

30 kW Class Arcjet Advanced Technology Transition Development (ATTD)

Mary M. Kriebel

**TRW Space & Technology Division
Space & Electronics Group
One Space Park
Redondo Beach, CA 90278**

June 2000

Final Report

20010327 148

APPROVED FOR PUBLIC RELEASE; DISTRIBUTION UNLIMITED.



**AIR FORCE RESEARCH LABORATORY
AIR FORCE MATERIEL COMMAND
EDWARDS AIR FORCE BASE CA 93524-7048**

REPORT DOCUMENTATION PAGE			Form Approved OMB No 0704-0188	
Public reporting burden for this collection of information is estimated to average 1 hour per response, including the time for reviewing instructions, searching existing data sources, gathering and maintaining the data needed, and completing and reviewing the collection of information. Send comments regarding this burden estimate or any other aspect of this collection of information, including suggestions for reducing this burden to Washington Headquarters Services, Directorate for Information Operations and Reports, 1215 Jefferson Davis Highway, Suite 1204, Arlington , VA 22202-4302, and to the Office of Management and Budget, Paperwork Reduction Project (0740-0188), Washington DC 20503.				
1. AGENCY USE ONLY (LEAVE BLANK)		2. REPORT DATE June 2000	3. REPORT TYPE AND DATES COVERED Final – February 1990 through October 1999	
4. TITLE AND SUBTITLE 30 kW Class Arcjet Advanced Technology Transition Development (ATTD)			5. FUNDING NUMBERS C: F04611-90-C-0005 PE: 63302F PR: 6340 TA: 00IT	
6. AUTHOR(S) Mary M. Kriebel				
7. PERFORMING ORGANIZATION NAME(S) AND ADDRESS(ES) TRW Space & Technology Division Space & Electronics Group One Space Park Redondo Beach, CA 90278			8. PERFORMING ORGANIZATION REPORT NUMBER 00.M230-024	
9. SPONSORING/MONITORING AGENCY NAME(S) AND ADDRESS(ES) Air Force Research Laboratory (AFMC) AFRL/PRRS 4 Draco Drive Edwards AFB CA 93524-7160			10. SPONSORING/MONITORING AGENCY REPORT NUMBER AFRL-PR-ED-TR-1999-0034	
11. SUPPLEMENTARY NOTES COSATI CODE(S):				
12a. DISTRIBUTION/AVAILABILITY STATEMENT Approved for public release; distribution unlimited.			12b. DISTRIBUTION CODE A	
13. ABSTRACT (MAXIMUM 200 WORDS) The Arcjet Advanced Technology Transition Demonstration (ATTD) Program developed and demonstrated a flight qualified 30 kW arcjet propulsion flight unit. Once it successfully completed qualification testing, the flight unit was integrated as the Electric Propulsion Space Experiment (ESEX) flight experiment onto the Air Force Advanced Research and Global Observation Satellite (ARGOS). The objectives of the flight unit space test were to measure arcjet plume deposition, electromagnetic interference, thermal radiation, and performance in space. These measurements were chosen to address specific operational issues that are commonly raised for EP systems. There were a total of eight firings conducted over the course of the 60-day mission, for a total duration of 2,023 seconds. All of the demonstration aspects of the experiment were completed successfully and the arcjet, PCU, PFS and overall system operated very well. All of the data analyzed to date indicate the thruster operated nominally, and operated completely independently of the normal operations of the host spacecraft.				
14. SUBJECT TERMS electric propulsion; arcjet; ESEX; ARGOS; flight experiment; high power; spacecraft; orbit transfer; ammonia; 30 kW; diagnostics; TQCM			15. NUMBER OF PAGES 144	
			16. PRICE CODE	
17. SECURITY CLASSIFICATION OF REPORT Unclassified	18. SECURITY CLASSIFICATION OF THIS PAGE Unclassified	19. SECURITY CLASSIFICATION OF ABSTRACT Unclassified	20. LIMITATION OF ABSTRACT SAR	

NOTICE

When U.S. Government drawings, specifications, or other data are used for any purpose other than a definitely related Government procurement operation, the fact that the Government may have formulated, furnished, or in any way supplied the said drawings, specifications, or other data, is not to be regarded by implication or otherwise, or in any way licensing the holder or any other person or corporation, or conveying any rights or permission to manufacture, use or sell any patented invention that may be related thereto.

ACKNOWLEDGEMENTS

The report contained herein documents the invaluable contributions made by many dedicated, exceptionally talented individuals across many different disciplines. These individuals performed as exceptionally as a team as they did in performing their separate responsibilities and the success of this program is as much a result of the collective teamwork as it was a result of the individual contributions. Hence, this acknowledgement is in recognition of the program team members from TRW's Space and Technology Group, Primex Aerospace Company, Orbital Sciences Corporation, the Air Force's Research Laboratory and Space and Missiles Systems Center, Boeing and the number of subcontractors that supported these team members.

FOREWORD

This Final Technical Report was prepared by TRW, Redondo Beach, CA, under Contract F04611-90-C-0005, for the Air Force Research Laboratory (AFRL), Edwards AFB, CA. The Project Manager(s) for AFRL is Daron Bromaghim.

This report has been reviewed and is approved for release and distribution in accordance with the distribution statement on the cover and on the SF Form 298.


DARON R. BROMAGHIM
Project Manager


RONALD A. SPORES
Chief, Spacecraft Propulsion Branch


LAWRENCE P. QUINN
Technical Advisor,
Rocket Propulsion Division

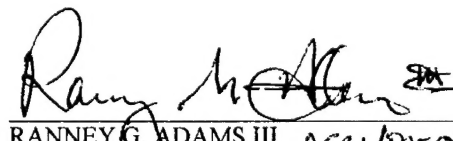

RANNEY G. ADAMS III
Public Affairs Director
AFRL/PASCO-062

TABLE OF CONTENTS

Section	Page
1.0 INTRODUCTION	1
2.0 OBJECTIVE	1
3.0 APPROACH	2
3.1 PHASE I - SYSTEM DESIGN	4
3.1.1 SYSTEM DESIGN	4
3.1.2 ARCJET DESIGN	4
3.1.3 PCU DESIGN	6
3.1.4 PROPELLANT FEED SUBSYSTEM DESIGN	7
3.1.5 COMMAND/CONTROL SUBSYSTEM DESIGN	8
3.1.6 DIAGNOSTIC PACKAGE DESIGN	9
3.1.6.1 PERFORMANCE	12
3.1.6.2 CONTAMINATION	12
3.1.6.3 OPTICAL	13
3.1.6.4 ELECTROMAGNETIC INTERFERENCE	13
3.1.7 POWER SUBSYSTEM DESIGN	14
3.1.8 THERMAL MANAGEMENT SUBSYSTEM DESIGN	14
3.1.9 STRUCTURE DESIGN	15
3.2 PHASE II - DEVELOPMENT TEST VEHICLE BUILD-UP, TEST AND INTEGRATION	16
3.2.1 SYSTEM DESIGN	16
3.2.1.1 POWER	16
3.2.1.2 ALIGNMENT	16
3.2.1.3 SOFTWARE	17
3.2.1.4 HIGH VOLTAGE	20
3.2.1.5 BATTERY DISCHARGE	20
3.2.1.6 INTEGRATED MISSION SIMULATION (IMS) TESTING	22
3.2.1.7 EMI ANALYSIS	24
3.2.1.8 VENTING ANALYSIS	24
3.2.2 ARCJET DESIGN	25
3.2.2.1 TUNGSTEN TO Mo/41Re WELD DEVELOPMENT	25
3.2.2.2 INCONEL TM 625 TO Mo/41Re BRAZE DEVELOPMENT	28
3.2.2.3 ARCJET ELECTRICAL PASS-THROUGH DEVELOPMENT	28
3.2.2.4 EM' and EM'' ARCJETS	29
3.2.2.5 IMS TESTS	32
3.2.2.6 FLIGHT ARCJET	33
3.2.3 PCU	37
3.2.3.1 ARCJET START TRANSITION	38
3.2.3.2 ARCJET LOW MODE TRANSITION	38
3.2.3.3 PCU INPUT VOLTAGE TRANSIENTS	41

TABLE OF CONTENTS (continued)

Section		Page
	3.2.3.4 PCU/ARCJET POWER RAMP	41
	3.2.3.5 PCU EFFICIENCY WITH AN ARCJET LOAD	41
	3.2.3.6 BREAKDOWN VOLTAGE VERSUS MASS FLOW RATE	41
	3.2.3.7 ARCJET BREAKDOWN INVESTIGATION	42
	3.2.3.8 PCU EM TESTING	45
	3.2.3.9 IMS TESTING	47
	3.2.3.10 FLIGHT BUILDUP	51
3.2.4	PROPELLANT FEED SUBSYSTEM DESIGN	53
	3.2.4.1 EFH DEVELOPMENT	54
	3.2.4.1.1 LIQUID INGESTION TESTS	56
	3.2.4.1.2 VAPOR OUTFLOW TESTS	56
	3.2.4.2 EM PFS DEVELOPMENT AND TESTING	57
	3.2.4.3 PFS IMS TESTING	58
	3.2.4.4 FLIGHT PFS FABRICATION AND TEST	60
3.2.5	COMMAND/CONTROL SUBSYSTEM DESIGN	60
3.2.6	DIAGNOSTIC PACKAGE DESIGN	61
	3.2.6.1 PERFORMANCE	61
	3.2.6.2 CONTAMINATION	62
	3.2.6.2.1 RADIOMETERS	62
	3.2.6.2.2 SOLAR CELLS	63
	3.2.6.2.3 TQCMs	63
	3.2.6.3 OPTICAL	63
	3.2.6.4 EMI	64
3.2.7	POWER SUBSYSTEM DESIGN	65
3.2.8	THERMAL MANAGEMENT SUBSYSTEM DESIGN	70
	3.2.8.1 MISSION PHASE 0/I ANALYSES	71
	3.2.8.2 MISSION PHASE II ANALYSES	72
	3.2.8.3 MISSION PHASE III ANALYSES	73
3.2.9	STRUCTURE DESIGN	73
3.2.10	FLIGHT UNIT INTEGRATION	75
3.3	PHASE III - FLIGHT QUALIFICATION AND DELIVERY	79
	3.3.1 ACCELEROMETER REWORK	79
	3.3.2 SOFTWARE VERIFICATION	79
	3.3.3 ELECTROMAGNETIC COMPATIBILITY TESTING	80
	3.3.4 RANDOM VIBRATION TEST	83
	3.3.5 THERMAL VACUUM TEST	85
	3.3.6 MASS PROPERTIES	97
	3.3.7 STORAGE PREPARATIONS	98
	3.3.8 POST-STORAGE ACTIVITIES	99
3.4	POST-DELIVERY OPERATIONS	101
	3.4.1 TRW ACTIVITIES	101
	3.4.2 BOEING ACTIVITIES	102

TABLE OF CONTENTS (continued)

Section	Page
3.4.2.1 ISV TESTING	102
3.4.2.2 INITIAL ESEX/ARGOS MATING	103
3.4.2.3 EMC TESTS	104
3.4.2.4 ACOUSTIC AND PYRO SHOCK	105
3.4.2.5 THERMAL VACUUM	105
3.4.2.6 ESEX GROUND OPERATIONS	106
3.4.2.7 ARCJET ALIGNMENT MEASUREMENTS	107
3.4.2.8 LAUNCH PAD ACTIVITIES	108
3.5 FLIGHT OPERATIONS	108
3.5.1 PHASE I OPERATIONS	108
3.5.2 PHASE II OPERATIONS	109
3.5.3 PRELIMINARY SCIENCE RESULTS	111
3.5.3.1 PERFORMANCE	111
3.5.3.2 CONTAMINATION	113
3.5.3.3 OPTICAL	114
3.5.3.4 ELECTROMAGNETIC INTERFERENCE	115
3.5.4 FLIGHT ANOMALIES	117
3.5.4.1 BATTERY PERFORMANCE	117
3.5.4.2 PFS LIQUID INGESTION	118
4.0 SUMMARY	119
5.0 RELATED PUBLICATIONS	121
6.0 REFERENCES	122

APPENDIX

APPENDIX A - MATERIALS RESEARCH AND DEVELOPMENT REPORT	124
---	-----

LIST OF FIGURES

Figure	Page
1 Arcjet ATTD Flight Unit Components	2
2 Phase I Flight Arcjet Design	5
3 Phase I Flight Power Cable	5
4 Preliminary PFS Block Diagram	9
5 Preliminary Diagnostic Package Deck: Top View	10
6 Predicted Plume Flow Field	11
7 E Field Along Centerline of 26 kW Arcjet	11
8 Phase II Power Profile	17
9 Arcjet ATTD Alignment Requirement and Capability	18
10 Battery Discharge Circuit Design	21
11 Battery Panel Load Resistor Circuit (Top View)	21
12 Battery Panel Load Resistor Circuit (Side View)	22
13 Analyzed Anode Joint Configuration	26
14 Alternate Anode Configuration with Tungsten Insert	27
15 Location on RTV Secondary Seal Material	30
16 EM' Arcjet Fractured Anode	30
17 EM'' Arcjet Thermal Performance	32
18 Development Arcjet Thruster Load sleeve and Nut	34
19 Flight Arcjet Thruster Load Sleeve and Nut	34
20 Development PCU Configuration	38
21 Pulser Current To PCU Current Transition	43
22 Arcjet Breakdown Voltage versus Voltage-Time Integral	44
23 Representative PCU Output Power Profile Measured During IMS Testing	49
24 Representative EM Battery Voltage Profile Measured During IMS Testing	49
25 Representative IM Battery Discharge Voltage Profile Measured During IMS Testing	50
26 Schematic Representation of the Propellant Feed System	54
27 Engineering Model PFS with EFH Integrated	55
28 Prototype Flight Configuration EFH	57
29 PFS Mass Flow Rate Test Results	58
30 Representative PFS Mass Flow Rate Measured During IMS Test	59
31 Representative Enhanced Feedline Heater Temperature Measured During IMS Testing	59
32 Diagnostic Package Device Layout	62
33 PIU Telemetry Conditioning Board	66
34 PIU Command Interface Board	66
35 PIU Heater Board	67
36 PIU Equipment Converter Board	67
37 PIU Battery Charger Assembly	68
38 Battery Cell Voltage Performance	68
39 Arcjet ATTD Six-Point Mounting Configuration	74
40 Extra Clock Signal from EMI Electronics	77
41 EMI/CCU Interface Signals Captured During EMI Breadboard Testing	78

LIST OF FIGURES (continued)

Figure		Page
42	Test Adapter Modification for Flight	81
43	ESEX Vibration Configuration	84
44a	Photomicrograph Obtained from SEM Analysis of Type 1 Particulate Contamination	89
44b	Spectrum Obtained from the EDX Analysis of Type 1 Particulate Contamination	89
45a	Photomicrograph Obtained from SEM Analysis of Type 2 Particulate Contamination	90
45b	Spectrum Obtained from the EDX Analysis of Type 2 Particulate Contamination	90
46	Spectrum Obtained from the FTIR Analysis of Particle Collected from PFS Platform	91
47	Spectrum Obtained from FTIR Analysis of Type 3 Contamination From Inside Battery	91
48	Thermal Vacuum Test Timeline	93
49	"As-Built" Thermocouple Circuit	94
50	All-Splice Thermocouple Option	94
51	PFS Test 1 - Steady State Response at 160 mg/second	96
52	PFS Test 2 - 200 mg/second ramping to 240 mg/second	96
53	Arcjet ATTD Flight Unit Delivery Ceremony	101
54a	Mating ARGOS to the ESEX Flight Unit	104
54b	ISV installed in the acoustic chamber for the acoustic and pyro-shock tests	104
55	Typical Operational Profile Of An Arcjet Firing Showing The Ramp To Full Power And Steady-State Operation	112
56	Arcjet On-Orbit Performance Uncorrected for Any Power Deviation	113
57	Summary Of TQCM Effects From The Arcjet Firings Over The First 65 Days From Launch	114
58	Series Of Images Acquired From The On-Board Video Camera Showing the Ramp To Full Power	115
59	Representative Bit Error Rate Data For Firing #2 (F-2) Displayed With Baseline Pass Taken Under Similar Conditions	116
60	Typical Battery Charging Circuit Instability	117

LIST OF TABLES

Table	Page
1 Arcjet Power Ramp Test	7
2 Diagnostic Package Instrumentation	10
3 IMS Test Summary	23
4 Arcjet ATTD Flight Unit Electromagnetic Interference Safety Margins	24
5 Stress Summary for Anode Weld Alternatives	27
6 EM" Arcjet Hot Fire Test Data	31
7 PCU/Arcjet Hardware Changes And Resulting Breakdown Testing	39
8 Pulser Circuit Discharge Characterization	42
9 Development PCU Performance with Resistive Load	43
10 Average Breakdown Data	44
11 PCU Anomaly Resolution Summary	50
12 Battery Effluent Test Results	69
13 ESEX Component Temperatures (°F) at 90 Minutes after Liftoff	72
14 Arcjet ATTD Flight Unit Modal Frequencies	75
15 Result Summary for Particulate Collected from Battery and the Arcjet Flight Unit	88
16 Flight Unit Mass Properties	97
17 Summary of ESEX Arcjet Firings and Propellant Releases	110

APPENDIX A: MATERIALS RESEARCH AND DEVELOPMENT REPORT

TABLE OF CONTENTS

Section	Page
A.1 High Density Tungsten Development	124
A.2 Tungsten to Mo/41Re Weld Development	124
A.3 Inconel TM 625-to-Mo/41Re Braze Development	131

LIST OF FIGURES

Figure	Page
A1. Analyzed Anode Joint Configurations	125
A2. Finite Element Model of Weld Joint with W25Re Transition Element	126
A3. Anode Stresses in Weld Region of Modified Joint	127
A4. Finite Element Model of Weld Joint with -30° Scarf Angle	128
A5. S _{yy} Anode Stresses in Weld Region of Scarf Joint	129
A6. Finite Element Model of Weld Joint with Thinned Anode at Weld Interface	129
A7. Alternate EB Weld Configuration with a W24/Re Ring	130
A8. EM” Anode Design	131

LIST OF TABLES

Table	Page
A1. Stress Summary for Anode Weld Alternatives	130

GLOSSARY

AFRL	Air Force Research Laboratory
AFSCN	Air Force Satellite Control Network
ARGOS	Advanced Research and Global Observation Satellite
ASID	Arcjet System Integration Demonstration
ATC	Ammonia transfer cart
ATTD	Advanced Technology Transition Demonstration
CCA	Circuit card assemblies
CCS	Command/control subsystem
CCU	Command and Control Unit
CDR	Critical Design Review
CEU	Camera electronics unit
CG	Center of gravity
CIA	Command interface assembly
CIV	Critical Ionization Velocity
CPCA	Camp Parks Communications Annex
CSFT	Combined Systems Functional Test
CTE	Coefficient of thermal expansion
DPC	Dual pressure control
DRD	Design Requirements Document
EB	Electron beam
EDX	Energy Dispersive X-ray
EFH	Enhanced Feedline heater
EM	Engineering model
EMC	Electromagnetic Compatibility
EMI	Electromagnetic interference
ESD	Electro-static discharge
ESEX	Electric Propulsion Space Experiment
FGU	Frame grabber electronics
FTIR	Fourier Transform Infrared
GN ₂	Gaseous nitrogen
GPS	Global positioning satellite
GSE	Ground support equipment
IEU	Integrated electronics unit
IMS	Integrated Mission Simulation
I _{sp}	Specific impulse
IST	Integrated systems test
ISV	Integrated space vehicle

GLOSSARY (continued)

KOH	Potassium hydroxide
LCU	Load control unit
MLI	Multi-layered insulation
MSSS	Maui Space Surveillance Site
N	Newtons
NH ₃	Ammonia
OSC	Orbital Sciences Corporation
PAC	Primex Aerospace Company
PCM	Phase change material
PCU	Power conditioning unit
PDA	Power distribution assembly
PDR	Preliminary design review
PFS	Propellant feed subsystem
PIU	Power integration unit
PROM	Programmable read-only memory
PSS	Power subsystem
PWA	Printed wiring assembly
PWB	Printed wire board
Rx/Tx	Receiver/transmitter
SEM	Scanning electron microscope
SEMCAP	Specification and Electromagnetic Compatibility Analysis Program
SMC	Space and Missiles Systems Center
SOH	State of health
SPI	Space Power, Inc
SSR	Solid-state recorder (SSR)
STT	Silvered Teflon TM tape
TMS	Thermal management subsystem
TQCM	Thermoelectric quartz crystal microbalances
USAF	United States Air Force
W100	Tungsten

1.0 INTRODUCTION

Previously, the United States Air Force (USAF) has operated under a "launch on demand" philosophy for transporting military payloads to their operational orbit. Besides being the quickest way to transport payloads, liquid and solid rocket propulsion technology was mature enough to complete the mission. Over the years, as payloads grew in mass, liquid and solid rocket upper-stage transfer vehicles were built to complement the launch vehicles. As payloads continue to grow, space transport vehicles will be unable to meet the USAF's needs.

Due to this continuing increase in payload mass and the recent technological developments in space power and electric propulsion, a wide range of orbit transfer and maintenance missions can be greatly improved in terms of deliverable payloads, on-orbit lifetimes and reduced launch costs through the use of electric propulsion. Because of this, development of the key components needed for the near term and future operational electric propulsion systems is being pursued.

Such a near term operational electric propulsion system for an electric orbit transfer vehicle is an arcjet propulsion system. Towards this end, TRW Space and Technology Division, along with teammates Primex Aerospace Company (PAC) and Orbital Sciences Corporation (OSC) have designed, built, and space qualified a 30 kW class ammonia (NH_3) arcjet as a part of the 30 kW Class Arcjet Advanced Technology Transition Demonstration (Arcjet ATTD) Program. Subsequently, the Air Force Research Laboratory (AFRL) performed the flight operations of the Arcjet ATTD flight unit. (Note: During the course of the program, TRW's two major subcontractors changed company names. For clarity sake, the companies will be referred to by their current name. Therefore, the company name Primex Aerospace Company (PAC) will be used to refer to work performed as Rocket Research Company, Pacific Electro-Dynamics, and Olin Aerospace Company. The company name Orbital Sciences Corporation (OSC) will be used to refer to work performed as Defense Systems Incorporated and CTA Space Systems. In addition, when the program began, the contract was issued by the Air Force Astronautics Laboratory. During the course of the program, the laboratory's name was changed to the Air Force Phillips Laboratory and then the Air Force Research Laboratory (AFRL), the name by which it is known today. Therefore, AFRL is used throughout this report to refer to the government contracting organization.

2.0 OBJECTIVE

The objective of the Arcjet ATTD Program was to develop and demonstrate a flight qualified arcjet propulsion flight unit. The flight unit, shown in Figure 1, consisted of a low impedance 26 kW arcjet, power conditioning unit (PCU), propellant feed subsystem (PFS), command/control subsystem (CCS), diagnostic package, power source, thermal management subsystem (TMS), internal interfaces, and system packaging. TRW was responsible for the system engineering, mechanical, electrical and thermal integration engineering, and the design and development of the diagnostic package. PAC, together with its subcontractor, Space Power, Inc. (SPI), designed, developed and fabricated the arcjet, PCU and PFS. OSC was responsible for the CCS, structure and integration of the flight unit. TRW completed the hardware development effort by performing the qualification testing of the flight unit. The hardware was subsequently delivered to AFRL for integration as the Electric Propulsion Space Experiment (ESEX) flight experiment onto the Advanced Research and Global Observation Satellite (ARGOS).

The objectives of the flight unit space test were to measure plume deposition, electromagnetic interference, thermal radiation, and acceleration in space. These measurements

were chosen to address specific operational issues that are commonly raised for EP systems. The key features of this flight unit were: 1) use of existing arcjet, PCU and PFS technology as the basis for the flight hardware; 2) maximum use of existing space qualified diagnostic instruments for the arcjet flight unit diagnostic package; 3) use of space qualified design approaches for the remaining flight unit support hardware; and 4) use of the protoflight approach to flight unit qualification.

3.0 APPROACH

The approach taken to perform these tasks was to segment the program into three phases:

- Phase I - System Design
- Phase II - Development Test Vehicle Build-up, Test and Integration
- Phase III - Flight Qualification and Delivery.

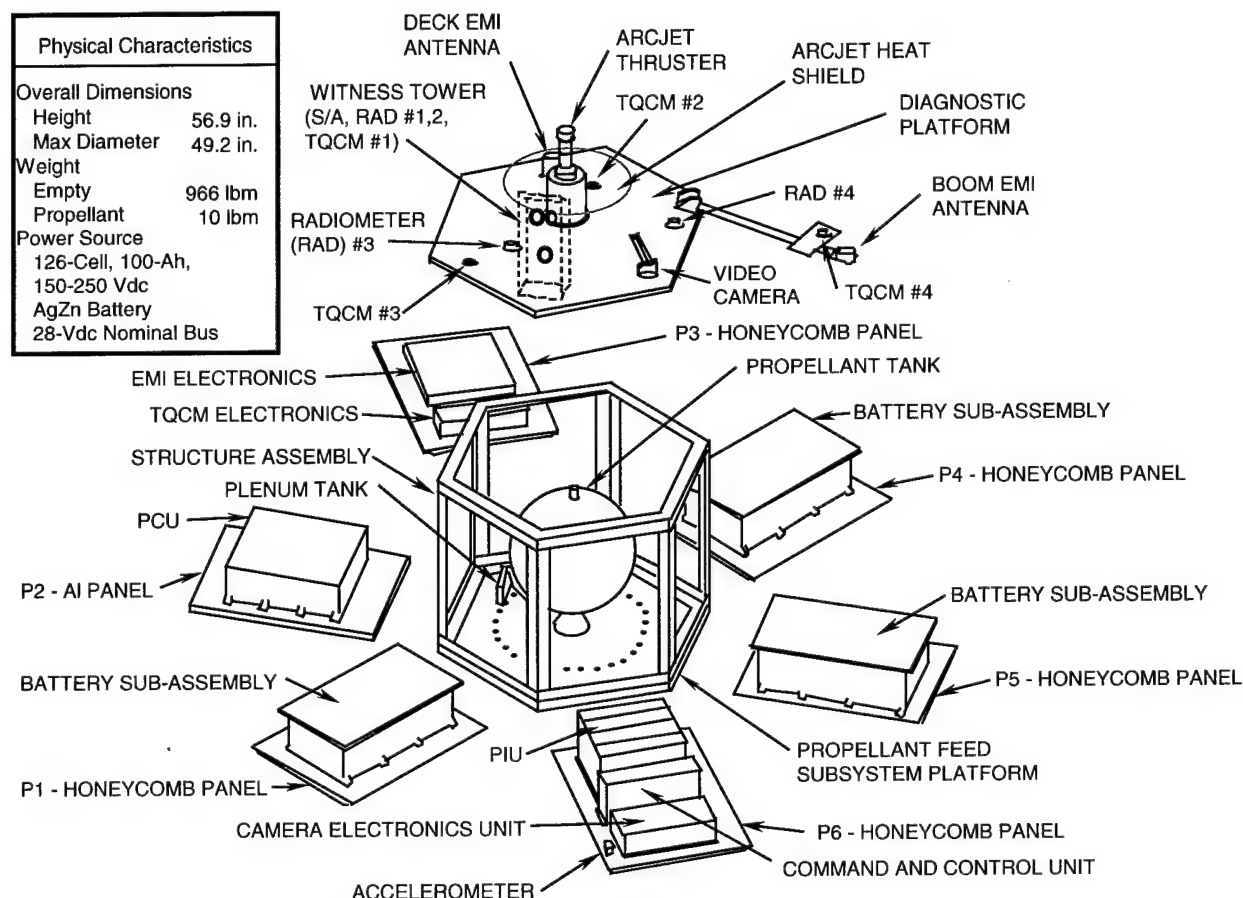


Figure 1. Arcjet ATTD Flight Unit Components

During Phase I, the engineering design of all the subsystems and the flight unit was performed. Preliminary developmental testing was also performed using a government-furnished arcjet and a breadboard PCU in order to establish detailed technical criteria regarding the start-up of the arcjet

with the PCU. Phase I was concluded with the presentation of the flight unit design to AFRL at the preliminary design review in July 1991.

During Phase II, fabrication and testing of development hardware was conducted and detailed design changes were incorporated based on these test results. Examples of these design changes include:

- Integrated testing of a development PCU with a government-furnished arcjet identified the inability of the PCU to break down (i.e. ignite) the thruster with the existing start circuit. Additional testing was accomplished and AFRL and PAC that defined the true start-up criteria for the arcjet. The necessary changes were successfully implemented into the PCU design.
- Numerous tests were conducted to develop a PFS which was capable of conditioning liquid NH_3 to vapor for the full 15 minute outflow required for thruster operation.
- Eagle PicherTM, a subcontractor to TRW, performed discharge tests using a 20-cell battery to verify performance capability and stability and to provide thermal design data before fabricating the full 126-cell battery.
- A development PCU, an engineering model (EM) arcjet, and an EM of the propellant feed subsystem were integrated and tested to verify performance. A full-scale EM of the battery was subsequently added to the entire system-level assembly to demonstrate the capability of the propulsion system end to end.
- EMs of the power integration unit (PIU) and the command and control unit (CCU) were assembled and functionally tested prior to and after a vibration test to verify functionality and their ability to endure the anticipated launch environment.
- A breadboard electromagnetic interference (EMI) electronics unit was upgraded to an EM and exposed to vibration, thermal cycle and burn-in tests to verify the integrity of the design for the Arcjet ATTD application.
- The flight unit structure was fabricated and subjected to a static load test and was inspected and verified to have survived the test without damage.

Following these tests, the overall flight unit design was presented to AFRL at the program Critical Design Review (CDR).

Following the CDR and AFRL approval of the flight unit design, some EM hardware was refurbished for flight use. Specifically, this hardware included the PIU, the EMI electronics unit, the CCU and the flight unit structure. PAC fabricated and assembled from all new components, the flight PFS, a flight arcjet and a flight PCU. Prior to integration into the flight unit, protoflight-level acceptance tests were conducted to verify compliance of the arcjet, PCU, and PFS with environmental requirements. TRW assembled the diagnostic package and the thermal management system. OSC integrated the various subsystems into the flight unit. Both TRW and OSC refurbished, as necessary, all hardware to assure its status as flight-ready.

Phase III of the program began at the completion of flight unit assembly and initial functional testing. During this phase, TRW subjected the flight unit to the protoflight acceptance

tests. This testing consisted of thermal vacuum, random vibration, electromagnetic compatibility (EMC), proof pressure and leak testing of the propulsion subsystem, and integrated system tests.

Having completed its ground qualification test, the flight unit was delivered to AFRL at the Boeing Company in Seal Beach, CA for integration onto the ARGOS spacecraft.

3.1 Phase I – System Design

The following paragraphs describe the work that was performed from the start of the program in February 1990 until the preliminary design review (PDR) which was held at AFRL in July 1991.

3.1.1 System Design. The primary design activity of this phase at the system level was the generation and continuous refinement of the system and subsystem level design requirements. These requirements were compiled into the Arcjet ATTD Design Requirements Document (DRD). This internal document identified all of the requirements for design, fabrication, test and delivery of the Arcjet ATTD flight experiment. This document also allocated these requirements to the major components and subsystems that comprised the experiment. The requirements included those provided in the customer statement of work, and the derived requirements presented at the Initial System Design Review. Also included in the DRD was a verification matrix that indicated the method used to verify compliance with all defined requirements. Generation of the DRD also required definition of the electrical, mechanical, thermal and functional interfaces between each subsystem and between the flight unit and the host vehicle.

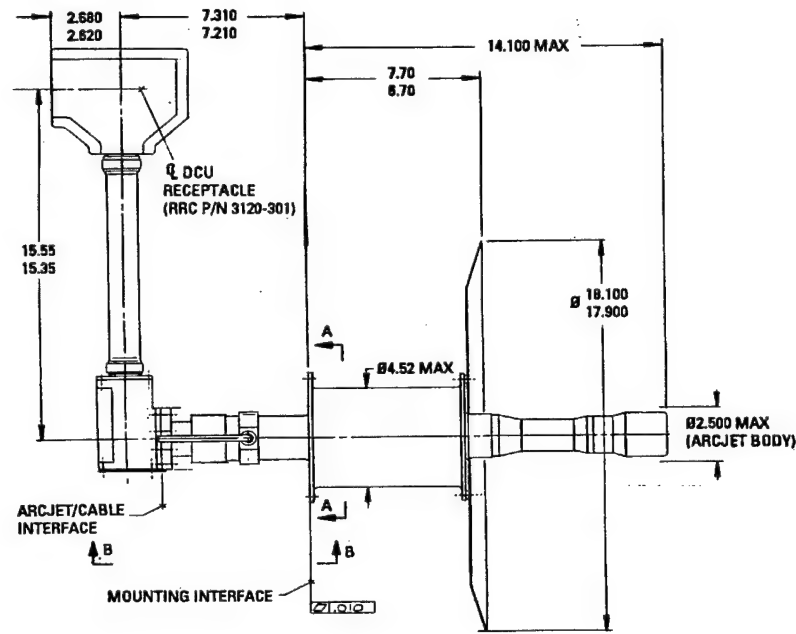
The initial physical design was driven by the requirement that the flight unit be compatible with the PegasusTM launch vehicle, but remain flexible enough to meet many other launch vehicle launch environments. This was due to the fact that the launch vehicle had not been identified at the time the contract was awarded. Therefore, the flight unit was designed to fit within the payload envelope of the PegasusTM fairing. Weight allocations were assigned to each subsystem and weight contingency held at the system level such that the total weight was within the PegasusTM launch capability. Since the flight unit design had been constrained in size and driven by very conservative launch environment requirements, the transition to the ARGOS spacecraft was fairly smooth. This is discussed in more detail in Section 3.2.

The high current nature of the power system of the Arcjet ATTD flight unit required significant attention be paid to the grounding philosophy. The requirements imposed on the grounding scheme were high power ground at the anode, low power ground for the solar array and 28 Vdc bus at the power integration unit (the solar array was later dropped from the design), and distributed signal grounds and isolated power for diagnostics and the command and control unit. This grounding philosophy also featured no power current flow through the structure. After the solar arrays were removed from the flight unit design, the grounding scheme was revised such that the host vehicle was grounded at the host vehicle power system and isolated power was sent to the PIU.

Initially, power for the Arcjet ATTD was to be provided by dedicated solar arrays on the flight unit. It was later decided that, as a payload aboard a host spacecraft, power would be supplied and that the solar arrays were not required. They were therefore dropped from the design and an accounting of required power was initiated.

3.1.2 Arcjet Design. The program approach was to start with the AFRL 26 kW arcjet design which had been previously developed for AFRL by PAC during the Arcjet Endurance Test

Program (contract number F04611-89-0013). Minimal internal design changes were made to the AFRL thruster as a part of the Arcjet ATTD program and the geometry of the electrodes was unchanged. The design work done during Phase I converted the laboratory model to the flight-weight, space qualified arcjet shown in Figure 2. Shown in Figure 3 is the power cable that supplies the high voltage, high current power to the arcjet from the PCU. This cable design was also developed during Phase I as an integral part of the arcjet design. Based on the performance achieved during the Arcjet Endurance Test Program, the arcjet was required to produce greater than 800 seconds



DIMENSIONS IN INCHES

Figure 2. Phase I Flight Arcjet Design

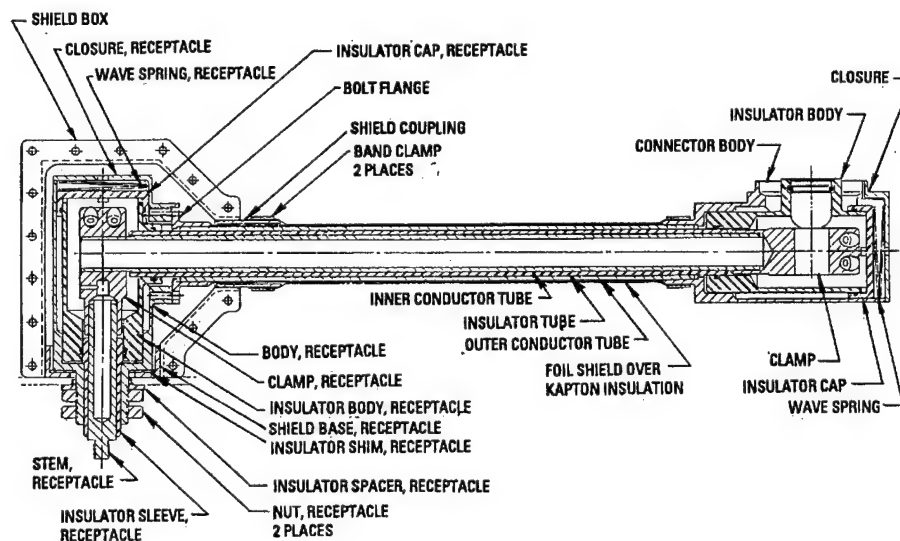


Figure 3. Phase I Flight Power Cable

specific impulse (I_{sp}) and approximately 2 Newtons (N) of thrust during each of the firings. Additional key design requirements for the cable were: (1) be able to operate at 26 kW of power; and (2) radiated emissions from the cable not interfere with the rest of the flight unit. Therefore, a triaxial cable with helical scoring for flexibility was designed and tested.

As a part of the overall arcjet development effort, three separate material process development efforts were undertaken. The first was to develop a process that would produce tungsten (W100) in densities high enough to be suitable for the high power/high temperature operating conditions anticipated for the 30 kW arcjet. This effort was conducted in Phase I while the two remaining development efforts were conducted in Phase II and are discussed in Section 3.2.2.

The process needed to produce the desired density of tungsten for the anode was initiated during Phase I of the program. This was a significant contribution to the development of the flight-unit arcjet. Tungsten is not usually fabricated in diameters greater than 1.5 inches and powder metallurgy does not produce full density material in the center of large bars where the critical anode dimensions are. To meet the density requirement of 99%, two-inch diameter by 7-inch long billets were forged into 3-inch diameter by 5-inch long billets and machined into the weld samples and anodes. The actual welding and testing of the samples was performed in Phase II.

3.1.3 PCU Design. The baseline PCU design incorporated the three-phase buck regulator concept developed for the AFRL by SPI. However, considerable design work was required to create a flight-qualified unit.

A testing opportunity presented itself early in the program when an SPI breadboard PCU (Number 03) and an AFRL arcjet were made available to the Arcjet ATTD program. This testing, the first integrated test of a high power arcjet and this PCU design, allowed the start-up parameters to be validated before fabrication of the development PCU. The specific objectives of the test were to measure the breakdown characteristics of the arcjet and PCU, determine the parameters of the power ramp-up, and determine the safest method of ramping the arcjet power from its initial starting level to steady-state.

The tests were initiated by testing the PCU with a resistive load to verify the PCU was operating within the expected limits. The PCU and arcjet were then integrated and preliminary attempts to start the arcjet were unsuccessful. The arcjet gap was reduced and a PAC capital PCU, which issues a start pulse of approximately 5kV, was used to successfully start the arcjet. The arcjet was run for approximately 45 minutes in order to condition the electrodes, and then the SPI breadboard PCU was re-integrated with the arcjet. Subsequently, breakdowns were repeatedly performed with a 2.1 kV pulse from the SPI PCU breadboard.

To characterize what is required for a stable power ramp-up, four computer controlled power ramps were performed at a constant propellant mass flowrate. Table 1 summarizes the results from these tests.

For these tests, it was determined that a limitation existed in the maximum rate of increase in arc current due to the possibility of forcing the arc into "low mode" - a constricted spot attachment. Further analysis was performed and the development unit was baselined and fabricated to initiate the ramp-up after a constant current level of 100 amps was maintained for 10 seconds.

Breadboard EMI filter testing was conducted to gather information on the effectiveness and stability of the EMI filter design proposed for use in the development PCU. The filter was integrated into an existing SPI breadboard PCU (Number 02) and initial testing was conducted to determine functional capability of the filter installation. These tests were followed by PCU

Table 1. Arcjet Power Ramp Test

Power Ramp	Constant Current (Amp)	Constant Current Duration (Sec)	Power Ramp Duration (Sec)
1	100	10	60
2	50	10	60
3	100	5	25
4	50	5	40

operation over a range of powers using a simple resistive load. The power level was increased gradually from approximately 5 kW to 10 kW with oscilloscope traces recording the input and output voltages. Once the PCU/filter combination was determined to be operating satisfactorily, the power was increased to 26 kW.

Voltage measurements were made at each of four locations: input to the EMI filter; output of the power supply; input to the PCU; and output of the PCU. These measurements were made at input voltage levels of 165 VDC and 180 VDC and at power levels of 15 kW and 26 kW. Conducted EMI measurements were also performed per MIL-STD-461 at these four locations. During these tests, two main issues were addressed: filter attenuation and filter stability during the start transient. The results showed that the actual start pulse transient stability of the EMI filter was better than expected. These tests also showed the ability of the EMI filter to attenuate the conducted current emissions on the input lines to the PCU to within the tailored limits of MIL-STD-461C.

As a result of start-up tests performed at PAC in February 1991, start circuit design changes were made to the PCU during Phase I of the program. These changes were made to increase the energy stored in the output inductors (which allows the start pulse to vary from 16 to 160 microseconds) and to modify the voltage ramp of the inductor energy charging characteristics.

3.1.4 Propellant Feed Subsystem Design. The baseline propellant feed subsystem was the TRW LES 8/9 feed system. However, it was determined that the design could not provide the flowrate of 240 ± 5 mg/sec required by the arcjet and still provide full vapor to the thruster during a 15 minute firing. Also, existing performance data for the LES 8/9 system indicate that the system produced pressure fluctuations greater than ± 10 %. The arcjet flowrate requirement only permitted fluctuations in pressure of ± 2 %. Deviations from this tight tolerance could result in damaging the arcjet or producing less than the required specific impulse. Therefore, analyses were conducted to determine alternate approaches for feeding gaseous NH_3 to the arcjet. One such approach was to determine how to withdraw only vapor from the propellant tank without significant modification to the current PFS hardware. However, since NH_3 is a wetting fluid, a continuous liquid film covering all internal surfaces of the tank, including the tank exit would most likely exist prior to arcjet operation resulting in liquid outflow.

To tap into the ullage gas, the gas bubble would have to be positioned at the tank outlet. Simple acceleration can move the bubble to the outlet region such as that produced by the arcjet, during cold flow or actual firings. Creating a dry spot at the exit or breaking the fluid film, however, requires an energy input that exceeded the surface tension. Preferential heating of one pole of the tank would produce the same effect, however, it is still necessary to break the bubble formed by the high bonding surface tension characteristics of NH_3 . Considerable analysis and testing was performed in Phase II to address and solve this technical issue.

In addition to the system performance issues, several hardware problems were identified and resolved. The tooling for the LES 8/9 tank was no longer available and the expense to procure a new tank was beyond the original budget. Therefore, a cost-effective, alternate approach was identified using two flight-qualified spare tanks. The first was from the PAC AtlasTM Roll Control Module and was used as the propellant tank for the flight unit PFS. A spare tank was also used as the plenum tank to contain the vaporized NH_3 .

The flow meter used within the PFS was comprised of an orificed manifold using output signals of two pressure transducers and one thermistor. The flow meter was tested to determine accuracy and sensitivity as a function of the inlet pressure, throat pressure or pressure drop across the throat and gas temperature. The data obtained from each test were used to refine correction factors for the imperial equations to determine the actual mass flow rate for a broad range of operating conditions. Four specific subtests were performed as described below:

Sub-Test 1: Evaluated the accuracy of the PFS flow meter at a constant mass flow rate (240 mg/sec) but with varying inlet pressure and throat pressure. Result: The test data confirmed that the flow orifice could be used to measure the flow rate of ambient temperature NH_3 and showed that NH_3 vapor does not condense in the venturi section.

Sub-Test 2: Evaluated the accuracy of the PFS flow meter during a simulated "cold flow" change in mass flow rate (130 mg/sec to 370 mg/sec) through the arcjet. Result: test showed good stability of the measurement over a wide range of propellant mass flowrates. The flowrate measured by the PFS orifice varied by no more than 3% from a calibrated flowmeter value over this flow rate range at a constant propellant temperature of 70°F.

Sub-Test 3: Investigated the response of the PFS flow meter due to changes in mass flow rate at different inlet pressures caused only by a change in the pressure drop across the throat. Result: test determined that the flow orifice choked at 26 psia for the nominal mass flow rate of 240 mg/s. This result was significant because the expected arcjet inlet pressure was 23 psia and the PFS flow meter orifice was re-sized to a smaller diameter to allow choked flow at higher arcjet inlet pressure.

Sub-Test 4: Investigated the sensitivity and accuracy of the PFS flow meter at a constant mass flow rate but with varying propellant inlet temperature and inlet pressure. Test results showed a total deviation of roughly 1% with respect to the calibrated flowmeter.

At PDR, the PFS consisted of the components shown in Figure 4. All components had flight heritage and the pre-PDR testing gave high confidence that it was a good-working design.

3.1.5 Command and Control Subsystem Design. The initial baseline CCS/host vehicle interface was based on the use of an existing RS 232 receiver/transmitter (Rx/Tx) controller board and communications software developed on existing OSC programs. The Rx/Tx interfaces between the host vehicle and the CCU were baselined to be one input line and one return line. A design assumption of the Arcjet ATTD program was that communication data would be transferred between the CCU and the host vehicle as a half-duplex serial bit stream. As discussed in Section 3.2.4, this RS 232 interface was changed to a MIL-STD-1553 interface when ESEX was manifested on the ARGOS spacecraft.

Fabrication of the boards that made up the CCU was not started until after PDR.

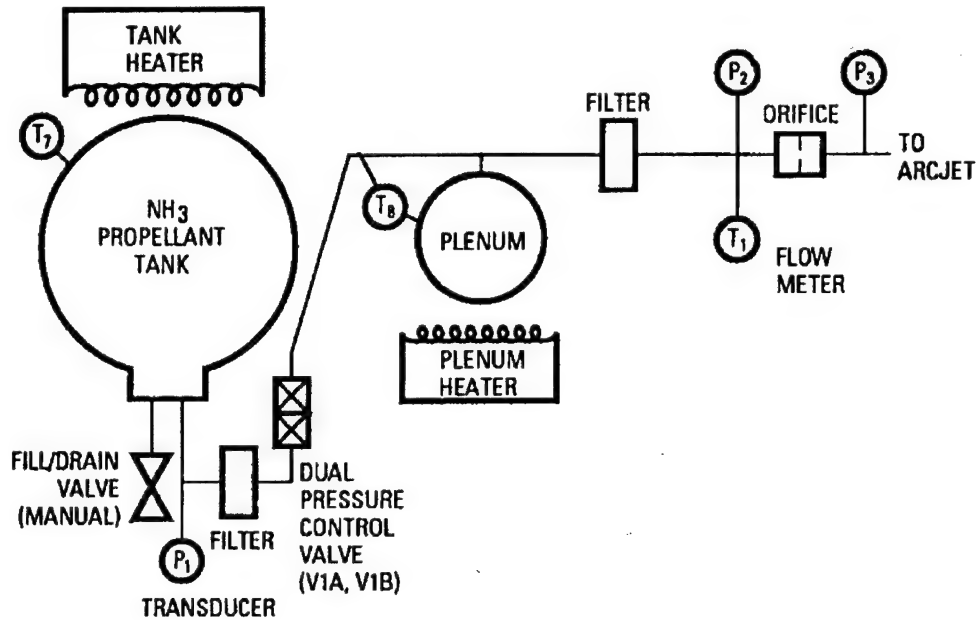


Figure 4. Preliminary PFS Block Diagram

3.1.6 Diagnostic Package Design. The key requirements for the diagnostics package were to measure thruster performance, plume contamination and thermal radiation flux of the arcjet, arcjet induced EMI, and the optical properties of the nozzle and plume luminescence. Furthermore, these results were required to help extrapolate the information to 30m from the arcjet, requiring near and far field measurements. The specific measurements and instrumentation used to make these measurements are listed in Table 2 and shown in Figure 5. These instruments were chosen to collect information regarding arcjet performance and spacecraft interaction that cannot be adequately quantified in ground tests.

In order to determine the optimum locations of the diagnostic package instruments, the arcjet thruster plume flow field was analytically modeled. Specifically, the results of these analyses helped to locate the four TQCMs and the solar cells, and were used to determine the potential condensation from the arcjet plume. Of the mass flux to the surfaces, only the NH and N₂ components were expected to condense.

One of the required tasks in the Statement of Work was to conduct an analysis to allow extrapolation of the measured effects to not less than 30 meters. The approach to accomplishing this was to predict plume flow field, EMI electric fields and thermal radiation to distances of 30 meters from the arcjet using the same analytical models developed to predict instrument performance. The assumption was that the measurements would validate the analytical models that were used for the extrapolation. The plume flow field and EMI electric fields at 30 meters are shown in Figures 6 and 7 respectively. Note that the models predicted uniform decay outside the spacecraft dimensions indicating numerical instabilities in the far flow field in the simple approximation code that was used.

Table 2. Diagnostic Package Instrumentation

Requirement	Source	Capability	Verification Method
Measure thruster performance	SOW 3.1.6	Accelerometer	Computed from measurement and mass
Thrust		Mass flow meter Voltmeter, ammeter } RRC	Measured
Mass flow			Measured
Thruster voltage and current			
Measure plume contamination (function of radius and angle)	SOW 3.1.6	TCQM	Measurements at four positions
Determine plume effects on	SOW 3.1.6	Solar array witness rate	Measurements
Solar arrays			Provide flow field for further analysis and test
Typical space vehicle structures			
Refractory metals			
Thermal radiation flux (function of radius and angle)	SOW 3.1.6	Radiometers	Measurements at four positions
Electromagnetic interference (function of radius and angle)	SOW 3.1.6	Radiated EMI experiment	Measurements at two positions
Document nozzle and plume luminescence	SOW 3.1.6	Video camera	Observation
Relate collected data to expected results at 30 m	SOW 3.1.6		Analysis

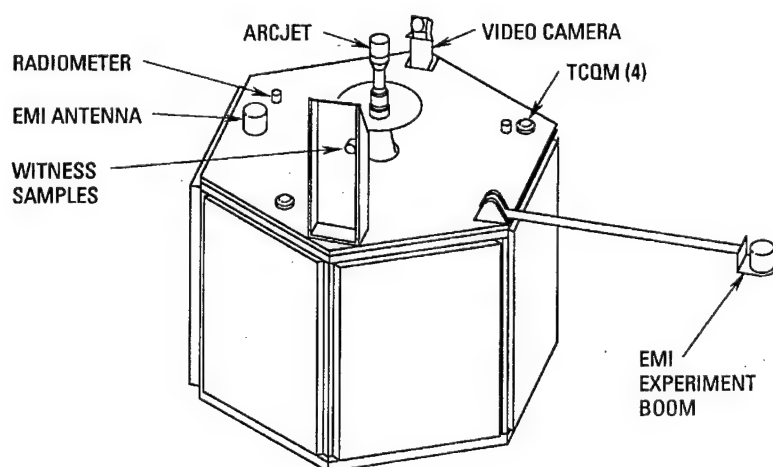


Figure 5. Preliminary Diagnostic Package Deck: Top View

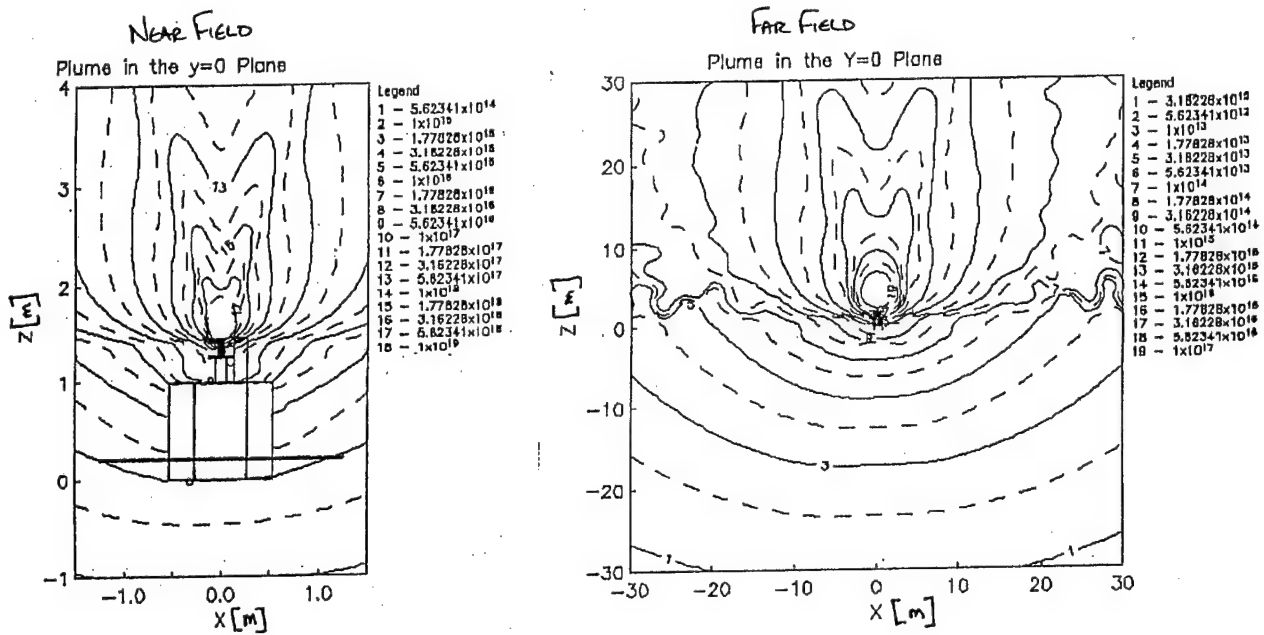


Figure 6. Predicted Plume Flow Field

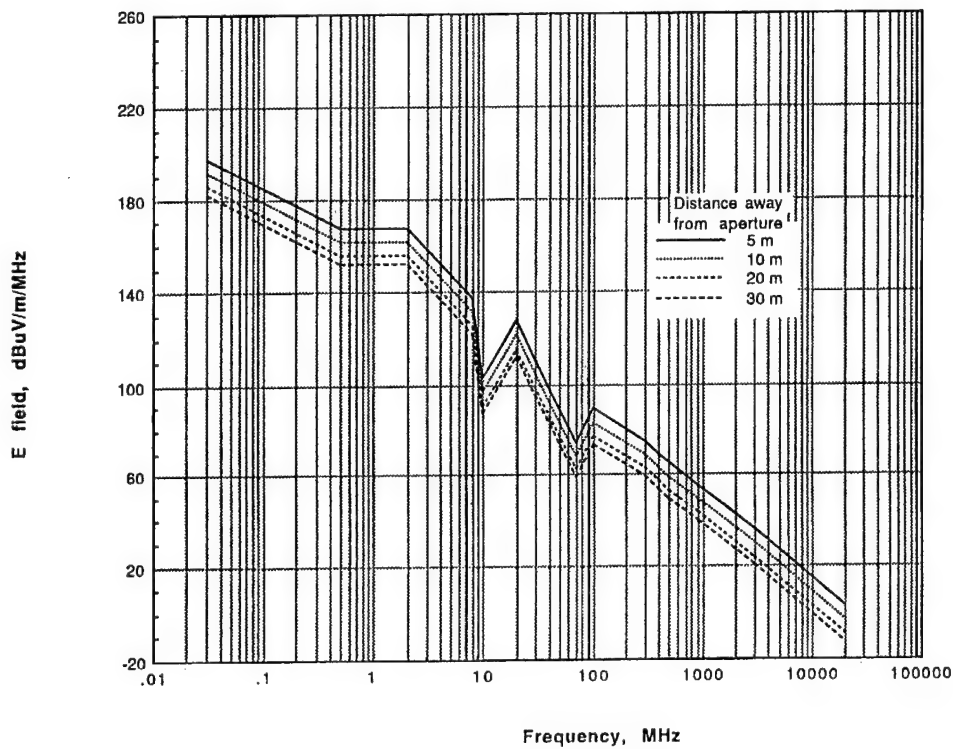


Figure 7. E Field Along Centerline of 26 kW Arcjet

3.1.6.1 Performance. An accelerometer was chosen in order to allow determination of the arcjet thrust. Having measured the spacecraft wet weight prior to launch, and measuring accelerations during arcjet firings, the thrust of the arcjet was calculated. The arcjet Isp was then calculated from the mass flow measurements made by the PFS, combined with the calculated thrust from the accelerometer measurements and spacecraft mass. Additional telemetry collected for the arcjet via the PCU included arcjet input current and input voltage. Using the thrust, mass flow, and power data, the arcjet efficiency was calculated.

3.1.6.2 Contamination. The instruments chosen for the plume contamination were thermoelectric quartz crystal microbalances (TQCM), solar cells, and radiometers. TQCMs measure deposition of contaminants per unit surface of an exposed crystal. The monitor consists of quartz crystal vibrating in shear mode that stabilizes at the resonant frequency of an oscillator. As the mass deposition on the surface increases, the beat frequency of the oscillator changes. There is a direct correlation between frequency and mass accumulation per unit surface area. These TQCMs were temperature controlled by means of a thermoelectric two-stage cooler set to a desired cold temperature for deposition measurements. The subsequent heating of the elements would ideally allow thermal gravimetric desorption of the crystals in flight. However, in practice, this proved difficult. This desorption technique permits identification of the collected contaminants by measuring the temperature at which vaporization occurs.

The diagnostic package had four TQCMs operating from a single electronics unit. The first sensor (TQCM #4) monitored contamination in the back flow region, where the contaminants were most likely to exist. The original location of this TQCM was planned to be either on the side of the flight experiment or located somewhere on the host spacecraft. However, the difficulty of the interfaces with this location caused it to be moved onto the deployable boom used for the far field EMI antenna. The three remaining sensors were positioned to take relative plume contamination measurements. Two of the TQCMs (TQCM #2 and #3) were mounted directly on the top of the diagnostic package platform. The last TQCM (TQCM #1) was mounted above the diagnostic platform at approximately the same height above the platform as the arcjet thruster exit plane next to the solar cells. This TQCM sensor could be used to help determine if plume contamination occurred on the witness samples and what the condensable deposits were.

During Phase I, analyses were conducted that determined the primary constituents of the arcjet plume would be molecular and atomic nitrogen and hydrogen, and NH. Metallic constituents, tungsten and thorium, from the arcjet, were also expected to condense, but the total deposition during the mission would be negligible.

The second element of the plume contamination experiment was the solar cell deposition experiment. Eight cells were mounted at a 45° angle from the arcjet centerline to receive exposure to the sun as well as the arcjet. There were two circuits of four cells in series; one circuit would measure the short circuit current while the second would measure load voltage. The type of solar cell chosen was gallium arsenide, which are less sensitive to the infrared frequencies expected from the arcjet. The spectral radiance of the arcjet anode is greatest in the wavelength range of 690 - 1200 nm while solar cells respond to light in the range of 300 - 1200 nm. This correlation allowed direct measurement of the effect of an arcjet on a solar array. A thermistor was also mounted on the back of the baseplate to provide temperature data during flight. The cell characteristics (open circuit voltage and closed-circuit current) were monitored prior to arcjet operations to obtain baseline data throughout the orbit cycle. The changes in these data observed during and after arcjet

operations, after correcting for temperature variations, could be viewed as possible plume deposition effects. Performing a TGA on TQCM #1 could then, potentially, provide insight into the source of the contamination.

The last element of the plume contamination experiment were four radiometers, chosen to measure heat energy flux during arcjet operations. At the beginning of this program, it was thought that flight qualified radiometers existed. Prior to PDR, however, that was found to be untrue and TRW embarked on an effort to design and qualify radiometers for this flight experiment.

The baseline locations for these radiometers were at various positions on the diagnostic platform and on the witness plate directly viewing the arcjet body. The specific locations and the radiometer thermistor data provided the necessary data to establish the heat flux during arcjet operations as a function of position and angle.

3.1.6.3 Optical. The video camera was designed to record plume luminescence. The camera originally had a 76-step grey scale, a spectral range of 0.45 to 0.9 μ m and a 20 centimeter diameter circular field of view 50 cm from the camera. The grey scale was to be calibrated so that the anode glow, estimated to be equivalent to one half sun intensity, would be just out of saturation and stepping down from this value. The camera had to be protected from stray light, earth glow and direct sunlight. Therefore, the witness plate mounting bracket was positioned to provide a background for the video camera. The camera was in line with the arcjet and witness plate blocking out background objects. For each arcjet firing, a series of frames from the camera were stored in the frame-grabber unit for transmission to the ground at a later time. Selection of when within the arcjet firing (i.e. start-up, shut-down, steady-state) these frames were taken and at what sample rate could be varied by ground command. These camera specifications and relative positioning were changed after PDR and is discussed in Section 3.2.6.

3.1.6.4 EMI. Analyses performed during Phase I provided a preliminary evaluation of the plume radiated fields based on plasma recombination in the plume. The calculated values were in the range of 1014 to 1015 Hertz. These frequencies were well outside the typical communication bands, so an EMI Experiment was designed to search for subharmonics in the communication bands from this source.

The original EMI Experiment was designed to monitor EMI in four communication frequency bands centered at 2, 8, 12 and 15 GHz. However, data gathered from another TRW program indicated that there would be null readings at these frequencies. The Arcjet System Integration Demonstration (ASID) Program sponsored by NASA Glenn Research Center, gathered EMI data for the 1.4 kW arcjet in a 30 foot diameter space simulator. These data, extrapolated for a 30 kW arcjet, indicated that the antennas would be saturated at 2 GHz and zeros would register at the remaining frequencies. Additional analysis was performed and the EMI Experiment was changed to record data at 2, 4, 8 and 12 GHz. A saturated reading was still expected at 2 GHz and a null reading was expected at 12 GHz, but these readings would help bound the EMI characteristics of the arcjet, as well as provide credibility to those taken at 4 and 8 GHz. A breadboard unit of the EMI electronics unit was built and tested during Phase I. The results of the testing showed that the EMI electronics unit performed as expected.

Two spiral cavity antennas that covered the desired frequency range were employed, one mounted on the diagnostic package platform. The second was originally secured to the host spacecraft in the back flow-field to allow measurements in both the near and far field regions. This antenna, however, was ultimately moved to the deployable boom due to interface issues.

3.1.7 Power Subsystem Design. The initial baseline design of the power subsystem (PSS) was a high voltage silver-zinc battery, which was recharged by a solar array to provide power for the entire system. This battery was to provide power at 150 Vdc, which the PCU could accept directly. However, an equipment converter was required to condition this power to 28 Vdc, ± 15 Vdc and ± 5 Vdc which were required by the ESEX electronic boxes. A trade study was performed to determine whether a two-battery system would be more simplistic and lower in cost since OSC had an existing low-voltage battery which may have been applicable to this system. The results of the trade study was that the two-battery system was 20 pounds heavier than the one-battery baseline and the added simplicity of the system was not significant enough to justify the added weight penalty. Therefore, the one-battery baseline was maintained.

This PSS baseline experienced one significant change during the design process. This major change was the deletion of the solar arrays from the flight unit, predicated by the likelihood that the host spacecraft (not assigned at this stage in the program) would provide unregulated 28 Vdc power. Therefore, the high voltage battery was dedicated to providing power to the PCU and arcjet, while the PIU was designated as the electrical interface for the host spacecraft. The PIU would distribute and convert host vehicle low voltage to the CCS, PFS, PCU, diagnostic experiment, and thermal management subsystem. The PIU was comprised of three units (or subassemblies): the equipment converter, the battery charger and PIU electronics (which consisted of the telemetry conditioning board, command interface board, and heater board.) During Phase I, the electrical design for the PIU was performed by TRW and provided to OSC.

Once the host spacecraft was identified, the PIU design was modified to be compatible with the ARGOS spacecraft. These changes were implemented in Phase II.

3.1.8 Thermal Management Subsystem Design. Two key requirements drove the TMS design. First, the design was to accommodate a broad range of space missions without dependence on the host vehicle for maintaining thermal control. The TMS was also required to maintain all components within their qualified temperature limits during any phase of the experiment including a steady-state arcjet firing. This requirement was important because of the high operating power of the arcjet and PCU. At an input power of 28 kW and a PCU efficiency of at least 93%, more than 1900 watts of heat were required to be removed from the PCU and radiated to space. The requirement of thermal independence from the host spacecraft over a broad range of missions allowed preliminary design work to proceed on the thermal management subsystem. This design work proceeded even though the host spacecraft and its mission (which would help define the external thermal environment) were not defined until after the program PDR.

In the baseline design, all electronic boxes of the flight experiment were mounted to the side panels of the flight experiment to allow internal box heat to be conducted to side panel silvered TeflonTM tape (STT) radiators. The one exception to this was the panel on which the PCU was mounted. The heat that would need to be rejected away from the PCU was greater than any amount that STT radiators alone could handle. The baseline design for removing heat from the PCU during and after an arcjet firing was to use a phase change material (PCM) panel. The panel is similar to a honeycomb panel, except that it is filled with a paraffin-like material that melts as it is heated. During the latter part of Phase I, an alternate design was analyzed and adopted in Phase II for the PCU heat rejection. The PCU panel was changed to a beryllium panel that stored the high PCU heat dissipation as sensible heat in the combined thermal mass of the beryllium panel and the PCU. The beryllium panel was chosen over the PCM panel because of the significant cost savings.

Development and fabrication costs for the PCM panel far exceeded the manufacturing costs of the beryllium panel, which did not require development. Also, for the beryllium panel, in-plane heat spreading would occur over the entire panel thickness, while for the PCM panel, the in-plane heat spreading would occur at the facesheets only. This results in much smaller gradients within the PCU baseplate. Much in the same manner, the silver-zinc battery sub-assemblies stored, as sensible heat, the 1600 watts generated per battery subassembly during the battery discharge (arcjet firing) and released it through STT radiator areas on the three battery panels.

During the battery recharge phase of an arcjet firing, the primary thermal management of the flight experiment was accomplished by the CCU with mechanical thermostatic control on select circuits. Actual thermistor data were compared to preset limits within the flight experiment software. Heaters turned on when minimum temperatures were reached and turned off at maximum temperatures. Thermal paints were used on both the interior and exterior of the flight experiment. The multi-layered insulation (MLI) covered the exterior of the flight experiment with cut-outs at the radiators.

On orbit environmental interface requirements to be imposed on the host spacecraft were also defined during Phase I. These requirements were necessary since the flight unit had a limited area it could use for radiating the heat generated by the electronic boxes mounted to the flight unit side panels. The maximum allowable orbit average heating rate on the PCU radiator panel was 19 watts/ft² and the maximum orbit average heating rate on any battery radiator panel was 23 watts/ft². These heating rates included all external heat sources such as solar heating, earth emission and albedo heating, and radiative heating from the host spacecraft. In addition, the radiator panels were designed assuming a view factor to deep space greater than 0.90.

3.1.9 Structure Design. During Phase I of the Arcjet ATTD program, the launch vehicle and loads for the flight experiment were undefined. Therefore, a major portion of the structure design effort was purposely delayed until after these interfaces were established. However, there were basic requirements that could be used to develop the preliminary design. The flight experiment envelope requirement was known, and the design was required to provide modularity to allow for quick and easy replacement of major components. As a derived requirement, the structure was to provide enough radiator area for all the electronic components.

To meet these requirements, a hexagonal body design was chosen which allowed the electronic boxes (battery subassemblies, PCU, PIU/CCU and diagnostic electronics) to be mounted to the six side panels, their radiators mounted on the exterior of the experiment for heat rejection to space. These side panels could be individually removed from the hexagonal structure for access to any of the components within the interior of the flight experiment. Two subsystem platforms were the top and bottom structural components. The propulsion platform provided the mounting surface for all PFS components, and the diagnostic platform is where the arcjet thruster and most of the diagnostic equipment were mounted. Aluminum honeycomb was used to manufacture all but one of the panels and the two platforms.

The core frame used for mounting of the platforms and panels was a stand-alone design such that it did not require either platform in order to integrate the side panels. This was an important integration feature that allowed PAC to build the flight PFS directly onto the flight propulsion platform at their facility while OSC concurrently integrated the remainder of the flight experiment in their Virginia facility.

In preparation for the preliminary design review, and after all of the subsystem preliminary design audits were conducted, the entire flight unit experiment layout was reviewed and updated to

incorporate the most updated equipment layouts into the overall design. Interference problems were revealed due to increased component sizes and added detail, such as the harness envelope. Due to the interference problems, and in anticipation of new envelope requirements, a worst case estimate was made to determine the maximum required flight envelope. The new dimensions were a maximum diameter of 48.2 inches and a maximum height of 59.3 inches.

3.2 PHASE II - DEVELOPMENT TEST VEHICLE BUILD-UP, TEST and INTEGRATION

The following paragraphs describe the work that was performed from the program PDR in July 1991 until the entire flight unit was integrated and ready for flight unit qualification testing in February of 1995. Specifically, Phase II consisted of fabricating development hardware, conducting subsystem development and EM tests, upgrading the detailed design to incorporate necessary changes prior to fabrication of the flight hardware, and integration of the flight unit. Also during this phase, the Arcjet ATTD CDR was conducted on December 17, 1993 at TRW. Representatives from AFRL, AF ST&T, TRW, Aerospace Corporation, Boeing, and other Air Force agencies were in attendance. A top-level review of the Arcjet ATTD system and subsystems was presented along with a status review of open action items. Several follow-up action items were generated at the CDR but none that required major design changes.

3.2.1 System Design. At the beginning of Phase II, a contract change was incorporated which officially identified the Arcjet ATTD host spacecraft as the ARGOS satellite. Along with this requirement change was the identification of new interfaces and launch environments. Many of these requirements were taken from the Air Force document MLV-90-XXXX-100. Therefore, the program requirements were revised to reflect these changes. Since the flight unit design had been constrained in size and driven by very conservative launch environment requirements, the transition to the ARGOS spacecraft was fairly smooth. Those areas affected by this change are specified in the appropriate subsystem sections.

3.2.1.1 Power. Throughout Phase II, the power profile for the flight unit saw many iterations as the requirements from ARGOS and the Arcjet ATTD flight unit design matured. The average power profile at the March 1993 quarterly review showed that the flight unit would require a maximum average power of 421 watts (including 5% contingency) during hours 75 to 80 of the typical 100-hour cycle between firings. This power profile was reviewed with the goal of reducing the peak average power of 421 watts to 331 watts with no contingency included. This was accomplished by delaying the use of the propellant tank heaters until after battery charging was completed, increasing the battery charging period from 60 to 67 hours, and increasing the cycle period from 100 hours to 108 hours per arcjet firing. Ultimately, ARGOS determined they would be able to accommodate concurrent propellant conditioning and battery charging. By the end of Phase II, the power profile for Phase II flight operations evolved to the one shown in Figure 8.

3.2.1.2 Alignment. The next concern raised by the ARGOS program was a requirement to have the arcjet thruster aligned to the ARGOS center of gravity (cg). The concern was that the arcjet could overwhelm the attitude control system and cause the vehicle to tumble. Therefore, an alignment requirement was generated that stipulated radial and angular offset limits. The requirement is defined by the line in Figure 9. Therefore, TRW, PAC, and OSC analyzed how the overall experiment design could be refined to meet this requirement. One specific assumption

that was agreed upon for this alignment analysis was that the thrust vector of the arcjet was coincident with the center-line of the thruster since that measurement had never been performed before. It was determined that the flight unit would meet the alignment requirement if adjustments to the alignment were performed iteratively during the assembly and integration process, while keeping the flight unit structure fully pinned. Furthermore, manufacturing control tolerances for the arcjet thruster, cable assembly, and structural frame were established, and structural tolerances and

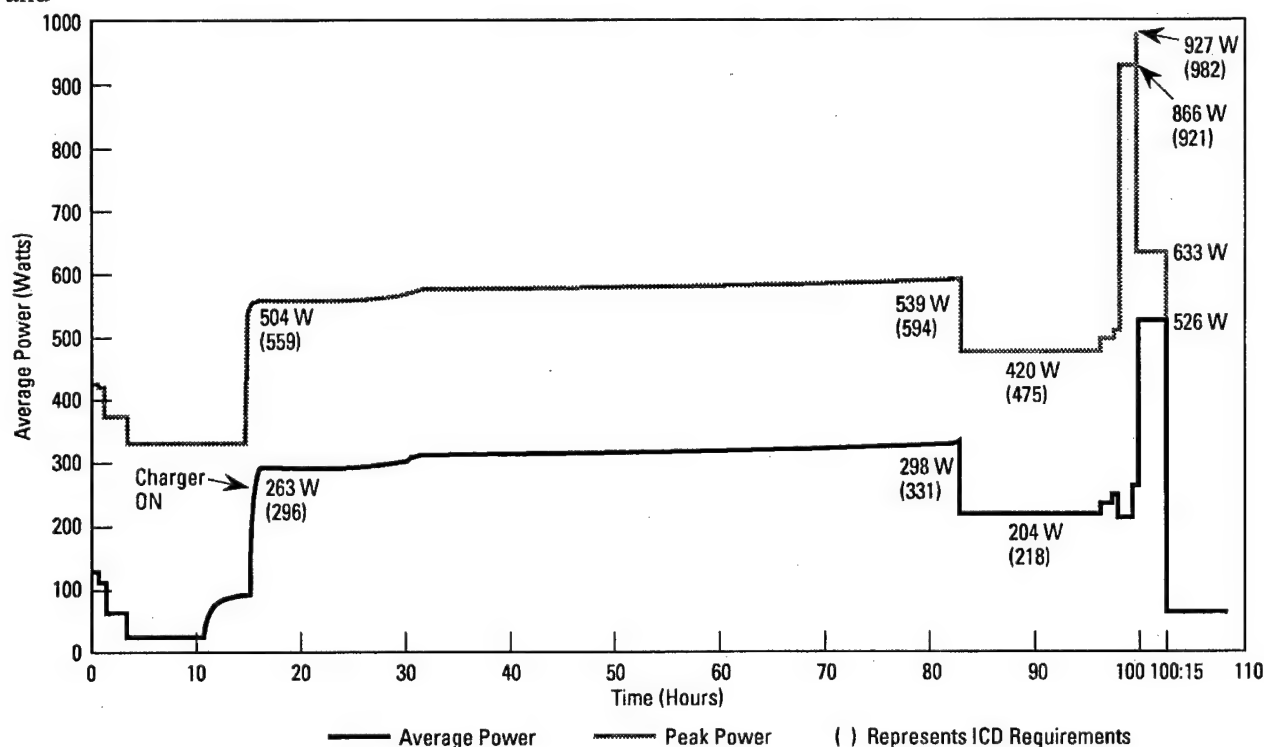


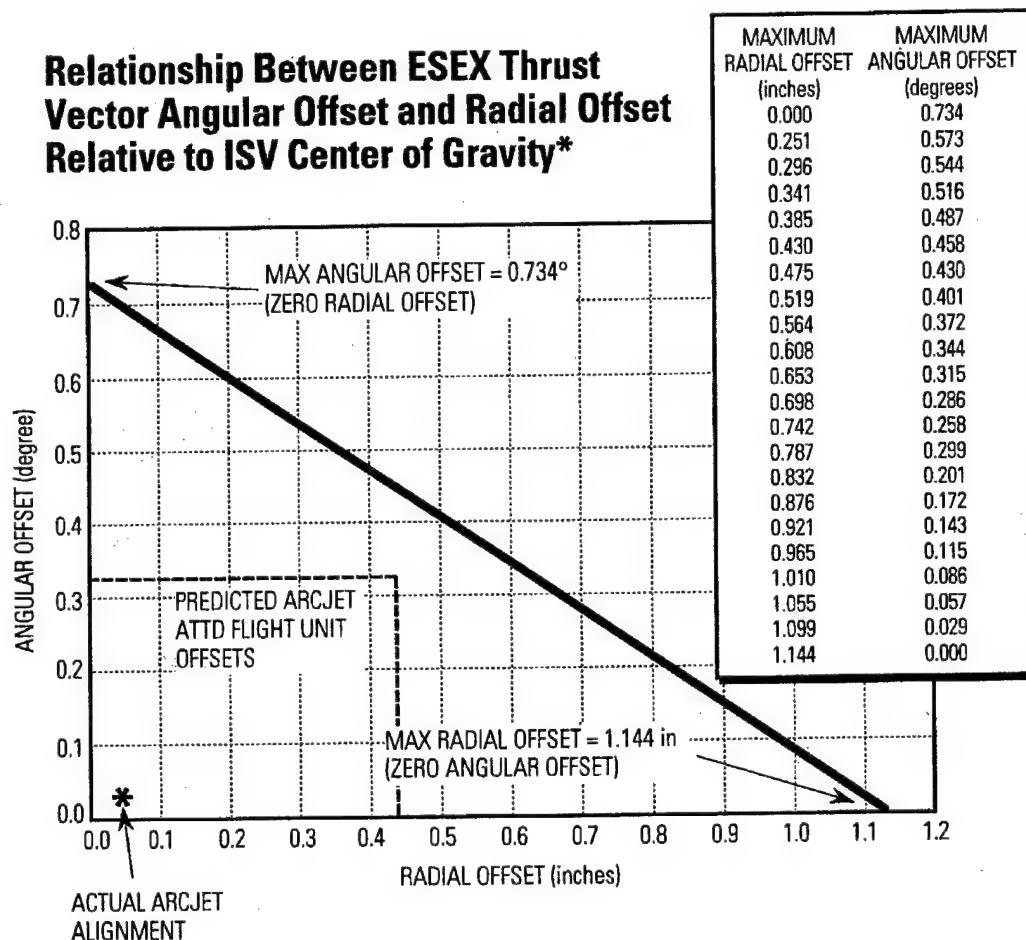
Figure 8. Phase II Power Profile

alignment control were maintained through the use of a coordinate measuring machine to measure the precise frame locations.

One of the key components that led to the success of the alignment requirement was the modification of the thruster adapter. The original design was a scalloped, conical adapter but this only allowed a maximum of 1.5° of movement when subjected to a 12 lb_f deflection force. Additionally, the scalloped conical adapter only allowed an adjustment for the angular offset, not the radial offset. This existing design was then replaced with two slotted plates with shim stacks which allowed adjustment for both radial and angular offsets. The adapter plates were painted with S13-GLO-13 paint to thermally match the surface of the diagnostic platform. This final alignment approach was such that no post-delivery alignment adjustments were required. The final analyzed and actual radial and lateral offsets on the flight unit are also shown in Figure 9.

3.2.1.3 Software. The software developed to operate the CCU was test software that interfaced with an operator workstation (personal computer) and allowed test verification that the flight unit was capable of performing all functions. However, this test software was insufficient

to perform flight operations and a flight software development effort was initiated. Since development of the flight programmable read-only memory (PROM) required access to an equivalent CCU, a cardcage was built to support the software development and verification. Once the first set of flight code was completed, a set of PROMs were burned and installed into this development CCU for formal testing. The testing was conducted "stand-alone" (no emulator) with the baseline code PROMs and a real 8086 processor.



* BASED ON 0.050 ft-lbs ALLOWABLE DISTURBANCE TORQUE, AND 0.45 lbs ESEX THRUST LEVEL

Figure 9. Arcjet ATTD Alignment Requirement and Capability

The flight unit coding and test effort involved 9 sub tasks: Boot Initialization Code; 1553 Code; Command Interface; Data Acquisition; Power Control; Heater Control; PFS Control; Diagnostics Control; and Event Sequence Control. The design task of the ground support equipment (GSE) software involved rapid prototyping, main loop design, interrupt design, and command/telemetry design. Rapid prototyping required setting up display screens and a user interface. This was accomplished using two software packages, Drovers Professional Toolbox and Graphics Server SDK. The main loop design was implemented using standard Windows 3.1 API. The GSE unit coding and test involved the following subtasks: User Menu; 1553 Code; Telemetry

Displays; Data Recording; Data Playback; Data Plotting; Data extracting; Video Display; and MT capability.

An Arcjet Flight Firmware Design Review was held at TRW on 25 July 1994. In attendance were representatives from the Air Force Research Laboratory, Aerospace Corporation and TRW. This day-long review covered the following topics:

- firmware, system and CCU hardware initialization
- main loop processing
- analog state of health (SOH) data acquisition
- temperature control
- EMI data and TQCM data bus acquisition
- continuous/single memory dump data acquisition
- video and heater data dumping
- command and event sequence processing
- PFS algorithm
- status

One issue that was raised during the review was regarding the CCU watchdog timer. The original design was hardwired for an elapsed time of 32 minutes. A more desirable value is 10 - 30 seconds and changes were made to the CCU to implement the revised duration.

During flight firmware development, the PFS mass flow rate conversion factor was found to be incorrect. This was determined by reading the measured value for the PFS pressure P2, and the temperature T1, computing the mass flow rate, and comparing it against measured value of mass flow rate. In doing so, the computed value and the measured value did not agree. This led to the discovery of an error in the mass flow constant. The mass flow equation was corrected to be

$$\text{PFS Mass Flow Rate} = \frac{(P2(\text{PSIA}) * 84.68)}{\sqrt{T1(^{\circ}\text{R})}} \quad (1)$$

The algorithm was successfully tested by comparing the floating point results to the integer math version of the algorithm. The output of the integer math version agreed in all cases to within 1 millisecond of the cycle width of the dual pressure control (DPC) valve. Most of the loss was due to truncation errors in the conversion.

The following flight firmware documentation was generated as an overall user's guide for the Arcjet Flight Experiment to provide a complete description of the Arcjet flight firmware and its operation:

- The Arcjet Command Description Document contained all the command definitions, formats, usage and restrictions.
- The Arcjet Software Error Codes document contained all the software error messages, and what actions to take (if any) upon receiving an error.
- The Arcjet Telemetry List contained all the telemetry mnemonics, location, size, units and expected range.
- Event Sequence Developers Guide which provided instructions for building, loading and executing a series of instructions (commands) at specific times
- Database document has all of the variable addresses assigned in the code execution

3.2.1.4 High Voltage. To protect against breakdowns occurring in the high voltage (250 Vdc) circuits, changes in the low power section of the Arcjet ATTD power subsystem (battery charger, harness, and PIU) were reviewed and implemented. In the battery charger and power distribution assembly (PDA) slice, several of the connectors were replaced with a single high voltage connector. A review of the new printed wire board (PWB) spacing on the battery charger and PDA slice showed that it was adequate. The existing harness wiring was replaced with high voltage wiring resulting in a minimal increase in harness weight, volume and cost. Other harness changes included replacing two existing test connectors (battery charger and battery voltage telemetry) with high voltage connectors.

3.2.1.5 Battery Discharge. Concern was raised regarding the state-of-charge of the battery at the completion of the ESEX operation. Since there were other ARGOS experiments operating after ESEX, verification that the battery sub-assemblies would not impact the other experiments was required. The specific concerns were electrolyte leakage and electrical shorting within the battery. The concern regarding electrolyte leakage was eliminated when it was confirmed that the existing cell design included an internal matting material that would help contain the electrolyte within the battery sub-assemblies. However, the concern regarding the potential for a battery short remained. Discharging the battery to zero volts would eliminate the potential for a dead short. However, the operational plan and electrical design for ESEX did not include any provisions for a complete discharge of the battery. An extended firing of the arcjet to fully discharge the battery was not an option since the arc cannot be maintained below ~150 Vdc. Other options were investigated including repetitive start attempts of the arcjet which could be performed to discharge the battery by pulsing the PCU start circuit once a second with this scenario, approximately 10 days would be required to completely discharge the battery sub-assemblies. The concern, however, was that the pulser would not last the full ten days at the 1 Hertz duty cycle.

The concept that was ultimately selected as the best approach was to place a resistive load on the battery and maintain the battery assemblies at acceptable temperatures during ARGOS mission Phase 3 until they were fully discharged. Each battery pack was outfitted with separate discharge circuits consisting of a thermostat and doghouse resistor circuit as shown in Figure 10. During ARGOS mission Phases 1 and 2, the battery sub-assemblies would be maintained above 40°F by the CCU controlling the battery heaters. The thermostat in the discharge circuit, with open/close set points of -20/+20°F respectively, would prevent the circuit from discharging the battery during ARGOS mission Phase 2. For ARGOS mission Phase 3, the CCU would be programmed such that the battery heaters maintain the battery sub-assemblies above the electrolyte freezing point (approximately -22°F) but turned off before the battery discharge thermostat reached +20°F. Theoretically, this design approach would allow continual discharge of each battery assembly. This design does, however, have three single point failures. In the event that the PIU fails during Phase 3, the battery heaters would be unable to prevent the battery sub-assemblies from overheating or freezing. If the CCU fails during Phase 3, no mechanism exists to control the battery heaters and the outcome would be the same as a PIU failure. One way to bypass these two single point failures would have been to have ARGOS route the mission Phase 3 battery heaters through the PIU so that neither the CCU or PIU would require power in this configuration. This approach, however, was abandoned and the identified risks were accepted to minimize the impact on the ARGOS system. The third single point failure is if one of the discharge circuit thermostats fails open and the corresponding battery assembly would remain charged. The remaining two battery packs would continue to discharge and would be unaffected by the open circuit. If the

thermostats failed closed, there was enough design margin in the battery charger to overcome the small voltage bleed.

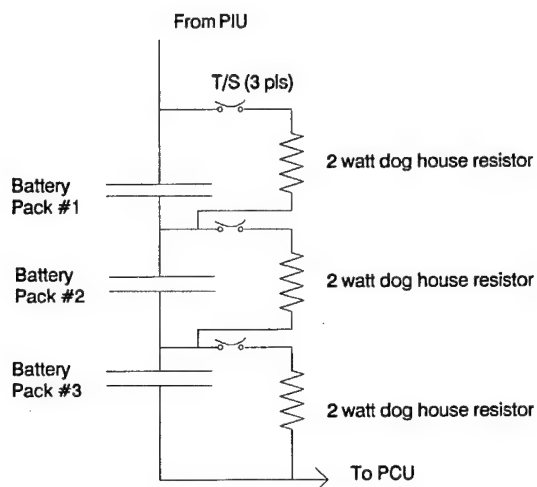


Figure 10. Battery Discharge Circuit Design

Figures 11 and 12 illustrate the implementation of the load resistor circuit and the location for the dedicated ARGOS mission Phase 3 heaters. The heater pairs shown on either side of the battery are the primary heaters. The mission Phase 3 heaters were located in the area available above and below the battery subassembly.

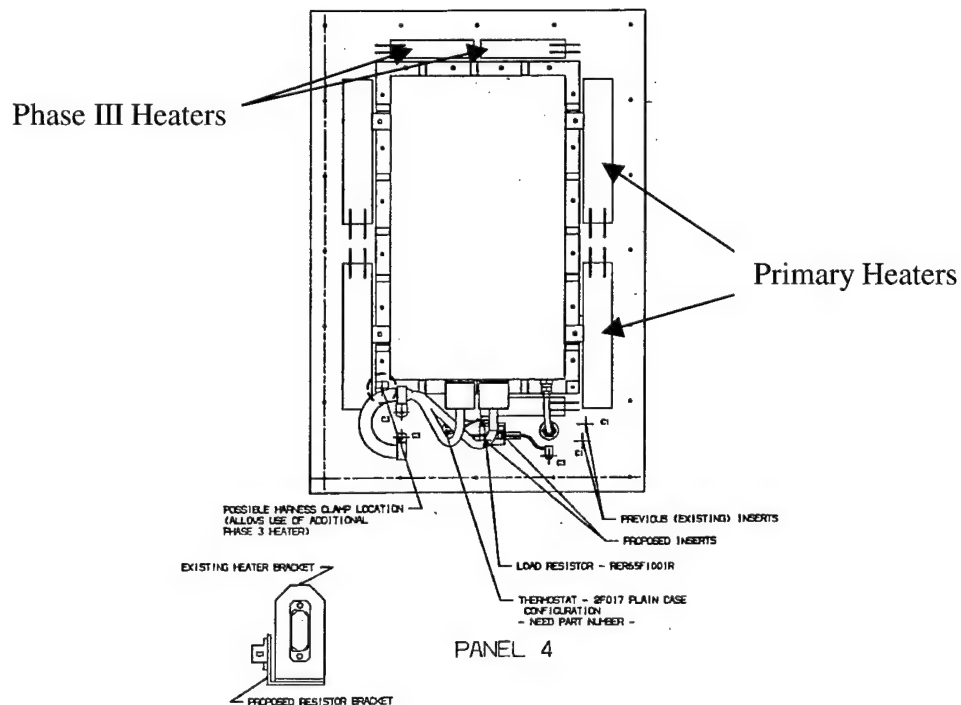


Figure 11. Battery Panel Load Resistor Circuit (Top View)

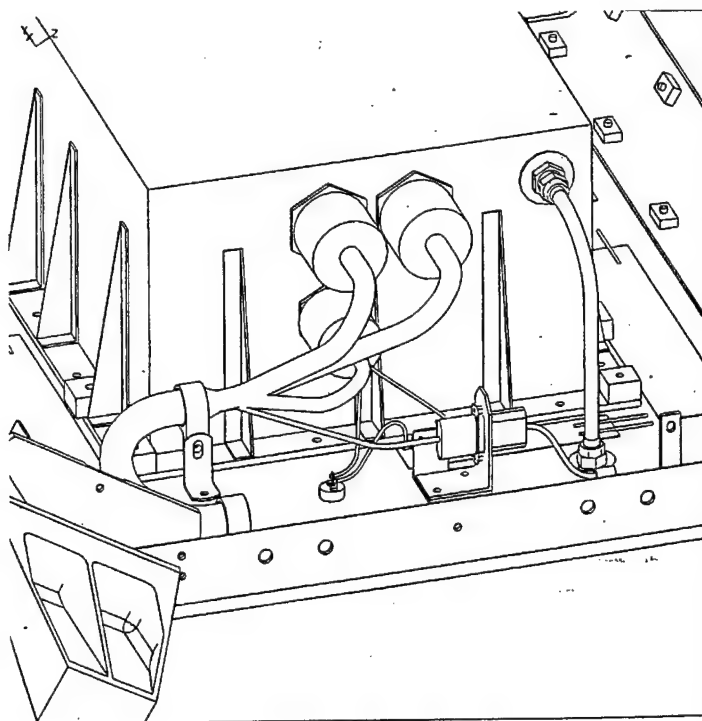


Figure 12. Battery Panel Load Resistor Circuit (Side View)

3.2.1.6 Integrated Mission Simulation (IMS) Testing. A key test performed during Phase II was the IMS test. The purpose of the test was to integrate as many aspects of the flight unit together to verify that all of the components would operate in a compatible manner as well as identify any interactions between them. Although the original intent was to test only the performance of the EM arcjet, PCU, PFS and battery together, the test opportunity attracted an expansion of this test objective. Added to this test were a solar cell witness plate to characterize how the solar cells would respond to the anode glow; a video camera in order to determine the appropriate shutter speed; a radiometer to characterize how it would perform relative to the radiated heat flux of the arcjet; and radiated and conducted EMI measurements of the arcjet and PCU. The reason for performing this early EMI test was due to the fact that facility limitations preclude any actual arcjet firings as part of the system level EMI testing at TRW.

The IMS test met all of its test objectives including the support of the TRW diagnostics evaluation testing. Table 3 documents the test firings completed during the IMS test. Details regarding how the individual components performed are provided in their specific sections of this report. A complete description of the measurements performed and the results obtained were documented in the EM Test Report¹.

The EMI data measured during the IMS test indicated that the radiated and conducted EMI from the arcjet and PCU were within the limits required by the program and documented in the Arcjet ATTD DRD. The exception to this was the broadband emissions below 0.6 MHz. However, there were no instruments aboard ARGOS which have sensitivities in this frequency range.

Table 3. IMS Test Summary

Firing No.	Date	Description	Duration (minutes)	Comments
1	10/4/93	Rapid Power Supply Checkout	5-10	Final checkout before battery firings
2	10/4/93	First Battery Firing	8	Shut-down prematurely, PCU interlayer board separation suspected, started with PCU at +40°F
3	10/5/93	Second Battery Firing	15	Started with PCU at -15°F
4	10/6/93	Third Battery Firing	15	Started with PCU at -5°F
5	10/6/93	Fourth Battery Firing	15	Started with PCU at +20°F
6	10/7/93	Fifth Battery Firing	11	Started with PCU at +40°F, shutdown occurred again
7	10/7/93	Sixth Battery Firing	15	Started with PCU at 0°F
8	10/8/93	Seventh Battery Firing	16.5	Conducted EMI data measured
9	10/8/93	None	0	Short through PCU discovered, no firing attempted
10	10/18/93	Eighth Battery Firing (A)	3.5	PCU was not uniformly cooled prior to firing, shutdown occurred
11	10/18/93	Eighth Battery Firing (B)	19	PCU cooled to 0°F, EMI data inside cell measured
12	10/19/93	Ninth Battery Firing	17	Did not start on first attempt, reduced flow to start, EMI data measured
13	10/19/93	Tenth Battery Firing	18	Rough start, but did start at full flow first time; shutdown when battery voltage dropped below 150 V
14	10/20/93	Cold Thruster Test	1-2	Demonstrated cold soak start capability

3.2.1.7 EMI Analysis. An electromagnetic compatibility analysis for the Arcjet ATTD flight unit was performed using the TRW Specification and Electromagnetic Compatibility Analysis Program (SEMCAP). The analysis was performed on the Arcjet CDR configuration and included selected command and telemetry, turn-on transients, and the transient expected while turning on the arcjet thruster.

The objectives of this analysis were to assess the electromagnetic compatibility of the Arcjet ATTD flight unit and electromagnetic interference safety margins of selected interfaces. The analysis studied and categorized the circuits identified into generator (potential interferer) and/or receptor (potential interference victim). Examples of generators include command and telemetry power interface turn-on transients for the experiment equipment serial clock pulses, and the large voltage transient developed from turning on the arcjet.

A total of 3 generators were included to act upon one worse case receptor circuit in the analysis modeled. A list of the generators and receptor is given in Table 4 below. Adequate margins (greater than 6 dB) were found for all generators on the receptor modeled. The margin on the receptor due to the sum of the generators is also provided.

Table 4. Arcjet ATTD Flight Unit Electromagnetic Interference Safety Margins

Generators	dB Margin	RSS Steady Margin	Transient
TQCM Telemetry Clock (Steady State noise)	79		
TQCM Turn-on Transient (Transient noise)	53		
ARCJET Thruster turn-on (Transient noise)	13		
Receptor State Margin			
Analog Input/Output with 1 millivolt threshold.		79	13

3.2.1.8 Venting Analysis. A venting analysis was also performed to assess the adequacy of the venting to relieve the pressure within the flight unit resulting from outgassing. Specifically, the objective was to determine if the pressure at the conclusion of the two-week on-orbit check-out period would be below the critical pressure of 1×10^{-3} torr that was specified as the upper limit permitted for powering up the high voltage circuitry within the PCU.

The flight unit was modeled geometrically as a single volume under the assumption that those boxes venting into the spacecraft had sufficiently large vent holes and that their internal pressures closely track that of the flight unit itself. The total outgassing mass flow rate was computed based on materials, areas and temperatures along with the available data on the outgassing rates of the materials. The two main outgassing sources were the Z306 black thermal paint (by virtue of its large surface area and moderate outgassing rate) and TeflonTM harnessing (by virtue of its high outgassing rate).

The flight unit was vented externally through two openings in the PFS platform with an equivalent opening of at least 12 square inches. If it was assumed that this vent was completely open (no blockage by MLI) then the pressure within the spacecraft at the end of the two weeks on-orbit was conservatively estimated to be 4×10^{-5} torr, a factor of 25 below the critical pressure.

However, the six-inch distance between the PFS platform and the ARGOS interface platform had to be closed with an MLI skirt which enclosed the 12 square inch opening in the PFS platform. Thus, the venting design was such as to guarantee at least one square inch of unimpeded vent area (i.e. a simple orifice). To accommodate this requirement, eleven half-inch diameter holes were added to the skirt to provide maximum vent capability while maintaining the thermal requirements.

3.2.2 Arcjet Design. As mentioned in Section 3.1.2, three separate material process development efforts were undertaken a part of the overall arcjet development effort. The first task, to develop a process to produce high-density tungsten, was conducted in Phase I is discussed in Section 3.1.2. The two remaining efforts were conducted in Phase II, and included a means by which to weld the high-density tungsten to Mo/41Re in order to join the anode body to the nozzle, and to develop a flight-qualified method to braze InconelTM 625 to Mo/41Re for the arcjet manifold-to-barrier-tube braze joint.

3.2.2.1 Tungsten to Mo/41Re Weld Development. At the end of Phase I, a process to produce the desired density of tungsten for the anode was completed. The output of this effort was a number of tungsten weld samples and anodes to be welded and tested in Phase II. Six sets of bi-metallic weld mock-ups were machined out of tungsten (W100) and Mo/41Re. The electron beam (EB) weld schedule parameters were established to join the Mo/41Re barrier tube to the tungsten anode. Three mock-ups were welded, of which two were subjected to thermal cycles between -150°F and 2300°F for up to 200 cycles and a single -320°F cold cycle. Post-thermal cycle penetrant inspections of the weld joint face and the weld heat affected zone revealed no defects in either the Mo/41Re or tungsten.

Two of the weld mock-ups were sectioned for metallographic weld quality inspection. One was in the post-weld stress relieved condition as noted above with 200 thermal cycles. The results of this metallographic cross sectioning revealed that both EB welds contained root cracks on the tungsten side of the weld in the heat affected zone. No external surface cracking, or weld leakage, was observed. It did appear, however, that the EB weld joint root heat affected zone of the tungsten was cracking during post-weld cooling and that cyclic thermal exposures did not cause through crack propagation. Therefore, an effort was undertaken to redesign these welds to reduce the post-weld residual stress. Three geometries, shown in Figure 13, were identified and analyzed.

The first proposed geometry change was to reduce the joint thickness to 0.088 inch from 0.125 inch to more closely approximate the joint geometry of the successful TelstarTM 4 anode weldment. A transition section was also considered in order to reduce the coefficient of thermal expansion (CTE) mismatch between the tungsten anode and the adjacent material. The selected transition material was W/25Re, which has a CTE that is very close to that of pure tungsten, but is less ductile than the Mo/41Re currently used in the joint. Changing the joint from a butt weld to a scarf weld was also examined. This geometry was thought to provide the benefit of retaining the current two materials, and requiring just one weld joint.

The three joint configurations were examined and compared to the existing design. Each case was analyzed using a linear axisymmetric finite element model with loading produced by

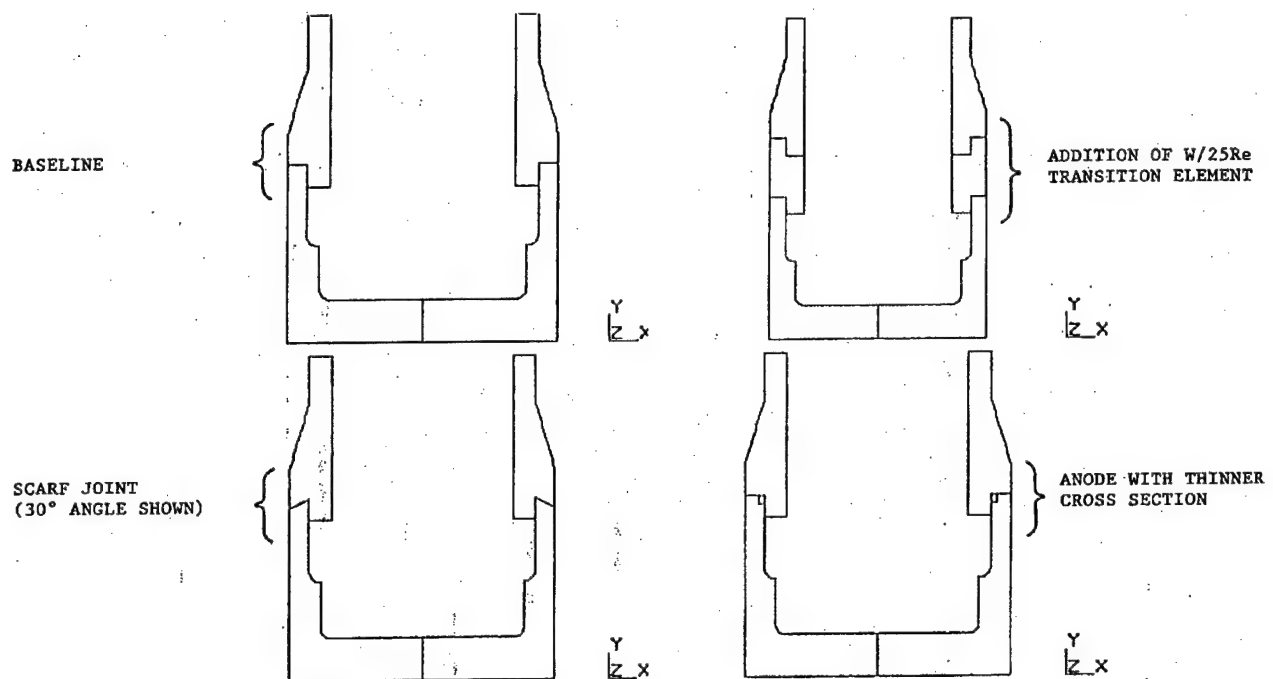


Figure 13. Analyzed Anode Joint Configurations

differential contraction of the various metals from a stress free state at the 2000°F welding temperature. For the transition sleeve and scarf joint options, various transition lengths and joint angles were modeled in order to identify the best possible geometries in each case.

Stress analysis results for the current design and the three proposed alternatives are tabulated in Table 5. The use of a scarf joint provided some benefits, but they were of a more incremental nature than those obtained by including the W/25Re in the anode weldment. The -15° scarf joint was less attractive from a stress minimization standpoint and was removed from consideration. The option of using a thinner anode section provided no benefit other than increasing the compressive axial load at the outer diameter (O.D.) of the weld. Addition of the W/25Re transition element was the only analyzed option that resulted in compressive loading of the anode weld root. A sample with a 0.350-inch long W/25Re element to connect the anode to the barrier tube was subsequently fabricated.

Since it was not anticipated that the cracks in the existing EM welded hardware would result in any hardware failure during EM testing, this EM arcjet fabrication using the baseline weld configuration proceeded in parallel with the weld-joint trade study. During the application of the TiC high emissivity coating of the EM arcjet anode, a circumferential crack formed approximately 0.25 inch from the tungsten to Mo/41Re EB weld on the tungsten side of the weld when the arcjet body assembly was grit blasted for surface preparation. This occurred in an area of known high external surface stress and was similar to a failure that occurred with one of the weld development samples. The grit blasting generated a flaw in the surface of the material that allowed the crack to form in the stress field. In order to minimize schedule impact, assembly and EB welding of a new EM arcjet was performed using the spare tungsten anode (formerly the flight anode), the original

Table 5. Stress Summary for Anode Weld Alternatives
(S_{yy} Stress Used as Figure of Merit)

Location	W Anode to Mo/41Re Barrier Tube	W Anode to 0.350 inch W/25Re Transition Sleeve	W Anode to Mo/41Re Barrier Tube With -15° Scarf Angle	W Anode to Mo/41Re Barrier Tube With 0.037 inch Relief at I.D.
Joint I.D.	79.3 ksi	-27.5 ksi	30.0 ksi	104.1 ksi
Joint O.D.	-13.0 ksi	13.3 ksi	30.0 ksi	-26.0 ksi
Anode Body	27.5 ksi	19.1 ksi	30.0 ksi	31.7 ksi

EM barrier tube and internal hardware, and a new manifold. The new assembly, referred to as EM', was not TiC coated to avoid introducing surface flaws.

Seven alternate flight configurations were also developed, but subsequently reduced to the W25/Re ring and a tapered-tungsten insert in a Mo/41Re anode tube. A sample with the W/25Re ring was welded, but the weld cracked in the heat-affected zone on the tungsten side of the tungsten-to-W/25Re weld. It became obvious the tungsten-to-molyrhenium weld had to be eliminated and the anode insert approach was pursued. The anode insert design is shown in Figure 14.

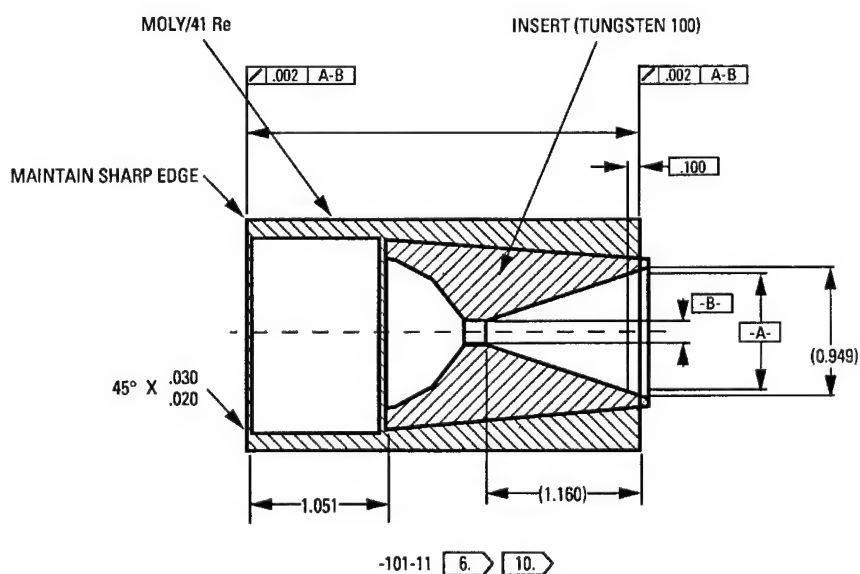


Figure 14. Alternate Anode Configuration with Tungsten Insert

3.2.2.2 Inconel™ 625-to-Mo/41Re Braze Development. A set of five Inconel™ 625-to-Mo/41Re braze samples was fabricated to duplicate the manifold-to-barrier-tube braze joint, but only three samples were actually brazed. The braze alloy filler metal rings were fabricated using 0.087-inch diameter gold wire. Internal visual inspection of the braze joints pull-through side was performed using a boroscope. The visual inspection showed braze material fillets around the entire circumference of all three samples, however, filler size was considered too small. An additional operation of adding gold braze powder to the external surface of the joint was performed on two of the samples as a technique for increasing alloy feed side fillet uniformity. Based on the resultant lack of success however, this technique was abandoned for use on the flight design but the samples were acceptable for proof testing. The flight braze used for the EM braze joint utilized 0.093-inch-diameter wire ring pre-flattened to obtain an oblong cross-section and did not require the use of gold powder filler.

All three braze samples were proof pressure tested using helium at 45-50 psig for five minutes minimum. They were then leak checked under an alcohol bath using helium at 30-35 psig for one-minute minimum. There was no leakage from any of the three samples.

Sample Number 2 was submitted for thermal cycling between 90°F and 150°F. The test fixture was a pneumatic cylinder driving a ¼" diameter CRES sample holder in and out of a quartz tube furnace with the temperature set at 90°F into a water jacket cooling zone. The atmosphere in the furnace was N₂, however, the port through the end plate was not sealed and some oxidation did occur. A programmable timer was used to cycle a solenoid 3-way valve (supplying the gas to the pneumatic cylinder) which controlled the position of the part with respect to the heating and cooling zones. Forty-five minutes in each position supplied adequate heating to obtain the desired temperature extremes.

The braze joint was checked at 29, 114, and 209 cycles for appearance and leak checked with bubble leak-check solution using 50 psig helium pressure. There was discoloration due to oxidation, but no evidence of leakage was found at any time. The braze joint was then sectioned for metallographic examination, and successfully completed inspection.

3.2.2.3 Arcjet Electrical Pass-Through Design. After completion of the assembly of the new EM arcjet EM', hot fire testing was initiated in May 1993. During the attempts to achieve successful arc breakdowns in the constrictor of the arcjet, breakdowns occurred in the cable assembly instead and a stream of hot plasma was observed to be exiting a vent hole on the cable. This indicated that a leak in the hermetic pass-through had occurred which was verified upon subsequent disassembly of the cable. A replacement unit also leaked after it had been installed into the thruster to replace the first leaking pass-through. At that point, arcjet testing was put on hold and a comprehensive examination of the hermetic pass-through design was initiated.

During 1992, PAC procured a total of five electrical pass-throughs from the manufacturer, Reynolds Industries™: two development units from one lot, and one qualification and two flight units from a second lot. As part of the acceptance tests, each unit was helium-leak-tested and verified to have a leak rate less than 10⁻⁸ scc/s. One of the development pass-throughs was welded onto the EM' arcjet during final assembly but not bench leak tested. After the unsuccessful attempt to hot fire test this EM' thruster, a bench top leak test on the thruster discovered a leak in the pass-through between the cathode and the alumina insulator at a rate easily detectable with a bubble solution and with the arcjet pressurized to less than 5 psig. Under magnification, a small crack in the braze between a COVAR washer and the alumina insulator that extended about 40° in the circumferential direction was visible. The washer is mechanically and electrically attached to the

cathode with other braze joints. It appeared that the washer had lifted away from the alumina. The pass-through was returned to Reynolds IndustriesTM for inspection.

After removal of first development pass-through, the second development pass-through was welded to the EM' arcjet assembly. Unlike the first pass-through, this second one was leak checked immediately upon completion of the assembly. This second pass-through, however, also leaked between the cathode and insulator at a rate comparable to the first pass-through. It was also noted that the cathode gap measurement decreased by 0.018 inches during the welding process.

The three remaining pass-throughs were leak tested with bubble solution at pressures up to 60 psig with no indication of leakage between the cathode and insulator. During this bubble test, however, the qualification unit showed a possible leak between the outer body and the insulator at approximately 10^{-4} scc/s. As a result of this potential leak, all three units were leak tested with a helium detector and found to be free of leaks to better than 10^{-8} scc/s.

The second development pass-through was repaired without disassembling it from the arcjet assembly. A tool was fabricated to pull the spacer ring just upstream of the insulator away from the insulator and low-viscosity, high-temperature (400-500 °F) GETM RTV-627 was injected between the cathode and insulator with the arcjet under vacuum. Leak tests performed at pressures up to 60 psig showed that no leakage occurred. This development pass-through withstood three 15-minute arcjet firings and a vibration test as part of the testing of the EM' arcjet assembly. A subsequent leak test with bubble solution (usually associated with a detection limit of 10^{-4} scc/sec) showed that it continued to be free of leaks up to 60 psig.

As a part of the effort to isolate the cause of the passthrough leak, dimensions were taken of the completed EM" arcjet thruster (see Section 3.2.2.4 for EM' and EM" discussion). These measurements showed that the TIG closure weld shrank by approximately 0.017 inches. Due to the asymmetry of this shrinkage as the weld was performed, this is the most likely source of the mechanical loads that caused the previous electrical pass-through failure. Hence, the welding process was modified such that the number of tack welds were increased to reduce the asymmetry of the loading. No leaks in the electrical pass-through occurred during subsequent testing of the EM" arcjet.

Because of the successful use of RTV on the EM' arcjet, the flight arcjet manufacturing process was also modified to include the use of RTV. For the flight unit, GETM RTV-566 was identified for use as an encapsulant for the braze region. The RTV was applied over the braze joint as shown in Figure 15 as a redundant seal in case of braze joint seal failure. RTV-566 is a low outgassing, high temperature RTV designed for space flight applications and is on the approved materials list of several spacecraft programs. The viability of this approach was validated by applying the RTV to the qualification pass-through on the EM" assembly.

3.2.2.4 EM', and EM" Arcjets. Subsequent to repairing the development pass-through, the EM' arcjet assembly was returned to hot-fire testing. Several start-pulse tests were conducted with the PCU power converters disabled to gather data on the breakdown characteristics and to verify arc breakdowns in the constrictor. After completion of the start pulse tests, a short firing was conducted in which the PCU started the arcjet, transitioned to an initial plateau current, and then shut down after a few seconds of operation. At approximately 1.2 seconds after the start, the anode fractured 0.8 inches upstream of the exit plane and the downstream portion of the anode including most of the divergent portion of the constrictor separated from the arcjet as shown in Figure 16. Although the arcjet continued to operate, the PCU was shut off about four seconds after

the start due to a failed laboratory power supply. A subsequent examination of the anode pieces revealed that the fracture started at the location of a type K thermocouple that was welded onto

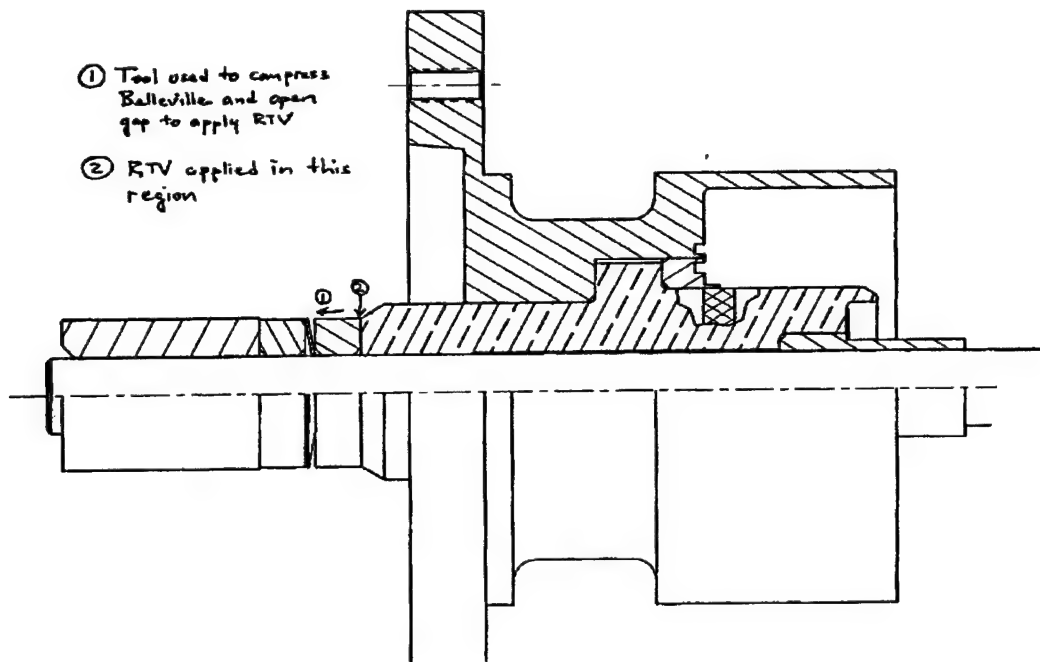


Figure 15. Location on RTV Secondary Seal Material

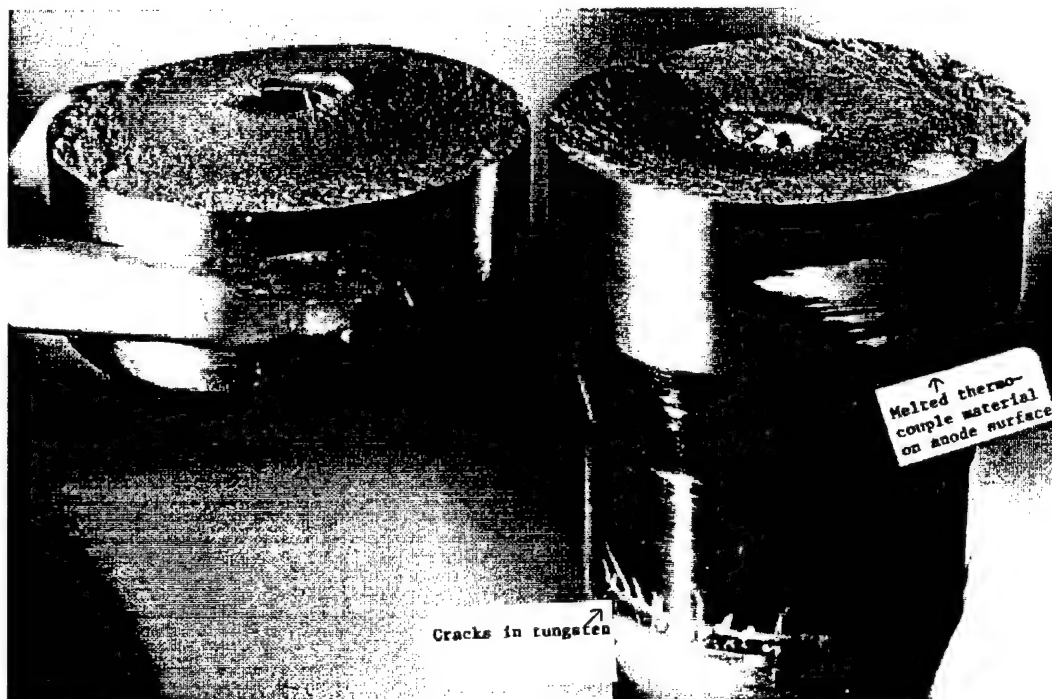


Figure 16. EM² Arcjet Fractured Anode

the outside of the anode 0.8 inches upstream of the exit plane. The fracture lines indicate that the crack traveled circumferentially in both directions until it met 180° from the thermocouple. This fracture effectively reduced the nozzle length from 1.162 to 0.25 inches and the area ratio from 40:1 to about 4:1. Welding of the thermocouple may have caused local surface flaws that propagated during the first firing.

In spite of the damaged nozzle, EM' testing continued once the faulty power supply was replaced. Six more short transition tests were conducted in which the arcjet was started and manually shut off after a few seconds. In each of these, the PCU successfully stabilized the current at the initial setting of approximately 90 A. After completion of the transition tests, three 15-minute arcjet test firings were performed. In each firing, the PCU started the arcjet on the first attempt, ramped the current up to full power, and ran stably at 26 kW.

Following completion of hot-fire testing, the EM' arcjet and power cable assembly were vibration tested along the axis perpendicular to both the arcjet and cable axes. The maximum level of 9.3 grms random vibration was held for 120 seconds without obvious damage in the anode.

After completion of vibration testing, the EM' arcjet assembly was returned to the manufacturing area to be cut apart so that various parts could be reused as part of the EM" assembly. The insulators showed no damage from the vibration and hot-fire tests, with the exception of a small chip in the long insulator tube, which may have been caused during disassembly. Inspection of the upstream end of the anode revealed very little erosion after ten full starts and three full firings. A new thruster was fabricated using a new arcjet manifold (with the tungsten insert nozzle) and refurbished portions of the EM' arcjet. This arcjet thruster was referred to as EM" and used in the IMS-testing.

Five 15-minute hot-fire tests of the EM" arcjet were successfully completed. The arcjet performed as shown in Table 6 (data from Run #3 was corrupted by a calibration error and is not included here).

Table 6. EM" Arcjet Hot Fire Test Data

Run No.	Thrust (mlbf)	Isp (sec)	Flowrate (lbm/sec)	Power (watts)	Run Time (sec)
1	435.6	761.9	0.57e-03	26667	1096
2	428.5	776.3	0.55e-03	26407	979
4	427.7	799.1	0.54e-03	26999	1272
5	435.9	797.2	0.55e-03	27175	985

As can be seen in Table 6, the thrust and Isp did not quite meet the program requirements of 0.5 lb_f and 800 seconds, respectively. Per discussions at PDR, the previous data used to derive the Isp requirement were limited to a few thruster firings and no tolerance associated with the Isp requirement existed. At PDR, it was decided to use data collected from these subsequent tests (and any other similar 30 kW arcjet tests) to determine an appropriate tolerance. From this data it was recommended that the Isp requirement be updated to reflect a tolerance of 3% or 800 ± 25 seconds.

The actual thermal performance of the EM" arcjet thruster was better than predicted as shown in Figure 17. The thruster ran much cooler than the thermal model had predicted with the exception of the anode. It is thought that more power was transferred into the anode than modeled (10,000 W instead of 3140 W).

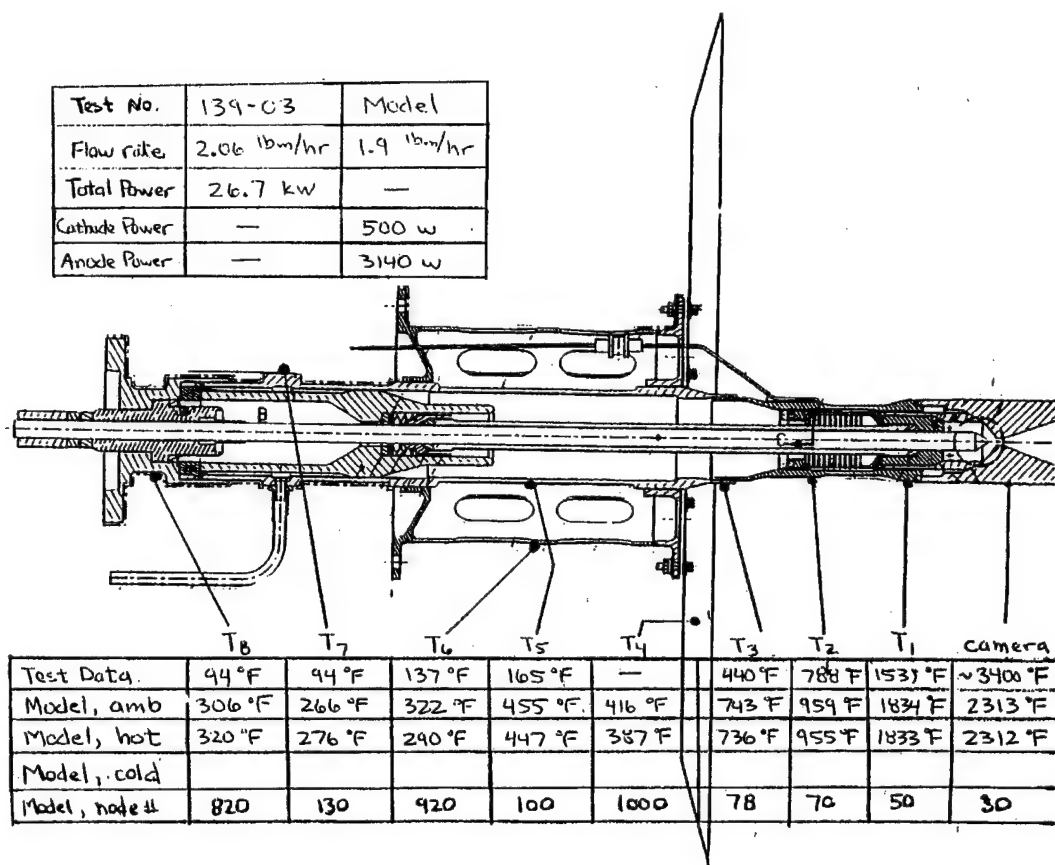


Figure 17. EM' Arcjet Thermal Performance

3.2.2.5 IMS Tests. Once the EM' component level testing was completed, the IMS test was initiated. More than twenty-six firings of the EM' arcjet were completed during the IMS test. A preliminary visual inspection of the thruster after the final firing revealed that some material had streamed from the upstream edge of the constrictor. The cathode tip appeared to be slightly eroded, although it was impossible to tell whether it was dimpled or not. It was also not apparent from this examination whether the material seen on the upstream edge of the constrictor was eroded from the anode or deposited from the cathode. None of the erosion observed would prevent the successful completion of the Arcjet ATTD mission.

Also noted was the movement of the tungsten insert. Measurements of the insert performed after the test showed that the insert protruded 0.035 inches from the Mo/41 Re sleeve. A comparable measurement acquired after assembly indicated that the insert protruded 0.009 inches from the sleeve. The movement of the insert provides an explanation for the increasing voltage measured during the period of the EM' arcjet and IMS testing.

Thruster temperatures were measured during all firings and compared well with previous measurements from the EM' arcjet testing as shown in Figure 17. The arcjet barrier tube temperature, taken using a flight-type thermistor, showed that the thruster does achieve steady state conditions during a 15-minute firing.

To prevent freezing of the NH₃ propellant during thruster operation, a heater mounted at the anode end of the arcjet thruster support structure was considered. Because two heaters totaling 50

to 100 watts would severely impact the power budget of the Arcjet ATTD flight unit, a cold thruster test was performed after the final IMS battery test firing to alleviate the concern of NH_3 condensing in the thruster passages and potentially causing a catastrophic start event. After the final IMS battery test firing, the arcjet was cooled using dry ice to approximately -40° . The dry ice was left in contact with the thruster anode while the vacuum chamber was pumped down. Arcjet flow was initiated when the temperature was between -30° and -40°F . No effect of the cold temperatures on the P3 or P2 pressure transducer telemetry was observed. The arcjet was successfully started when the arcjet temperature was -19°F and the start was completely normal, showing that the addition of a heater to the arcjet was not required.

During transport of the EM" arcjet from the IMS test cell to the vibration lab for an additional vibration test (to test the new anode design), a noise was heard from inside the thruster. No loose parts inside the thruster were observed before the start of the IMS testing and the thruster performed nominally during the testing. It is not clear whether this damage occurred during the testing or during disassembly from the test stand. The loose part caused a rattle when the thruster was tipped or rotated suddenly. Evaluation of the rattle in the thruster began with the X-ray examination of the area contained within the manifold on both sides of the upstream end of the mounting structure. The X-rays showed that the parts within the manifold were stable and there was no sign of foreign material in the area.

The evaluation of the area at the downstream end of the thruster by X-ray was precluded by the density of the barrier tube and other components that would necessitate extremely long exposure times. Therefore an evaluation of the tolerances and fitups was undertaken. Based on this analysis, the load sleeve, which provides a second source of preload on the vortex injector, was determined to be the most likely candidate. (This was subsequently confirmed when the EM" was disassembled after delivery to AFRL). The load sleeve was installed with a pre-load of 1/4 to 3/8 turn of the retainer nut. Assuming that the nut was seated squarely in the sleeve prior to any load being applied, this would result in a compression of 0.014 to 0.021 in. As shown in Figure 18, the tapered section of the retainer nut in the development thruster is approximately 0.020 in. smaller in diameter at the large end than the inside diameter of the load sleeve. Therefore, it was theorized that as soon as part wear equaled the pre-load, the load sleeve experienced a lateral movement of 0.020 in. In the flight thruster, the tapered section of the retainer nut is large enough such that the load sleeve rides on the tapered area. Any wear beyond the pre-load distance only causes a lateral movement equal to the longitudinal clearance due to the 30° angle, as seen in Figure 19. One additional difference between the flight and development thrusters is that the pre-load was increased to one full turn, or 0.055 inch, which virtually eliminated the problem. However, because of the loose part within the EM" arcjet, the thruster was not vibration tested.

3.2.2.6 Flight Arcjet. Following completion of the IMS testing, the final assembly of the flight arcjet was completed. The cathode hermetic pass-through weld was completed using the modified procedures developed on the engineering hardware. This procedure reduced the shrinkage at the weld joint from 0.017 inch to 0.006 inch, greatly reducing the side loads imparted to the ceramic to metal braze in the pass-through. As discussed above, the hermetic pass-through was treated with RTV 566 encapsulant material as a precaution to prevent leakage in the event the braze was compromised. The arcjet was leak checked and proof pressure checked with no leakage detected. The exterior surfaces of the arcjet were coated with Pyromark series 1200 black thermal control paint. The final assembly was completed with the attachment of the thermocouples in two

locations, however, the T3 thermocouple proved difficult to attach to the Mo/41 Re barrier tube. Therefore, the thermocouple was attached to the InconelTM body, just forward of the mounting structure. This location was approximately 2 inches further from the anode exit than the previously planned location, but had a much higher probability of successfully operating during the flight.

After completing fabrication of the flight arcjet, cable, and receptacle, ATP testing of the flight arcjet and cable was performed. The arcjet and cable were in the vacuum chamber, connected to the external PCU via a test adapter and approximately 40 feet of welding cable. The arcjet was mounted to the thrust stand so that its performance could be measured. The thrust test was preceded by breakdown checks of the thruster. Initially, breakdowns were occurring on every 3 or 4 start pulses. However, over the interval of firing approximately 100 start pulses, the frequency and repeatability of breakdowns decreased noticeably. Ultimately, it was observed that no output voltage was being measured at the output of the PCU. This was traced to a short in the start circuit. The problem was located and repaired and the thrust test was resumed. Additional breakdown tests confirmed operation of the start circuit. The thruster was then started without incident. Startup was observed to be very smooth with no sparks observed. The power ramp to 26 kW was also accomplished without incident. The thruster ran at the nominal mass flow rate of 240 mg/s for the 15 minute firing. No anomalies were observed during the steady state operation.

The shutdown procedure was commanded from the microDACS computer at the completion of fifteen minutes of operation. No response was seen, and the thruster continued to fire at full power. A second and third input command were given from the computer, again with no result. At this point, the PCU test fixture panel was used to shut off the "arcjet start" command, causing the thruster to drop to the 10 kW power level, and then to shut off the "PCU converter enable" command, which should have commanded the current level directly to zero amperes, extinguishing the arc. Unfortunately, the arcjet did not shutoff instantly and a bright flash was observed followed by a shower of at least two dozen sparks, uniformly distributed, exiting the nozzle. Video replay of the event showed that the plume brightness dropped for approximately 2.5 seconds prior to the event, indicating that the command to shut off the "arcjet start" was received and the power level did drop to 10 kW. The next single frame contained a bright luminous plume of a whitish-blue color. The following frame showed no plume, but many sparks exiting the nozzle in a symmetric pattern. In the third frame, the arcjet was out and no additional sparks were seen exiting the nozzle.

Post-test inspection of the thruster indicated the presence of molten material in the upstream region of the anode just prior to the entrance of the constrictor. Visual and borescope examinations were conducted, as were pin gauge measurements of the constrictor. The molten material was present from just upstream of the lip of the constrictor through about the first half to three-quarters of the constrictor in a fairly uniform manner around the circumference. Near the end of the constrictor and extending out into the nozzle the molten material was in the form of approximately 12 streaks uniformly distributed around the periphery. The streaks were approximately 0.05 inches high and 0.05 inches wide by 0.25 inches long. The pin gauge measurements indicate a reduction in constrictor diameter in at least part of the constrictor from 0.150 inches to 0.140 inches. The cathode showed normal wear. Functional measurements such as inlet pressure and thrust with cold NH₃ flow were performed with no significant deviation from the pre-firing values. Electrical isolation was also measured and found to be within specification.

A material review board (MRB) was convened to assess the damage and identify the required corrective action. It was decided to perform the required hot fire tests to complete the

thruster ATP and watch the start up and transition to steady state operating characteristics of the thruster - particularly the voltage. Since the voltage did not remain abnormally low and did not exhibit fluctuations, the hardware was judged flight-worthy and dispositioned to use as is. Further changes to the PCU which solved this problem are described in Section 3.2.3.10.

Following the thrust test, the arcjet and cable were removed from the test cell and prepared for the three axis vibration test. A vibration level of 9.6 grms was applied for a period of one minute per axis. The vibration test was conducted without incident. Post-test inspection revealed the T3 thermocouple had a cracked sheath, approximately 1/4 inch from the tip, adjacent to the weld pad. The crack did not result in a loss of continuity, but did cause the loss of structural integrity of the sheath. During handling, the thermocouple was extended unsupported and was frequently jostled inadvertently. An MRB action was initiated to redesign the thermocouple mounting and routing path. A new thermocouple was obtained and was installed prior to further testing.

A leak check of the flight arcjet was performed after the vibration test. Using leak detection liquid, a small leak was detected at the base of the cathode as it exits the hermetic passthrough. This was the same region where earlier leaks occurred on the EM hardware. This passthrough was re-welded in place using modified techniques designed to reduce the stress imparted into the passthrough ceramic-to-metal braze. As a secondary precaution, the interior surfaces of the passthrough were also potted with encapsulant material (GE RTV 566). Further potting of the exterior surface of the passthrough prior to final assembly was also planned, but was changed when the passthrough passed a leak check after the weld was completed. The exterior potting required a special tool that was misplaced between the EM build and the flight build. The decision to drop the exterior potting requirement from the final assembly procedure was made primarily based on schedule constraints and the belief that the reduced weld shrinkage (0.006 inches vs. 0.017 inches) would reduce the likelihood of cracking the braze joint. It was also reasoned that if another leak did occur, it was possible to apply the exterior potting at that time.

Ultimately it was decided to apply the exterior potting and repeat the vibration and leak tests. GETM RTV 566 encapsulant was applied while pulling a vacuum on the thruster interior to draw the RTV into the leak path. The RTV was applied successfully, but in compressing the Belleville washer to open a gap, the washer yielded, leaving no compression on the spacer ring and RTV. To prevent the spacer rings from chattering during re-vibe, a shim was fabricated with 0.020" lock wire to put tension on the Belleville.

The arcjet and power cable were re-vibed (9.6 g rms for 30 seconds in all 3 axes) and post vibe leak checks and electrical functional test showed no leaks and no problems. The arcjet was fired again to repeat the Performance Verification (thrust) Test. No instability was observed, the pressure and voltage of the arcjet was normal, and the Isp was measured to be 797 seconds.

The arcjet was found to leak again in a post firing leak check. The leak was small and not an issue as far as lost flow rate, but could be dangerous electrically by providing Paschen breakdown conditions inside the power cable on start-up. Therefore, a sleeve was designed to fit over the leak outlet area to seal the leak with two O-ring bore seals. The o-rings sealed against the alumina insulator and the copper lug on the passthrough. This sleeving was found to seal when leak tested with both high pressure (45 psia) and low pressure. As a final step, the arcjet was vacuum impregnated with RTV 566 as a safety measure. The arcjet was then hot fired twice and the seal was found to be leak tight.

The thruster and cable passed all ATP functional tests. The operational condition of the thruster was assessed to be excellent. No evidence of voltage instability due to the constrictor

damage was seen. The thruster started and transitioned cleanly. Sparks were seen intermittently during the first of the two hot firings, but were limited to a total of six during the entire 15 minute run. During the second and final hot firing, no sparks were observed.

Starts were more difficult than previously experienced in the same configuration during the IMS testing. Typically more than ten start pulses were required to get a breakdown at full flow rate. Breakdowns were achieved more readily at reduced flow rates. Since provisions had been made to baseline reduced flow rate starting on orbit, this was not seen as a serious problem. Starts were achieved at flow rates between 180 mg/s and 200 mg/s, both of which were well above the on orbit starting flow rate of 160 mg/s. Therefore, the arcjet and cable were shipped to OSC where it was integrated onto the flight unit and the alignment was performed.

3.2.3 PCU. Fabrication of the development PCU was initiated in Phase I and completed in Phase II. The development PCU is shown in Figure 20. The testing was started by SPI doing initial power-up tests using the power handling section of SPI breadboard PCU #02. Initial tests with the resistive load indicated good control loop stability and satisfactory current regulation. The unit was run incrementally higher in power from 2 kW up to 26 kW without incident. As a final test of the current regulation, the load resistor was replaced with the SPI arcjet simulator and a start pulse was used to initiate a discharge. The start pulse successfully broke down the arc simulator, but only seconds later the Gentron™ FETs in all three phases failed catastrophically. Troubleshooting revealed that a resistor value on one of the control boards was one-third the correct value and yielded one-third the correct voltage for the current sense circuit. As a result, when the arc discharge initiated, the current ran up to a very high value and overloaded the Gentron™ FETs. Overcurrent protection circuitry, planned for the development PCU, was not enabled for this test.

The Gentron™ FETs and resistors were replaced and the test was repeated, starting again at 2 kW. Once again, the resistive load testing uncovered no problems with control loop stability. Current regulation was improved over the previous test due to the change in the current sense resistors. After reaching 26 kW and successfully running on the resistive load, the unit was again connected to the SPI arcjet simulator. This time the PCU started and successfully regulated the arc load. Due to the nature of the SPI arc simulator, the maximum current was limited to 100 A. The PCU was run in this fashion for slightly more than one hour. It was then used to restart the arcjet simulator without problem and voluntarily shut down.

Power handling and functional tests of the complete development PCU were also performed with the PCU running into a resistive load. Preliminary PCU efficiency measurements were conducted during the power handling tests at 26 kW and three different input voltage levels with the following results: ~ 97.3 percent at 160 VDC; ~ 97.2 percent at 170 VDC; and ~ 96.8 percent at 180 VDC.

Minor changes were incorporated to allow the PCU to accommodate an input voltage of 150V, down from 165 Vdc. Specifically, the EMI input filter required redesign as determined by a SPICE™ analysis. Testing of the PCU with the development arcjet was initiated, however, the start circuit provided inadequate energy to achieve an arc breakdown in the thruster. Table 7 documents the PCU/arcjet hardware changes and resulting breakdown testing.

In order to minimize the schedule impact cause by the arcjet breakdown problem, steady state and performance verification testing with the PCU and arcjet was resumed per the test plan while design alternatives were worked in parallel. The following paragraphs summarize this testing effort.

3.2.3.1 Arcjet Start Transition. The pulser circuit was installed in parallel to the PCU output to initiate an arc discharge and transition to a steady state DC arc. Repeatable arcjet starts were conducted at a PCU input voltage of 225 Vdc and arcjet current of 100 amps. Figure 21 shows a typical transition from start circuit pulser current to PCU current supplied to the arcjet during startup. Start attempts at PCU input voltages less than 225 Vdc were unsuccessful due to the small difference between the input and output voltage which causes the blocking inductors to remain unsaturated, thereby preventing the PCU from supplying current to the arc. The pulser circuit was then modified by adding an additional parallel shorting switch to allow a higher level of stored start energy. After completing the modification, successful starts were obtained at PCU input voltages as low as 180 Vdc. The modification and test results verified that supplying higher sustaining current from the start circuit drives the arc voltage lower due to the negative impedance of the arc and increases the start up reliability.

3.2.3.2 Arcjet Low Mode Transition. Start tests were performed at different arc current levels and a constant mass flow rate. As the arc current (PCU plateau current) was varied between 50 and 100 amps, the transition from low mode operation, (approximately 50 Vdc) changed considerably. At an arc current of 75 and 100 amps, the voltage transitioned slowly over a 60 millisecond period after about 40 to 100 milliseconds of low mode operation. At an arc current of 50 amps, however, the voltage transitioned to the steady state level of 100 volts after about 40 milliseconds of low mode operation. When the arc voltage rapidly transitioned from 50 to 100 volts, it tended to overshoot to levels at or above the PCU input voltage (150 to 225 Vdc). When this occurred, the PCU output current was driven to zero thereby extinguishing the arc.

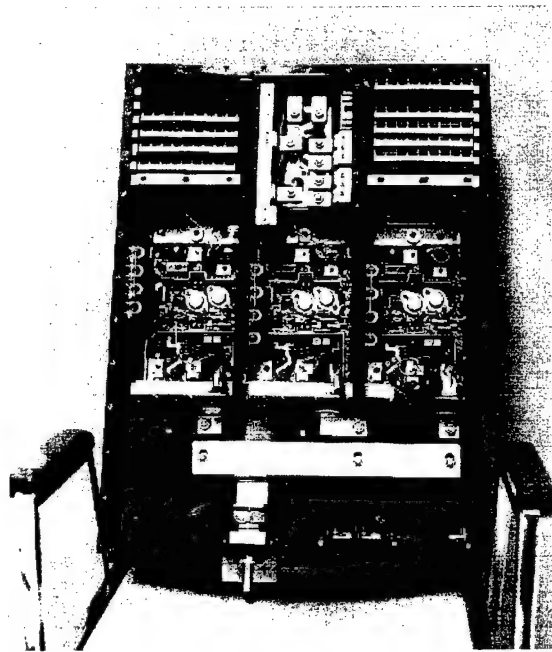


Figure 20. Development PCU Configuration

Table 7. PCU/Arcjet Hardware Changes And Resulting Breakdown Testing

TEST	PURPOSE	RESULT
Capacitive Loading Test	High voltage start circuit was tested into 15 feet of facility-type power cable terminated with varying capacitance (4800, 2400 and 1200 pF) to determine capacitive loading effects.	The pulse was measured at both the PCU output and at the arcjet input for comparison purposes.
Initial Arc Breakdown Tests	Characterize initial breakdowns over various starting conditions Start pulse (V_{IN} , mass flow)	2.5 kV start pulse voltage measured. Numerous start pulses following this breakdown and short duration firing were unsuccessful (with two exceptions) in achieving arc break down between 25 and 240 mg/sec.
Start Circuit/Procedure Modifications		
Higher Voltage Clamp	The zener diodes clamping the start FETs were replaced allowing a higher peak voltage.	Resulted in destroying the start FETs by exceeding their voltage rating
Start Pulse Waveform Shaping Circuit	Capacitance was added to increase the width of the start pulse to provide more time above 1000 volts which, at the time of this test, was thought to be the DC level necessary for breakdown based on HyPot TM testing at 240 mg/sec.	The resulting waveform failed to achieve an arc breakdown and had a lower peak voltage that had widened to roughly 1.2 micro-seconds at 1 kV from 0.6 micro-seconds without the added capacitance.
Increased Start Circuit Inductance	Two of the output inductors were disabled to increase the total output inductance to store more energy for the start pulse.	The resulting waveform into an open circuit looked very similar to waveforms with the three inductors.
Increased Inductor Current	Series/parallel arrangement of start FETs was modified to increase short circuit inductor current from 60 to 80 amps, providing more energy in the start pulse.	No appreciable changes were recorded in the resulting start pulse waveform and arc breakdown was not achieved due to this change.
Repetitive Start Pulse Circuit	Since the electrode properties may change a slight amount during each start pulse regardless of whether an arc breakdown occurs, repetitive start pulses were attempted as a potential method for achieving an arc breakdown	Two 120 mg/sec breakdowns achieved after 40 to 50 pulses. The start circuit was modified to automatically deliver repetitive pulses (10 per second) while checking for output current between each pulse. If output current was sensed, the circuit would terminate pulsing to prevent a perturbation that might possibly extinguish the arc causing a failed start.

Table 7. PCU/Arcjet Hardware Changes And Resulting Breakdown Testing (continued)

TEST	PURPOSE	RESULT
Facility Power Cable Modification	Series inductance of facility power cables reduces high voltage pulse at arcjet. Cables between the PCU and the vacuum chamber wall were shortened, twisted & wrapped with shielding to lower the inductance.	Following the cable modification, the inductance was measured to be 5 micro-Henries and the capacitance was measured to be 2000 Pico-Farads.
DC HyPot™ Testing	Determine if the level of breakdown voltage depended on polarity of the electrodes.	With NH ₃ mass flow of 240 mg/sec, initial breakdown was found to occur at 1.7 kVdc with the cathode charged positive and 2.7 kVdc with the cathode charged negative. This testing did not indicate the subsequent start problems since the PCU had been designed to provide a 2.5 kVdc start pulse.
Stepped Output Inductor	Added series 800 μ H inductor with each 50 μ H output inductor to add energy to the pulse causing a broader pulse width.	Although test results showed pulse width was roughly doubled from 1 to 2 microseconds, the waveform did not achieve an arc discharge.
10 X 2 Start Transistor Matrix	Obtain a higher peak voltage by replacing the original 4 X 2 matrix of 900 volt FETs with a 10 X 2 matrix of 500 volt FETs.	Test results did show that the peak voltage was increased by 1000 volts, from 2.8 kV to 3.8 kV, the waveform did not achieve an arc discharge.
10 X 2 Matrix with Stepped Output Inductor	This method combined both ideas above to yield both a broader and higher pulse waveform.	Test results showed pulse was the same height and twice as wide. With the 10 X 2 matrix alone, the waveform did not achieve arc discharge.
Continued DC HyPot™ Tests	Try a new test procedure for conducting the HyPot™ tests	The negative DC level required for breakdown at 240 mg/sec varies between 3-4 kV. If the voltage was allowed to ramp up to 4 kV in 150 msec, arc discharge would occur at that point. If the voltage is ramped to only 3 kV, arc discharge may not occur until after 500 to 1000 msec.
10 X 2 Matrix with Increased Inductance	Increase peak voltage beyond the 10 X 2 matrix by increasing stored inductance by adding a 3 mH inductor in series with only 2 of 3 50 μ H output inductors.	Test results showed that the peak voltage increased by 300 volts, from 3.8 kV to 4.1 kV. Although two arc discharges were achieved at 4.1 kV, the success rate was only 2 to 3 %.
Pulser Circuit Checkout	Utilized variable high voltage pulser circuit, (no steady state power capability), to investigate the breakdown characteristics of the arcjet.	Varied peak voltage and pulse width. Table 8 is the pulser settings, peak voltage, voltage rise time, breakdown voltage, number of pulses and number of successful/failed breakdowns.

Table 7. PCU/Arcjet Hardware Changes And Resulting Breakdown Testing (continued)

TEST	PURPOSE	RESULT
Continued DC HyPot™ Tests	Try a new test procedure for conducting the HyPot™ tests	The negative DC level required for breakdown at 240 mg/sec varies between 3-4 kV. If the voltage was allowed to ramp up to 4 kV in 150 msec, arc discharge would occur at that point. If the voltage is ramped to only 3 kV, arc discharge may not occur until after 500 to 1000 msec.
10 X 2 Matrix with Increased Inductance	Obtain a higher peak voltage yet beyond the 10 X 2 matrix by increasing the amount of stored inductance by adding a 3 mH inductor in series with only 2 of 3 50 microH output inductors.	Test results showed that the peak voltage increased by 300 volts, from 3.8 kV to 4.1 kV. Although two arc discharges were achieved at the 4.1 kV level, the success rate was only 2 to 3 %.
Pulser Circuit Checkout	Utilize a variable high voltage pulser circuit, (no steady state power capability), to investigate the breakdown characteristics of the arcjet.	A test matrix that varied both the peak voltage and pulse width was conducted. Table 8 is the pulser settings, peak voltage obtained, voltage rise time, breakdown voltage, number of pulses at a given setting and the number of successful or failed breakdowns.

3.2.3.3 PCU Input Voltage Transients. PCU input voltage transients were measured both directly at the input studs and at the output of the EMI filter. The noise levels were lower after the filter as expected.

3.2.3.4 PCU/Arcjet Power Ramp. An internal power ramp board was utilized to reach the 26 kW power level following arcjet startup. The PCU initially sets the plateau current at 100 amps (approximately 10 kW) for approximately 12 seconds. The power is then ramped linearly to the 26 kW level within 70 seconds of start up. All power ramps were conducted successfully without any anomalies or instabilities.

3.2.3.5 PCU Efficiency with an Arcjet Load. After reaching a steady state arc voltage and current at the 26 kW power level, measurements of the PCU input voltages and currents were made to calculate a PCU efficiency. The results are shown in Table 9.

3.2.3.6 Breakdown Voltage versus Mass Flow Rate. In June, 1992, testing was conducted to determine the arcjet breakdown voltage as a function of NH₃ mass flow rate with a set of "burned-in" electrodes. The pulser circuit attached in parallel with the PCU output was used to generate the narrow width high voltage pulse. For reference, the rise time of the pulse, (a function of circuit capacitance), was 800 nanoseconds at the 4.5 to 5 KV breakdown level. Test results

showed that the breakdown voltage varied in a nearly linear manner between 2 KV at 50 mg/s to 5 KV at 270 mg/s.

Table 8. Pulser Circuit Discharge Characterization

Pulser Height (%)	Settings Width (kV)	Peak Voltage (kV)	Rise Time (ns)	Breakdown Voltage (kV)	Number of Pulses (#)	Number of Breakdowns (#)
0	0	3	900	Failed	20	0
10	0	4.2	800	Failed	21	0
11	0	4.9	750	4.9	30	18
15	0	NA	650	5.2	20	20
20	0	NA	500	5.4	20	20
30	0	NA	500	6.3	11	11
			640	6.8		
40	0	NA	450	6.0	6	6
50	0	NA	350	5.0	6	6
60	0	NA	520	7.0	2	2
70	0	NA	500	6 to 7	2	2
80	0	NA	500	6 to 7	2	2
90	0	NA	500	6 to 7	2	2
100	0	NA	500	6 to 7	2	2
0	0.1	1.4	1500	Failed	1	0
10	0.1	2.4	2000	Failed	1	0
20	0.1	3.6	2000	Failed	1	0
30	0.1	4.2	1500	Failed	1	0
40	0.1	4.8	1500	Failed	1	0
50	0.1	NA	1500	5.0	1	1

3.2.3.7 Arcjet Breakdown Investigation. Having conducted an extensive series of tests, TRW, PAC, and AFRL met in November, 1992 to discuss the arcjet starting problem and its potential effects on the PCU start circuit. A general consensus was reached that additional data were needed to verify that a slower dV/dT ramp rate for the arcjet may produce a lower voltage arcjet breakdown condition. A discussion was held regarding the requirements for the start pulse and the potential impact on the PCU and arcjet design. There was concern that simply increasing the voltage to greater than 5000 V could lead to voltage holdoff problems and corona within the PCU, cable, and arcjet. The meeting attendees also concurred that a pulser circuit parametric test approach seemed to have the best probability for successfully identifying a design to ensure arcjet breakdown. As a result, a plan was set in place to conduct additional testing and AFRL agreed to perform these tests. The results of these tests would ultimately have to be implemented to the current flyback inductor start circuit since it was only capable of producing a 2500 V pulse for approximately one microsecond.

The two main goals of the pulser circuit testing were to get data on the effect of start pulse rise rate on breakdown voltage and to resolve differences between static breakdown voltages measured previously (with the HypotTM by PAC and with a Glassman high voltage supply by AFRL.)

All testing was conducted by AFRL using as Air Force GFE arcjet with the baseline anode and the burned-in cathode with a rounded tip. The cathode gap was set to 0.240 inch and NH_3 was

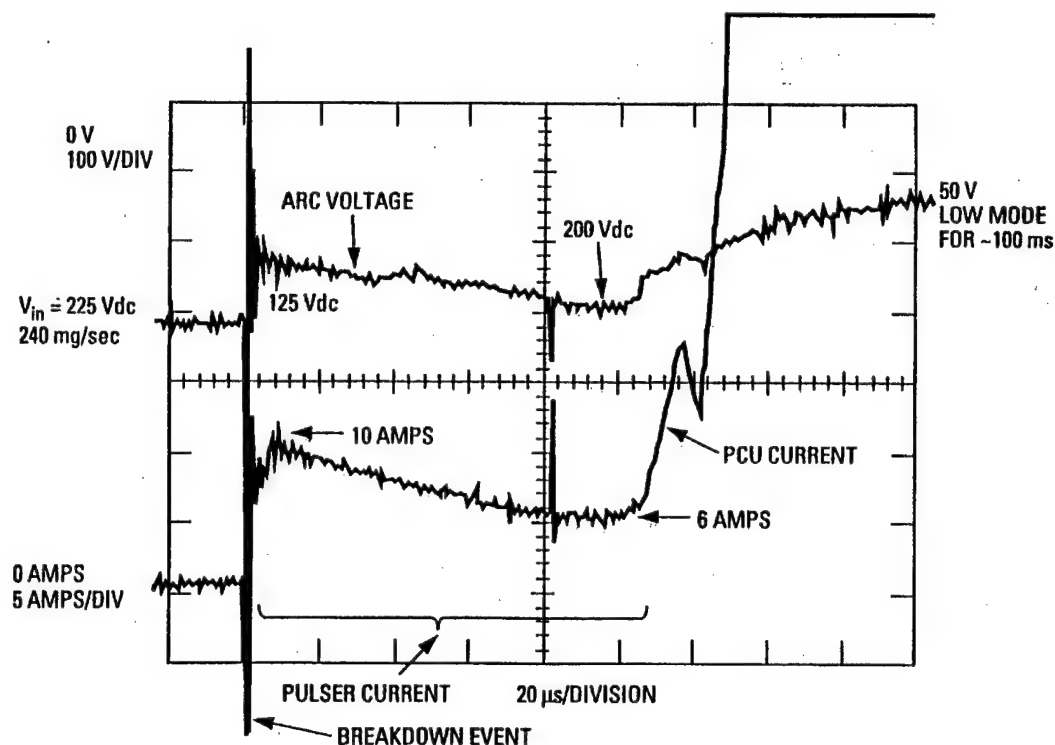


Figure 21. Pulser Current To PCU Current Transition

Table 9. Development PCU Performance with Resistive Load

Voltage (volts)	INPUT Current (amps)	Power (watts)	Voltage (volts)	OUTPUT Current (amps)	Power (watts)	Efficiency (%)
225.2	122.9	27,766	100.3	260.6	26,138	94.4
185.66	148.1	27,496	100.5	259.4	26,070	94.8
150.16	181.9	27,314	100.7	259.1	26,092	95.5

used for all tests. The arcjet was refurbished by replacing several insulators that had become slightly conducting or had broken.

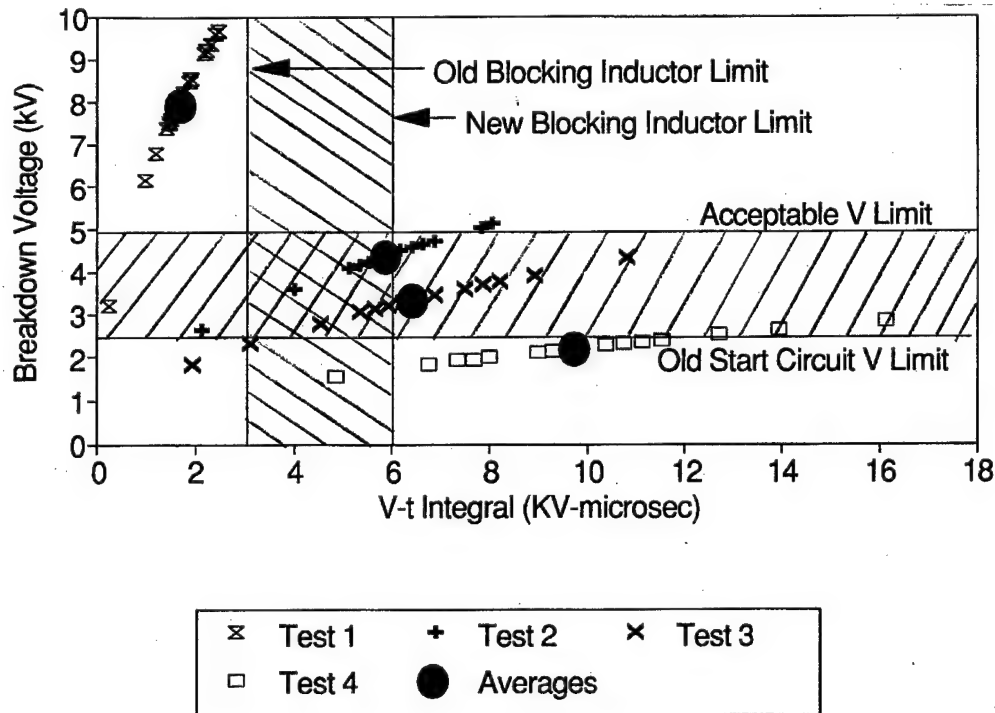
For the first test objective, measurements were made with four different voltage rise rates obtained by adding combinations of capacitance to the pulser output and to the flyback snubber. All results for this portion of the tests were obtained at 240 mg/s flow rate after cleaning the electrode with a glow discharge for 10 minutes. For each rise rate tested, 18 to 20 repetitions were made to get good statistical average results. The average values for each of the four cases are presented in Table 10.

Table 10. Average Breakdown Data

Test	Snubber (uF)	Output Caps (pF)	Rise Rate (KV/us)	Breakdown Voltage (KV)	Volt-Time Integral (KV/us)
1	0	0	19	7.95	1.72
2	0	4700/2400	1.62	4.33	5.87
3	1	4700/2400	0.86	3.28	6.44
4	4	4700/2400	0.25	2.2	9.83

The individual and average data points are plotted in Figure 22. The individual data points give an idea of the scatter in measured breakdown voltages. It should be noted that breakdown was achieved at a significantly lower voltage than the average if multiple start attempts were made. As the voltage rise rate was decreased, the average voltage required to ignite the arcjet dropped. Figure 20 shows the voltage limit of the original start circuit at about 2500 V. For all but the slowest rise time tested, the voltage required to breakdown exceeded that limit. However, for that slower rise time the original start circuit does not retain enough energy to supply adequate current to make the transition to a stable arc.

While the required voltages dropped with slower rise times, the voltage-time integral also increased. If this integral is too long, the blocking inductors that prevent start-up currents from traveling through the PCU saturate and stop working, allowing start energy to be diverted from the



arcjet. The development PCU blocking inductors could handle approximately 3 kV- μ s with margin. Increasing this limit to roughly 6 kV- μ s was therefore considered. Overall, the results were encouraging since it appeared that an effective start pulse could be generated from a compromise between breakdown voltage and volt-time integral.

For the second test objective, head-to-head comparisons of static breakdown voltages between the PAC HypotTM tester originally used and the Air Force Glassman high voltage power supply were made. There were enough differences in breakdown voltages to indicate variations expected in parameters that were difficult to control, such as microscopic surface condition, which suggested the necessity to build margin into the capabilities of the final design. Hence, the start circuit was redesigned to increase the start pulse voltage to 8 Vdc with a pulse width of 5 -10 ms.

3.2.3.8 PCU EM Testing. High power functional testing of the modified PCU determined the following parameters:

- The measured PCU efficiency at 165 and 232 Vdc exceeded the design goal of 94%.
- Ground isolation was measured to be greater than 1 megohm.
- The EMI input filter response at 165 and 232 Vdc showed that the filter was well damped and close to the SPICETM prediction.
- The high input line operation at 230 Vdc input showed that included spikes from the voltage swing across the hybrid FETs is below 300 Vdc; well below the hybrid limit of 400 Vdc. There was no evidence of the suppression circuit turning on.
- The maximum output ripple at the Hi/Lo Line was less than 11% at 230 Vdc and 10 kW output. The specification limit is 15% peak to peak.
- The PCU satisfactorily performed regulation of the auxiliary power supply over the low voltage dc input range of 24 to 32 Vdc.
- The EMC measurements at the PCU line input at 165 Vdc and 10 kW output and 230 Vdc and 26 kW output were very close to the SPICETM predictions and very similar to data obtained from the breadboard tests. One data point at 120 kHz and 165 Vdc input exceeded the specification goal limit by about 2 dB. All other points meet the specification criteria.
- EMC measurements at the PCU line output were made at 165 Vdc and 10 kW output and 230 Vdc and 26 kW output.

The PCU was then subjected to ten thermal cycles between -20°F and 132°F. Following exposure to thermal cycling, the unit was functionally tested and full power and start circuit evaluations were performed. Full power functional tests were performed on the resistive load prior to the start circuit tests.

On the first application of a start pulse to the GFE arcjet thruster, a successful start was achieved with the new breadboard starter circuit. Testing over the range of 150 to 240 Vdc was performed and start-ups were successfully achieved. Due to the poor condition of the GFE thruster anode, a steady-state arcjet voltage of only about 60 Vdc was achieved at a mass flow rate of 240 mg/sec. By increasing the mass flow rate to over 500 mg/sec, the voltage was maintained at about 80 Vdc that allowed a single full-power ramp up.

The development PCU with the breadboard start circuit was also successfully tested with the EM' arcjet assembly. By using no output capacitor, a 1000 pf capacitor, and a 4700 pf capacitor, voltage rise rates of approximately 7, 5, and 2.4 kV/ms were observed, respectively. The breakdown voltages at a propellant flow rate of 240 mg/sec ranged from 6.8 kV with no capacitor

to about 6 kV with the 4700 pf capacitor. The lowest breakdown voltage recorded was 3.5 kV at 110 mg/sec with the 4700 pf capacitor.

Three consecutive 15-minute firings of the EM' arcjet assembly and development PCU at 26 kW were performed. Although a PCU input voltage of 160 V did not support a start on the first attempt, the PCU started the arcjet successfully on all subsequent attempts with an input voltage of 180 V. The PCU ramped up the power as expected and held the 26 kW level with good stability. Although no measurements of the breakdown voltage were made at the start of these firings, the arcjet started without a problem each time.

Following completion of the hot-fire testing, it was determined that the breakdown voltages increased significantly from the pre-test levels. One possible explanation for the anomaly is that the cathode had become contaminated with molten thermocouple material when the anode fractured at the location of the test thermocouple (Reference Section 3.2.2).

After completion of testing, the PCU was reconfigured into the full EM assembly. As a result of start voltage data obtained during the EM' arcjet testing, the start circuit transformer design was modified to provide approximately 1000 V higher output capability.

Following the EM' Arcjet/EM PCU testing, the EM PCU was tested with the EM" arcjet thruster. The PCU performed as expected; breakdown voltages of 5.5 kV were consistently obtained for propellant mass flow rates ranging from 175 to 240 mg/sec.

In order to control the amount of outgassing in the PCU and eliminate any internal arcing during the high voltage start pulse, a technical survey of the design criteria used in the past on high power space electronic components was conducted. From this review, basic guidelines for the ATTD program were established to ensure that the PCU would meet its operational lifetime.

In high voltage equipment, the principal design criteria are to have corona-free operation by maintaining a low internal pressure during the high voltage operation. The breakdown pressure is a function of the spacing of the high voltage conductors. A corona event could cause a failure of the insulation leading to an equipment failure. When there is corona and the right pressure/distance relationship, a breakdown will occur and components could fail due to the high surge current. When there is internal outgassing due to the component materials and processes, the internal pressure will increase, increasing the probability of an internal breakdown. Venting must be provided to allow the outgassing to be vented and maintain the internal pressure below 10^{-5} torr.

Three references^{2,3,4} were used to establish the basic design criteria for high voltage space flight equipment for NASA programs, and were also directly applicable to the Arcjet ATTD program. Based on the information gathered from these references, the following recommendations were generated for the PCU design, development, and testing program:

- High Voltage Insulation Design - References 2 and 3 should be used as the basic high voltage design criteria for components and material selection and for the detail mechanical design.
- Venting Criteria - Since the PCU is a large unit, with higher power and higher operating temperature, two (2) square centimeters effective vent area per 1000 cubic centimeter volume as a minimum should be used as the venting criteria. Vents should be distributed around the external surface of the PCU. Vents should be located near the high voltage boards and where the heat producing components are located. The high operating temperature would increase the rate of outgassing in these areas. Screen venting material to minimize internal contamination should be utilized.
- Test Program - The PCU must be baked out in a vacuum for 48 hours at its highest estimated operating temperature before initial turn-on in a vacuum environment. After a

- period of high power operation, the PCU must be allowed sufficient venting time to allow outgassing to the ambient vacuum before the next high voltage start pulse is generated.
- Spacecraft Integration - The spacecraft venting can not interfere with the PCU venting criteria. The non-operating on-orbit time before initial turn-on should be at least 48 hours to ensure that adequate venting has occurred.

Tests were performed to measure the internal PCU pressure. With the box closed and the conditioning plate heated to 132°F the measured internal pressure was never more than 1 mtorr greater than the external pressure. This test was performed prior to the addition of venting holes in the lid and with the unit inoperative to minimize risk. As a precaution, additional screened vent holes were added to raise the vent area to the recommended 2 cm²/liter. The unit was operated at 78°F and 132°F, but the internal pressure did not exceed the outer pressure by more than 1 mtorr. The arc breakdown points in question would require an estimated pressure of about 300 mtorr.

The PCU CDA was conducted on September 8, 1993 at PAC with representatives from PAC, and TRW in attendance. The status of the PCU design was reviewed and outstanding issues were discussed. One key suggestion raised during the review was to perform a volt-second characterization test of the blocking inductor magnetics to address concerns about the start circuit design margin. A new source for the magnetic cores that would provide an increased start voltage capability of approximately 2000 V was identified and PAC agreed to evaluate by test the use of the new core in the inductor for the flight unit start circuit and compare the results with the core currently being used.

The test was performed using three different core or multicore samples:

- The original three-core ferrite blocker utilized for testing the arcjet thruster as an external part to the output 50 mH inductor of the EM PCU.
- A two-core blocker incorporated in the output composite inductor of the EM PCU.
- A single-core blocker manufactured by Ceramic Magnetics Co. that was selected for use in the upgraded composite inductor. It was anticipated that this core should provide greater volt-second capability than the existing two-core blocker.

The test results showed that the increased peak voltage achieved with the proposed Ceramic Magnetics core blocker provided extra margin of breakdown capability of at least 1000 volts. The higher inductance was also beneficial because less leakage current flowed back into the PCU from the start pulse. Consequently, more energy was available for establishing the arc at this higher inductance without causing any transition problems. Based on the tests performed, PAC recommended that the proposed Ceramic Magnetics ferrite core blocker be used in the composite inductor for the flight unit start circuit. With this final design change identified, fabrication of the flight PCU was initiated.

3.2.3.9 IMS Testing. Two anomalies associated with the PCU were noted during the IMS testing. First, a drift problem was encountered with the telemetry circuits for conditioning the P1, P2, and P3 PFS pressure transducer signals. After two attempts to fix the drift problem, PAC decided to continue with the testing by routing the control of the PFS through the micro-DACS computer directly. The P1, P2, and P3 signals were still monitored during the IMS test to search for signs of interference when the arcjet was firing but were not used to control the PFS.

A second problem that was encountered involved a nonlinearity in the telemetry signal for the PCU output voltage. Subsequently, a calibration was performed between 100 V and 130 V (the

range of interest), which yielded an accuracy of 0.3 percent over that range. This linear fit was used in place of straight scaling of the data output from the telemetry board to the micro-DACS.

After resolving these telemetry circuit problems, the PCU was used to fire two breakdown pulses into the arcjet to check for start pulse adequacy and correct thruster operation. Both pulses resulted in breakdowns in the nozzle with a breakdown voltage of approximately 5500 V. Subsequently, the PCU was used to start and run the arcjet through a power transition test up to full power using the Rapid Electric Power Supply. The arcjet started and transitioned to full power without incident, thus verifying that the PCU start circuit and power converters were functioning properly. At this point, the EM battery was connected to the PCU input to begin the actual IMS test series. (A summary of the IMS test is given in Table 3.)

The initial battery test firing was started with a PCU baseplate temperature of +40°F. The start and transition were accomplished without incident. The battery voltage transient concerns at arc initiation were alleviated, however another problem occurred during this firing. At approximately 8 minutes elapsed time into the run, the test configuration shut down. It was suspected that the PCU caused the shutdown because of the instantaneous nature of the shutdown (e.g., no instabilities, no plume oscillations, no sparks were observed). Interlayer board separation known to be present in some of the circuit card assemblies (CCA) in the EM PCU was found to be the ultimate cause of the shutdown. The solution to the problem was to start the test with the PCU baseplate at a colder temperature since the board separation had been previously correlated with thermal transients as the boards heated up.

Before the start of the second battery test firing, the PCU baseplate was cooled to -15°F. The firing was completed without incident. The same was true of the subsequent two firings, which were started at increasingly high PCU baseplate temperatures. Before the fifth battery test firing, the PCU baseplate was returned to +40°F and again, the test prematurely shut down. The power profile of the fifth battery test firing is shown in Figure 23. The very rapid shutdown correlates well with the theory of interlayer board separation leading to a temporary open circuit. All the remaining IMS tests were run with the baseplate cooled to approximately 0°F and, with one exception, there were no further unplanned shutdowns. The one exception was battery test firing #8A where the PCU baseplate had been heated to drive off volatile material and was rapidly cooled just prior to firing. This probably resulted in a temperature gradient inside the PCU, interlayer separation, and ultimately to the unplanned shutdown.

The final PCU anomaly was a short through the PCU that was discovered just prior to the eighth battery test firing. This anomaly was traced to the FET board and subsequently to one of the hybrid FET devices located on the board. The FET was from the same lot of parts that had exhibited similar failures which were linked to either sodium contamination or wire bonding problems. Both of these failure modes were resolved before the purchase of the flight FETs for the flight PCU by modifying the fabrication process to eliminate the problems. The other FET on the board was exhibiting an anomalous source to gate voltage. Both of the FETs were sent to HiRel Laboratories to determine the causes of their failures.

An example of the charge and discharge battery voltage profiles measured during the IMS test is shown in Figures 24 and 25 respectively. The discharge profile shown in Figure 25 shows more detail of the early voltage fluctuations since it was measured during a short firing. The minimum battery voltage was typically about 160 V.

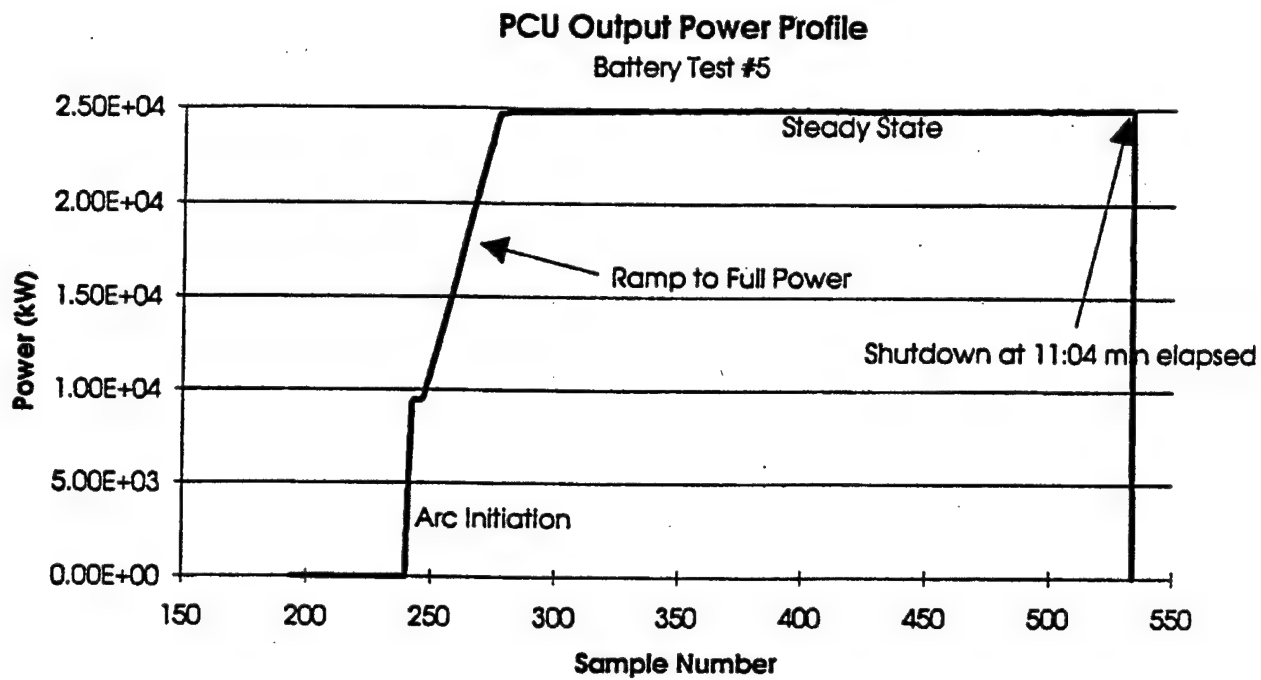


Figure 23. Representative PCU Output Power Profile Measured During IMS Testing

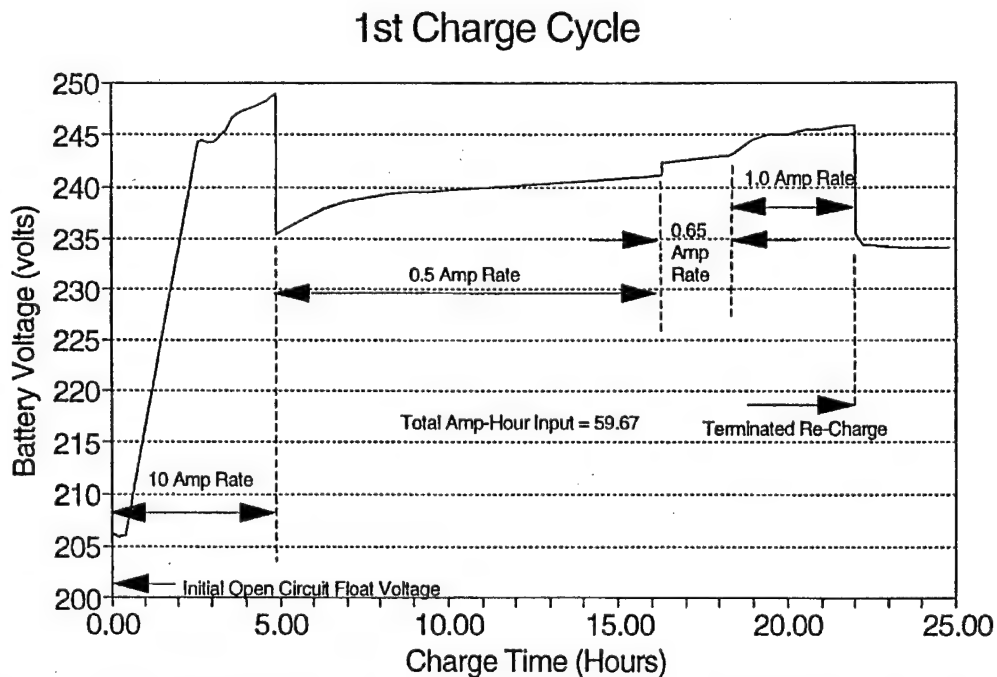


Figure 24. Representative EM Battery Voltage Profile Measured During IMS Testing

8th "Partial" Firing/Battery Discharge

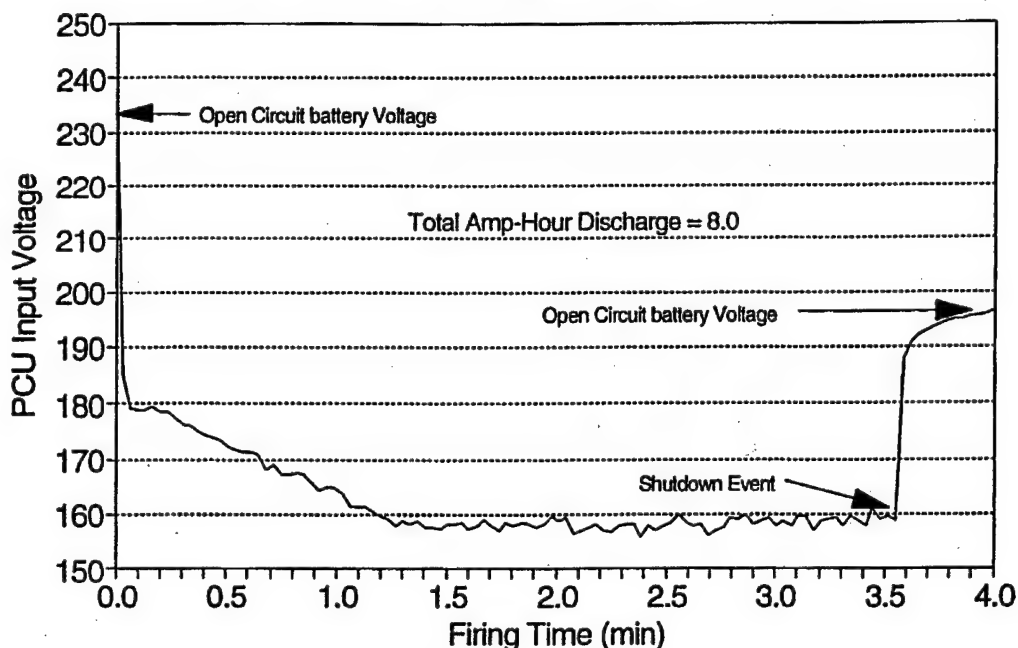


Figure 25. Representative EM Battery Discharge Voltage Profile Measured During IMS Testing

The PCU was inspected after removal from the IMS test chamber and evidence of breakdowns near the motherboard was found. Data collected indicated that there is considerable voltage ripple on the PCU telemetry line during arcjet firings. Additional engineering effort was expended to resolve some of the difficulties encountered during the IMS testing. A summary of the difficulties and the resolution of each is given in Table 11. Verification that the corrective actions were successful was obtained during the ATP testing of the flight PCU.

Table 11. PCU Anomaly Resolution Summary

Anomaly	Probable Cause	Resolution
PCU shutdowns	Board Fine line separation	Boards repocured for flight unit
Telemetry drift	Thermal effects	Circuit redesigned to be more stable
Voltage non-linearity	Failed capacitor circuit	Higher screened part (JANTX) in flight unit
Hybrid FET failure (short)	Manufacturing defect	Class B screening of hybrid FETs for flight unit
Hybrid FET failure (drive voltage)	Overheating due to failure of partner FET	None Required

3.2.3.10 Flight Buildup. Following the IMS test, the assembly of the flight PCU was completed, and ATP testing was started. All functional checkouts of the PCU were completed successfully. During preliminary high power testing with the resistive load, however, an anomaly was detected in the output current level, which was traced to the current sense transformers. The flight unit current sense transformers were built according to the drawings that specified a winding of 200 turns. This value was in error and did not represent the as-built configuration of the EM PCU which used 250 turns and provided the correct current output. The lead-time for procuring replacement magnetic cores containing 250 turns was eight weeks. PAC and TRW engineering and quality determined that swapping the current transformers from the EM unit with those from the flight unit was the best alternative and this was done.

The flight PCU successfully completed ATP testing per released ATP procedures prior to being integrated with the arcjet for hot fire testing. The ATP tests included resistive load testing to 26 kW, conducted EMI testing, and a 24 hour burn in test. Several functional tests were performed throughout the test series, as well.

While doing early breakdown tests with the flight PCU and arcjet, a short circuit developed in the start circuit, effectively connecting the PCU cathode and anode outputs. The short circuit was later determined to be between the anode side of the start circuit transformer output and the PCU chassis. Mechanically, the short occurred when a chassis mounting post rubbed through the conformal coating to contact a trace in the card. An insulating pad was installed between all chassis mounting surfaces and the card.

Before the Performance Verification Test Firing, further breakdown tests were conducted successfully. The arcjet was then started at 180 mg/s and fired for approximately 15 minutes. The lower flow rate was necessary due to the impedance of the long cables connecting the PCU and arcjet. After ignition, the PCU ramped power up to 26 kW and operated stably for the entire firing.

During shut down, two PCU related problems occurred. First, the PCU would not shut down from the microDACs computer. The "Converter On/Off" command off was issued at least twice from the computer, but the arcjet continued running at 26 kW. A manual shut down sequence was initiated from the test control fixture, but this too proved unsuccessful. This inability to command the PCU off was replicated later running the PCU on a resistive load. With the microDACs command line in the off position, a digital volt meter on the command line pins at the test control fixture read 4 V, instead of the expected < 0.5 V. In addition, lights on the test control fixture that normally indicate operation of the propellant feed valve driver were observed to flicker faintly, although no valve was connected to the PCU at the time. Finally, an unrelated test experienced unscheduled firings in another cell that shares the same 28 V laboratory power supply as the microDACs command signals use.

It is theorized that high frequency noise on the PCU resulted in the false "on" command at the TCF. It is also thought that this same noise was travelling through the positive leg of the 28 V laboratory supply and through the common shield grounds in such a fashion as to send a false "on" command to the valve driver. The problem was traced to poor regulation of the small power supply supplying the 28 V power to the PCU (as distinct from the laboratory's 28 V command line power supply common to all tests). Replacement of this power supply with one less susceptible to feedback from the PCU eliminated the inability to command the PCU off and the flickering of the propellant feed valve driver. The problem was thought to originate from the active regulation of the output voltage in these power supplies. Since a spacecraft 28 V power source is considerably stiffer and involves no active regulation, the PCU was expected to be less susceptible to such problems. The microDACs command circuits were also moved to their own 28 V supply, separate

from the rest of the lab, preventing further interference with other tests. This experience also demonstrated the desirability of low output impedance on the command circuitry external to the PCU. This test set up had a 1 k Ω resistor across the command lines to bleed off leakage current from the microDACs when in the "off" condition. An even lower impedance to command ground would have ensured a successful "off" command in the noisy environment.

As described in Section 3.2.2.6, the second problem that occurred during the shutdown of the flight arcjet firing was a flash and sparks that were observed coming from the arcjet. This problem was traced to a missing jumper wire that enabled the normal shutdown circuit. The missing jumper wire was potted in the cable bundle connecting the left and right motherboards in the EM unit and therefore not apparent during visual inspection when the flight circuits were being verified. This jumper appeared to be a late modification to the cable assembly and may not have been adequately documented in the EM schematics; resulting in a drawing error, that led to a fabrication error.

In normal operation, upon receiving an "off" command on either of the logic or converter command lines, the PCU would drive the current reference voltage negative, which would drive the regulated current level to zero to extinguish the arc. The control circuit auxiliary power supplies would be shut down at the same time, but they tend to maintain their voltages for about 60 ms before decaying. Upon decaying, they lose the ability to control the FETs. Subsequent measurements on the .5 Ohm resistive load demonstrated that the current jumps to 360 A for about 10 ms at that point, indicating that the FETs momentarily apply the input open circuit voltage across the output. This was the operating sequence for the EM PCU and all EM testing. With the jumper wire missing, the first step of driving the current to zero did not occur in the flight unit firing. The effect was that the arc continued to operate at 90 A for 60 ms, at which point the auxiliary power supplies began to decay allowing a 10 ms burst of high current to pass through the arcjet.

Initially, it was felt that the 60 ms interval over which the arc was out would be sufficient to prevent the arc from relighting in an uncontrolled fashion when the control circuit momentarily allowed the open circuit voltage of about 200 V to be applied to the arcjet. Video-tapes of over 24 EM firings were reviewed for evidence of arcjets re-lighting at shut down. There were no observations of an increase in plume brightness or sparks immediately before or after any shut downs, except for the occurrence of a single spark at the shut down of the eighth battery firing during the IMS tests. In this firing, a premature shut down occurred a few minutes into the firing, probably due to the fine line separation in the EM cards causing the auxiliary power supplies to turn off suddenly. This event easily could have caused an uncontrolled shut down of the arc, which would not necessarily drive the current to zero before the control circuits lost power. Nevertheless, there was concern that open circuit voltage across the hot electrodes could cause a momentary re-light on orbit. Therefore, the PCU was altered such that the current could be shut off indefinitely before shutting off the auxiliary power supplies. This was most expediently accomplished by changing the arcjet start command such that it ramps the output current to zero, rather than 90 A. As long as the "Converter On/Off" command is "on", the auxiliary power supplies remain active and provide positive control of the FETs. When the "Converter On/Off" command is shut "off" after waiting several minutes, the FETs still apply open circuit voltage to the electrodes for the 10 ms burst, but the electrodes are too cool to re-light.

The first resistive load tests of the flight PCU with the missing jumper re-connected exhibited slight instabilities as evidenced by the 90 A plateau level running at 87 A and the ramp up behaving erratically. These problems were traced to noise propagated across the cable bundle

connecting the two motherboards in the PCU. The noise was eliminated and stability restored by adding filter capacitance to the control lines.

This current shunt, which supplies the current telemetry signal, was found to have drifted about 7% off of nominal and had been drifting ever since construction of the unit. The flight current shunt was replaced with the EM current shunt and no further shifts were observed in ground testing. However, flight data ultimately indicated further drifts.

The Performance Verification Test firing data indicated that the PCU efficiency was only 90.5%, a loss of 6% or almost 2 kW since the ATP on the resistive load. This issue was in addition to two existing PCU issues: the drifting current telemetry and the instability at input voltages below 170 V. A multi-tracked investigation was started covering all of these problems.

The perceived performance loss and telemetry issues were actually both symptoms of the drifting current shunt. A subsequent re-test of the PCU efficiency confirmed earlier measurements made during the ATP tests of 96% or higher.

The low voltage instability problem proved to be the most elusive of the three. Originally, it manifested itself at approximately 165 volts input voltage. As the testing progressed, it appeared to grow worse. It began appearing at voltages as high as 175 volts. After an extensive review of the hardware, two failed components were found and replaced. This improved but did not eliminate the instability. The threshold changed from approximately 172 V to approximately 168 V, but was still nowhere near the required spec value of 160 V. At this point it was determined that the inductance of the lines running between the Rapid Electric power supply and the PCU may be playing a role. The inductance was measured to be 10 microhenries with the welding cable running parallel over a total distance of approximately 60 feet. The cables, when twisted about one another to reduce the inductance, resulted in a measured inductance value of 7 microhenries. When the test was repeated with this change only, the PCU ran stably down to an input voltage of less than 160 V. The estimated inductance of the flight cable between the battery and the PCU is 4.5 micro Henries.

After resolving these performance issues, the PCU was subjected to three-axis vibration at 9.6 grms. After completing vibration testing, the PCU was visually inspected for workmanship and a final ATP was performed verifying all electrical functions.

The PCU was then integrated with the PFS and checks were made on the pressure transducer signal conditioning and telemetry circuits. These tests showed that a drift and an offset were generated when the PCU input voltage was varied. The drift was significant relative to the signal output. Filtering capacitors were put on the input lines of these signal conditioning boards, which eliminated the drift and offset, and the signal conditioning circuits performed without problems during integrated PFS testing.

After a final physical inspection was performed, the PCU was shipped to OSC for flight unit integration.

3.2.4 Propellant Feed Subsystem Design. As introduced in Section 1.4, a design alternative was needed since the LES 8/9 propellant feed subsystem was not sufficient for the Arcjet ATTD mission. Although the analyses conducted in Phase I suggested that vapor-outflow could be expected utilizing thermal stratification to position the liquid NH_3 away from the tank outlet, there was no clear method for design verification in a 1-g environment. Therefore, specific design changes to the PFS were considered, and ultimately a design change was adopted to add an enhanced feedline heater (EFH) to the PFS.

As shown in Figure 26, The EFH is a segment added to the propellant line immediately downstream of the propellant tank outlet which is packed with a metallic wick and can be heated with 300 watt heaters. This design was tested extensively with the EM PFS to verify it would provide vapor to the arcjet under full liquid outflow from the propellant tank for a full fifteen minute firing. The tests were not only to verify the operation of the EFH, but also to verify the PFS could operate with the EFH and meet the flowrate and control requirements of the arcjet.

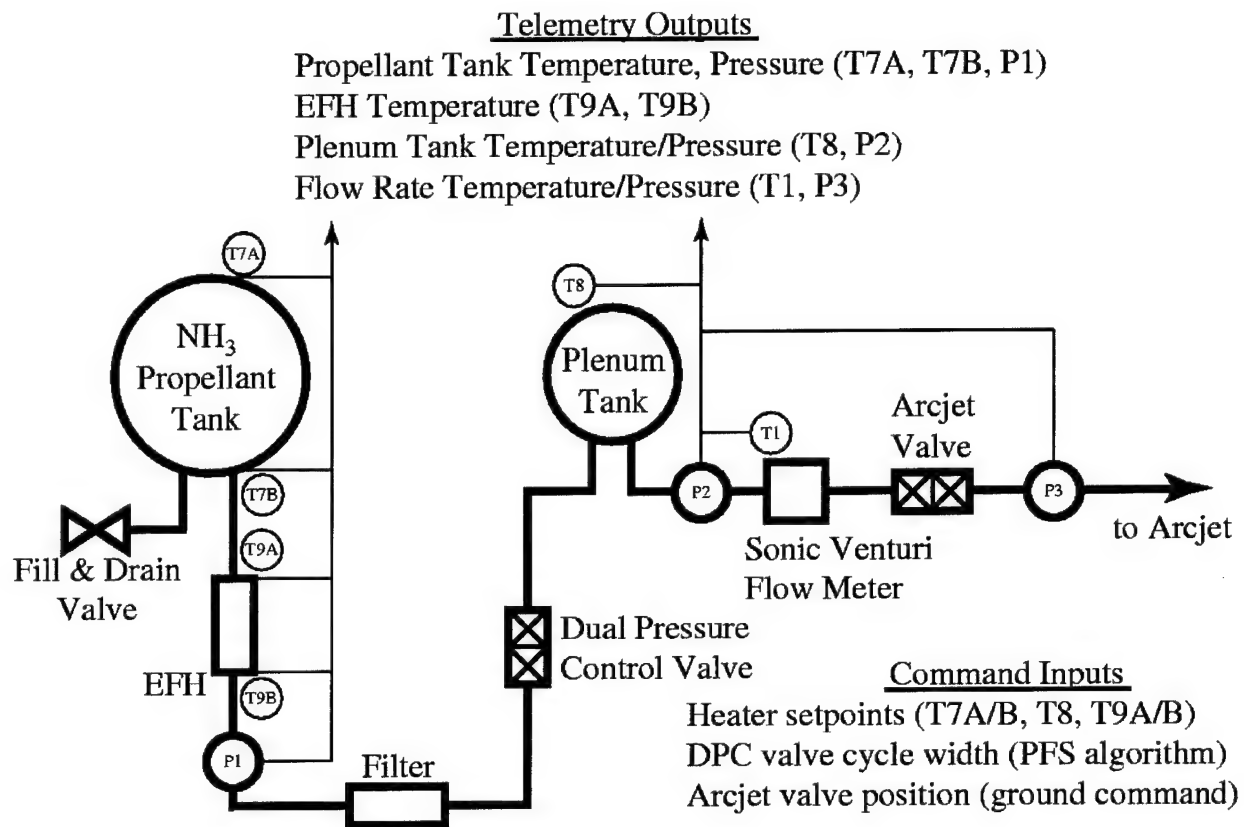


Figure 26 - Schematic Representation of the Propellant Feed System

3.2.4.1 EFH Development. A subscale bench test, a full-scale bench test, and an integrated test series with the full scale EFH installed in the development subsystem were completed.

In the subscale EFH tests, the power level and mass flow rate were roughly 60% of the PFS baseline values. The heater operated acceptably at a mass flow rate of 136 mg/sec and a power level of 200 watts. Oscillating movement of the liquid front was indicated by periodic temperature variations, however, continuous vapor feed was successfully achieved. Test results indicated high quality flow even when liquid penetrated down into approximately 75% of the EFH.

In another test, the heater was intentionally washed out by removing heater power until the flowmeter indicated substantial liquid flow. At this point, full heater power was applied to verify the system could recover from a full liquid flow condition. Several minutes after heater power was applied, the system was exhibiting flow behavior consistent with full vapor outflow.

The mass flow rate readings did not vary more than $\pm 10\%$ during the vaporization runs. This important result implied that a NH_3 flow of less than 100% quality may be supplied to the flow control valve without an appreciable impact to the mass flow through the valve, hence the response of the control system would not be significantly altered. In light of these results, it was believed that the EFH did not need to be fine tuned to provide 100% vapor to the control valve in all inlet conditions.

An 18 inch long, 300 watt full scale development version of the EFH was built and bench tested to verify performance. Two 15 minute liquid outflows at the full mass flow rate of 240 mg/sec were performed. Performance scaled from the 60% sub-scale test version as expected.

Based on these results, the EFH was installed in the EM PFS (shown in Figure 27) and several subsystem tests (15 minute liquid outflows at the full mass flow of 240 mg/sec) were performed. The integrated performance was stable and robust (capable of maintaining mass flow control with aerosols induced at the EFH inlet) and the flow remained within the specification limits.

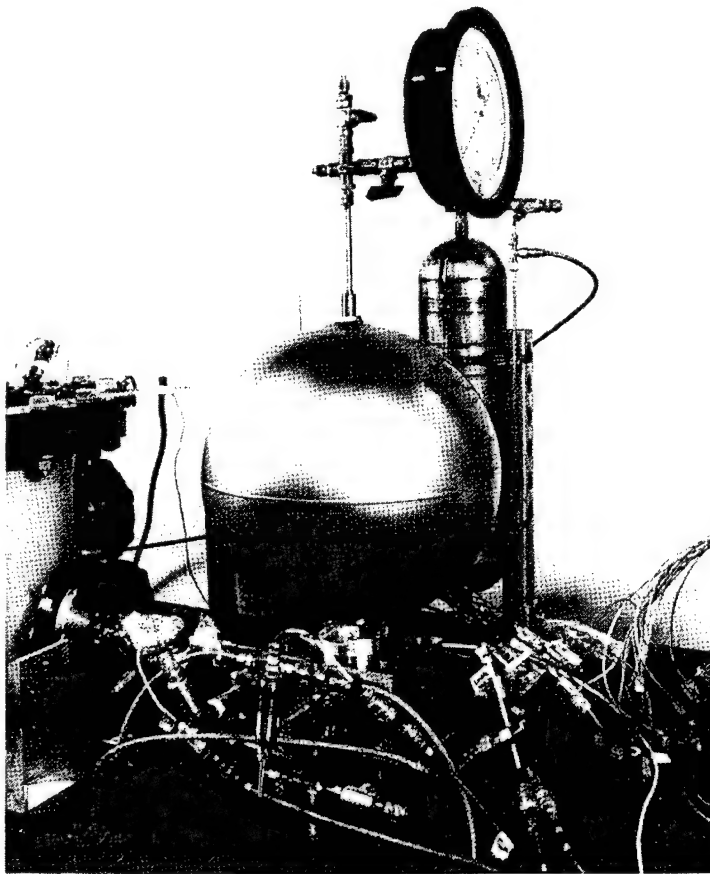


Figure 27. Engineering Model PFS with EFH Integrated

The majority of the test results for both the full scale and subsystem testing were conducted employing heater densities of 20.76 kW/m^2 with the inlet of the feedline heater positioned such that the liquid flowed downward (i.e. 1g flow). A single test was conducted at the same power density,

but with the heater inlet inverted (i.e., -1g flow). The results of this test were very nearly the same as compared to the 1g flow testing which suggested that the flow boiling in this configuration was independent of gravity. An additional 1g flow test was conducted with a power density of 33.90 kW/m² which indicated that the EFH was effectively vaporizing the ingested liquid (as characterized by acceptable mass flow rates throughout the run) with no indication of liquid at the inlet to the venturi flow meter.

With the successful completion of these tests the EM PFS and development EFH were integrated with the arcjet for additional testing. Liquid ingestion tests were conducted which successfully demonstrated the ability of the PFS to maintain acceptable mass flow rate control during all phases of arcjet operation (i.e., cold flow, ramp up, and steady-state) as summarized below.

3.2.4.1.1 Liquid Ingestion Tests. Several test runs were performed to characterize the performance of the PFS during 100% liquid outflows from the propellant tank. A liquid ingestion test with the EFH inverted was repeated to ascertain the influence of gravity on the performance of the EFH. The test was conducted at ambient temperature (approximately 65°F) with the EFH power setting at 346 watts. Manual thermostatic control was provided to maintain EFH wall temperatures near 280°F. The test sequence was initiated with a 3 minute vapor flow (EFH active) to pressurize the plenum. The propellant tank was then rotated to provide 100% liquid to the tank outlet. Liquid outflow was maintained for 18 minutes with nominal flow control results. The results of this test confirm the development unit results that gravity has a negligible influence on the performance of the EFH.

A second liquid outflow test was conducted to determine the effects of increased line voltage on the operation/performance of the EFH and subsequently the performance of the PFS. This 21-minute test was conducted with the propellant tank conditioned to 120°F, the EFH power set to 520 watts, and manual thermostatic control of EHF outlet wall temperature to 280°F. The results of this test verified that the higher power levels do not adversely effect the performance of either the EFH or the PFS. These final liquid ingestion tests verified the start-up algorithm prevented excessive liquid flow during an evacuated start, demonstrated improved mass flow rate control and automated thermostatic control, and demonstrated the ability of the PFS to maintain acceptable mass flow rate control during all phases of arcjet operation (i.e., cold flow, ramp up, and steady-state).

3.2.4.1.2 Vapor Outflow Tests. A vapor outflow test, conducted with the same operating conditions as those of the liquid outflow with the exception that the power was reduced to 300 watts, was performed to ascertain if the presence of the EFH had any observable effects on the performance of the PFS. During the vapor outflow portion, the EFH fluid outlet temperature oscillations were considerably smaller than those associated with liquid outflow, as would be expected. This test also showed that the presence of an aerosol at the EFH outlet (i.e., control valve inlet) had no discernible influence on the mass flow rate control - verifying the robustness of the flow control system.

A 28-minute vapor outflow test with the propellant tank at ambient temperature (~55°F), the EFH power set to 180 watts, and manual thermostatic control with a control temperature of 280°F was performed. During the first 13 minutes, the tank pressure dropped until the mass flow rate through the control valve was less than the desired flow rate and the valve cycle width saturated to open indicating that an operating temperature of 55°F was too low. A subsequent test with the

propellant tank conditioned to ~75 °F was successfully run for 15 minutes with the PFS providing the desired nominal control throughput. The results of this test demonstrated that an operating temperature of 75°F was acceptable. Since the operating temperature was baselined at 120°F and the thermal control and power subsystems had been designed to provide this higher operating temperature, there was sufficient margin to ensure acceptable system operation for the ATTD mission.

With the success of the integrated arcjet/PFS (and EFH) testing, the design of a flight type EFH was completed as shown in Figure 28. This design was also subjected to the same development testing conducted with the proof-of-concept EFH by performing stand alone and integrated operation tests. Following successful checkout tests, vibration and thermal/vacuum tests were conducted.

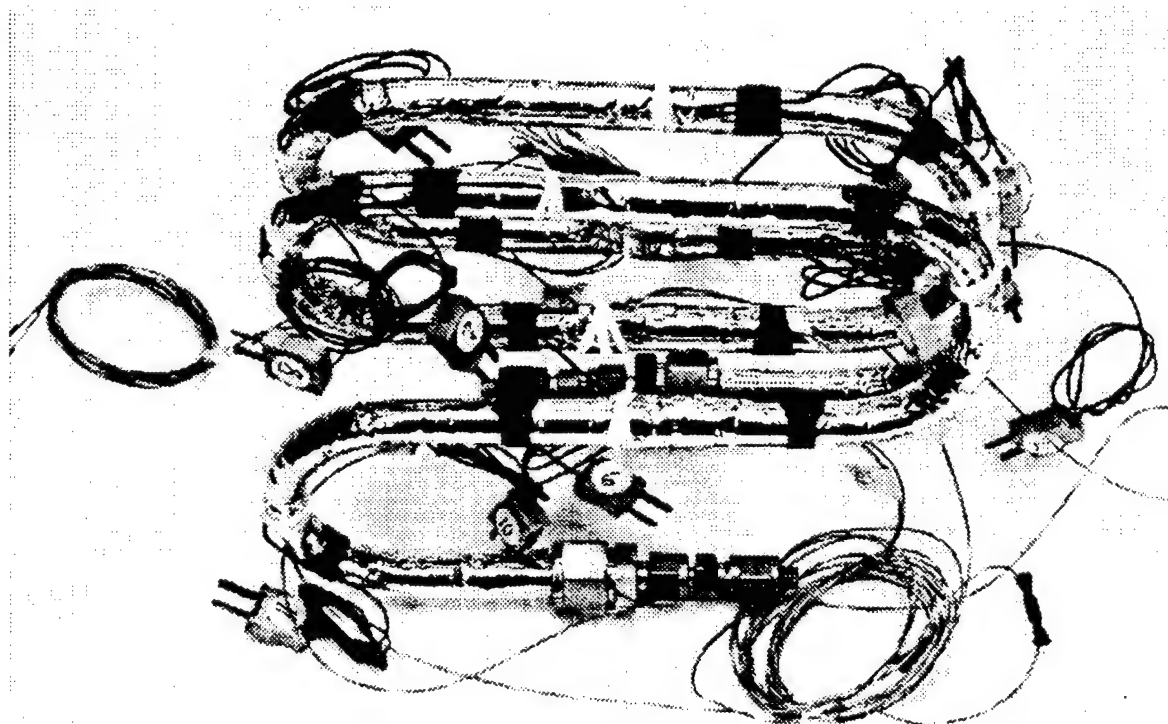


Figure 28. EM Configuration EFH

3.2.4.2 EM PFS Development and Testing. After assembly of the EM EFH into the EM PFS was completed, a series of vacuum tests were successfully completed. The propellant tank heater increased the temperature of the liquid NH_3 to approximately 100°F while the EFH was heated to an operating temperature of approximately 200°F using power ranging from 300 to 400 W. The system was tilted at an angle of 50° to allow depletion of liquid at the propellant tank outlet during the series of ten outflows. Mass flow rates were successfully regulated within the desired tolerance of 240 ± 5 mg/sec as shown in Figure 29 and pressures and temperatures were within expected ranges during operation. The software properly controlled the initiation sequence,

heaters, and valve operations. The locations of the control thermistors were also confirmed for use on the flight unit.

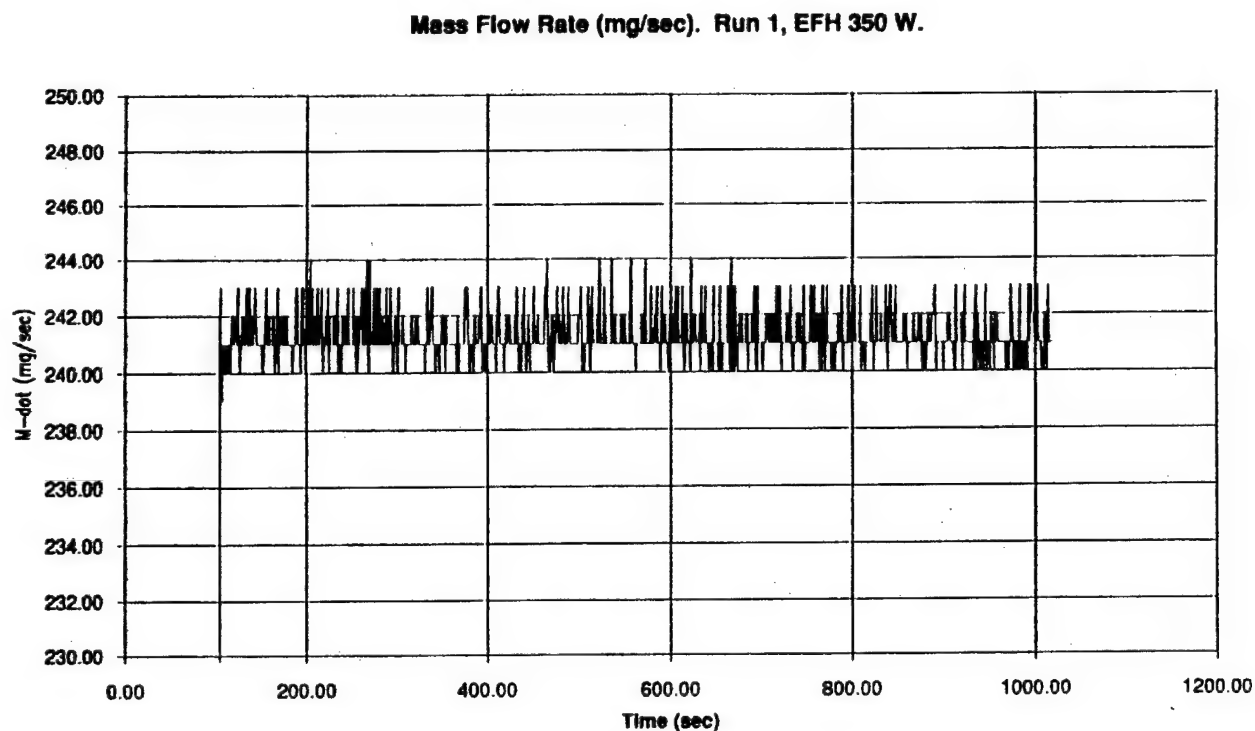


Figure 29. PFS Mass Flow Rate Test Results

A contamination problem with the pressure control valve involving some unknown material was encountered during the development EFH testing. The pressure control valves were exchanged and the testing proceeded without further incident. The former flow control valve was not fitted with a control orifice, so the valve duty cycle was not optimum, however, this had no effect on the successful outcome of the test.

The PFS CDA was conducted on June 7, 1993 at TRW via video-conference. Representatives from the Air Force, TRW, PAC, and Aerospace Corporation were in attendance. Provisional approval to proceed with the fabrication of the flight unit was received and manufacturing activity was initiated. Source control drawings for the propellant and EFH line heaters and the propellant and plenum tank heaters were completed and released.

3.2.4.3 PFS IMS Testing. After completion of the EM PFS verification testing, the EM PFS was installed in the PAC test chamber, instrumented, and the propellant tank loaded with 15 lbm of NH_3 in preparation for the IMS testing. The EM PFS operated flawlessly during the IMS testing. The mass flow rate and temperature data measured during the IMS test confirmed that the PFS operated in a stable manner. Figures 30 and 31 show representative mass flow rates and EFH temperatures, respectively, measured during the fifth battery test firing.

Several small problems were encountered with pressure transducers and propellant valves. However, after switching out some of the faulty hardware, the IMS tests were successfully concluded. One of the failed valves, the propellant tank valve, was inspected and tested to determine the cause of the failure and whether any evidence existed that it was related to dry cycle

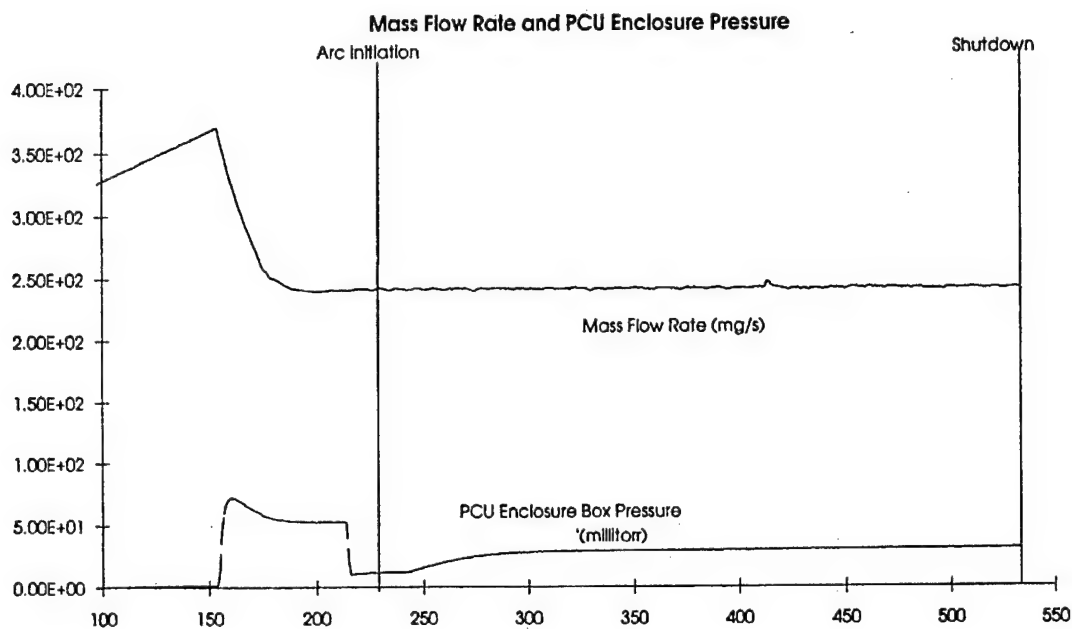


Figure 30. Representative PFS Mass Flow Rate Measured During IMS Test

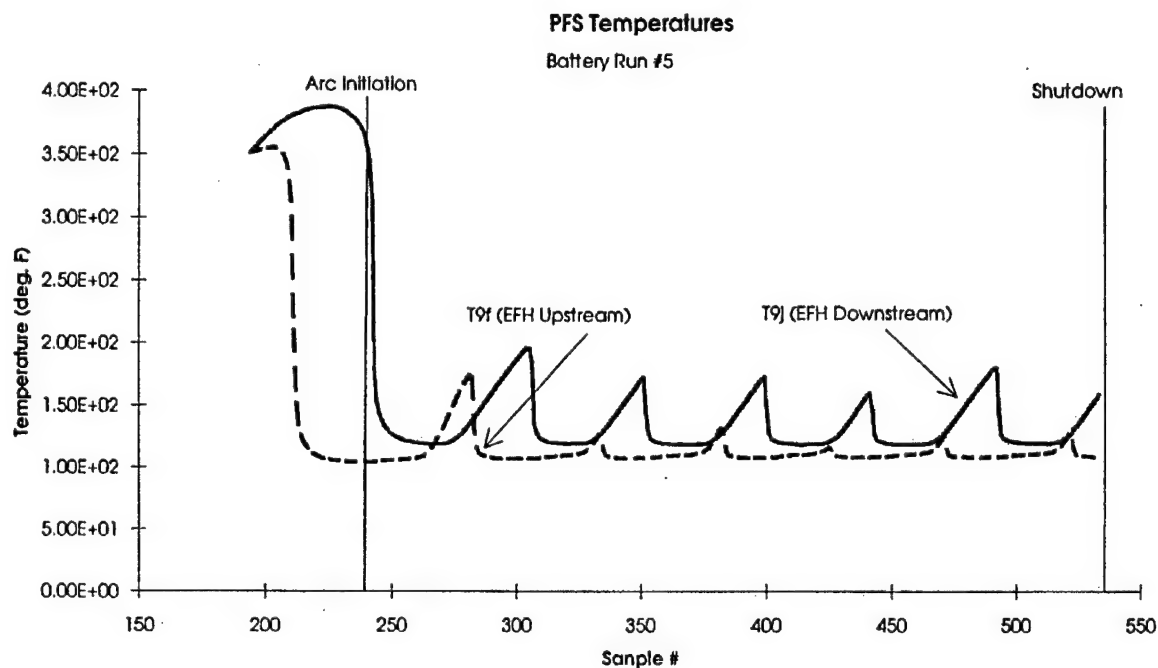


Figure 31. Representative Enhanced Feedline Heater Temperature Measured During IMS Testing

operation of the valve. This particular valve was found to be contaminated during previous PFS testing (Reference 3.2.4.2), subsequently cleaned and re-installed into the EM PFS. At the time of the failure of this valve during the IMS testing, it had accumulated over 40,000 dry cycles. Another valve in the system continued to function well after 41,000 cycles and so this failure was not thought to be related to dry cycle operation but attributable to swelling or looseness of the elastomeric seal material resulting in restriction of the flow through the valve. Since the flight requirement for these valves is 10,000 cycles each, no design or component change was required.

3.2.4.4 Flight PFS Fabrication and Test. In parallel with EM testing and the IMS test, the flight PFS was manufactured. After mechanical assembly, the flight PFS underwent weld inspection where x-rays verified all 15 weld joints in the lines and tubing. Following the weld inspection, proof and leak testing of the PFS was successfully conducted.

During electrical functional checks, one of the pressure transducers was found to have a resistance value that was out-of-specification. Upon further examination, it was determined that one of the thin film resistors in the transducer had been damaged, probably from ESD during handling. Since all three transducers had experienced the same environment and potential for static build-up, PAC decided to replace them all. At the same time, an ESD protection program was implemented for all handling operations, which was based on PAC's electronics department plan.

As part of the flight PFS acceptance testing, three five-minute outflows were conducted at different mass flow rates. In addition, the ability to ramp up the mass flow rate was demonstrated. The PFS was run with liquid, two-phase, and vapor tank outflow conditions, and all data indicated operation of the EFH and the control system was nominal. Detailed results of these tests are documented in the PFS ATP data package. Once this final testing was completed, the flight PFS was integrated onto the PFS platform and shipped to OSC for integration.

3.2.5 Command and Control Subsystem Design. A requirement change that resulted from the designation of ARGOS as the Arcjet ATTD host spacecraft was that the flight unit CCS was to be compatible with a MIL-STD-1553B data bus. Since the CCU design had already begun, and some hardware built, software and hardware modifications were required to implement the 1553B interface board. The test software was also redesigned to incorporate the 1553B interface. OSC reviewed the ARGOS implementation of the 1553B Interface Specification and then reviewed existing OSC 1553B interface hardware and software designs. This review determined that the existing hardware design met all the interface requirements except for the internally hardwired 1553B remote terminal addressing. Therefore, the ARGOS program designated a specific remote terminal address for the Arcjet ATTD payload that allowed the existing OSC 1553 data bus design to be used without modification.

To support testing of the CCU flight boards, a wire-wrap motherboard card cage and interface test unit were fabricated. Prior to its use, the interface test unit was tested to verify correct analog input voltages, bi-level commands, and telemetry to the analog I/O boards. The testing then performed on the flight boards included:

- The two analog interface boards were tested to verify proper operation.
- The general purpose CPU board was tested and the real time clock, interrupt controller, and RAM memory were verified.
- The memory I/O board was tested and the watch dog timer circuit, board control output port, and RAM memory were verified.
- The computer power switchboard was tested and programmable timers were verified.

- The f-megabyte memory board was tested to verify the 2 megabyte of RAM and memory control circuitry.
- The 1553B interface board was tested along with the bus controller PC-AT hardware to transmit and receive test data.

The device drivers, diagnostics, and test software were also used to test the CCU flight boards. All interfaces were verified including the diagnostic board that interfaces to the TQCM, EMI, and video camera electronic units.

During testing of the PFS floating point control algorithm in the CCU test software, a jitter problem was identified from the ON/OFF timing of the DPC valve. The CCU could not generate a precise 500 ms valve ON/OFF cycle because of the cumulative effect of the demands on the CCU processor. The error of the 500 ms valve ON/OFF cycle was between 0 and 42 ms, which would cause an error in the mass flow control. The acceptable error margin was defined to be 2% or 10 ms.. A hardware timing circuit was developed to implement the control of the PFS dual pressure control valve duty cycle via hardware instead of software. Subsequent testing of a breadboard circuit based on this design was successful in eliminating the timing control problem. The hardware design used two programmable timers and logic to generate the variable duty cycle pulse. The programmable timers could be updated asynchronously by software while the 57.6 kHz input clock for the timers generated a precise 500 ms control pulse. The existing flight computer power switch printed wiring assembly (PWA) in the CCU contained spare programmable timers and logic suitable for implementing this circuit in the CCU, and was reworked to include these devices.

The PFS software was modified to implement the hardware timer duty cycle pulse generation for testing of the hardware timing circuitry. The hardware and software were tested and correct operation confirmed. Protoflight qualification thermal and vibration testing of the flight CCU, including post-vibe electrical verification testing was then successfully completed.

3.2.6 Diagnostic Package Design. After being assigned as a payload aboard the ARGOS spacecraft, the diagnostic package design baselined at PDR was reviewed and the locations of the instrumentation were definitized. The primary design constraints for locating the instruments were:

- Maximize the exposure of the solar cells to sunlight
- Deploy EMI antenna boom into the Y-plane to avoid interference with the reaction control thrusters of the ARGOS spacecraft
- Minimize EMI cable lengths to minimize losses within the cables
- Prohibit instrument interference with other instruments or equipment

All instruments were located as shown in Figure 32 and Figure 1.

The diagnostic package CDA was conducted on July 7, 1993 at TRW with representatives from the TRW Arcjet ATTD project, electrical systems design and integration department, and materials and processes department in attendance.

3.2.6.1 Performance. During Phase II, an accelerometer system built by Endevco™ was chosen for the flight experiment since a better estimate of the entire spacecraft weight was known. The Endevco™ system was designed to measure 32 µg, well below the 78 µg expected. Since the accelerometer system was an off-the-shelf component, there was no activity design surrounding the accelerometer during Phase II. At the appropriate time during the flight unit integration activities, the Endevco™ accelerometer system was mounted onto panel 6 of the flight unit (Reference Figure 1). In testing the accelerometer, it was found that the unit would not provide a reading due to what looked to be a saturated signal, even in the absence of active stimulation. Reviewing the unit

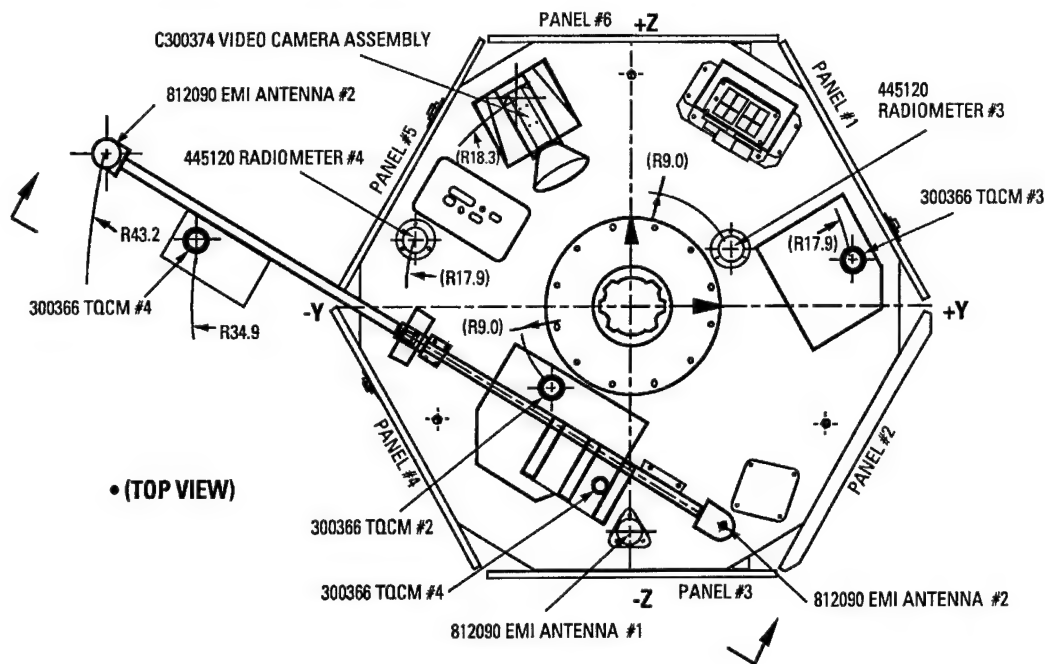


Figure 32. Diagnostic Package Device Layout

design with the supplier, it was determined that the installed accelerometer system was designed for a frequency response that was greater (0.05 Hz) than that produced by the arcjet thruster. The thruster produced a slow acceleration over 85 seconds, essentially resulting in a dc-like signal. This accelerometer, although capable of measuring micro-g accelerations, was designed to measure sudden accelerations that produce ac-like signals. The solution was to replace the existing piezo-electric accelerometer system with a servo accelerometer. The space-qualified accelerometer system selected was the Allied SignalTM QA3000 accelerometer. Because the accelerometer is very sensitive to temperature changes ($25 \mu\text{g}/^\circ\text{C}$), it was imbedded into a large aluminum block to reduce its susceptibility to thermal fluctuations. Thermal standoffs were also initially used to minimize its susceptibility to conducted thermal fluctuations from the panel. TRW built up a circuit breadboard and, after successfully completing functional testing at TRW, the unit was provided to OSC to perform an integrated functional verification of the unit and its interfaces. The accelerometer was placed on Panel 6, which was in the open, horizontal configuration. Power to the appropriate accelerometer pins was verified to be ± 15 Vdc. The accelerometer output signal and temperature measurements were also verified at the unit and at the CCU. The unit was tilted to verify correlation to positive and negative accelerations. Ultimately, however, additional modifications were needed to the unit design as discussed in Section 3.3.1.

3.2.6.2 Contamination.

3.2.6.2.1 Radiometers. The results from an assessment of the thermistor requirements for radiometer #1 indicated that one thermistor would not be able to cover the entire -10 to +3008F temperature range. If only one thermistor was used, some of the predicted temperatures experienced by the radiometer could not be measured during the mission. Therefore, two thermistors were used to cover the expected operational temperature range; one thermistor for the colder temperatures and a second one for the higher temperatures. With this design change

implemented, an EM radiometer was fabricated and vibrated to qualification levels to verify the design's mechanical integrity.

The EM radiometer was then tested at PAC during the IMS test. The device was instrumented with two additional thermistors such that the heat flux down the titanium stem could be determined. A comparison of the heat flow down the stem with the flight thermistor temperature difference would allow the radiometer to be calibrated for any unknown heat leaks. After the IMS test, fabrication of the flight radiometer was initiated. The radiometers were painted at the piece-part level, assembled into four sensors, and then the units were delivered to OSC for flight unit integration.

3.2.6.2.2 Solar Cells. During Phase II, one change was incorporated into the solar cell design. At PDR, only the load voltage and short circuit current of the gallium arsenide solar cells was to be measured. However, because the cells would be traveling into and out of the solar illumination, variation in the measurements would be difficult to determine. Any variation in the readings was required to determine the effect of the arcjet firings on the cells. Therefore, it was decided to take measurements of open circuit voltage instead of load voltage.

The TRW-supplied solar cell was tested during the IMS Test with the cell mounted in the proposed flight orientation relative to the arcjet exit plane. Measured open circuit voltages ranged from 725 mV at 360 sec after start to 685 mV at 850 sec. A short circuit current of 28 mA and a cell temperature of 285°F were measured at a later time. The cell showed a 30% increase in short circuit current after exposure to the arcjet firings, although changes in check lamp output cannot be ruled out.

During final inspection of the solar array assembly, it was determined that the entire backside of the array substrate had been painted with thermal paint, leaving no where to mount the assembly thermistor. After a small amount of paint was removed for mounting the thermistor, the solar array witness plate was shipped to OSC for integration into the flight unit.

3.2.6.2.3 TQCMs. The hardware for this part of the contamination experiment was off the shelf and no activities were conducted relative to this instrument in Phase II of the ESEX program.

3.2.6.3 Optical. During Phase II, two changes were considered for the optical experiment on ESEX. The first change was the addition of a filter to the camera. The baseline camera for the program was one used on the Air Force STEP program which was approximately 4 inches in length. This length grew to 7 inches over the course of the STEP program, necessitating the relocation of this camera on the diagnostic deck. As a result of the move, the camera would now see the bright arcjet anode which would overwhelm any other image within the camera's view, specifically the arcjet plume. Therefore, a permanent filter was added to attenuate the anode glow so that the plume could be viewed. PAC had previous ground experience with a 900 nm filter for observing anode effects and a 656 nm filter for observing anode and plume effects (the hydrogen alpha line radiates at 656 nm). With the filter in place, the camera would collect the optical image normally and provide the data to the CCU to process. The processing results in a color-coded temperature band in the anode to indicate whether or not hot spots have developed due to arc attachment problems with the plume showing up as an intense colored area. After some technical trades were performed, the 656 nm filter was chosen for the flight camera.

The second change considered was the addition of a baffle to the camera to prevent stray light from entering the lens and adversely affecting camera operation. It was ultimately determined that the baffle would cause excessive heating of the camera and camera filter by trapping radiated heat from the arcjet. The maximum predicted temperature of the baffle at the end of a 15-minute thruster firing was 305 °F, mostly because of its low thermal mass, relatively high thermal radiation heating of the baffle surfaces from the thruster and plume, and high convective plume heating of the surfaces. The maximum predicted temperatures for the filter and camera at the end of a 15-minute thruster firing were 220 °F and 106 °F, respectively. Cases were run for various alternate baffle design options including increasing the thermal mass of the baffle and providing thermal isolation between the baffle and the camera with the use of fiberglass washers. None of these options were successful in maintaining the camera and filter within their temperature limits. While the camera body might survive high temperatures with no degradation in video performance, the filter was a major concern. The 656-nm Balmer hydrogen spectral line pass band of the filter is temperature dependent, and the glass window in front of the filter has a reflective surface blocking band that is also temperature dependent. The combined temperature shifts of these two optical elements in series with the camera field of view was thought to be great enough to cause unacceptable video quality. It was determined, however, that without the baffle, the maximum camera and filter temperatures achieved were acceptable (81 °F and 93 °F, respectively). Without the baffle, sunlight could have interfered with the camera imaging, but this would only have occurred during a small part of an arcjet firing (approximately 7% of total firing time) and was deemed acceptable. Furthermore, no damage to the internal CCD of the camera was anticipated to occur if sunlight did enter the lens, hence, the baffle was removed from the camera design.

After completion of final open slice and integration testing of the flight video camera and frame grabber electronics (FGU) at TRW, the camera was potted and subjected to thermal, vibration, and acceptance tests. Subsequently, the camera was integrated with the assembled FGU and flight housing.

A laboratory video camera equivalent to the flight video camera was used during the IMS to determine the optimum aperture setting for the flight camera since this could not be varied on-orbit. Based upon the video camera images of the arcjet plume taken during the IMS test, an optimum camera f-stop number of 8.0 was selected. The shutter can be controlled from full open to almost closed.

The video camera IR optical filter was temperature cycled from 14°F to +122°F for functional testing and -40°F to +122°F for mechanical inspection. No cracks were found in the filter after this testing. Final assembly of the flight camera and filter was then completed. The camera and filter assembly were vibrated and successfully passed functional testing with the FGU. Both units, camera and electronics, were shipped to OSC and integrated into the flight unit.

3.2.6.4 EMI. The diagnostic package thermal analysis was performed assuming that the EMI antennas would be painted with S13GLO white paint. Giving the antenna a known thermal surface and known thermal characteristics, detailed analysis or testing of the EMI antenna was avoided. TRW planned to paint the antennas in the same way as satellite antennas, however, the Arcjet ATTD antennas are encased in a TeflonTM-based radome cylinder that can not be prepped for painting without damaging the antenna. TRW investigated alternate means by which to paint the antennas without damaging them, and identified a method to place an S13GLO-painted 5-mil kapton radome over the antennas. Since TRW typically does not use these types of spiral

antennas, AFRL was consulted. AFRL saw no issues regarding performance degradation or use of the antennas for the ESEX application with the radome, and this solution was implemented.

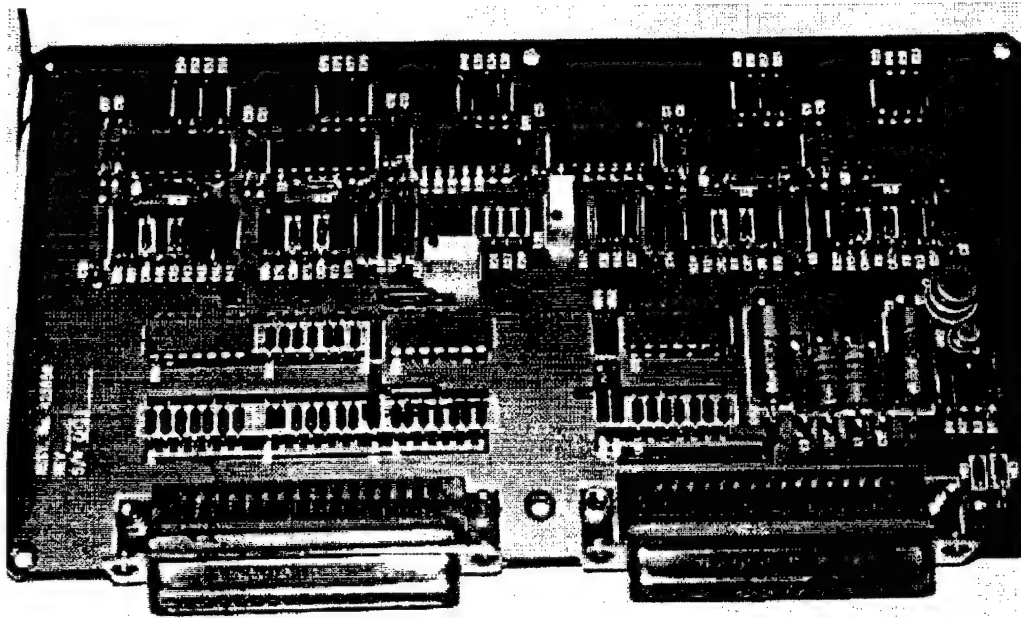
The second issue for the EMI antennas was that the predicted operating temperatures were below their specified temperature range of -65° to +160°F. The temperatures predicted for the antenna on the deployable boom with the S13GLO paint were -85° to +94°F. It was determined that the antenna cannot be maintained within acceptable temperature limits without active thermal control. An existing camera heater circuit had adequate margin to support both the camera heater and the heater selected for the EMI antenna. The set points for the camera heater circuit were eliminated so power would be supplied to the circuit continuously. A mechanical thermostat was added to the camera heater circuit and mounted to the camera body to control the camera within the acceptable temperature limits. The EMI antenna heater circuit was spliced in with its own mechanical thermostat (and mounted to the antenna body) which had set points appropriate for the EMI antenna thermal control.

3.2.7 Power Subsystem Design. During the first half of Phase II, the design of the PIU was completed, some of the components were built into breadboards and ultimately a protoflight PIU was fabricated. This work was conducted at the board level prior to integrating the individual boards together to make the PIU. These boards included: the telemetry conditioning board, the heater control board, the equipment converter, the command interface board, the battery charger, and power distribution assembly (PDA). The completed telemetry conditioning board, command interface board, heater board, equipment converter assembly, and battery charger assembly are shown in Figures 33 to 37, respectively.

Selection of the battery supplier was also performed during Phase II. Proposals were received from Eagle-Picher Industries, Inc.TM and Yardney Technical Products, Inc.TM Yardney'sTM primary battery design did not meet the operating voltage range required by the arcjet and PCU and the alternate design, which did meet the voltage range requirement, had insufficient margin at the lower voltage limit. The data provided on the battery design proposed by Eagle-PicherTM showed the capability to perform its required mission. Based on Eagle-Picher'sTM technical capability as well as their ability to provide support, hardware and testing within the program schedule, they were chosen to be the Arcjet ATTD battery supplier.

One of Eagle-Picher'sTM initial tasks was to complete nine charge/discharge cycles of a twenty (20) cell silver-zinc battery. Results indicated that there was minimal voltage degradation after nine cycles. The lowest voltage reached was 1.272 volts/cell (average), as shown in Figure 38, and this occurs at 40 seconds into the discharge. This was at the point where the current first reached its maximum value of 175 amperes. The maximum temperature, corresponding to a rise of approximately 80°F, was reached approximately five minutes after the discharge was completed. As a result of the 20-cell testing, Eagle-PicherTM proposed a battery that contained 126 silver-zinc cells, equally divided into three subassemblies, each containing 42 cells.

Qualification testing of a single silver zinc battery subassembly was completed by Eagle-PicherTM. The testing verified the satisfactory performance of the battery subassembly during and after exposure to the dynamic and static test conditions simulating actual mission requirements. The battery subassembly successfully met or exceeded all the specified requirements of the qualification test procedure (QTP-589) with the exception of four anomalies. Each anomaly was in regards to the requirement that the battery output voltage be within a range of 52.5 to 61.0 volts. The anomalies occurred as follows:



Figures 33. PIU Telemetry Conditioning Board

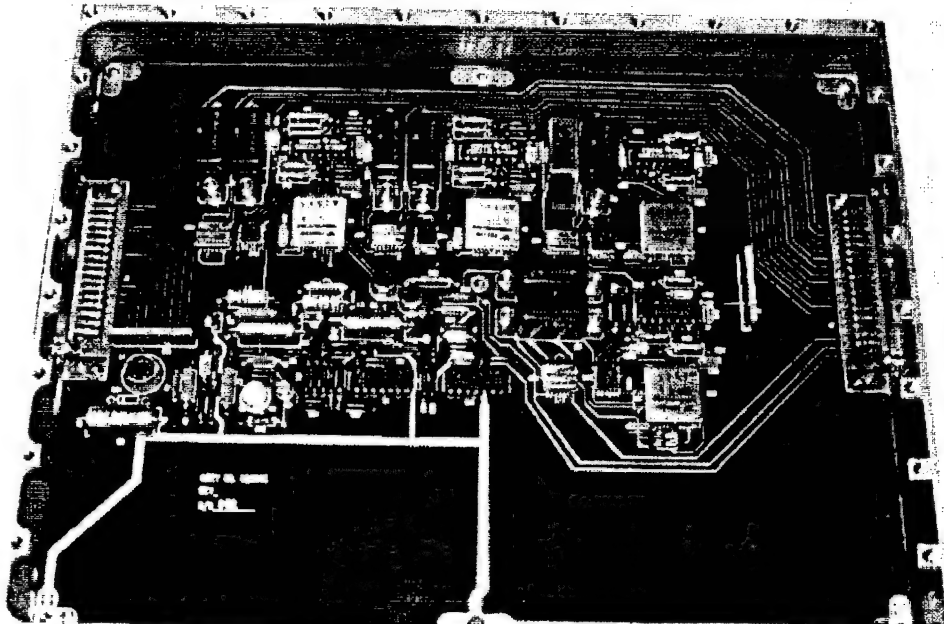


Figure 34. PIU Command Interface Board

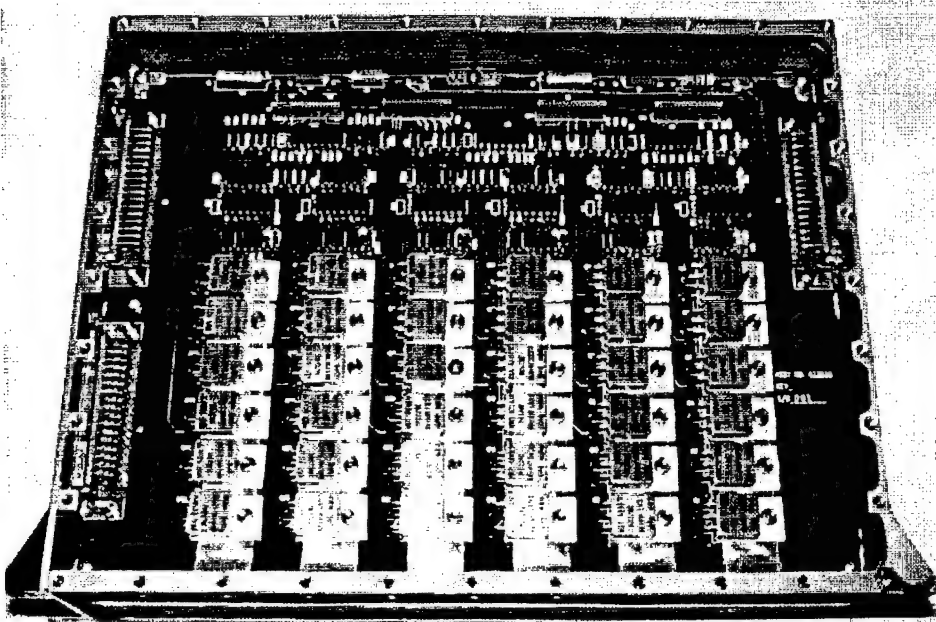


Figure 35. PIU Heater Board

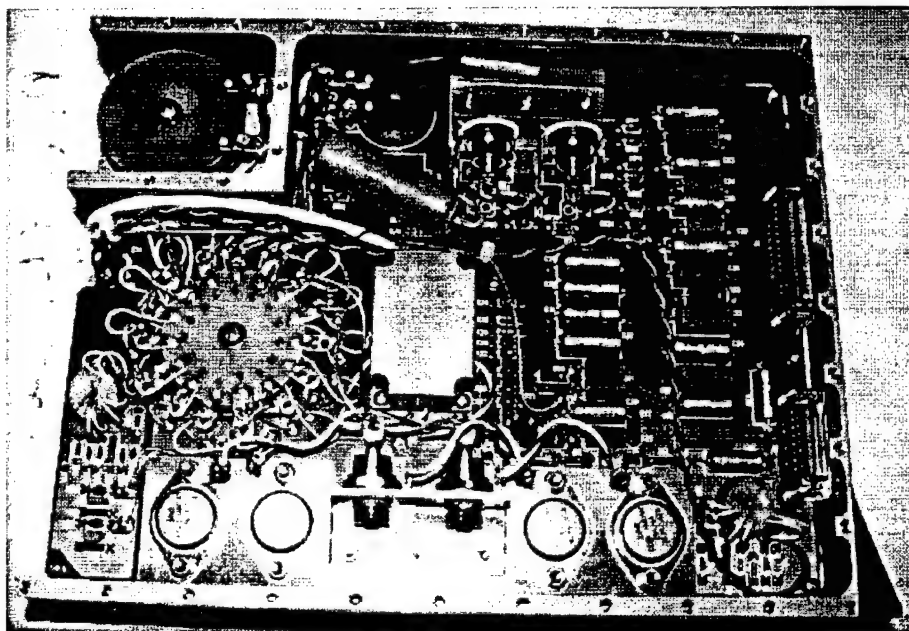


Figure 36. PIU Equipment Converter Board

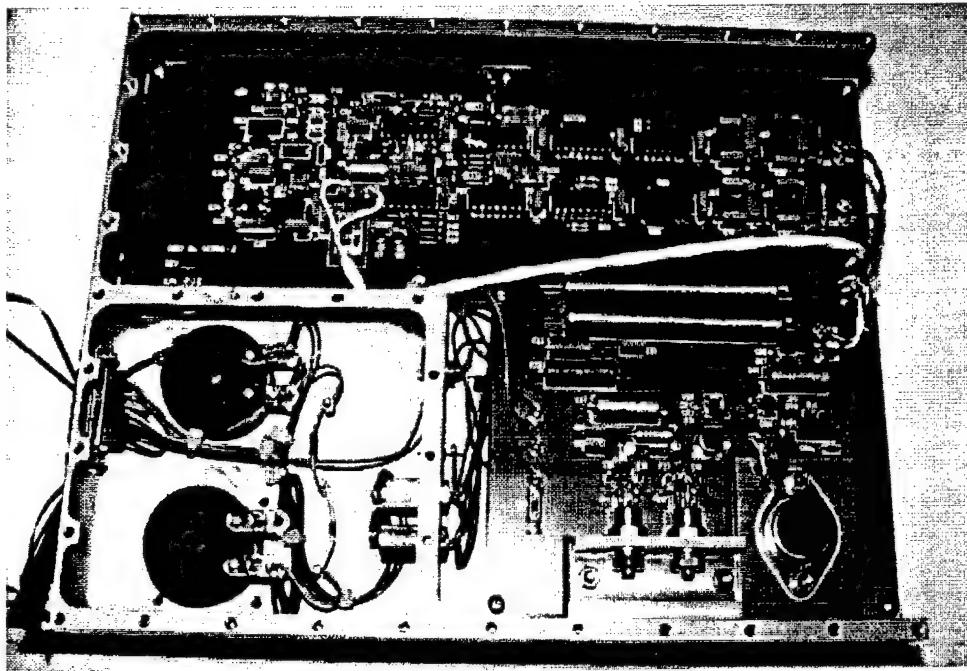


Figure 37. PIU Battery Charger Assembly

PACK (20 CELLS) VOLTAGE vs TIME
DISCHARGE CYCLE

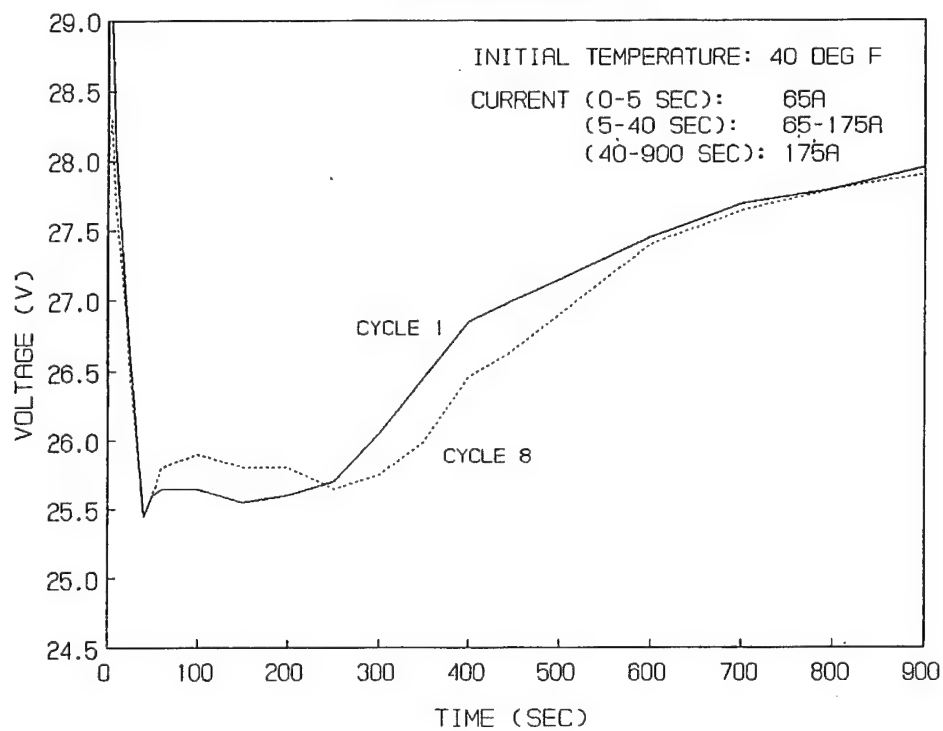


Figure 38. Battery Cell Voltage Performance

- The discharge voltage during the random vibration test exceeded the maximum voltage limit of 61.0 Vdc. The maximum voltage recorded during vibration discharge was 62.85 Vdc.
- The discharge voltage during thermal vacuum cycle #1 exceeded the maximum voltage limit. The maximum voltage recorded during thermal vacuum discharge was 62.45 Vdc.
- The discharge voltage during thermal vacuum cycle #2 dropped below the minimum voltage limit of 52.5 Vdc. The minimum voltage recorded during the thermal vacuum discharge was 50.25 Vdc.
- The discharge voltage during the final functional load test dropped below the minimum voltage limit. The minimum voltage recorded during the final functional discharge was 51.05 Vdc.

These anomalies demonstrated the inherent design characteristics of the battery and were not indicative of a hardware problem. Hence, the test was deemed successful.

Over the course of the program it was discovered that silver zinc batteries vent a gas during discharge and that the effluent consists of a combustible mixture of hydrogen, oxygen, water vapor, and potassium hydroxide vapor. However, the composition and quantities of these constituents had never been quantified since previous uses of the silver zinc cell had consisted of single-use applications (i.e. launch vehicles.) Therefore, the Arcjet ATTD program developed a methodology to capture the battery effluents during a discharge and determine its composition through chemical analysis. This effluent testing was conducted during the battery assembly qualification test.

The results from the test and analysis of the effluents are summarized in Table 12. The quantity of oxygen was calculated to be one-half of the hydrogen amount. It was not possible to experimentally quantify the amount of oxygen and nitrogen in the gas sample because the composition of the gases resident in the battery before start of discharge was not known. The battery ullage was filled with air and subsequently pressure leak tested with nitrogen - diluting the air to an unknown extent. Because hydrogen can only be formed via electrolysis of water, oxygen is reported at a calculated value of one-half that found for hydrogen. These results apply to the discharge products from one battery subassembly. Since the Arcjet ATTD flight unit has three subassemblies, these results must be multiplied by three to determine the total effluent quantity.

Table 12. Battery Effluent Test Results

Test Parameters	
Test Duration	75 Minutes
Maximum Battery Temperature	115 °F
Analytical Data	
Constituent	Amount ¹
Water	0.28 mg
Potassium Hydroxide	3.3 µg
Hydrogen	35.3 µg
Oxygen	17.7 cc ²

1 Reported amounts are corrected for battery and sampler ullages, pressure (battery pressure = sampler pressure + 5 psi) and temperature (battery temp max = 115 °F)

2 Oxygen calculated as ½ the amount of hydrogen

Electrical testing of the battery charger unit showed that a noise coupling problem occurred at high temperatures; between 122 - 140 °F. The concerns regarding the noise were: (1) the noise levels were equal to the allowable noise levels per the ARGOS ICD and (2) the noise was a result of the charger switching between the current mode and voltage mode. This switching could overstress the components within the PIU and cause a failure which could result in an overcharged battery (if the other battery charging safeguards also failed.) Values were changed for several charger components that improved the stability of the battery charger at high temperatures in the voltage control mode, but did not remove it. Therefore, it was decided to accept the PIU with the noise-reducing changes and terminate further efforts to isolate the cause. This decision was based on several factors: (1) the PIU maximum expected temperature is 82°F, significantly less than where the problem occurred; (2) the PIU is also operated in the current mode, not voltage mode; and (3) the resultant noise is well within the radiated noise requirements of the ARGOS ICD. The unit was reworked, inspected and underwent protoflight vibration testing. After successfully passing post-vibration functional testing, the PIU was installed into the flight unit at OSC.

One other change was made to the PIU as required by the EMI Electronics. The EMI Electronics needs continuous -15V power (3 watts) to prevent a potential overstress of the A/D converters within the unit. If this power was not present before the main +15V and +5V power was applied, an over-current condition could result and overstress the converters. Therefore, a simple fix was implemented within the PIU to hardwire the -15V line to the EMI electronics.

Two prototype KilovacTM relays were tested in the Arcjet system at PAC to switch the high power battery voltage to the PCU. Other relays from the same lot were subsequently qualification tested. Concerns arose regarding the dynamic flight worthiness of the prototype parts and to the exact mounting configuration. A shock mount pad was considered, however, shock mounts do not always yield definitive and acceptable results. The KilovacTM relays flight qualification indicated that there is considerable margin to the Arcjet requirements as long as the structure did not have any high resonant peaks. To determine if there was an adequate acceptance level vibration margin, the KilovacTM relays were instrumented and tested during the structure vibration testing and subjected to the flight unit random vibration levels according to TRW's vibration test plan for the Arcjet KilovacTM relays. One monitor accelerometer was placed on the underside of the PFS platform between the two relays and connected to a data recorder. The relays were connected to a power supply, load resistor and oscilloscope. This test set up allowed determination of whether or not the relays chattered during exposure to the flight random vibration loads. The relays were manually opened and closed to verify proper operation before and after each vibration test. The digital storage scope was set for 1 ms/div and to trigger at 12.0 Vdc. The relay contacts were connected to +25.0 Vdc through a 2.5 Ohm, 1 watt resistor as specified in the test plan. No triggering from contact closure was detected during the vibration test.

KilovacTM expressed further concern to TRW regarding the use of prototype parts in space flight applications. This was a known risk, but these parts were selected since no other relays were available which met the requirements. This risk was reduced by the testing performed on the relays, such as the random vibration test described above, since this was the best means to verify these relays were flight ready without subjecting them to a full component qualification program. In addition, the flight requirements were also small (1 cycle). Flight results confirmed the successful operation of these components.

3.2.8 Thermal Management Subsystem Design. During Phase II, an overall flight unit thermal model was developed. In order to adequately represent the thruster and propellant feed

subsystems, PAC provided TRW with simplified thermal models and thermal interface data for the PFS and arcjet.

Preliminary hot case analyses for the overall flight unit were performed to help size the initial panel radiator areas. All equipment panel temperatures were maintained within their prediction limits with the exception of the camera electronics unit (CEU). With all of the available panel area for the CEU utilized as radiator area, the maximum predicted panel temperature exceeded the prediction limit by approximately 7°F. Only a 22°F margin existed between the maximum predicted panel temperature and the acceptance limit (29°F margin is required by MIL-STD-1540). The final thermal analysis would not change this result significantly, but implementing any design changes could wait for a more definitive analysis.

The thermal management subsystem CDA was conducted on July 12, 1993 at TRW with representatives from the TRW Arcjet ATTD project and thermal systems design and test engineering project in attendance.

Development of the flight unit MLI included a fit check of the ESEX MLI templates and to develop MLI templates for more complicated geometries, such as the boot around the EMI antenna hinge. After manufacturing of the flight unit thermal blankets was completed, some of these blankets were painted with S13GLO paint, and the thermal blankets (with the exception of the side panel blankets) were installed. Included in this effort was the verification testing of the thermal "dog house" for the EMI antenna boom hinge.

3.2.8.1 Mission Phase 0/I Analyses. A thermal analysis of the Arcjet ATTD flight unit during the ARGOS ascent phase (Mission Phase 0) was also completed. The purpose of this analysis was to define the time after liftoff that power was required by the ESEX flight unit from the ARGOS host vehicle. Heaters were required to eliminate the possibility of equipment temperatures exceeding cold survival limits. According to ARGOS (i.e. Boeing) personnel, power would be provided between 84 to 90 minutes after liftoff. A conservative cold case analysis was performed to determine whether this was acceptable. The goal was to demonstrate that the predicted component temperatures had at least a 20°F margin over their survival limit temperatures.

Key launch vehicle and host vehicle interface assumptions included the following:

- ESEX and the host vehicle were maintained at $50 \pm 2^\circ\text{F}$ prior to liftoff by the launch vehicle air conditioning system.
- Prior to separation, ESEX is enclosed in the launch vehicle payload adapter
- Holes in the payload adapter and the payload attach fitting truss were closed out with MLI (although ultimately not true in the liftoff configuration).
- Spacecraft separation occurred at 63.3 minutes after liftoff.
- The ESEX mounting platform on the host vehicle was maintained above 9°F by the host vehicle thermal control system.

The first analysis, which was very conservative, determined that it would be acceptable to provide power to ESEX between 84 and 90 minutes after liftoff as shown in Table 13. After the flight unit had been delivered to AFRL, this analysis was refined to identify the specific time at which survival limits of the ESEX hardware would be exceeded in case ARGOS had trouble supplying power to ESEX. This initial 90-minute period was then expanded to approximately 4 hours. Ultimately, it was determined that if the flight unit was preheated on the launch pad, it could survive for up to seven hours on-orbit without heater power. This preheat approach was implemented using the flight unit's internal heaters, but the added thermal margin was not required.

Table 13. ESEX Component Temperatures (°F) at 90 Minutes after Liftoff

Component	Predicted Temperatures (°F)	Survival Limit Temperatures (°F)	Temperature Margin (°F)
Compartment			
Battery Cell (P1)	45	20	25
PCU	45	-20 ¹	65
EMIE	42	14 ¹	28
TQCME	42	-20 ¹	62
Battery Cell (P4)	44	20	24
Battery Cell (P5)	44	20	24
CCU	20	-40 ¹	60
CEU (FGU)	18	-67	85
PIU	30	-20 ¹	50
Relay	42	-67 ¹	109
Diagnostic Platform			
Camera	-10	-40	30
Camera Filter	-11	-40	29
Radiometer #1 Thermistor ²	-46	-67	21
Radiometer #2 Thermistor ²	-44	-67	23
Radiometer #3 Thermistor ²	-16	-67	51
Radiometer #4 Thermistor ²	-1	-67	66
Solar Cell Thermistor	-44	-67	23
TQCM Sensor #1 ³	-39 ³	-387	348
TQCM Sensor #2 ³	-41 ³	-387	346
TQCM Sensor #3 ³	-53 ³	-387	334

¹ Temperature given is lower protoflight (operating) limit.

² Thermistor temperatures for radiometers are at the sensor (not the base).

³ TQCM sensor temperatures predicted assuming maximum conduction to platform(unconservatively). Not a concern since survival limit is extremely low.

3.2.8.2 Mission Phase II Analyses. A thermal analysis of the baseline configuration showed that the maximum predicted temperatures of TQCM #2 and #3 during an arcjet firing exceeded the maximum temperature limit specified by the vendor. The performance of the TQCMs at temperatures above 60°C was uncertain. To adequately dissipate the heat from TQCMs #2 and #3, silvered TeflonTM tape radiators with areas of approximately 59 and 90 in² respectively were added to the thermal design. To avoid unacceptable heating of the radiators from

the flight unit structure during arcjet thruster firing, the TQCMs were thermally isolated from the diagnostic platform with stainless steel fasteners and standoffs consisting of fiberglass washers.

The final detailed analysis of the PCU panel was also completed. Thermal control for the PCU was to be provided by cooling the panel to a low temperature prior to thruster firing. During the firing when the PCU heat dissipation was high, the PCU was maintained within its temperature limits by storing the dissipated power as sensible heat in the thermal mass of the PCU and the panel. Design requirements for the panel changed significantly during the course of the program. The efficiency of the PCU increased from 93 percent to over 95.5 percent. In addition, excessive panel weight became a non-issue since significant weight margin existed on the ARGOS host spacecraft. Beryllium was originally selected as the baseline panel material because of its high specific heat (0.4 Btu/lbm-8°F versus 0.2 Btu/lbm-8°F for aluminum) and it was determined that the PCU temperature requirements could be met with a beryllium panel weighing 51.7 pounds. Similar temperature results were obtained with an aluminum panel weighing 85.1 pounds. Due to the tremendous cost advantage of using aluminum over beryllium, the aluminum panel was selected as the recommended design.

A thermal analysis of the EMI antenna boom was performed to verify the preliminary thermal design accommodations for the TQCM sensor mounted on the boom. Worst hot and cold operating cases were considered. The analysis was performed assuming silvered Teflon™ as the radiator surface for the TQCM radiator. However, since the cold temperature extreme of the radiator plate was near the temperature limits of the adhesives used to bond the silvered Teflon™, second surface mirrors were used instead. The predicted temperature extremes of the EMI antenna were found to be well within their temperature limits.

3.2.8.3 Mission Phase III Analyses. An analysis was performed using the overall flight unit model to determine the minimum battery temperature expected during battery discharge portion of the ARGOS mission Phase III operation. The purpose of this analysis was to determine whether the battery sub-assemblies would be able to survive without any heaters. The minimum battery temperature was predicted to reach approximately -50°F which is below the minimum temperature of -22°F specified by Eagle-Picher™. As a result heaters were incorporated into the thermal design for ARGOS mission Phase 3 operation.

3.2.9 Structure Design. During Phase II, extensive use was made of the CATIA capabilities that existed between TRW and OSC. TRW was responsible for the overall flight unit design and OSC was responsible for the detailed structure design and the integration of the flight unit. CATIA models of the overall flight unit layout were frequently updated by TRW and transferred to OSC in support of their work. CATIA models were also shared with Boeing after the ARGOS was designated as the Arcjet ATTD host spacecraft.

As a result of assignment to the ARGOS spacecraft, the design of the mechanical adapter of the flight unit was changed. At PDR, the mechanical adapter was of a conical configuration. This was changed to a six-point mount as shown in Figure 39 to minimize the thermal conductance across the physical interface between the host spacecraft and the Arcjet ATTD flight unit. This six-point configuration was very easy to implement with the core frame approach used for the flight unit, and also provided better access to electrical connections between the two vehicles.

A change in the mounting adapter material was also made from aluminum to titanium. The thermal conductivity of titanium is approximately 1/25th that of aluminum. Therefore,

significantly less heat would be transferred across this interface to the ARGOS spacecraft. Alternative approaches, such as placing insulators below the structure mounting feet, were

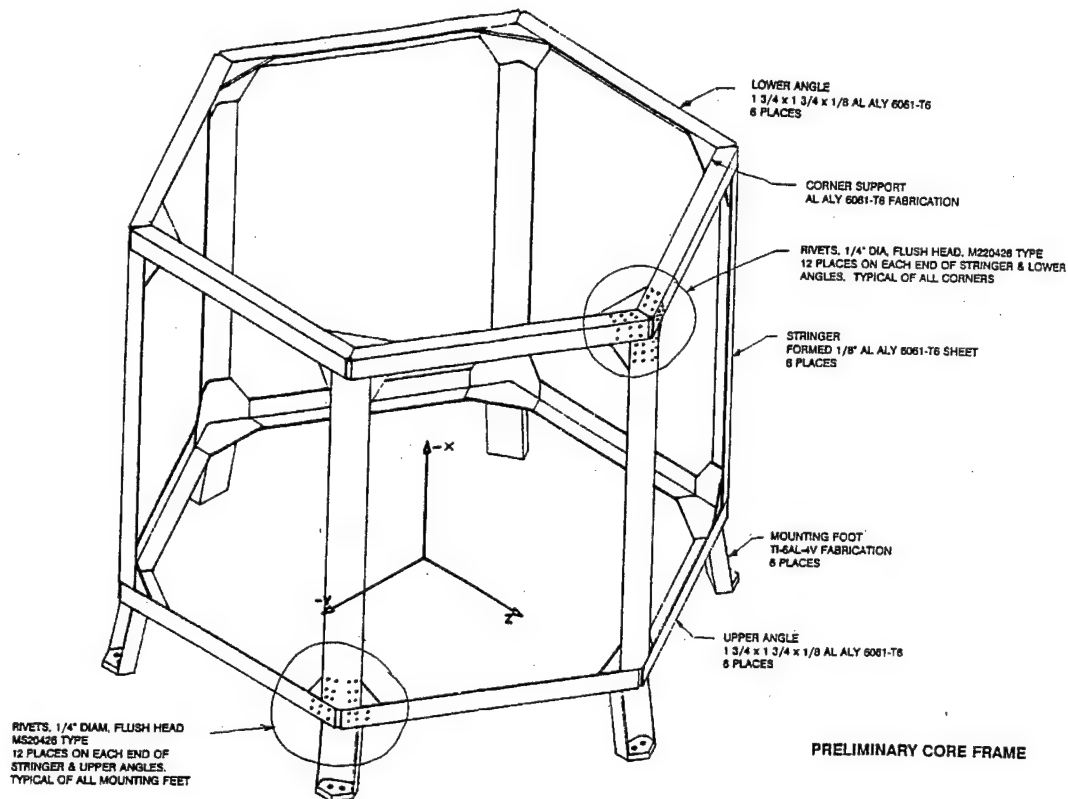


Figure 39. Arcjet ATTD Six-Point Mounting Configuration

considered but found to be less reliable than the titanium material substitution. The six adapter feet were of a bolt-on design to allow for adjustment in aligning the frame with the spacecraft axes.

Based upon NASTRANTM dynamic simulations performed by Swales, OSC increased the diagnostic and PFS platform thicknesses from 0.75 inches to 1.125 inches. Once the PFS platform was manufactured, it was shipped to PAC for integration of the PFS System.

OSC performed two deployment tests of the EMI boom, one at ambient temperature and one after a cold soak at -50°F. In both tests, a zero-g environment was not simulated. The boom could not be deployed in the vertical plane since the spring was unable to overcome the force of gravity and counterbalances were not available; therefore, it was deployed in the horizontal plane instead. The tests utilized a flight antenna, a TQCM radiator, a TQCM mass mockup, cable harness, and MLI blankets located on the boom hinge. The boom failed to deploy fully the first time. Investigation into the cause of the failure led to the discovery that one of the damper mounting screws had loosened, backed out and jammed the hinge mechanism. These screws were from the original assembly of the boom, and the locking elements had worn off. It appeared that the screws loosened during handling and/or shipment of the boom to the test facility. New patch type locking element screws were installed and the hinge reassembled. The subsequent cold

deployment test was successful. It was also demonstrated that the boom hinge blanket provided no impediment to the deployment.

After fabrication of the core frame assembly was completed, source inspection of the frame, side panels, and platforms was completed, and a measurement of alignment critical tolerances was completed successfully.

3.2.10 Flight Unit Integration. The flight structure was integrated with mass mockups and successfully completed a structural qualification testing. The modal frequencies measured during this test are provided in Table 14.

Table 14. Arcjet ATTD Flight Unit Modal Frequencies

Mode	Frequency (Hz)		Description
	Actual	Required	
1	50	25	Lateral plate mode of Panel 4
2	50	25	Lateral plate mode of Panel 5
3	51	25	Lateral plate mode of Panel 6
4	55	25	Lateral plate mode of Panel 1
5	61	50	Axial plate mode of PFS platform
6	65	50	Axial plate mode of diagnostics platform

Following the test, the structure was inspected and no damage was found. The mass mockups were removed and mechanical integration of the experiment components was initiated. The thruster, power cable and PCU were the first components integrated with the structure, and the alignment of the thruster was completed. Measured alignment of the thruster (including measurement error) was 0.221" radial offset and 0.049° angular offset. This was well within the allowable limits of 0.360" and 0.14°. The PFS platform was integrated with the structure next and the propellant line connected to the thruster. The tank tripod was then fixtured to the core frame and matched drilled.

The diagnostics platform was built up with the EMI antenna boom, witness bracket, camera, radiometers, and the TQCM radiators. The camera, TQCM and EMI electronics boxes, the CCU and PIU were mounted to the side panels which were mounted to the core frame. Following hipot testing and thermal vacuum bakeout, interfacing harnesses were integrated, trimmed to length, and completed.

During integration of the harness with the PCU, a problem with the 100-pin connector installed on the PCU for command/telemetry was discovered. The connector was cadmium plated, which differed from the connector type specified on the source control drawing. TRW materials and processes (M&P) engineers were consulted and it was their consensus that the option of least risk was to remove and replace the connector. The next best option was to coat the connector, and the option of most risk was to use the connector as is. M&P reviewed drawings and hardware photos and verified that coating the connector was feasible with the PCU in the integrated configuration it was in. Aerospace Corporation was also consulted and provided connector data, location and expected temperature information. Aerospace's consensus was that as long as the expected temperature data was accurate, the PCU connector should be acceptable as is. This was based on a NASA Goddard study (MTR No. 313-004, June 1981) which showed that cadmium

does not outgas at the temperatures the PCU connector was expected to reach (87-104°F). At this point, it was decided to use the PCU cadmium coated connector as is.

The functional testing of the flight unit performed by OSC consisted of interface testing between the individual subsystems and the CCU (1553 data bus). Interface testing consisted of integrating the PIU and monitoring the lines before connecting the rest of the subsystems. After checkout of the PIU interface was completed, the CCU was connected, followed by the rest of the subsystems. Aliveness tests were also performed as part of the interface testing including the monitoring of bus current and voltage as a function of subsystem on/off operation.

Functional testing of the pressure control valve and the arcjet flow control valve was also conducted. This test verified valve voltage and pulsewidth with a resistive load applied on the line. No cycle testing of the valves was performed in order to limit the dry cycles accumulated.

During the system level integration testing at OSC, the following problems were found:

- The differential inputs to the analog I/O were not connected to ground by the cable harnessing and resulted in the CCU not being able to read various thermistors and transducers. An adapter cable that connects the inputs to ground was fabricated and installed.

- The CCU was not able to turn on several heater circuits. The analog I/O boards were pulled from the CCU and inspected, and several chip resistors were of the wrong value. The chip resistors were replaced, and proper operation of the boards was verified.

- Two heater circuits failed in the on condition during retesting after the chip resistor repair. Two of the MOSFETs and drivers on the heater control board in the PIU were damaged by electrostatic discharge (ESD). The parts were replaced and the circuits successfully retested. The failure was the result of poor grounding of the equipment panels during testing.

- Thermostatically controlled heaters on the camera and EMI antenna boom failed to operate. The thermostats would not close at cold temperatures. New thermostats were received, passed bench testing, and were installed on the spacecraft. The "faulty" thermostats were later found to operate nominally during a bench test. It was theorized that the thermostats, in their flight configuration, could not get cold enough to close during the ground test.

- Testing of the TQCM system verified the CCU interface with the TQCM electronics, but a problem was found while commanding the sensors,. Commanding the sensors to cool resulted in them heating up. Commanding the sensors to heat resulted in them cooling down. It was determined that the output command lines from the TQCM Electronics to the TQCM sensors were reversed. The reversed signals were "un-reversed" with the use of an adapter harness, which routed signals to produce the correct responses in the sensors as commanded by the electronics.

- Commanding of the KilovacTM relays to the enabled state resulted in damage to some transistors within the PIU. Troubleshooting determined that the relay circuit was wired incorrectly to open and close simultaneously by the PIU, causing no action by the relays and causing the driving transistors to fail. The damaged transistors within the PIU were replaced and the KilovacTM relay circuit was rewired with the use of an adapter harness and some rewiring of the PIU command interface assembly (CIA) board.

- In testing the EMI Experiment, oscilloscope data showed that the EMI Electronics allowed generation of an extra clock signal. The EMI Electronics should only have generated 18 clock signals, but, as shown in Figure 40, 18 ½ signals were actually being generated. After the extra signal was discovered, the unit appeared to stop processing antenna inputs and stayed in calibrate mode. Although these inputs were strictly ambient noise, the unit seemed to stop registering any change in the noise floor. The EMI Electronics Unit was directly connected to a noise generator, which produced a 2 GHz signal, and still the unit did not respond, which is typical of a latch-up

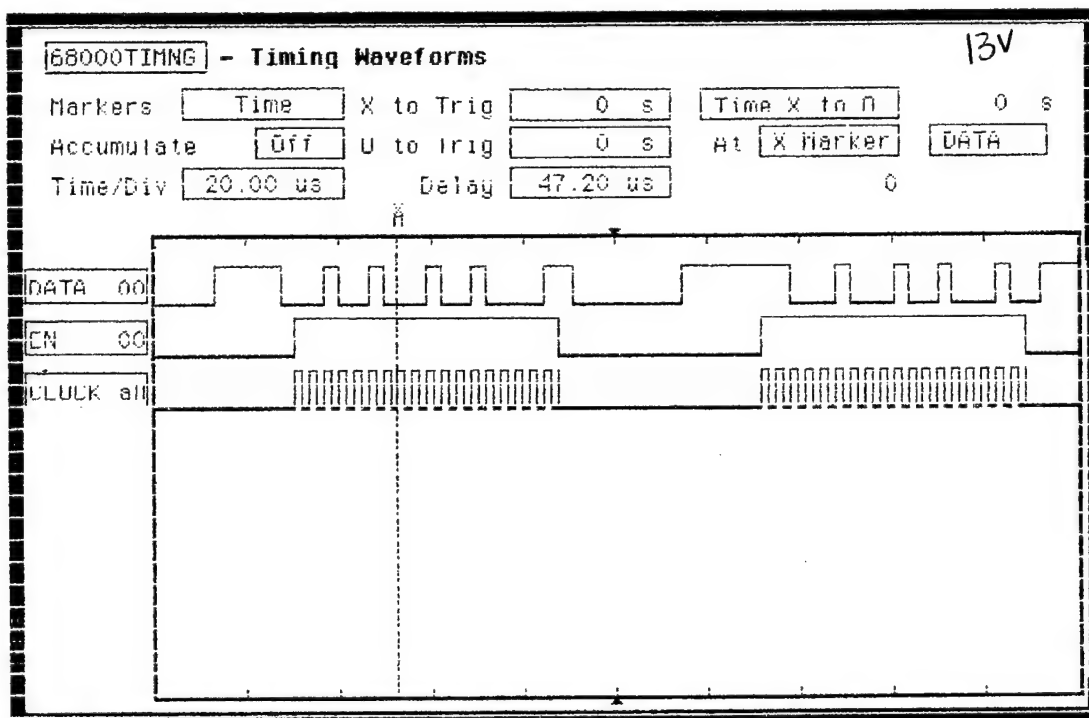


Figure 40. Extra Clock Signal from EMI Electronics

condition. At this point, the problem appeared to be in the EMI Unit and it was removed from the flight unit and returned to TRW for unit level troubleshooting.

At TRW, the suspect electronics box was integrated with the original test set used to qualification test the unit. In this configuration, however, the unit performed as expected and per specification. The electronics were then integrated with the CCU cardcage. Again, the unit performed acceptably with the exception of the additional clock signal. One theory behind the latch up condition was that the CCU and EMI units got out of synch and caused a latch up to occur. It was also determined that the EMI electronics design did not have power on reset capability, which might allow for such latch ups to clear.

A timing analysis was performed of the signals sent to the EMI unit by the CCU. Based on this analysis, the EMI Electronics timing requirements were reviewed and the appropriate modifications implemented. A Schmitt Trigger, inverter and resistors were added to the timing circuit to provide a more compatible, higher drive capability interface between the EMI Electronics and the Command and control Unit (CCU). These changes were first incorporated into the EMI Electronics breadboard and successfully tested in the Arcjet ATTD flight unit. The EMI/CCU interface signals were connected to a logic analyzer and digital storage oscilloscope and verified to be correct. Pictures of these displays were taken and are provided in Figure 41. The two top photos show the 18 clock signals from the CCU and the data read by the EMI Electronics. The bottom right photo shows the EMI Electronics in the data enable mode and the data generated by the unit. The bottom left photo shows the data captured by the CCU. These data show that the unit is toggling between the two antennas and not stuck in the calibrate mode which it seemed to be when the unit problem was first discovered.

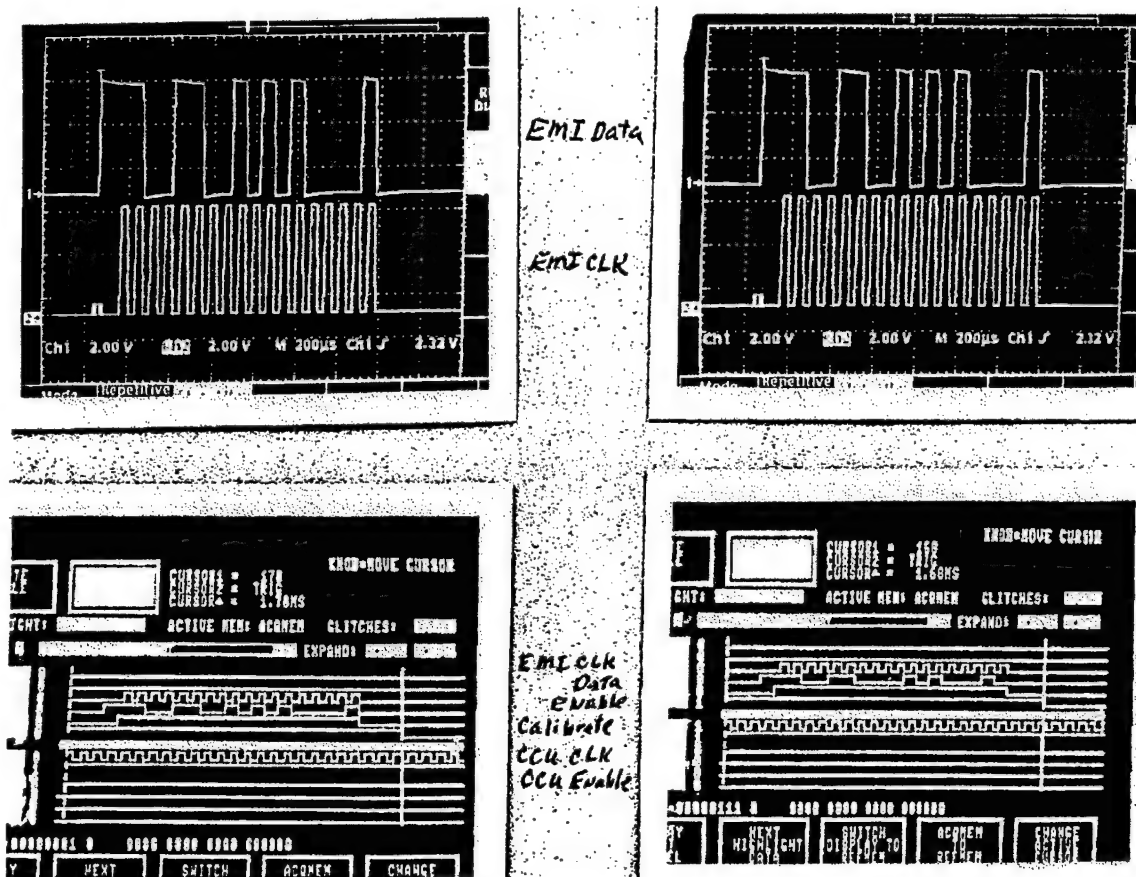


Figure 41. EMI/CCU Interface Signals Captured During EMI Breadboard Testing

- In testing the accelerometer, the signal appeared to be saturated, even in the absence of active stimulation. It was determined that the current accelerometer system was designed to respond to a frequency response that is greater than that produced by the arcjet thruster. The thruster produced a slow rise in acceleration over a period of 85 seconds, essentially producing a dc-like signal. Sections 3.2.6.2.1 and 3.3.1 explain the details of the problem and the solution implemented.

Prior to shipment of the integrated flight unit from OSC to TRW, the TRW system engineer/program manager and quality engineer performed an on-site review of the hardware and the test data. No significant hardware problems were found and the flight unit was deemed acceptable for shipment. TRW witnessed the flight unit close up, loading into the shipping container and loading of the shipping container onto the air-ride truck. The flight unit left OSC on 30 January 1995 and arrived at TRW on 2 February 1995. None of the shock indicators placed on or in the shipping container were triggered to indicate any rough handling during transportation. The unit was secured onto the in-plant transporter and moved to the Arcjet Integration and Test Facility.

The flight firmware was then modified to acquire accelerometer data ten times per second (super sampling) in order to prevent aliasing of the data. The data addresses were also revised to reflect the changes necessary in the CCU to accommodate the accelerometer.

3.3 PHASE III - FLIGHT QUALIFICATION and DELIVERY

3.3.1 Accelerometer Rework. The re-worked flight unit accelerometer (see Section 3.2.6.2.1) was fabricated and acceptance tested, functionally and environmentally, in a unit-level vibration test. During the burn-in testing of the flight accelerometer, it was observed that the unit output was not stabilizing within the expected timeframe after turn-on. According to the accelerometer manufacturer, the accelerometer output should stabilize within minutes of turn-on, but the flight accelerometer was not stable even after 24 hours. It was suspected that the accelerometer was damaged during protoflight vibration testing. Therefore, the flight unit was instrumented with a triaxial accelerometer and a low level sine sweep test performed from 20 - 2000 Hz. This test showed that the accelerometer was subjected to extremely high accelerations at its resonance frequency of approximately 1300 Hz. It was determined that the mounting configuration, which was designed for thermal isolation of the accelerometer assembly, did not provide enough structural stiffness to prevent damaging the accelerometer. Different dampening materials were tested with the assembly, but no acceptable material was found that would ensure the accelerometer would survive launch vibration levels. Therefore, the accelerometer housing was redesigned such that the unit was hard mounted to the flight unit side panel instead of being elevated. The lack of thermal isolation was accounted for in the ground processing of the accelerometer data. The accelerometer circuit card assembly and a new accelerometer were installed in the new housing, the unit was inspected, and pre-vibration functional testing was successfully completed. The accelerometer assembly was then vibrated at the unit level successfully integrated into the flight unit and functionally tested as part of the flight unit pre-vibration functional test. The accelerometer continued to work within specification for the rest of the environmental testing.

3.3.2 Software Verification. The first test performed on the flight unit was a combined post shipment functional/flight software acceptance test. This testing served two purposes: to verify the functionality of the flight hardware and to verify the ability of the flight software to control it. Some of the results from this testing were as follows:

- Calibration curves were revised for telemetry parameters T7A, T7B, T5 and T6 to correct the telemetry processing.
- The software that controlled the timing of the TQCM and EMI experiment data had to be refined to properly synch the data between those units and the CCU.
- During the low power PCU test, it was determined that three signal return lines from the PCU were not connected to chassis ground. A harness adapter was installed which brought these return lines out from the PCU and grounded them close to the CCU on Panel 6. The PCU was then successfully operated at 4 kW approximately one year since its last functional test and after two ground transports.
- The propellant feed valve and the pressure control valve were both cycled. The feed valve was cycled twice and valve opening was verified by the expulsion of GN₂ into a bag on the end of the thruster. The dual pressure control valve was cycled 20 times but the duty cycle was too short to produce a measurable change of pressure. However, the valve could be heard cycling.
- Some software modifications were required and implemented to enable the frame grabber unit and the video camera to interact and exchange commands and telemetry.

- The EMI Experiment was stimulated using a 1-18 GHz source. Both antennas showed proper responses in the 2, 4, 8 and 12 GHz frequency ranges.
- The breadboard accelerometer was integrated into the flight unit and Panel 6 was lowered to a point where the accelerometer was not saturated in the 1g environment. With small movement of the panel, the flight telemetry showed the appropriate response.
- The PIU battery charger indicated a 10 volt drop between the battery simulator and the telemetry being read by the CCU. Oscilloscope data showed that the battery charger generated high frequency noise that interfered with the battery telemetry circuit. A capacitive filter was added to the PIU PDA slice and the retest verified correlation between battery voltage and telemetry voltage within 0.2 volts.

In preparation for PCU high power testing, the arcjet power cable adapter end was fit checked with the test adapter used to shunt the PCU power to the arcjet resistive load. During that fit check, the test adapter galled, preventing removal of the adapter. The Arcjet ATTD development engineer from PAC was brought in to support the removal efforts. Many different attempts were made in order to free the galled part with no success. There were limitations on what could be done to correct the problem due to the fully integrated level of the hardware and the amount of torque that could be comfortably put on the adapter without potentially damaging flight hardware. In order to allow testing to continue, it became evident that the only approach was to work with the adapter in this configuration and to determine how the adapter could be modified for flight. The adapter was shortened and a larger diameter, coarser thread hole was drilled into the shortened adapter. A new test adapter piece was fabricated and installed, also with the coarser threads. Figure 42 represents the flight configuration of the cable at the test adapter end.

3.3.3 EMC Testing. Following the functionality and software verification tests, the Arcjet ATTD Flight Unit EMC test was performed, during which the PCU was operated at full power, 26 kW, for the first time in the fully integrated flight unit. During these tests, the PCU was operated at full power approximately sixty times. Eighty percent of these runs were ten minutes in duration or longer. Efficiency ranged from 95 - 96%. Input and output current was monitored to verify stability and operations of all three output stages of the PCU.

The results of the EMC testing are provided in a full test report (TRW Document Number 95.M541.4-035)⁵ and included the full suite of tests identified in MIL-STD-461C and MIL-STD-1540. The following paragraphs summarize all of the results of these tests that were anomalous. The CE07 test was performed and no limits (+42Vdc, -14 Vdc) were exceeded. During the CS01 test, the PCU exhibited susceptibility at 8V P-P at high (30 Vdc) and low (26 Vdc) bus voltage in the 20-50 kHz range. The PCU showed no susceptibility up to 6V P-P at both high and low bus voltage on either power or return in the same range. It was decided at this point that these results were sufficient.

During CS01 testing, the valve driver for the thruster feed valve within the PCU showed susceptibility in the 30 - 400 kHz range at 8V P-P at 30 Vdc bus voltage, on the return line, but showed no susceptibility at 6V P-P. The susceptibility was noted when the pressure downstream of this valve dropped from approximately 30 psi to 20 psi. The valve driver provided enough voltage to the valve in order for it to open and release pressure from the plenum tank to ambient. This does not raise concern regarding on-orbit operations since (1) this is not the valve that maintains propellant in the system, and (2) the plenum section of the PFS is charged with NH₃ gas before every arcjet firing.

6. SEAL IN PC

7. UPON FINAL
PER MANUFA



Figure 42. Test Adapter Modification for Flight

During the CS02 test, the PCU exhibited susceptibility at 30 - 60 MHz in the power to chassis configuration at 1V and 0.75V, but showed no susceptibility in this range at 0.5V. However, there was no susceptibility in this range up to 1.0V on the return to chassis test nor the line-to-line test. Therefore, the PCU was retested in the 30-60 MHz range in order to determine if the susceptibility noted in the power to chassis configuration was real. The test was successfully repeated (i.e. no susceptibility was observed) up to the 0.75 V level when the test was stopped due to lack of disk space that prevented further data logging (this is discussed in detail below). At this

point the test was terminated and it was concluded that the PCU exhibited no susceptibility up to 0.75V in the power-to-chassis configuration.

The CS06 test was completed in two modes; battery charger ON and PCU/Diagnostics ON. The PIU was found to be damaged as a result of this test when, during EMC in-rush current testing, current leakage was found on two of the three heater buses. Although the heaters were disabled, current was still being drawn by the heaters when power was applied to the heater bus. A heater control functional test was performed in order to determine the cause of the problem, and troubleshooting determined that the transistors for each of the heater circuits were exposed to twice their design rating voltage during EMC testing. In discussions with AFRL, Space and Missiles Systems Center (SMC), Boeing and Aerospace, it was determined that the spacecraft bus would not inject more than 20 V at the ESEX interface, which would mean that only approximately 16V would reach the heater control board transistors. Therefore, a design change of the board was not required. However, although only two of the 36 were found to be damaged, all 36 transistors were replaced since they were most likely overstressed. Unit level testing (functional, vibration and thermal cycle) was performed prior to re-installation into the flight unit. Further testing of the inrush current and input surge test were completed with no limits exceeded.

During RS03 testing, Antenna #2 of the EMI Experiment remained saturated after the 5 GHz test. Reducing the 5 GHz signal did not remove the saturation. Resetting the EMI Experiment by powering it OFF and ON did not clear the saturated state. After turning off some of the test equipment, the saturation of Antenna #2 went away. To verify the EMI Electronics and its antennas had not been damaged, the EMI electronics was commanded into the calibration mode, and the expected response was received. A functional test of the EMI Experiment was performed and all data were nominal. To prevent unrealistic antenna inputs from damaging the EMI Electronics, test-only 50 Ω terminations were installed on the EMI Electronics antenna inputs and the testing was continued.

Also, during the RS03 testing, in the middle of a 26 kW PCU run, the test facility power was momentarily brought down due to a lightening storm. As a result of this loss of power, the flight unit GSE power supply was shut down which resulted in a shut down of the flight unit. To determine the flight unit state-of-health, the agreed test approach was to perform the flight unit power up sequence and check the functions of the PIU and the PCU. The PCU was tested by performing a gradual power up test and all functions and data were nominal. It was also determined that when power was removed from the flight unit: (1) it remained off, (2) the power relays between the high power supply and the PCU remained closed, and (3) the CCU was not able to re-boot. These were important points because it meant that high power was not removed, and then immediately re-supplied to the PCU, which could have damaged the unit. Based on this event, the following additions were incorporated into the GSE to prevent damage to the flight unit in the event of a facility power shut down: (1) an uninterruptable power supply was integrated with the GSE in order to keep (a) the computer operational to enable the flight unit to be "safed" until facility power was restored and (b) the flight unit 28 Vdc bus powered until the flight unit could be "safed", preventing a sudden power down of the flight unit; and (2) the flight software boot-up procedure was revised to protect the PCU from a sudden power down and power up event.

As noted above, during the CS02 test, a non-EMC related shut-down of the system occurred during a PCU full power test. Throughout testing, the CCU time was closely monitored in order to determine if the CCU was being upset by any of the susceptibility signals being injected on the power bus. For this event, the CCU time stopped updating every second. Commanding was not possible through the GSE, therefore, the PCU was shut-down through the PCU test fixture and the

flight unit was shut down by powering it down through the GSE. Before any testing continued, it was determined that the computer disk to which the flight unit test data was being recorded had filled up and no further data logging and commanding was permitted. Although there was a software warning implemented to inform the operator of this condition, it was not generated (this code was subsequently reviewed and corrected). An incremental turn-on of the flight unit was performed to verify flight unit state-of-health and all systems were nominal. In addition, a step was added to the flight unit data-logging procedure to check available disk space before powering up the flight unit.

Another anomaly observed during EMC testing was that the video camera system would not provide pictures on a consistent basis. The EMC testing was postponed in order to determine the cause of the video camera problem. Troubleshooting testing indicated that the pixel clock between the video camera and the FGU was not being transmitted correctly. The FGU was verified to generate the clock signal, however, it was unclear if the camera was processing it. Therefore, the camera was removed from the flight unit for functional testing. The camera was found to be functioning as required, so troubleshooting turned to investigating the harness between both units. The individual connectors were inspected and found to have contamination visible when a magnifying glass was used. Each cable connector was then cleaned using isopropyl alcohol (IPA) and a nylon brush. The cable was then reconnected and the total resistance measurement was as expected, $\approx 3.5 \Omega$. Loose connections were checked for, but none were found. The pixel clock cable was re-connected to the camera and the FGU, and a functional test performed on the system. This functional test produced a very clean video picture. Based on this effort, it was concluded that the video camera pixel clock signal was unable to be transferred between the FGU and the camera due to a high cable resistance caused by connector contamination.

3.3.4 Random Vibration Test. The flight unit vibration testing was conducted following the EMC test and the results are documented in TRW Report M533.5.95-071⁶. Figure 43 shows the flight unit on the vibration test fixture. Prior to the vibration test, the following tasks were performed in preparation for the test:

- Nineteen test accelerometers were installed throughout the flight unit.
- A pre-vibration leak test was performed on the thruster to verify no leakage. A post vibration thruster leak test was also performed, in the same manner as the pre-vibration leak test. No pressure decay was measured in either test.
- The PCU test adapter plug was secured with a flange that mated to the bolt circle of the PCU receptacle in order to prevent the plug from moving in a radial direction within the power cable inner conductor. The outer shield box was also installed for the test.
- A ten pound mass simulator constructed of TeflonTM was secured around the equator of the NH₃ propellant tank.
- The flight battery mass simulators were installed.
- The flight unit was secured to the vibration table using a flight torque value of 35 ft-lbs.

The unit was first tested in the Z axis, and was subjected to a 0.25 g sine sweep from 5-100 Hz. This test was followed by a vibration test whose overall level was only 6.6 grms, 3 dB less than the intended level. The responses of the 19 test accelerometers were reviewed and it was determined that some notching was required in the lower frequency range to account for the first bending moment of the flight unit. The vibration test was then repeated at an overall level of 9.3 grms. The unit was subjected to another 0.25 g sine sweep from 5-100 Hz in order to determine if

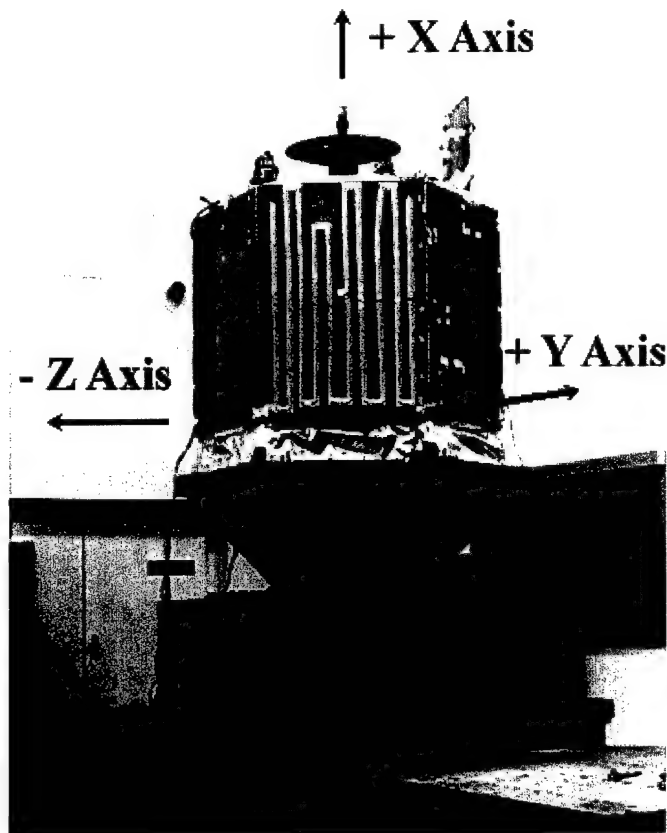


Figure 43. ESEX Vibration Configuration

any resonant frequencies of the unit changed. No frequency changes were noted, indicating no changes in the structural integrity of the vehicle.

The unit was then tested in the Y axis. As in the z-axis, the unit was subjected to a 0.25 g sine sweep from 5-100 Hz. During this initial sweep, the test was aborted based on responses measured by one of the control accelerometers. The data from the accelerometers located on the propellant tank tripod showed that the tank was impacting the tripod ring, sending a shock into the tripod that was in plane with the Y axis. This shock was then transmitted through the structure longeron and attachment foot to the vibration fixture where the control accelerometer was located. The filtering on the control accelerometer was adjusted to account for this impacting and the sine sweep was repeated at 0.1 g from 5-100 Hz. After the data was reviewed, a 0.25 g sine sweep from 5-100 Hz was performed and similar, positive results were observed. This test was followed by a vibration test at an overall level of 9.3 grms. The unit was subjected to a post-vibration 0.25 g sine sweep from 5-100 Hz. No frequency changes were noted.

The flight unit was repositioned for the X axis test and a 0.1 g sine sweep was performed from 5-100 Hz. Based on the data from this test, a 20 second 3.75 grms random vibration test was performed to better characterize the response of the flight unit in this axis. Notching in this axis was implemented to limit response of the PFS and diagnostic platforms to less than the 11.5 g axial design limit. In addition, there was a fixture frequency at 1000 Hz that required notching. The X-axis vibration test was performed to an overall level of 8.7 grms. The PFS platform fundamental

frequency occurred at 63 Hz with $Q = 25$. The diagnostic platform had high- Q responses at 86 and 150 Hz. The PFS platform response to the notched environment was 20 g. The unit was subjected to a 0.1 g sine sweep from 5- 100 Hz in order to determine if any resonant frequencies of the unit changed. No frequency changes were noted, indicating no changes in the structural integrity of the vehicle.

One of the results of the notching done during the random vibration test was that the vibration spectrum was notched below the ARGOS ICD levels between 55 – 160 Hz and 900 – 1000 Hz. Therefore, a waiver was submitted to SMC requesting acceptance of the flight unit as tested. Aerospace conducted a statistical energy analysis that showed that the expected levels were sufficiently below the tested levels and the waiver was granted.

Following the vibration test, a post-vibration functional test was performed on the flight unit. During this test, two hardware problems were found. The first problem was that the video camera system did not produce a nominal video frame. The video camera problem was investigated first to determine the state of health of the video camera and the frame grabber electronics. Both units performed as expected. Therefore, the harness was checked again (similar to the EMC test) and a loose connection was found on the pixel clock connector. This cable was removed and replaced with a new one and the video camera system performed nominally. The resistance of the other pixel clock cables was checked and found to be nominal. The faulty cable was x-rayed and it was found that the inner conductor of the cable had pulled away from the crimp within the flight unit connector, providing a very poor connection. The other coax cables were x-rayed and it was determined that no other connectors needed to be replaced.

The second hardware problem was identified in the TQCM located on the diagnostic tower (TQCM Sensor #1) which measured a significantly lower frequency than expected. The problem was isolated to the sensor itself, which was removed from the spacecraft and returned to the supplier for disassembly, inspection and rework. The rework involved adding additional potting material to support the flexure of the internal crystal mount. This repair was used on previous TQCMs on other flight programs.

Post-vibration testing included a verification of the PCU start circuit. The flight unit was configured with the PCU electrical test equipment in order to measure the start pulse on an oscilloscope. The pulse was compared to the start pulse generated when the PCU was first functionally tested in February and no degradation in the pulse shape or magnitude was found.

3.3.5 Thermal Vacuum Test. Following the post vibration functional test, the flight unit was prepared for the thermal vacuum test.

- The EM battery sub-assemblies and the corresponding vent lines were installed.
- Two ion gages were temporarily installed in the flight unit in order to read internal flight unit pressures during the thermal vacuum test.
- The flight software PROMS were removed from the flight unit CCU to be updated with software changes which (1) included a modified reboot routine that would better protect the flight unit in the event the CCU gets rebooted during an arcjet firing on orbit, (2) provided the ability to open the dual pressure control valve and hold it open for system pressurization and (3) modified the default for maximum PCU internal temperatures.
- Flight and test thermal insulation was installed and a thermal simulator for TQCM Sensor #1 was installed.

- Just prior to thermal vacuum testing, the propellant feed subsystem was pressurized to 298 psia using a 90% GN₂, 10% GHe mixture. This was done in preparation for the leak testing to be performed after the thermal vacuum test.

Prior to installing the EM battery sub-assemblies, a series of tests were performed to verify the integrity of the battery sub-assemblies – especially since they had been activated well beyond their design life. Each battery was charged and discharged and each battery cell checked to determine their state of health. Although the capacity of the battery sub-assemblies was lower than when they were first activated (50 A-hrs versus 70 A-hrs), there was no indication the battery sub-assemblies would be unable to support the test. As a precaution, it was decided that the PCU firings would be reduced from 15 minutes to ten during the thermal vacuum test. The EM battery sub-assemblies were then charged to this limit with an external power supply so the battery sub-assemblies could be charged at a rate of approximately 4.5 amps. The flight battery charger was exercised at the beginning of the charge operation and at the end to verify that the charger did function with the battery sub-assemblies installed. The internal battery thermistors were monitored during the charging in order to ensure safe charging temperatures. The battery sub-assemblies were charged to 245.81 volts when the external charging was completed.

While final preparations were underway for the testing, a high temperature was noted on the internal battery thermistor for the battery on Panel #1. This temperature reached a maximum of approximately 138 °F before decreasing. (throughout the charging, this temperature never exceeded 90 °F.) and a distinct odor was also present in the thermal vacuum chamber. Battery Panel #1 was promptly removed from the spacecraft. Upon inspection of the flight unit and the battery assembly, a hole approximately 1/4-inch in diameter was discovered in the battery case, and some contamination of the flight unit was evident.

After the EM battery was removed, its lid was removed and a black residue was found on the top surface of the battery. A tape test was performed to determine the extent of contamination within the flight unit. Eleven samples were collected from various locations within the vehicle and were analyzed. Scanning Electron Microscopy (SEM) samples were also taken to determine the composition of the contamination. To determine if any electrolyte was released from the battery, a litmus test was performed on various surfaces within the vehicle. The battery electrolyte is potassium hydroxide (KOH) which is alkaline in nature. All samples taken showed the surfaces to be neutral. Therefore, it was concluded that no electrolyte contamination occurred.

Composition determination of the particulate samples collected from both the spacecraft and the battery was performed. To confirm the source of residual contamination on the spacecraft was from the battery, SEM/Energy Dispersive X-ray (EDX) analysis and Fourier Transform Infrared (FTIR) analyses were performed. Morphology information obtained from the SEM analysis and composition information obtained from the EDX and FTIR analysis were used as criteria for comparing the residues. Samples were collected from representative locations from within the spacecraft.

A summary of the results obtained from the EDX and FTIR analysis of samples taken before the residue was removed from the flight unit are presented in Table 15. Three general types of particulate were removed from the battery. A darkly colored fine particulate, mostly less than 20 microns in size, with an elemental composition of mostly copper, oxygen and carbon, was collected from internal surfaces of the battery (see Figure 44a and b). FTIR analysis of this residue revealed a negligible infrared signature that indicates the residue was mostly copper oxide and/or inorganic carbon, both of which show negligible absorbance in the infrared. This residue was also collected

from all of the areas sampled on the PFS platform and on both internal and external surfaces of the PCU. The results of the SEM analysis showed high concentrations of copper and carbon in the contamination. This raised concern since both materials can be highly conductive and Battery Panel #1 is immediately adjacent to the PCU which controls all of the ESEX high power. Furthermore, the hole, which was generated in the battery case, coincided with a series of vent holes in the side of the PCU. Upon opening the PCU for contamination inspection, it was determined that a terminal block had been mounted over the PCU vent holes closest to where the battery hole had formed on Battery Panel #1. This terminal block protected the PCU from collecting considerable contamination. All horizontal surfaces were carefully vacuumed and wiped with IPA. Surface resistance measurements were also taken on the PCU output inductors and the contamination within Battery sub-assembly #1 to determine if the contamination was conductive. The measurements, taken with an ohm meter and copper probes (0.25 inches in diameter) placed approximately 1 inch apart, showed an open circuit in the PCU and in the lightly contaminated area of the battery. In the heavily contaminated area within the battery, the resistance was 100 k Ω . The conclusion from these measurements is that the contamination from the battery was virtually non-conductive.

A second particulate type, with an elemental composition of iron, chromium, nickel and oxygen, and a uniquely spherical shape approximately 5 to 10 microns in size, was collected from both internal surfaces of the battery and most of the PFS platform surfaces (see Figure 45a and b). This type of residue was not observed on the internal surfaces of the PCU. Because of the close physical and chemical resemblance to a stainless steel weld slag, a proposed source of this material is the "burned through" stainless steel battery side panel.

The third particulate, collected from inboard of panel #1 on the PFS platform, was a polymeric silicone/epoxy type material of unconfirmed origin (see Figure 46 for FTIR spectrum). A proposed source of this material is a mixture of the PT401 epoxy coating and ethylene propylene potting materials used in the battery. An FTIR spectrum of a polymeric type particle collected from within the battery is shown Figure 47. Both Figure 46 and 47 spectra show peaks characteristic of epoxy. A notable difference is that the Figure 39 material shows peaks at 1244 cm^{-1} , 1023 cm^{-1} and 837 cm^{-1} which are characteristic of silicone. This suggests that the source of the epoxy/silicone material was different, nonetheless, possibly still from within the battery.

The cause of the failure was believed to be a result of exceeding the design life of the battery. The wet life of the battery (i. e. how long the battery is useful once activated) is 18 months. The EM battery sub-assemblies were activated in September 1993 - 19 months prior (used for six months and then placed in cold storage for approximately 13 months.) This scenario could readily lead to dendrite formation, for instance, and cause a short circuit within a cell. In addition, the design specified only ten charge/discharge cycles - while the EM battery sub-assemblies had been charged 12 times. AFRL decided that any further analysis to determine the exact cause of the failure would be conducted at their discretion.

The spacecraft was cleaned per a special test procedure. The cleaning consisted of systematically vacuuming the entire spacecraft followed by an alcohol wipe of all interior surfaces. Tape pull samples were collected to provide a comparative measure of cleanliness relative to before the cleaning was performed. A dramatic improvement in the post-cleaning particulate concentration values over the pre-cleaning values was apparent. Pre-cleaning samples average about 290 particles per square inch, whereas post-cleaning samples average about 70.

Table 15. Result Summary for Particulate Collected from the Battery and the Arcjet Flight Unit

Sample location	EDX Results Primary elements	FTIR Results	Source of sample
PCU 1	Cu, O, C, Si, Cl, Fe	not analyzed	from battery
PCU 2	Cu, Fe, Cr, Si, O	not analyzed	from battery
PCU 3	C, O, Fe, Na, Al, Si	not analyzed	unknown source
PCU 4	Fe, Ni	not analyzed	unknown source
PCU 5	O, Al, Si, Ca	not analyzed	unknown source
PCU 6	Cu, C, Si, Fe	not analyzed	from battery
PFS 1	1) C, Cu, O, Cl, Si, Fe 2) Fe, Cr, Ni, O	1) not analyzed 2) not analyzed	from battery
PFS 2	1) C, Cu, O, Cl, Si, Fe 2) Fe, Cr, Ni, O	1) not analyzed 2) not analyzed	from battery
PFS 3	1) C, Cu, O, Cl, Si, Fe 2) Fe, Cr, Ni, O	1) not analyzed 2) not analyzed	from battery
PFS 4	1) C, Cu, O, Cl, Si, Fe 2) Fe, Cr, Ni, O	1) not analyzed 2) not analyzed	from battery
PFS 5	C, Cu, O, Cl, Si, Fe	not analyzed	from battery
PFS 6	C, O	epoxy-silicone	from battery
Battery 1	1) C, Cu, O, Cl, Si, Fe 2) Fe, Cr, Ni, O	1) not analyzed 2) not analyzed	from battery
Battery 2	1) C, Cu, O, Cl, Si, Fe 2) Fe, Cr, Ni, O 3) C, O	1) not analyzed 2) not analyzed 3) epoxy	from battery

PCU 1 vertical panel of the PCU box adjacent to the battery below the vent holes
PCU 2 horizontal surface of the FET compartment
PCU 3 vertical surface below cable / FET compartment
PCU 4 horizontal surface of the EMI filter compartment
PCU 5 vertical surface on the output inductor bus bar
PCU 6 inside surface of the PCU cover panel
PFS 1 +y PFS platform corner of structure between panels #1 and #2
PFS 2 +z PFS platform corner of structure between panels #1 and #6
PFS 3 PFS platform inboard of panel #1 near the plenum tank support bracket
PFS 4 -y PFS platform corner of structure between panels #4 and #5
PFS 5 PFS platform inboard of panel #4
PFS 6 inboard of panel #1 on the PFS platform
Battery 1 underside of battery cover plate
Battery 2 free residue collected from inside battery after removing the cover panel

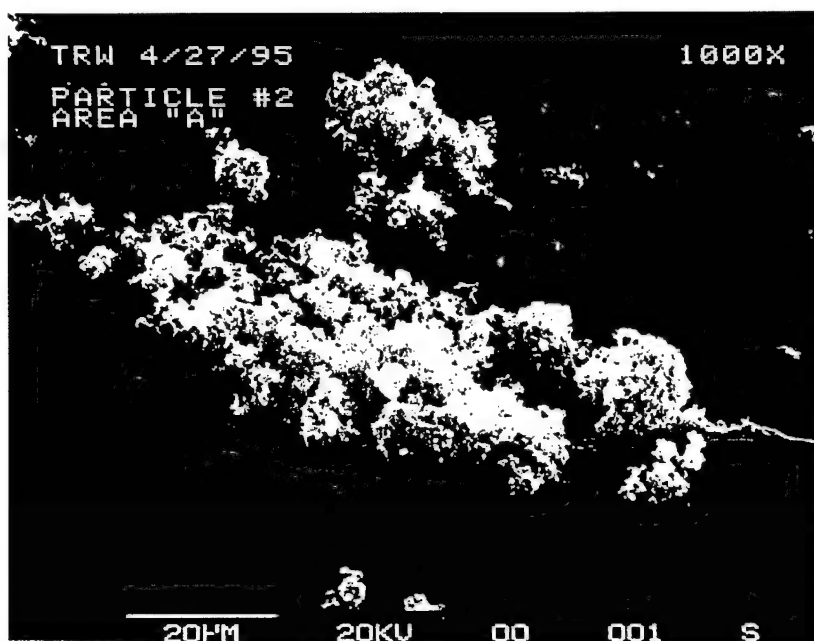


Figure 44a. Photomicrograph Obtained from SEM Analysis of Type 1 Particulate Contamination

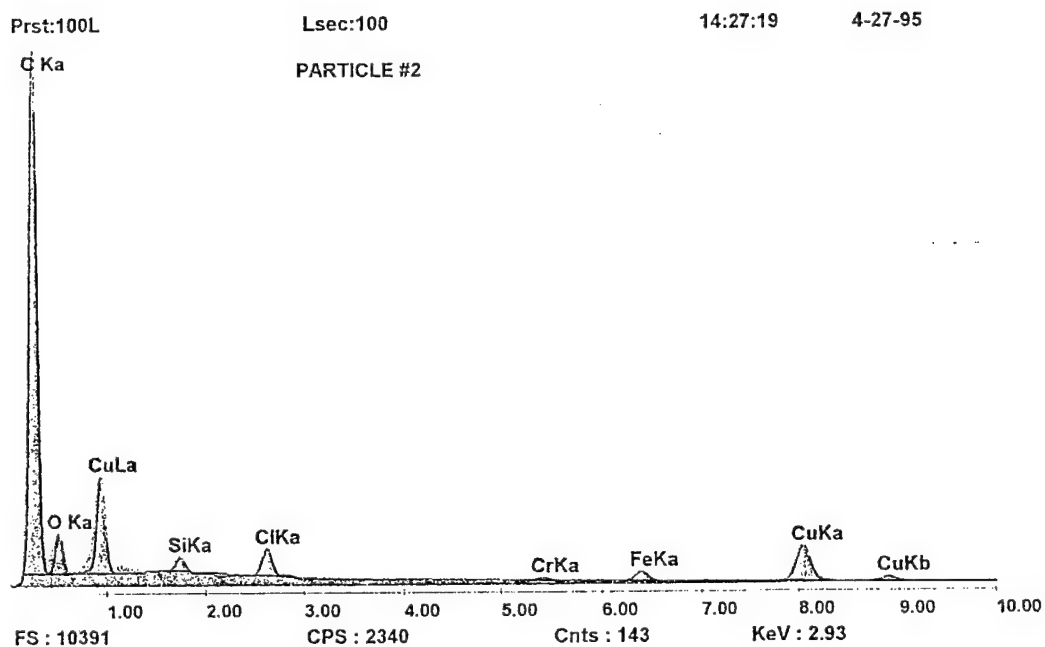


Figure 44b. Spectrum Obtained from the EDX Analysis of Type 1 Particulate Contamination

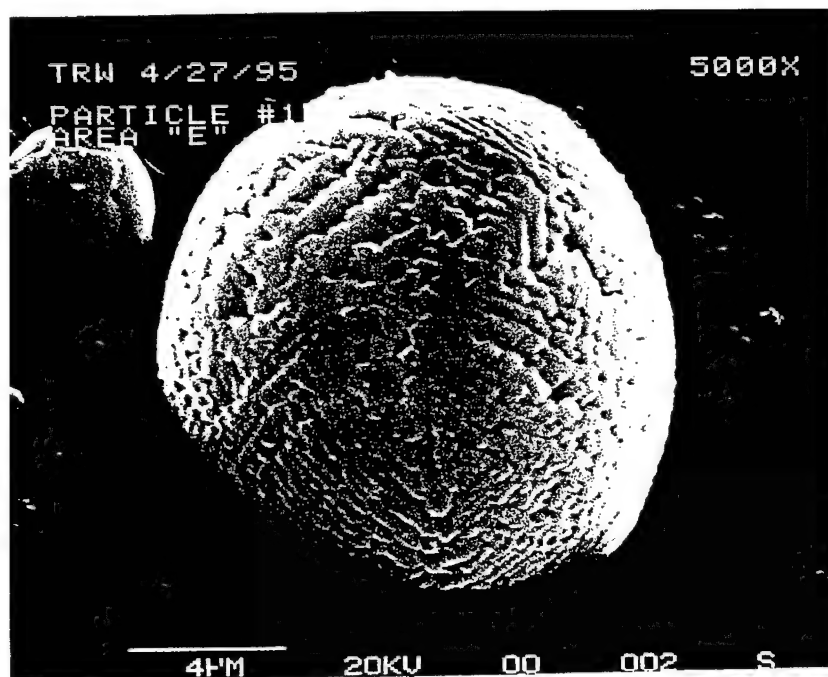


Figure 45a. Photomicrograph Obtained from SEM Analysis of Type 2 Particulate Contamination

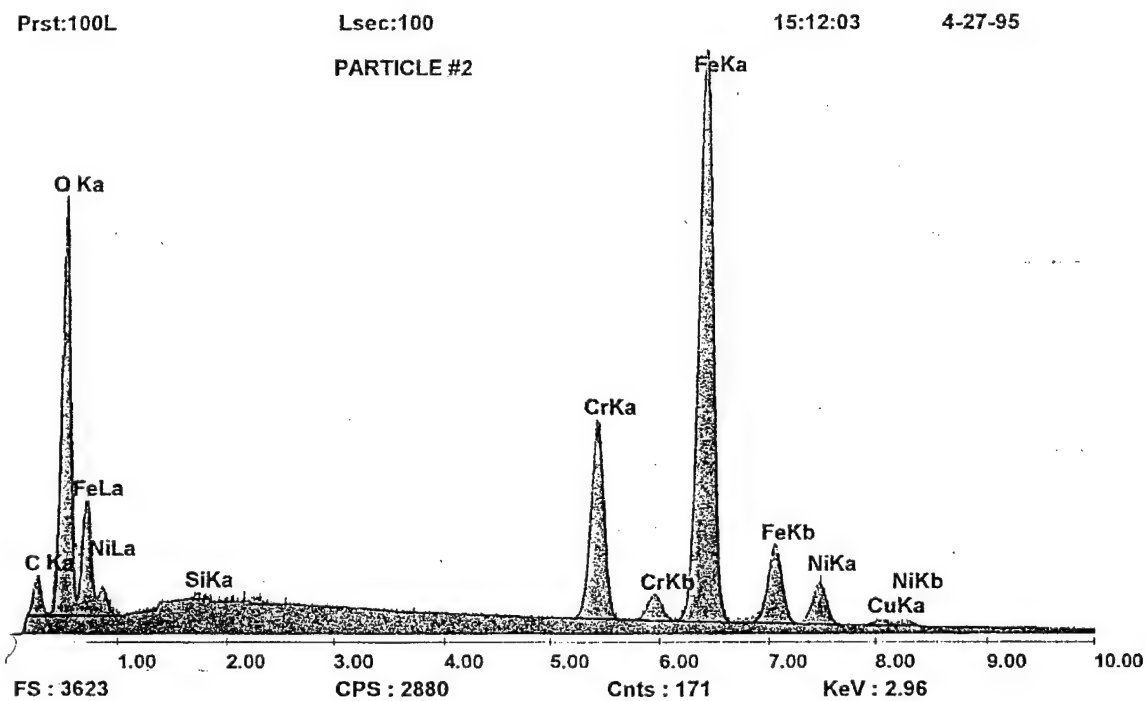


Figure 45b. Spectrum Obtained from the EDX Analysis of Type 2 Particulate Contamination

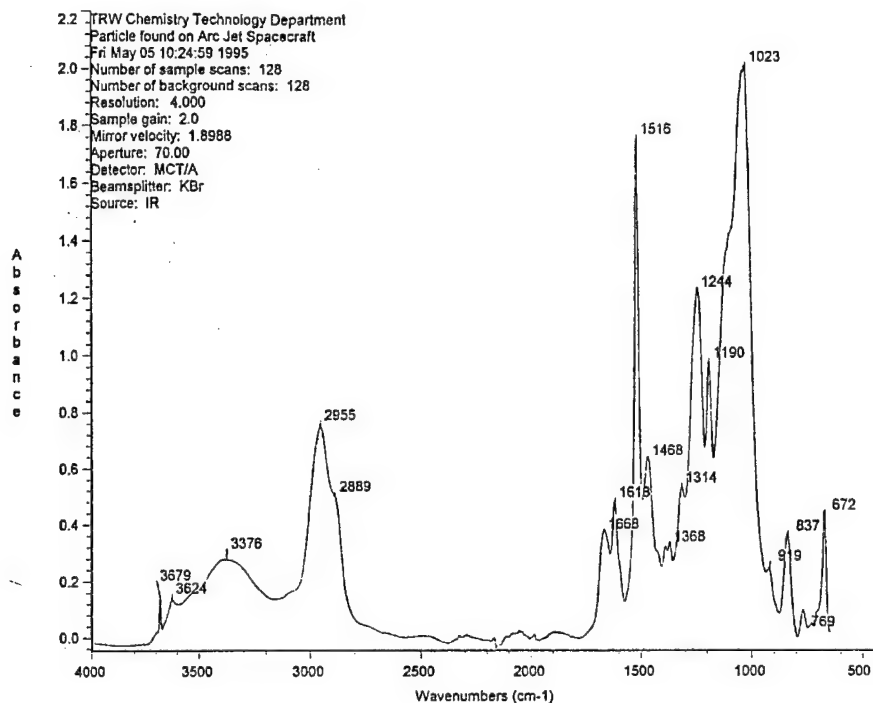


Figure 46. Spectrum Obtained from the FTIR Analysis of Particle Collected from PFS Platform

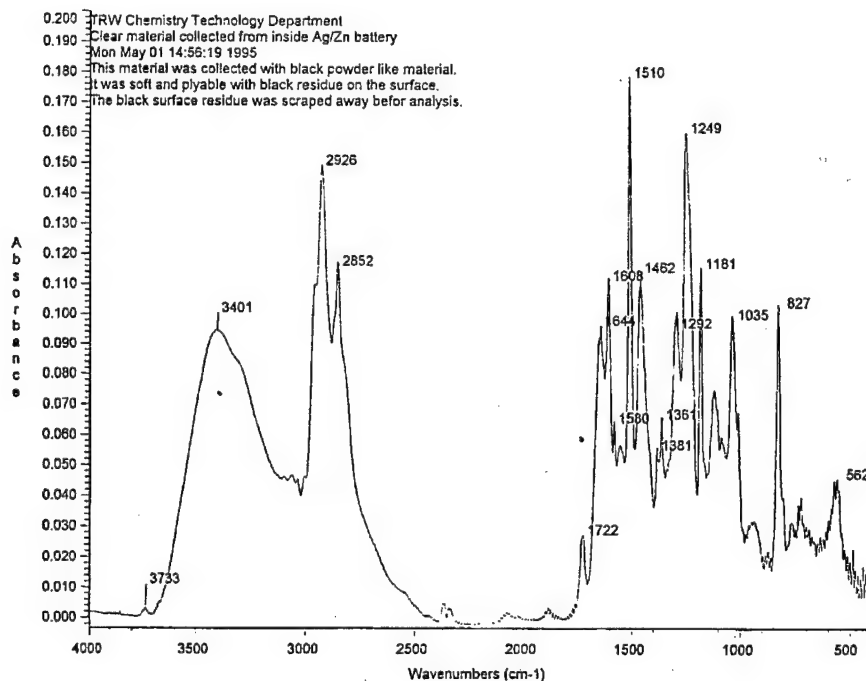


Figure 47. Spectrum Obtained from FTIR Analysis of Type 3 Contamination From Inside Battery

With the cleaning complete, the flight unit was prepared for thermal vacuum testing. The remaining two battery sub-assemblies were removed from the flight unit and fully discharged. The battery sub-assembly on panel #5 was re-installed into the spacecraft to provide data from the internal battery test thermistor. The vent line was installed onto Battery Panel #5 as a precautionary measure although no venting of the battery was anticipated. Battery Panels #1 and #4 had no battery sub-assembly or simulator installed. The flight unit was also re-configured to be powered through the thermal vacuum chamber wall using the Rapid Electric Power Supply. The PCU was prepared for the thermal vacuum test by connecting it to the resistive load. To ensure no shorts between the inner and outer conductor leads to the load, multiple layers of clear kapton were wrapped between the leads (> 8 mils thickness). These wrapped leads were then wrapped with a second layer of clear kapton to prevent shorting of the test insulation to the leads.

The thermal vacuum test was performed per Figure 48. Deviations taken during the test were as follows:

- Since the full compliment of battery sub-assemblies were not installed during thermal vacuum, battery, charging was not performed.
- The first firing of the PCU during the first hot transition lasted only three minutes, not the originally planned fifteen minutes. The ion gages within the flight unit indicated pressures were increasing within the flight unit as the PCU was warming up. Therefore, the PCU was commanded off after three minutes when the ion gages registered a pressure of 1×10^{-4} torr. It was decided to let the flight unit complete the first hot soak to help drive off more outgassing products while the PCU was not running.
- Since the first PCU firing was truncated due to increasing flight unit pressure, the first full firing of the PCU during the second hot transition was not performed after a hot soak. The hot soak in this phase was deleted in order to increase the potential for a full fifteen minute firing. This approach proved to be successful. The pressure within the flight unit increased from approximately 1.6×10^{-5} torr to 5.2×10^{-5} torr during the firing.
- The third hot transition included a three hour hot soak prior to running the PCU at high power. Flight unit pressure increased from 2.3×10^{-5} to 8.3×10^{-5} torr during the firing.
- The last hot transition did not include a hot soak prior to running the PCU at full power.
- Time to achieve cold and hot thermal balance was considerably longer than anticipated due to the testing criteria that temperatures could not fluctuate by more than $1^\circ\text{F}/\text{hour}$.

Two test discrepancies were found during the thermal vacuum test. The first problem was discovered just after the cold turn on of the CCU was performed. During pump down and filling of the cold wall, the flight unit was powered and telemetry was monitored for any anomalies. The flight unit was then successfully turned off during the first cold transition in order to simulate the cold turn on of the CCU and the flight unit on orbit. However, when the analog telemetry became available with the CCU power, it was discovered that T3 and T4, arcjet thermocouple temperatures, were not reading as expected. The test thermocouple placed on the thruster barrier tube registered -49°F . T3 telemetry showed 162°F and T4 showed 52°F .

Analysis of the thermocouple circuits determined that multiple thermocouple junctions were inadvertently created in the harness between the thermocouple and the PCU conditioning circuit. The "as-built" thermocouple circuit is shown in Figure 49. It was determined that the thermocouple junctions could be replaced by splicing in new, continuous thermocouple wire around the different thermocouple junctions and either (1) rework the PCU connector and put the thermocouple wire right into the connector or (2) splice the thermocouple wire into the PCU

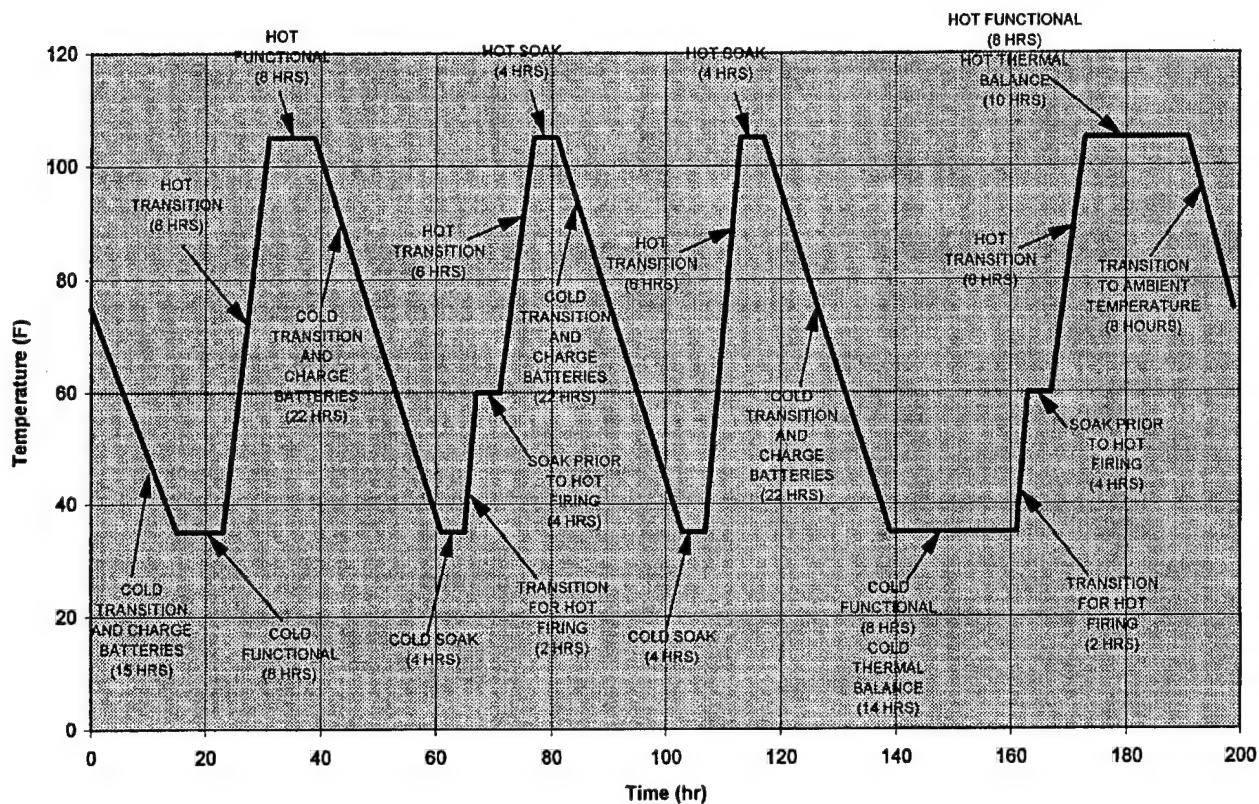


Figure 48. Thermal Vacuum Test Timeline

harness as close to the PCU connector as possible. In order to determine whether the option of reworking the PCU connector would provide significantly better results over the “all-splice” option, a simple bench-top test was performed. The splice was heated to determine its affect on the actual reading. The actual reading changed almost directly proportional to the splice temperature. Since the worst case temperature differential expected in the area of the splice would be less than 20 °F, the option of splicing into the PCU harness was selected. This option is illustrated in Figure 50. Thermocouple wire was spliced into the PCU harness and then routed along the existing harness bundle to where the thruster thermocouple splices were made when the thruster was first integrated. The old splice was demated and the new thermocouple wire was installed.

The second thermal vacuum test discrepancy was found during the first hot functional test. The functional test included turning on the precharge circuit and verifying that 100 mA of charge current was sent to the PCU input capacitors. During the first hot functional test, the 100 mA did not register on the milliamp meter that was part of the external test set up. The command was sent numerous times with no current indications. This circuit was successfully tested during the first cold functional test. As the thermal vacuum test progressed, the precharge circuit ON command was sent at various temperatures during hot and cold transitions to try and determine if (1) the circuit consistently did and did not operate, and (2) if the temperatures at which it did or did not operate were consistent. Through the test, the precharge circuit operated nominally at the colder temperatures and did not operate at temperatures greater than ≈ 125 °F. An independent review of the precharge circuit design determined that the circuit contained a transistor that becomes more conductive with increasing temperature. Therefore, this transistor was allowing current to “leak”

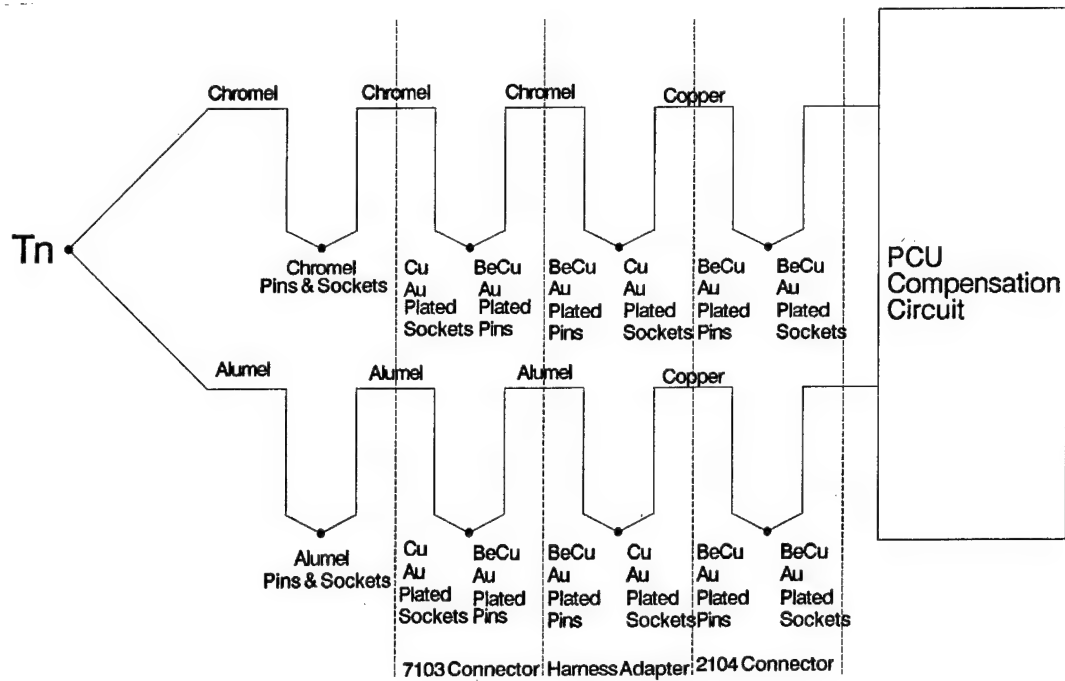


Figure 49. "As-Built" Thermocouple Circuit

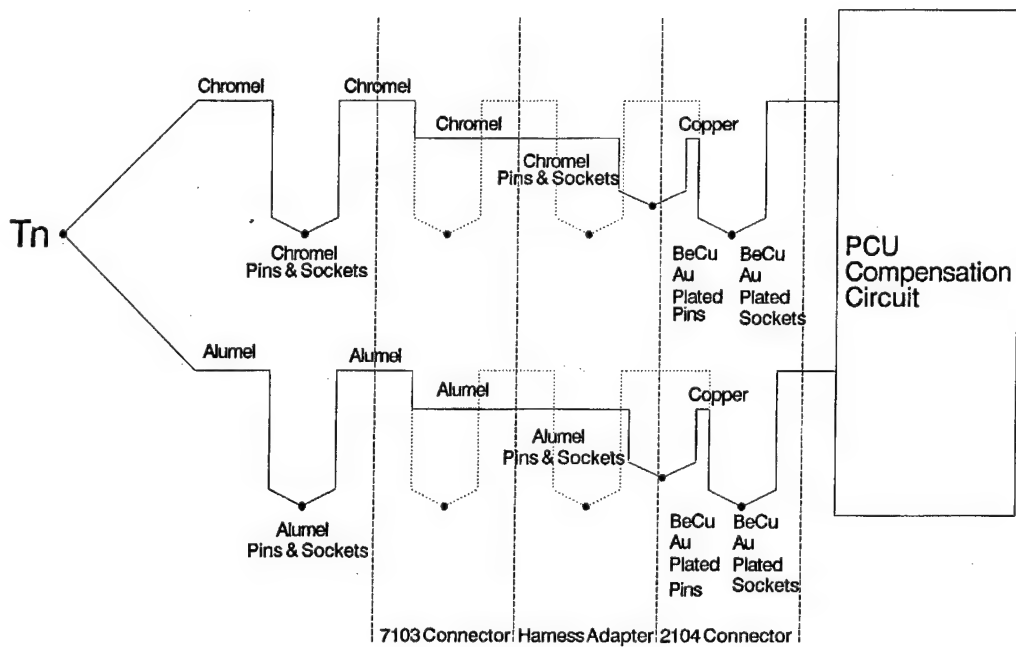


Figure 50. All-Splice Thermocouple Option

through the circuit to the PCU input capacitors as the flight unit temperature was being increased for hot soak conditions. Therefore, the capacitors were actually being pre-charged before the circuit commanded the precharge to occur. The current leakage, although low, was enough to charge the PCU capacitors and cause current not to be drawn when the pre-charge circuit was commanded on. To correct this leakage, a resistor was added to the circuit to reduce the leakage to the nanoamp level so the PCU capacitors will not be pre-charged without commanding the circuit. After the resistor was added to the circuit, this nanoamp leakage current was verified in test up to 152 °F.

After the thermal vacuum test was complete and before the thermal vacuum chamber was brought back to atmospheric pressure, an external leak test of the PFS was performed. A standard leak was introduced into the vacuum chamber and measured by a mass spectrometer within the pumping system. After the chamber stabilized again, a second measurement was taken of the gas being pumped from the chamber. Any helium registered during this measurement would be attributed to a leak of the PFS or background helium. The measured leakage was less than the required 1×10^{-4} scc/sec.

After the completion of this test, the chamber was returned to atmospheric pressure and a PFS Algorithm Verification Test was performed. The purpose of this test was to verify the proper incorporation of the PFS flow control algorithm into the flight software. Verification would be indicated by proper convergence to the programmed flowrates. Figure 51 shows the results of the first test where the PFS was commanded to control to a flowrate setpoint of 160 mg/sec. The test was started at a pressure that correlated to an expected flowrate higher than 160 mg/sec in order to minimize the number of cycles accumulated on the dual pressure control valve. The operational sequence allows for flowrate stabilization within two minutes, which was demonstrated in this test. Figure 52 illustrates the PFS performance when it was programmed to establish an initial flowrate of 200 mg/sec and then ramp up to 240 mg/sec. This test represented the situation where the current system pressure correlated to a flowrate lower than the desired. This test also demonstrated the ramp up capability, although a premature shutdown of the test due to an incorrectly entered test time did not allow the system to stabilize at the final desired flowrate.

Following the PFS Algorithm Test, the PFS propellant tank was repressurized to approximately 285 psia and an internal leak test of the dual pressure control valve was performed. Using a bubble method, a tygon tube was placed on the thruster leak check fixture with the other end placed into an inverted pipette filled with alcohol. The thruster feed valve was then opened for approximately 5.5 minutes, exposing the closed dual pressure control valve to the alcohol-filled pipette. If any bubbles were generated, this would indicate a leak across the dual pressure control valve. The open time of the thruster feed valve was limited by the valve temperature, which had to be closed if the valve reached 150°F. Although only 4 minutes of test time was necessary to determine if an out-of-specification leak was present, additional test time was planned to provide adequate test margin. The first 5.5 minute test did not generate any bubbles. The second time the thruster feed valve was opened, bubbles were generated and liquid displaced from the pipette. It was decided to let the system temperature stabilize since the heat generated by the valve could cause a false indication. The system was left to stabilize overnight and the test performed again the next day. The feed valve was kept open for 6.5 minutes during this test and no bubbles were observed. Therefore, it was determined that the dual pressure control valve internal leak rate was less than the allowable 3 scc/hr.

At the completion of the PFS testing, the flight unit was removed from the vacuum chamber and a fit check of the interface between the flight unit and the GFE ground transporter was

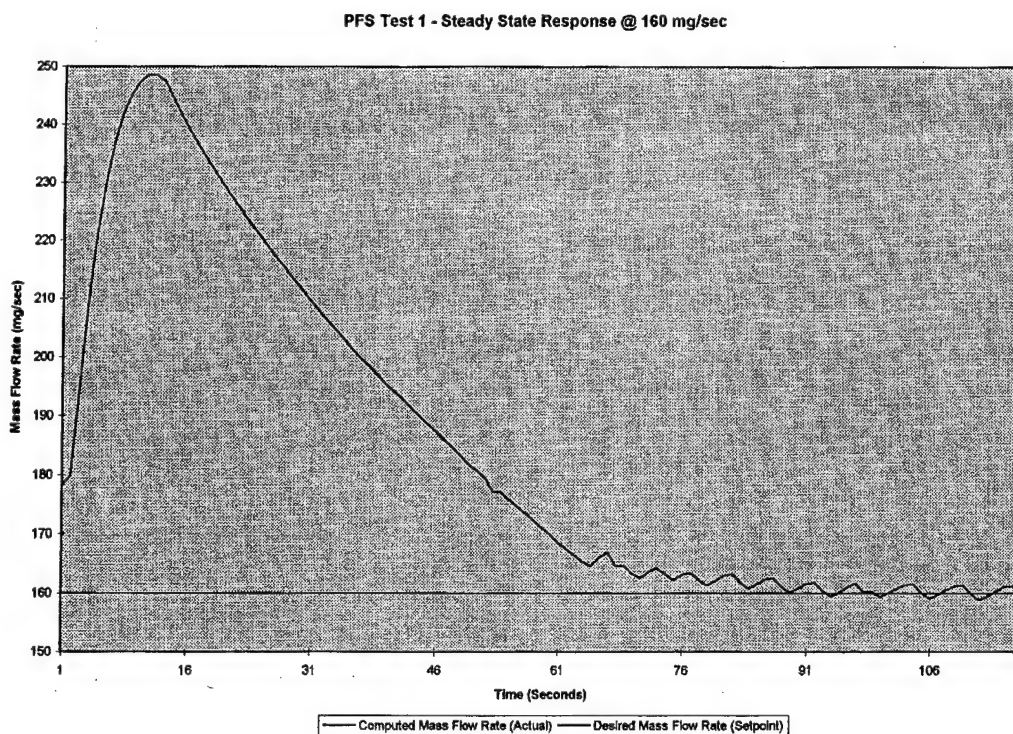


Figure 51. PFS Test 1 - Steady State Response at 160 mg/second

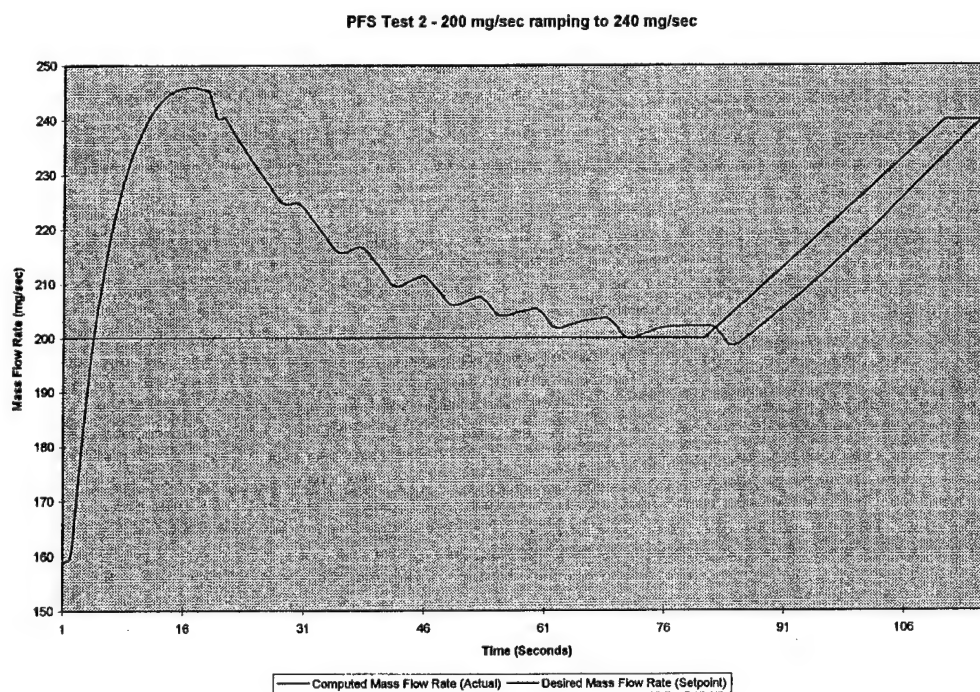


Figure 52. PFS Test 2 - 200 mg/second ramping to 240 mg/second

performed. During the check, the clearance between the flight unit and the mounting pads was identified as too small. These mounting pads were re-worked to remove 0.5 inches and make this interface more reasonable.

3.3.6 Mass Properties. After the flight unit was removed from the thermal vacuum chamber, it was configured for mass properties testing. The following deviations from the Arcjet ATTD flight configuration were in place during the flight unit mass properties test:

- The EM battery sub-assemblies were installed but connectors to these battery sub-assemblies were only tied in place and not electrically mated.
- The battery vent lines for the battery sub-assemblies on Panels #1 and #4 were tied to the battery sub-assemblies and not mechanically installed.
- Only a few pieces of the flight MLI were installed
- TQCM #1 was not installed. A mass model was installed in its place.
- Thirteen test thermocouples remained in the vehicle from the thermal vacuum test.
- Protective covers were installed on three of the TQCM sensors.
- Propellant was not simulated for these measurements.
- Shorting plugs for ordnance were installed during the test. These shorting plugs will not be installed for flight.
- Four close-out bolts on Panel 6 were not installed.
- Six close out bolts on top corners of structure were not installed.
- The twelve fasteners that secure the flight unit to the host spacecraft were not installed.

These deviations all involve low-mass items and were not expected to generate a noticeable change in the overall mass and cg location of the flight unit.

The weight and lateral Y and Z CG values were determined using the Space Electronics Mass Properties System WCG-15/5. The machine was calibrated per the operator's manual for weight and distance data and the machine calibration was verified by the TRW Equipment Management Center. The holding fixture for the flight unit was installed on the machine and a tare measurement was performed. The flight unit was then installed on the machine and three data runs were performed with the flight unit -Y axis (Reference Figure 40) at the +X axis of the machine. The flight unit was then hoisted slightly and rotated 180 degrees about its vertical axis (X) and re-installed on the machine with the flight unit +Y axis at the +X axis of the machine and three data runs were performed. The data from these runs are provided in Table 16.

Table 16. Flight Unit Mass Properties

Run Number	Weight (lb _m)	Y CG offset (inches)	Z CG offset (inches)
1	951.260	1.017	0.185
2	951.487	1.023	0.190
3	951.422	1.022	0.188
4	951.545	1.033	0.139
5	951.349	1.035	0.141
6	951.414	1.036	0.142
	Average Weight (lb _m)	Average Y CG offset (inches)	Average Z CG offset (inches)
	951.412	1.027	0.164

The Arcjet flight unit thruster alignment was performed immediately following the mass properties measurements using the same fixture. The flight unit was lowered onto the fixture using two 0.25 diameter guide pins to tightly control the orientation of the vehicle. A reference theodolite (TR) was positioned to a line of sight along two tooling balls and the azimuth compass of the theodolite was set to 180°. Two additional theodolites were set up, TX and TY, to provide the actual alignment measurements. An alignment fixture was centered on top of the arcjet thruster. In the center of this fixture was a machinist block that had two magnetic mirrors placed on two adjoining sides of the block. Around the perimeter of this fixture, eight 45° degree targets were placed so they faced radially outward. The line of sight of theodolite TX was adjusted relative to theodolite TR and then to the magnetic mirror on the thruster alignment fixture. The horizontal and azimuth readings for theodolite TX were recorded:

- Theodolite TX azimuth: 180 deg 52 min 47 sec (nominal is 180)
- Theodolite TX vertical: 90 deg 02 min 26 sec (nominal is 90)

Next, the line of sight of theodolite TX was adjusted relative to theodolite TR and then to the magnetic mirror on the thruster alignment fixture. The horizontal and azimuth readings for theodolite TY were recorded

- Theodolite TX azimuth: 270 deg 52 min 47 sec (nominal is 270)
- Theodolite TX vertical: 89 deg 59 min 25 sec (nominal is 90)

Photogrammetry was used to verify the theodolite alignment measurements. Photoreflective targets were placed on the mass properties machine in four locations. Hemispherical reflective targets were placed in each of the two bolt holes of the six flight unit mounting feet. The eight targets on the perimeter of the thruster alignment fixture were also used for these measurements. A video camera was used to take a series of still photos of the flight unit and the reflective alignment targets. The alignment photos were computer processed and verified the theodolite measurements.

3.3.7 Storage Preparations. In order to establish the flight unit's functionality prior to storage, a final functional test was performed. During this testing, the flight camera thermostat could not be actuated even though it was chilled with cold GN₂. The problem was a result of the thermal mass of the camera which prohibited the thermostat from closing. Since it was functionally tested during the thermal vacuum test, the thermostat was left in place on the flight unit with high confidence that the device is functional.

As part of the pre-storage functional test, the thermocouple rework was tested. A thermocouple generator was connected to the flight PCU harness at the thermocouple splice to simulate T3 and T4. The thermocouple generator was then set to various temperature readings and the PCU output for T3 and T4 were recorded. A second test was performed similar to the first except that the thermocouple splice near the PCU was elevated approximately 10°F to measure the effect of the temperature gradient on the actual PCU output for T3 and T4. The data generated during this testing was used to produce calibration plots for T3 and T4.

At the completion of the pre-storage functional test and before the panels were closed, a pre-storage cleaning was performed. All surfaces were vacuumed with a clean-room vacuum and residue left from thermal vacuum test heaters was removed using isopropyl alcohol. All test cables were removed from the flight unit and ESD covers were placed on all exposed connectors. The flight unit was then moved to the storage area and was placed under the following storage conditions:

Humidity: The flight unit was placed in an ESD-safe storage bag that had a continuous dry GN₂ purge. This GN₂ met TRW specification C795936-1; containing ≤ 1 ppm moisture and 99.9987% pure. The humidity of the storage was also maintained at 30 - 55% relative humidity.

Temperature: The ambient temperature was maintained at 50 - 80°F.

Monitoring: A temperature/humidity monitor was placed within twenty feet of the flight unit and checked twice a week to verify temperature and humidity requirements were not exceeded and that the GN₂ purge was still active.

Facility Ground: During storage, the flight unit was tied to static facility ground.

In addition to storing the flight unit in a dry GN₂ environment, 50 Ω terminations were put on the antenna input connectors of the EMI Electronics to prevent any damage to the input amplifiers.

During the flight unit storage period, correlation of the thermal vacuum test data and the flight unit thermal model was completed. The flight thermal model was modified and analyses re-performed to determine flight radiator sizes and verify the thermal system, as built, was acceptable. The detailed results of this effort are provided in a separate TRW report, 96.M532.1.15-001⁷.

3.3.8 Post-Storage Activities. According to the flight unit's original design, the PIU was to be secured to Panel #6 at the corner of each slice from the inside of the panel, as well as from the outside of the panel into the center of each slice chassis. The purpose of these outside center fasteners was to produce better contact between the slice and the panel for thermal heat conductance. These fasteners were not installed at OSC and not noticed until the flight unit was ready to go into thermal vacuum testing. It was decided at that time to let the test proceed without the fasteners and to use the actual thermal vacuum data to determine whether the center fasteners were truly necessary. During the correlation of the thermal model with the thermal vacuum test data, it was determined that only the battery charger slice center screws should be installed. Upon examining the panel holes and the location of the battery charger slice center holes, considerable offset between these holes was found. Therefore, the panel holes were slotted to accommodate for the offset. In order to perform this work, the battery charger slice was removed and a protective cover was put in place to catch any particles generated during the drilling. Once the holes were slotted, the battery charger slice was re-installed and the appropriate fasteners were installed.

One other hardware modification was performed as a result of the thermal model correlation. The thermistor that was located directly between the CCU and the PIU was moved for better thermal control of the CCU. This thermistor was moved less than one inch to directly at the baseplate of the CCU.

In January of 1996, the flight unit was removed from storage and moved to a clean room integration area for some rework and the pre-delivery functional test. The first rework performed was to move the secondary heater thermostat, the discharge thermostat and the panel thermistor for panels #1, 4 and 5 from the inside of the panel to the outside of the panel. This change was implemented because thermal vacuum data indicated that the original placement of these sensors would not provide adequate control of the panel heaters, and hence the flight battery sub-assemblies.

As a part of the post-storage test, two tests of the EMI boom were performed with the assistance of an OSC engineer. The first test was to verify free movement of the boom by removing the retaining nuts that held the boom in place. The boom was then manually deployed

approximately 135°. The boom was not fully deployed since doing so would result in the boom getting locked in place. This would have required complete disassembly and reassembly of the boom hinge to free the boom. No movement resistance was noted during this test.

The second test verified the functionality of the boom ordnance. A 5 amp, 20 millisecond pulse was sent to the bolt cutter ordnance and both bolt cutters actuated verifying the total ordnance circuit. The expended ordnance was removed and the ordnance housing returned to OSC to be refurbished. The housing was then reinstalled on the flight unit by an OSC engineer.

During pre-shipment preparations, TQCM #1 was re-installed onto the flight unit. This sensor was repaired after it was damaged during the flight unit vibration test, but was not re-installed before the flight unit was put into storage.

Also during pre-shipment preparations, a dent was found on the inside of Panel #1. It is hypothesized that the dent was a result of closing a small harness bundle in between the panel and the structure frame. The depth of the dent was measured and then the NASTRANTM model was run to determine whether a repair of this panel was necessary. The model indicated that no repair would be required if the dent was no deeper than 0.040 inches. The dent measured approximately 0.050 inches. Therefore, an aluminum doubler, 0.020 inches thick, was bonded to the panel in the area of the dent to restore the necessary strength to this panel.

Following the completion of all of the re-work, the post-storage/pre-delivery functional test was performed. Upon powering up the flight unit, it was immediately noticed that although the GSE power supply was providing power at 28 volts, the flight unit telemetry indicated a bus voltage of only 18 volts. Troubleshooting determined that there was not good contact of the ground wire with the GSE test fixture. Once a better ground was provided for the test set, the bus voltage telemetry matched that of the GSE power supply and the functional test continued.

The functional testing proceeded nominally with the exception of the telemetry from the T3 thermocouple on the arcjet thruster. The thermocouple telemetry indicated a thruster temperature of over 1700 °F. Since the thruster was at ambient temperature, this reading was known to be incorrect. Upon examining the thermocouple circuit, it was determined that the thermocouple splice on the underside of the diagnostic platform had come loose and an open circuit resulted. This was confirmed by applying pressure on the splice and getting the splice to make sufficient contact to provide a reasonable temperature reading. It was determined that the splice material used was too big for the size of the thermocouple wire. Therefore, this splice, along with the other three in the two circuits, was successfully reworked with smaller diameter splice sleeving and verified.

The PCU was run at high power during this functional test. It was tested by using the gradual power up procedure used throughout the program to verify the state of health of the PCU prior to running at full power. The final test of the PCU was 16 minutes long, at 26 kW, and the unit ran at an efficiency of over 95%. At the completion of this test, the PCU power cable test port was configured for flight, including the modification of the stuck test adapter piece that was drilled-out as originally planned (see Figure 36). This modification allowed for the installation of the torlon cap but did not completely remove the adapter piece in order to prevent contamination of the inside of the power cable.

After successful completion of the functional test, preparations were made for delivery to Boeing in Seal Beach, Ca. One such preparation was to change out the fasteners used by OSC to secure the arcjet thruster top adapter plate to the lower adapter plate. Since the fasteners called out in the drawing were too long, OSC substituted different fasteners. TRW determined that these fasteners would not be sufficient to securely hold the thruster in place due to thermal loads. The

high temperatures could cause a relaxing of the pre-load of the fasteners and allow some shift of the thruster, affecting thruster alignment. Therefore, TRW substituted a higher strength, shorter length screw in place of the OSC fasteners. The fasteners were systematically replaced, one at a time, to prevent any movement and misalignment of the thruster.

The Arcjet ATTD Flight Unit Delivery Ceremony was conducted on 23 February 1996. The ceremony was attended by various representatives from the Air Force, TRW, PAC, OSC, and Aerospace and is shown in Figure 53.

The flight unit was loaded into the AFRL shipping container, and a pre-shipment aliveness test was performed. This consisted of powering up the vehicle and verifying the flight unit was able to communicate with the ground support equipment. The flight unit was then delivered to Boeing on 6 March 1996. Prior to shipment, 1, 5 and 15g shock indicators were placed on the shipping container. One 5g indicator was set off during its installation. One 1g indicator was set off during the transport and one 1g indicator was set off during the off-load operations at Boeing. The fact that these indicators were triggered was not a concern.

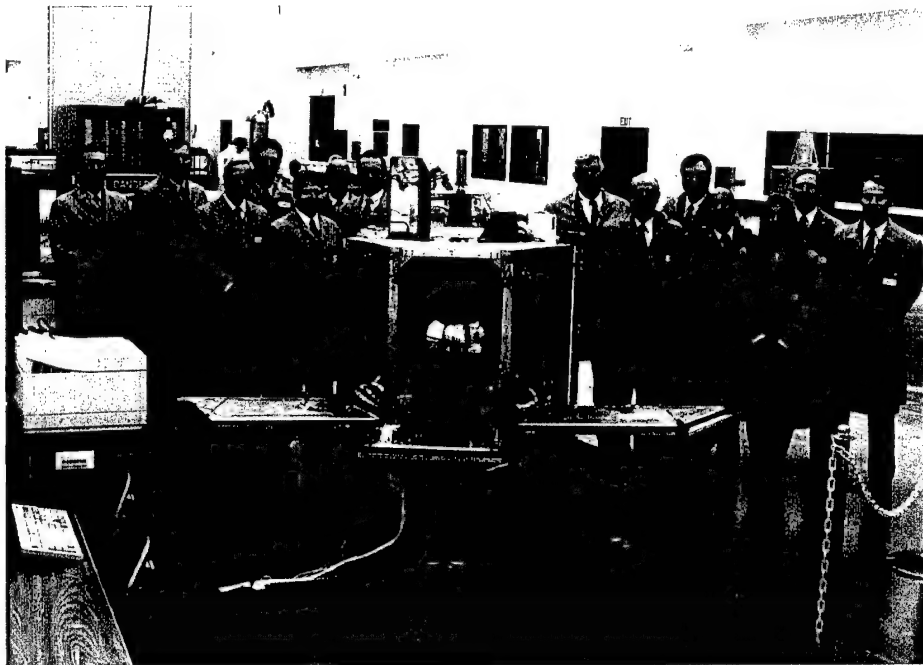


Figure 53. Arcjet ATTD Flight Unit Delivery Ceremony

3.4 POST DELIVERY OPERATIONS

3.4.1 TRW Activities. The thermal analysis of the video camera was updated in order to assess the affect of the higher temperatures expected from the arcjet during a firing on the filter and coverglass. Because of the uncertainties in this analysis related to the (1) thruster emittances and (2) the camera surface absorptances, the maximum predicted temperatures covered a wide range. Additional runs of the camera model did show that a significant thermal benefit could be achieved with a reflective coating on the front of the coverglass. A second issue was identified with the structural integrity of the filter holder assembly currently installed on the camera. The holder was

designed to withstand a maximum temperature of 120 °F, based on the preliminary thermal analysis. Based on the updated analysis with the thruster test data, the holder could see temperatures greater than 200 °F. A program decision was made to accept the diagnostic thermal design as it was configured, despite the higher anticipated temperatures from the arcjet.

3.4.2 Boeing Activities. As described above, the delivery to ARGOS was completed in early March, 1996 when the flight unit arrived at Boeing. Once the flight unit, now officially known as ESEX, was secured in the Boeing clean room, a post-delivery functional test was performed to verify the integrity and functionality of the flight unit. This was the same test performed at TRW during the final functional test prior to delivery, and all systems operated nominally. Items that could not be tested were the high power operation of the PCU and the mechanical thermostats on the flight unit. The PCU could no longer be tested at high power due to the test configuration required. The thermostats were not tested due to lack of accessibility. They were later verified during the ARGOS thermal vacuum test.

Once the ARGOS build-up was complete, ESEX was integrated with ARGOS and underwent a system-level flight qualification program on the integrated space vehicle (ISV). These tests included electromagnetic interference and compatibility (EMI/EMC), an acoustic and pyro-shock environment verification, and a thermal vacuum/balance test. Since the ESEX flight unit had already been flight qualified, the ISV testing primarily served to verify the interface between ESEX and ARGOS.

3.4.2.1 ISV Testing. ESEX was not mechanically integrated with ARGOS immediately, in order to allow maximum flexibility during the ISV checkout. Extender cables were used for the 28 Vdc power, command and telemetry, and structure current return connections. A full functional test was conducted on the ESEX/ARGOS interface in this configuration in order to verify the operational status of the flight unit. This test, identified as the pre-integrated systems test (IST), verified all of the interfaces between ESEX and ARGOS (power, command, and telemetry), and only a few problems were identified. Most of these anomalies occurred because of a misunderstanding of the most significant and least significant bits in the command and telemetry definition. The resolution involved writing a simple piece of software that inverted the least and most significant bits on a byte-by-byte level.

Following the successful verification of the functionality of the spacecraft, a series of tests were performed to verify the communications subsystem and the electromagnetic compatibility of the ISV. In order to ensure that ARGOS could communicate with the ground during flight operations, a test was performed to verify the commanding, telemetry, and ranging of the vehicle. This test consisted of commanding and receiving telemetry in the same way as that on-orbit, with a pre-determined command sequence uploaded to the vehicle. The proper execution of this sequence was verified via GSE as well as by downlinked telemetry.

The remainder of the IST proceeded based according to a more operational timeline. The test was divided into phases to simulate the mission profile - Phase I for the launch and early orbit operations, Phase II for ESEX and Critical Ionization Velocity experiment (CIV) operations, and Phase III for the remainder of the experiments. The majority of the ESEX test activity for IST was focused in Phase II and was based on the demonstration of the sequence commanding capability for the ESEX mission. A basic sequence was built which turned several boxes on and off at preset times during the test. This test was then repeated with CIV releases overlaid, and was then followed by a heater functional test. IST also verified the capability of the ESEX flight unit to

recover from an ARGOS switchover from the primary to the redundant side of the flight computer and the power distribution system. The only outstanding anomaly from IST was a spurious EMI antenna signal at or near 2 GHz that was observed on both EMI antennas at fluctuating intensity. Both EMI antennas measured a 8-10 dB signal above normal at 2 GHz. During initial testing, the signal from the boom antenna (antenna #2) was slightly stronger than that of the antenna on the deck (antenna #1). After the switchover of the ARGOS flight computer, however, the effect reversed so that antenna #1 saw a slightly stronger signal. The anomaly did not reappear after this occurrence. Troubleshooting was conducted to check for stray 2 GHz signals in the clean room due to ARGOS antennas, GPS antennas, electronics, etc but no spurious source was discovered. Further testing was performed to verify the functionality of the antennas at each frequency by using a simple signal generator and a log-periodic antenna. These tests verified the antennas functioned within their specifications and yielded no further spurious data. Since no further anomalous data were observed on the antennas, they were used for flight without further modification. Once Phase II of the IST was completed, the test was stopped in order to perform the EMC test as described below. The Phase III portion of the IST was performed following the successful completion of the EMC test.

3.4.2.2 Initial ESEX/ARGOS Mating. The original test plan was to complete IST prior to EMC, but flight hardware availability dictated the performance of the EMC test out of sequence - prior to the completion of IST. In order to accomplish the EMC verification, the ESEX flight unit was mechanically mated to the vehicle in order to simulate the flight configuration as closely as possible.

The ESEX/ARGOS mating, Figure 54, was accomplished via four leveling jacks that are a part of the ESEX ground transporter. The ESEX flight unit was placed in close proximity to the ARGOS vehicle, which was raised above ESEX using a facility crane. ARGOS was then lowered down onto the six ESEX feet using a hydraset to limit the loading on each of the feet to approximately 100 lb. Since the ESEX feet were measured to be coplanar to less than 0.003 inches prior to shipment, and the ARGOS bulkhead was measured to be flat within 0.003 inches over a 12-inch span, only a small gap was expected between the ESEX feet and the ARGOS bulkhead. However, once the mating was initiated, there was a relatively large gap (0.019 to 0.041 in) on four of the ESEX feet.

The explanation for this discrepancy can most likely be attributed to the difference in the ESEX configuration between the pre-delivery measurements and the ISV mating. For the ESEX measurement, mass mockups of each of the three battery sub-assemblies were installed on the ESEX battery panels, as the flight battery would be in the launch configuration. These mass mockups were removed prior to this initial mating and the ESEX panels (which act as shear panels) had been opened and closed several times. These factors suggest that some twisting of the ESEX structure could have occurred between the two measurements. There were a total of four mating/de-mating operations conducted throughout the ground tests in order to accommodate the test flow. Although these operations were performed in several different configurations, the gaps observed during the first mating remained unchanged. Flight shims were fabricated to account for the gap and installed prior to launch.

On subsequent operations, a revised mating procedure was devised to lower the risk of damaging the ESEX flight unit. This procedure was implemented as a result of an incident during the first de-mating operation that resulted in an overload on the ESEX structure. Since the ESEX transporter has four leveling jacks, the procedure was modified to raise the ESEX jacks

incrementally rather than lower ARGOS via the hydraset. This method provided much finer control over the mating, and avoided any further incidents. (see comments summary)

3.4.2.3 EMC Tests. Once ESEX was mechanically mated to the vehicle, the ISV was installed on a ground support fixture and the EMC test was initiated. As described above, the ESEX flight unit already passed a rigorous test sequence for EMC, as did all of the experiments, prior to delivery to Boeing. This previous testing enabled the system-level EMC to be a verification of the compatibility of the individual experiments with the ARGOS bus in a worst case susceptibility and emission environment.

There were two main objectives for the EMC test: verification of the bus power quality and ISV system-level compatibility. For the first objective, each of the experiment and space vehicle loads were switched on and off while measurements were made on an oscilloscope of the bus voltage and current ripple. For the compatibility portion, each of the experiments were placed in one of two modes in which the hardware was either in its noisiest state (while others were in the most susceptible state), or in its most susceptible state (while others were in their noisiest state). An evaluation was then performed of the state of health data transmitted from each experiment for a duration of six hours. No ESEX anomalies were observed. Following the completion of the EMC

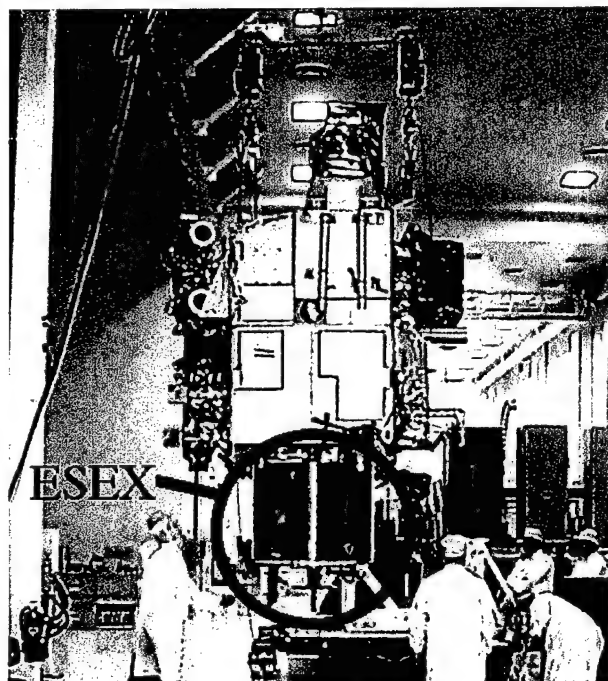


Figure a

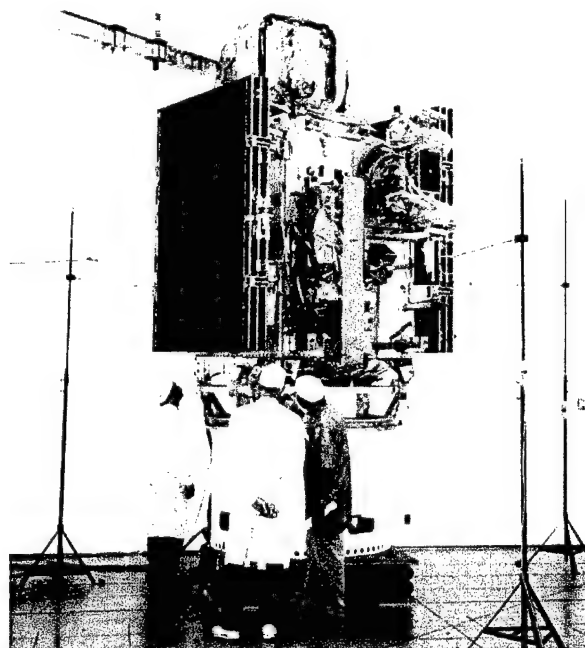


Figure b

Figure 54. Mating ARGOS to the ESEX flight unit (a) and the ISV installed in the acoustic chamber for the acoustic and pyro-shock tests (b)

test, the ESEX flight unit was de-mated from the ISV for the completion of the Phase III portion of IST.

The remainder of the IST was conducted for the Phase III portion of the mission by conducting a whole series of tests including nominal and anomalous operations for the seven Phase III experiments. For ESEX, Phase III is a benign operational regime in which the only activity is

battery discharging. For this portion of IST, then, ESEX was placed in a mode to simulate the battery discharge, and verify a proper shutdown if a software-detected fault occurred. No ESEX anomalies were observed for the duration of IST.

Upon completing IST, a combined systems functional test (CSFT) was completed as a vehicle performance baseline for the remaining environmental tests. The CSFT was a limited functional of all of the interfaces - both internal boxes and external experiments to the ARGOS bus. For ESEX, this consisted of an abbreviated version of the Pre-IST functional checkout, which validated complete ESEX functionality except for the high power operations involved with starting the arcjet.

3.4.2.4 Acoustic and Pyro-Shock. Following the EMI/EMC and IST tests, the next series of tests were initiated to verify the structural integrity of the ISV in an acoustic chamber (see Figure 51b). The overall test level for the spacecraft was 143 dB for a total of one minute, corresponding to the expected launch environment. The ISV was unpowered and in a configuration similar to launch with some minor differences such as MLI and ordnance. The ISV was mounted with the payload adapter fairing and the adapter ring mounted on an isolation system inside of the acoustic chamber. Since there was some concern regarding low frequency modes detected in the ESEX random vibration testing, the ESEX/ARGOS interface bulkhead was instrumented with several accelerometers in order to monitor the input into the ESEX structure during testing. After completion of a low-level preliminary sweep, several accelerometers were observed to have recorded high responses. These levels were all eventually traced to 60 Hz noise on the signal lines with one exception - the accelerometer mounted to the ESEX witness tower. There was some concern regarding the TQCM on the tower since this was the one that failed during the ESEX vibration test, but a CSFT following the acoustic test validated the diagnostics on the tower all operated normally.

The pyro-shock test immediately followed the acoustic test in order to verify the ISV could survive the shock spectrum expected at separation from the launch vehicle, and when the solar arrays were deployed. The ISV was in the same configuration as that of the acoustic test - unpowered, and mounted within the adaptor fairing and onto the adapter ring - and all of the same instrumentation remained including the two tri-axial accelerometers mounted to ESEX. The separation bolts for the fairing adaptor assembly were fired, followed by the bolts that secure the solar arrays onto ARGOS. After each test, the data from all of the accelerometers were analyzed to verify the response was as predicted. No anomalous results were observed.

3.4.2.5 Thermal Vacuum. The thermal vacuum/balance test was conducted to verify the functionality of the ISV in a thermal and vacuum environment similar to that on-orbit, as well as to verify the ISV analytical thermal model. Since ESEX completed a thermal vacuum/balance test, the ESEX flight unit was typically maintained within 35-55 °F in order to avoid overstressing any of the ESEX components. However, a thorough verification of the interface was accomplished by several CSFTs at the cold and hot temperature plateaus. There was also a considerable effort to calibrate the TQCMs during the ARGOS thermal vacuum test, an effort that ultimately proved only somewhat useful. Because the operation of the TQCMs was not well documented (for cost reasons), the commanding scheme used during the thermal vacuum test did not adequately cool the sensors to obtain a good frequency profile as a function of temperature.

The ARGOS thermal vacuum test was actually performed twice. The first test identified several box-level anomalies that dictated a second test to validate the fixes. Furthermore, the first

test was stopped midway through to change some of the panel radiators because the overall ISV temperature was 18-36 °F lower than predicted. Boeing analyses determined that the heat loss from the internal ARGOS boxes was lower than predicted. This lower heat rejection resulted in a lower requirement for radiator area on the ARGOS panels - which resulted in a colder ISV than expected. Once the first test was accomplished, including a validation of the new radiator areas, a series of fixes were implemented for the ARGOS integrated electronics unit (IEU), the load control unit (LCU) the solid-state recorder (SSR) and the GPS receiver. These fixes were completed in mid-1998, verified at the box-level, and the ISV was put back into the thermal vacuum chamber for the second test.

One ESEX anomaly was also identified and repaired during the thermal vacuum test preparations. Just prior to the first thermal vacuum test, the TRW thermal engineer observed that the silver-TeflonTM tape installed for the ESEX radiators was the incorrect thickness. Unfortunately, this oversight was not identified until after a significant portion of the tape was installed. In order to conserve ARGOS schedule, the ESEX re-work was delayed until after the first thermal vacuum test was complete. The re-work was performed in-between the two tests, and validated in the second thermal vacuum test. The second ARGOS thermal vacuum test was completed with no anomalies.

3.4.2.6 ESEX Ground Operations. Following the completion of the second thermal-vacuum test, the ESEX flight unit was removed from the ISV. While ESEX was de-mated, a series of ground operations were performed including the final flight software PROM installation, loading the NH₃ propellant, and battery activation and installation. These activities were accomplished in parallel with several ARGOS activities (which could not be accomplished with ESEX mated) including the weight and CG measurement, final thruster alignments, and a solar array deployment test.

The final flight PROMs were installed by the original TRW software engineer, who was brought out specifically for this task. The PROMs were finalized at TRW, transported to Boeing, and installed on the flight unit. Once installed, a complete ESEX functional test was accomplished which verified everything was working as expected (except for the high power operation associated with an arcjet firing). This included cycling both of the valves, the high voltage KilovacTM relays, and executing all of the final command sequences to be used for the flight operations. All of these tests were performed without any anomalies, although a couple of iterations on the final flight code were required for the correct sunsafe procedure implementation.

Following the flight PROM installation, AFRL personnel loaded the NH₃ propellant into the ESEX flight tank using AFRL-developed GSE. This effort was conducted outside of the clean room to avoid any possible NH₃ hardware contamination, and to eliminate the potential personnel hazard. In order to maintain the ESEX cleanliness levels, the flight unit was installed in an airtight container with a constant trickle purge of GN₂ to maintain positive pressure prior to exiting the clean room. The NH₃ transfer cart (ATC) worked simply on a pressure differential system using a small vacuum pump to evacuate the ESEX flight tank. Care was taken to minimize the amount of residual GN₂ in the flight tank (which was loaded prior to shipment from PAC to OSC) including several NH₃ flash/evacuation steps, in order to ensure that no GN₂ reached the thruster while it was operating. A total of 10.1 ± 0.05 lbs of anhydrous NH₃ was loaded into the flight tank from the ATC.

The battery installation was performed immediately following the NH₃ loading, but met with two anomalies prior to completion. The first of these was observed after the cells were

activated by Eagle-PicherTM at TRW, when one of the cells failed to hold a charge. This sub-assembly was ultimately sent back to Eagle-PicherTM and the cell replaced. While this cell was being replaced, the remaining two sub-assemblies were installed on the flight unit with only minor issues (usually as a result of missing fasteners, etc.). The third sub-assembly was delivered to Boeing and installed, while a set of test hardware was delivered to conduct the battery conditioning and system-level verification tests with the fully assembled flight unit. The battery verification tests consisted of performing a charge/discharge cycle with an external power supply and load. This test also verified the ability of the battery charger to operate stably at several states of charge, although never for more than 30 minutes because of the thermal limitations of the battery charger in ambient conditions. Higher frequency measurements were made of the battery charger output on an oscilloscope, and no anomalies were observed. The battery charging instabilities observed on-orbit (Reference 3.5.4) were not observed during these tests, presumably because the charger was not on long enough for the effect to begin. Once the charging tests were complete, the battery was discharged to approximately 173 Vdc (~ 1.37 Vdc/cell) in order to be at a low state of charge for launch, and the flight unit underwent its final cleaning. The remove-before-flight covers were also installed.

The second anomaly occurred after all of the battery testing was complete and the flight unit was undergoing the final packaging for launch. While closing panel #5, part of the battery harness was apparently pinched between the panel and the structure, causing a battery short to ground. The damage to the flight unit consisted of several damaged wires in the harness, a hole in the structure, and several depleted battery cells. After securing the flight unit, a full functional test was performed to verify the integrity of the remaining ESEX boxes, and no other anomalies were observed. The damaged wires in the harness were repaired or replaced, and the harness routing was re-worked to make sure there was adequate clearance between the panels, the ESEX structure, and the harness. Furthermore, the high and low sides of the harness were separated and insulated from each other, and to provide further protection from impingement on any sharp corners. The damage to the structure was repaired by grinding out the affected area (in order to reduce stress concentration zones), and installing a doubler to carry the stress load in the damaged rib. Finally, the four battery cells that were depleted (3 on panel #5 and 1 on panel #1) were re-charged with an external power supply. The charging was performed twice, because the first top-off did not charge the cells enough to keep them on that energy plateau when the power was removed. The battery state of charge was increased to approximately 201 Vdc (~1.6 Vdc/cell) to ensure the cells would not drop off this plateau. A final functional test was performed after all of the re-work was completed and no anomalies were observed.

Finally, the ESEX flight unit was closed up and installed on the ISV for the final time. This was completed in the same way as the previous mating operations, using the jacks on the transporter to raise ESEX up to the ARGOS bulkhead. The ESEX flight weight was measured to be 976 lbs without some of the interface MLI installed, but with the addition of several remove-before-flight covers, and the guide pins used to mount ESEX onto the transporter. Once mated, the final MLI was installed, the battery thermostats were verified, the final arcjet alignment measurements were made, and the final factory functional test was conducted.

3.4.2.7 Arcjet Alignment Measurements. A validation of the arcjet alignment to the ISV CG was required in order to ensure the arcjet firing would not saturate the ARGOS reaction control system. Unfortunately, a direct measurement could not be made because there was not a good line-of-sight while ESEX was mated to ARGOS and the two were in the ARGOS

transporter. In order to perform the alignment validation, two measurements were made - one of the thruster exit plane to the ESEX feet, and then one from the ESEX feet to the vehicle CG - and the results of the two were added together analytically. Both of these measurements were made with theodolites and reflective mirrors, typical of many thruster alignments. The first measurement (from the nozzle to the ESEX feet) was made before IST when ESEX was de-mated from ARGOS and the thruster was pointing up. The final alignment measurement was performed after ESEX was mated to the ISV for the final time and the ISV CG location was known. The results of this test confirmed the measurements made at TRW - in spite of the gaps between the ESEX feet and the ARGOS bulkhead - and confirmed that the arcjet nozzle was pointing at the CG within the specified limit.

3.4.2.8 Launch Pad Activities. Following the successful completion of the final functional test at Boeing, the vehicle was packaged in the transporter and shipped via air-ride truck to VAFB for launch. Once the vehicle arrived at VAFB, it was unpacked, purges were re-established, and a post-delivery functional verification was performed. During this test, it was observed that the ESEX battery voltage was lower than expected, decreasing to approximately to 160 Vdc. After consultation with Eagle-PicherTM, and a review of the battery telemetry circuit, a 368 k Ω load from two resistors in the PIU was discovered across the battery - draining the charge. Since there was no way external power could be used to charge the battery without a significant amount of on-stand re-work, and because of the thermal limitations of the battery charger in ambient, a re-charge plan was initiated that used the flight charger in a cyclical manner. The method would turn the flight charger on for 30 minutes, and then leave it off for 60 minutes before turning it on again. Although this technique required 31 cycles (46.5 hours of test time) to keep the battery at an acceptable state of charge, it proved to be effective. The final pre-launch activity was the extraction of the remove-before-flight items which was performed on 4 Jan 99, and the vehicle was prepared for the scheduled launch on 12 Jan 99. Several anomalies occurred which delayed the launch until 23 Feb 99 including ground telemetry errors and a bad vernier engine on the Delta II, but the weather (primarily high winds) proved to be the biggest problem through the ten launch slips. Ultimately, the vehicle was launched successfully on 23 Feb 99 at 10:29:55 GMT, and was inserted to within 1% of the nominal orbit.

3.5 FLIGHT OPERATIONS

This section draws a great deal of its material from References 8-12 which are conference papers written by a number of USAF Research Laboratory personnel. As detailed below, data from all of the on-board diagnostics were collected for each of the firings. Several ground-based measurements were also performed for specific firings. In general, the performance of the thruster was nominal and, while there were measurable effects observed, none of the on-board or remote diagnostics indicate any issues with integrating high power electric propulsion onto spacecraft. Furthermore, none of the firings had any effect on the ARGOS operations.

3.5.1 Phase I Operations. After the successful launch and first acquisition, the operations focused on verifying the spacecraft bus and ESEX were fully operational. ARGOS completed its nominal initialization except for two issues. The first prevented the use of the Global Positioning System to support ESEX operations as originally planned. The second issue, an inability to perform ranging, commanding, and telemetry downlink simultaneously with the AFSCN standard uplink

power and command modulation index, made some of the ESEX electromagnetic test objectives difficult to accomplish.

The first ESEX activity following turn-on was to initialize the TQCMs and begin cooling these sensors in order to characterize the vehicle outgassing. The second objective was to enable battery charging to prepare for the upcoming firings and prevent energy loss from the PIU bleed resistors. On the second day of charging, the first of two ESEX anomalies were observed. High oscillations on the battery charger output were observed when the battery voltage approached -225 Vdc (the arcjet and battery were connected so that the anode is at ground potential, thus a more negative voltage is "higher"). This was probably related to the overall problem with the battery (as discussed below) which ultimately led to the battery failure.

As the ESEX battery was charging, the remainder of the ESEX initialization and checkout was completed. This checkout included a verification of all of the electronic boxes, the thermal control system, and the command sequences used to control the majority of the ESEX operations. The ESEX EMI boom was deployed on day 14, after data were gathered on TQCM sensor #4 with the sensor pointed at the ESEX diagnostic deck. Once all of the initialization activities were completed successfully, Phase II began.

3.5.2 Phase II Operations. Phase II was dedicated to two primary experiments - ESEX and the CIV experiment. The original operations plan called for integrating ESEX firings with CIV releases for the duration of the mission. This concept, however, did not prove logistically feasible due to a shorter amount of time between ESEX firings coupled with weather and instrument problems at the ground observation sites. This change, however, did not dramatically affect either the CIV or ESEX total mission success.

The first ESEX activity in Phase II was to perform a series of outflows from the PFS, first of GN_2 , and then of NH_3 while monitoring the ESEX and ARGOS state of health telemetry. These activities are summarized in Table 17. The objective of these outflows was four-fold: to bleed the GN_2 blanket from the plenum tank; to verify the operation of the PFS; to verify the arcjet cold flow thrust would not have a detrimental affect on the ARGOS attitude control system; and to measure any off-axis thrust (which there was none). The GN_2 outflow was conducted over two passes, to allow enough time to evacuate the plenum tank to < 1 psia, by opening the arcjet valve (i.e. the PFS algorithm was not activated). During the NH_3 outflow, the PFS exhibited nominal behavior except for a momentary ingestion of a slug of liquid NH_3 at the initialization of the PFS algorithm.

PFS heater performance prior to the outflows indicated that the bulk of the NH_3 liquid remained away from the outlet of the propellant tank. This was the intended operational profile (Reference 3.2.5), accomplished by differential heating of the propellant tank poles and possibly aided by the angular momentum of the spacecraft in orbit. During the NH_3 outflow (and throughout the mission), temperatures of the EFH indicated relatively little liquid entering the EFH, and 100% vapor outflow at the exit. The duty cycle of the flow control valve showed a large control margin with the measured flow rate often within ± 0.3 mg/sec of the setpoint, well within the specified requirement of ± 5 mg/sec.

The ingestion of liquid NH_3 at the initialization of the PFS algorithm was unexpected since it was not detected in any ground tests. While the liquid ingestion was brief and confined to the initial valve pulse, it occurred for every outflow except the last firing (F-8). This minor problem was overcome by implementing an operational delay after opening the arcjet valve - allowing the plenum tank to "dry out" and the flow to stabilize before starting the arcjet.

Table 17 - Summary of ESEX Arcjet Firings and Propellant Releases

Firing (F) or Release (R) No.	Date/Time	Duration	Location	Comments
R-1 (GN ₂)	11 Mar 99 1928 Z	8:29 (509 sec)	Not observed	Initial GN ₂ bleed required majority of pass.
R-2 (GN ₂ /NH ₃)	12 Mar 99 0027 Z	1:13 (73 sec)	Not observed	GN ₂ bleed completed. NH ₃ aborted due to overly conservative software constraints on PFS heaters.
R-3 (GN ₂ /NH ₃)	12 Mar 99 1258 Z	1:59/3:59 (119/239 sec)	Not observed	All systems operated nominally. Liquid ingestion first observed.
F-1A	13 Mar 99 1240 Z	N/A	MSSS	First arcjet ignition (on 10 th start pulse) - firing aborted due to overly conservative software constraints on mass flow rate.
F-1B	15 Mar 99 1210 Z	N/A	MSSS	Firing attempt aborted due to overly conservative software constraints on PFS heaters.
F-1C	15 Mar 99 2155 Z	2:21 (141 sec)	CPCA	Modified firing sequence to account for liquid ingestion and ensure vapor outflow to arcjet. CPCA performed passive data collection.
F-2	19 Mar 99 2232 Z	5:01 (301 sec)	CPCA	Flow rate setpoint increased to 250 mg/sec. All systems operated nominally. CPCA acquires first active data set.
F-3	21 Mar 99 1224 Z	5:33 (333 sec)	MSSS	All systems operated nominally. No MSSS data acquired due to inclement weather.
F-4	23 Mar 99 2127 Z	8:02 (482 sec)	CPCA	All systems operate nominally except for low battery output voltage - causes arcjet to shut off early. First indication of battery trouble.
F-5	26 Mar 99 2145 Z	5:04 (364 sec)	MSSS	Low battery voltage forces early termination. Telemetry problem makes operating arcjet difficult. MSSS acquires first space-based arcjet firing spectra.
R-4 (NH ₃)	30 Mar 99 0636 Z	9:54 (504 sec)	N/A	Attempted PFS heater modifications to eliminate liquid ingestion do not succeed.
F-6	31 Mar 99 1305 Z	4:30 (270 sec)	MSSS	Low battery voltage forces early termination. Telemetry problem reduced by increasing ground transmitter power. No firing spectra acquired.
F-7A/B	2 Apr 99 2209 Z	53 sec/38 sec	CPCA	Attempt to discharge battery as much as possible prior to reconditioning. Arcjet stopped/re-started due to PCU command logic. CPCA acquires start and stop transient data.
R-5 (NH ₃)	9 Apr 99 1548 Z	9:06 (456 sec)	N/A	Further attempts to eliminate liquid ingestion with PFS heater modifications do not succeed.
F-8	21 Apr 99 1222 Z	42 sec	MSSS	Battery reconditioning has no effect on arcjet firing time. No MSSS data acquired. No liquid ingestion observed.

Once the PFS operation was verified, the arcjet firings were initiated. The firings were all conducted over two ground sites to facilitate ground-based observations. These two sites were the 1.6m telescope at the Maui Space Surveillance Site (MSSS) for optical observations and the Camp Parks Communications Annex (CPCA) in Dublin, CA for the communication experiments.

The first two firing attempts (F-1A and -1B) were aborted due to overly conservative software constraints. Initial adjustments to the ESEX system were expected, and did not reflect system behavior that was anomalous or out-of-specification. Subsequent data review showed the arcjet actually ignited on the first firing attempt (F-1A) on the tenth start pulse, but was aborted within 2-3 seconds due to a mass flow rate limit that was too tight for the ramp up phase. The second firing attempt (F-1B) was aborted by a temperature software limit prior to the arcjet start.

The need for ten start pulses to ignite the arc on the first attempt is consistent with ground test experience, where multiple start pulses were often used. Additionally, flight experience with other arcjets has typically shown the first on-orbit ignition to be slightly more difficult than all subsequent starts, possibly due to oxidation or slight, unavoidable contamination of the cathode from ground handling, cleanliness levels, etc. Interestingly, all subsequent ESEX firings ignited on the first pulse, validating the work done early in the program (Reference 3.2.3.7) to ensure reliable arcjet starts. The first successful arcjet firing (F-1C) was completed after a thorough review of all software limits. The planned duration for the first firing was four minutes, but was terminated after 141 seconds because the contact support was ending - mostly as a result of the delay from the liquid ingestion. This firing was performed over CPCA, which passively acquired data on the ARGOS transmission spectra. The results acquired from CPCA are discussed briefly below, and detailed in another article.⁶

Subsequent firings proceeded much in the same manner as F-1C. The mass flow rate for the remaining firings was increased, however, since the arcjet power appeared higher than the nominal 26 kW. Later analysis suggested this may not have been the case as discussed below and elsewhere.⁷ Figure 55 illustrates a typical operational data set for a firing (in this case from firing F-4 on 23 Mar 99). As shown, the arcjet, PCU, and PFS (all of the demonstration components) operated well - typically well within the specifications set forth at program initiation. The liquid ingestion and the drop in battery output voltage can also be seen in this figure. The drop in battery output voltage ultimately caused the arcjet to stop since it was below the acceptable PCU input voltage.

Battery charging was conducted between each of the firings, which were scheduled on high elevation passes at either MSSS or CPCA. This scheduling philosophy maximized the opportunities to collect data, but forced the duration of each firing to be limited by the amount of charging performed.

Phase II proceeded with seven additional firings and the remainder of the ARGOS mission Phase II operations. Besides the liquid ingestion and the battery failure, and minor telemetry issues with the arcjet current and inlet pressure, the entire ESEX flight unit performed flawlessly. Ultimately, however, the battery failed completely, eliminating any chance of further ESEX firings. Since this failure occurred within days of the scheduled end of Phase II and the majority of science data had been collected, the result was only a minor impact on the overall mission success. Once the battery condition was stabilized, ESEX was placed into a long-term discharge configuration for the Phase III portion of the ARGOS mission. ESEX will continue to collect data from the on-board sensors until the flight unit power is disabled.

3.5.3 Preliminary Science Results. The science data collected during ESEX operations was divided into sections corresponding to the scientific objectives and the specific sensors. These areas are performance, contamination, optical and EMI. The following data are the initial results from the experiment, and constitute the preliminary analyses performed to date.

3.5.3.1 Performance. The arcjet performance was measured by three different techniques: an on-board accelerometer, AFSCN tracking, and the ARGOS GPS receiver. The ΔV derived from each of these three different techniques agree to within 1%.

The on-board accelerometer data were collected for all eight firings. There are a number of uncertainties in the thrust derived from the acceleration measurement dominated by the

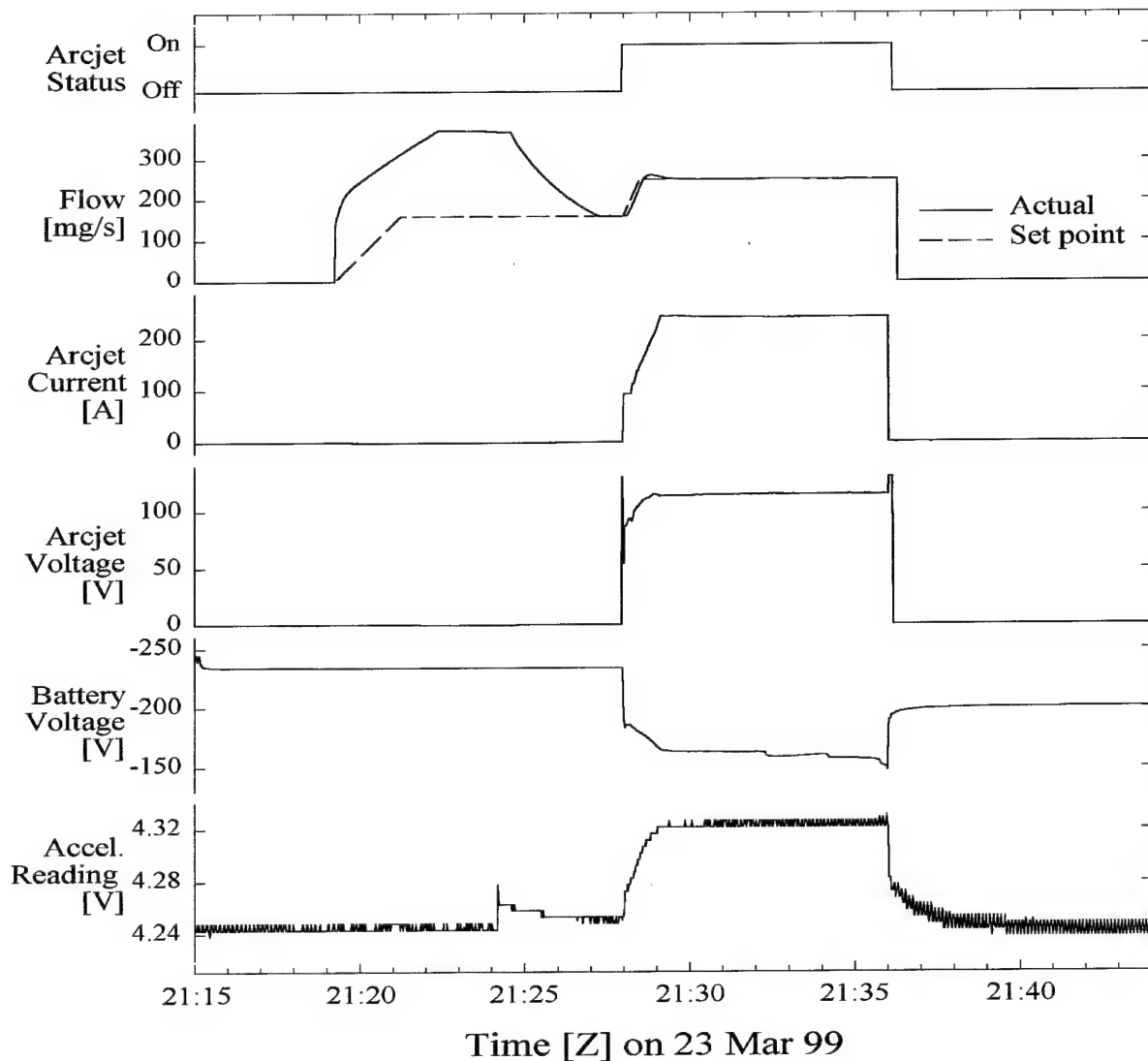


Figure 55 - Typical Operational Profile Of An Arcjet Firing (F-4) Showing The Ramp To Full Power And Steady-State Operation

systematic uncertainties associated with the accelerometer, PFS, and PCU. Figure 56 shows a summary of the I_{sp} for all of the firings plotted against the ground test data on the EM hardware. The preliminary analyses conducted to date suggest the arcjet current telemetry was repeatedly reading approximately 7% high. Since this has not been confirmed, although much of the data examined to date appear to agree with the corrected numbers, the data presented here are uncorrected for the higher power readings. This figure does show, however, the mean of the corrected performance as an illustration of the effect of the 7% difference. In summary, the measured I_{sp} was 786.2 ± 49.8 seconds, the efficiency was $26.7 \pm 2.7\%$, and the thrust was 1.93 ± 0.09 N.

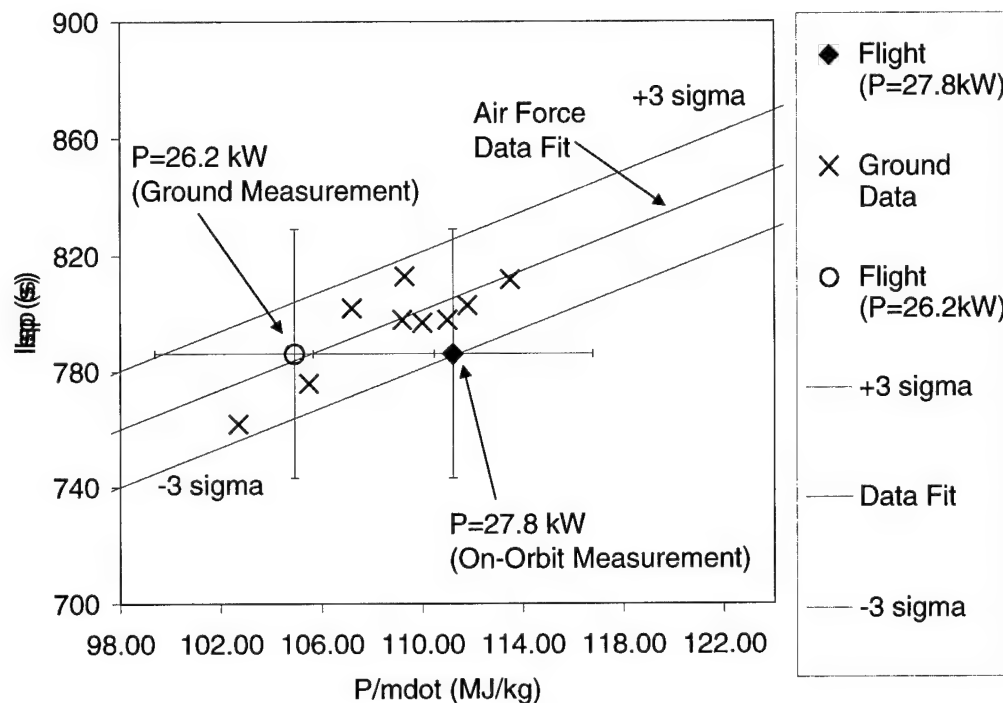


Figure 56 - Arcjet On-Orbit Performance Uncorrected For Any Power Deviations

3.5.3.2 Contamination. An array of sensors were positioned at strategic locations of the ESEX package in order to assess the contamination effects of the arcjet firings. Mass deposition, which can impact satellite optical and thermal control surfaces, is measured using the four TQCMs. Thermal flux from the arcjet firing is measured using the four radiometers coated with S13-GLO, a common thermal surface material with low solar absorptivity and high emissivity. Measurement of heat transfer through the coating identifies the degradation of the S13-GLO when subjected to the spectral emission of the high-power arcjet. This degradation affects the thermal design of spacecraft using high power electric propulsion. A sample Ga-As solar array segment placed near the arcjet nozzle determined the potential for plasma-solar array interactions or obscuration of the solar flux, which can have a deleterious impact on satellite power generation capability.

A summary of the ESEX TQCM data is presented in Figure 57. During eight firings of the ESEX arcjet, no measurable material deposition is observed that is attributable to the steady-state operation of the arcjet. Material is collected on the sensor nearest the thruster exit plane (TQCM sensor #1) on the first firing, however the lack of similar collection on subsequent firings suggests this material was a one-time efflux indicative of the fabrication and handling, and not indicative of steady-state contamination rates. TQCM sensor #2 (which is not in the line-of-sight of the arcjet body or the plume) shows essentially no effect from the firings. Surprisingly, the TQCM sensors within this line-of-sight generally show a removal of previously deposited mass with each firing.

In a similar effect, the radiometers placed near the thruster exit, with a view of both the arcjet plume and body, show degradation of the sensor material from the arcjet firings. Radiometers with no view of the arcjet, or a view of only the plume, show no measurable degradation. Thermal transient analysis, required to determine the heat flux to the spacecraft from the arcjet firing, has not yet been performed.

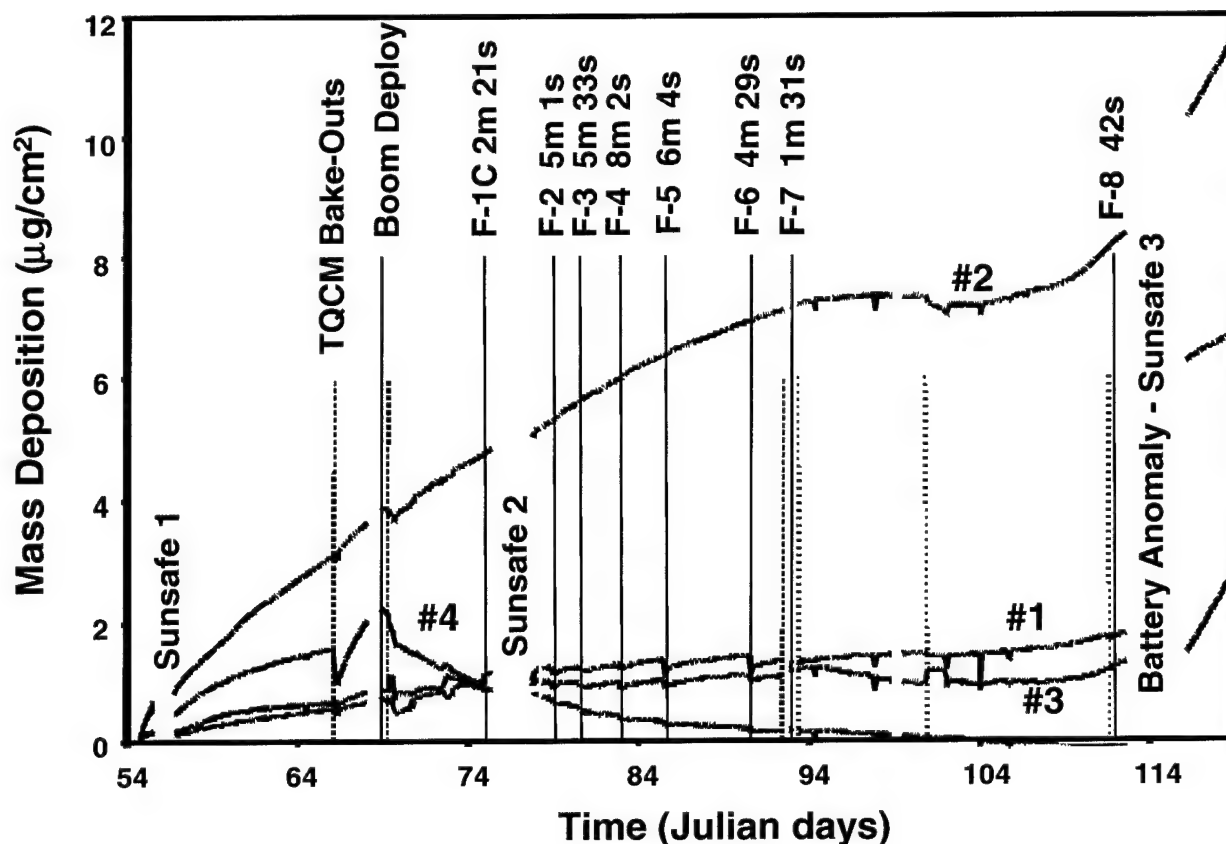


Figure 57. Summary Of TQCM Effects From The Arcjet Firings Over The First 65 Days From Launch

Solar cell segments placed near the thruster exhaust show increasing degradation through the experiment, attributable to the exhaust plasma partially shorting the solar cell load. The solar array measurements also show a 3% decrease in power generation over the 60-day time period in which the arcjet was fired, attributable to degradation in the solar transmissivity of the cover glass material. No deleterious effects associated with the arcjet firings were observed on the main ARGOS solar arrays.

3.5.3.3 Optical. Optical observations were made from a ground-based sensor, the 1.6m spectrograph/telescope at MSSS, and an on-board sensor, the still frame video camera. The objective of these observations was to characterize the emitting excited states both from a spectroscopic and spatial perspective. Emission more than a few millimeters from the nozzle arises from recombination and consequently the measurement environment is expected to be significant to the observations. The ESEX flight was the first opportunity to observe a high-power plume expansion under molecular flow conditions, since ground emission measurements have all been performed at considerably higher background pressure.

Spectroscopic data were expected to yield information about the energy distribution of excited states (and thus contribute to the overall understanding of losses in the arcjet). The specific

intent was to closely examine the NH (A-X) transition at moderately high resolution in an effort to determine vibrational and rotational temperatures. The spectroscopic data also include continuum emission from the hot arcjet nozzle that can be compared to nozzle temperatures measured in ground test. A very small subset of the anticipated ground based spectroscopic data were obtained during the flight campaign. The single firing usefully observed recorded arcjet emission over the spectral range 320-670 nm at low resolution. In addition, the poor weather conditions during the observed pass make unambiguous spectral intensity calibration difficult, and unfortunately the spectral resolution is not high enough to make the best estimates of the NH temperatures. However, the principal features observed from the flight agree with ground tests, namely, atomic hydrogen lines dominate the line spectrum, along with the NH complex at near-UV wavelengths; and the emission lines sit on top of a greybody continuum rising to the red end of the spectrum. Further analysis and interpretation of the results are underway.

The video camera provided a verification of normal arcjet operation and was partly intended as a diagnostic for anomalous operation. More important, however, was the expectation that the video images would reveal the extent of the emitting part of the plume to be smaller than that observed on the ground, since a small recombination volume is expected in space. Finally, the video camera was expected to confirm temporal and spatial aspects of arcjet nozzle heating models.

The on-board camera acquired images during each of the eight firings with several different shutter speed settings. Unfortunately, there were not enough firings to test the full dynamic range of the camera, and the bright thruster at full power mostly washed out several images. There was obtained, however, a significantly useful survey of images of the arcjet during the first 90 seconds of operation illustrating the rapid heating of the anode and extent of the plume. Part of this series is shown in Figure 58, which shows the startup and most of the 70-second ramp to full power.

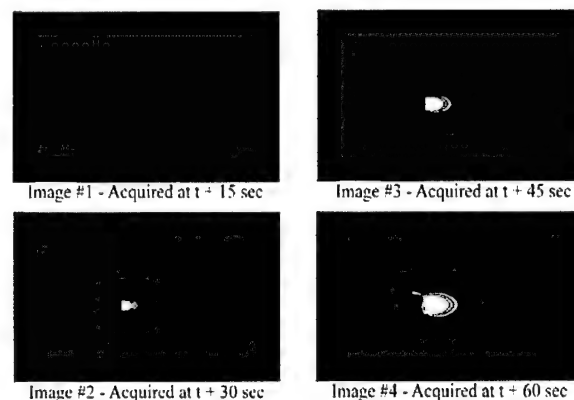


Figure 58 - Series Of Images Acquired From The On-Board Video Camera Showing The Ramp To Full Power

3.5.3.4 EMI. The impacts of a 30 kW class arcjet on spacecraft communications and operations have always been a major integration concern. In order to address as many of these potential issues as possible, a series of tests were performed during the ESEX mission. These tests included measurements from the on-board EMI antennas, communication bit error rate (BER) tests to quantify the effect of the arcjet on the ranging signal, and uplink/downlink tests to qualitatively

verify the communication link integrity. The results from the uplink/downlink test, and other qualitative results from the performance of the ARGOS sub-systems, are still being evaluated.

The on-board EMI antennas measured the radiated emission from the arcjet in the lower gigahertz communication frequencies (e.g., S-band, X-band, etc.) The antennas sample 2, 4, 8, and 12 GHz signals with a $\pm 5\%$ bandpass filter on each channel. Data were gathered on the antennas for each of the firings, during quiescent spacecraft periods, and during routine spacecraft operations. The firing and non-firing data sets were then compared to identify any effects from the arcjet operation. The antenna measurements during arcjet firing periods did not differ from non-firing data which correspond to ground test data.

The BER test enabled a quantified assessment of the effect of the arcjet on the satellite ranging channel. This test is performed by replacing the normal ranging pattern with a test pattern from CPCA and determining the number of bit errors on the return signal using a BER counter. A series of baseline measurements were made while the arcjet was off, and with the vehicle in several transmit configurations for comparison with firing data. Figure 59 shows a representative data set from the BER tests with an arcjet firing vs. a baseline measurement. These data were recorded at transmit rates of 1.024×10^6 bits/sec, with typical error rates less than 2 bits in 10,000.

In total, three arcjet firings and over thirty baseline BER curves were recorded during the ESEX flight. Preliminary analyses of the data did not reveal a clear correlation between features observed in the arcjet firing curves and the operation of the arcjet, since similar features are identifiable in both baseline and arcjet firing curves. Further analyses are underway to isolate the causes of the observed features in order to determine the impact, if any, of high power arcjet operations on communications.

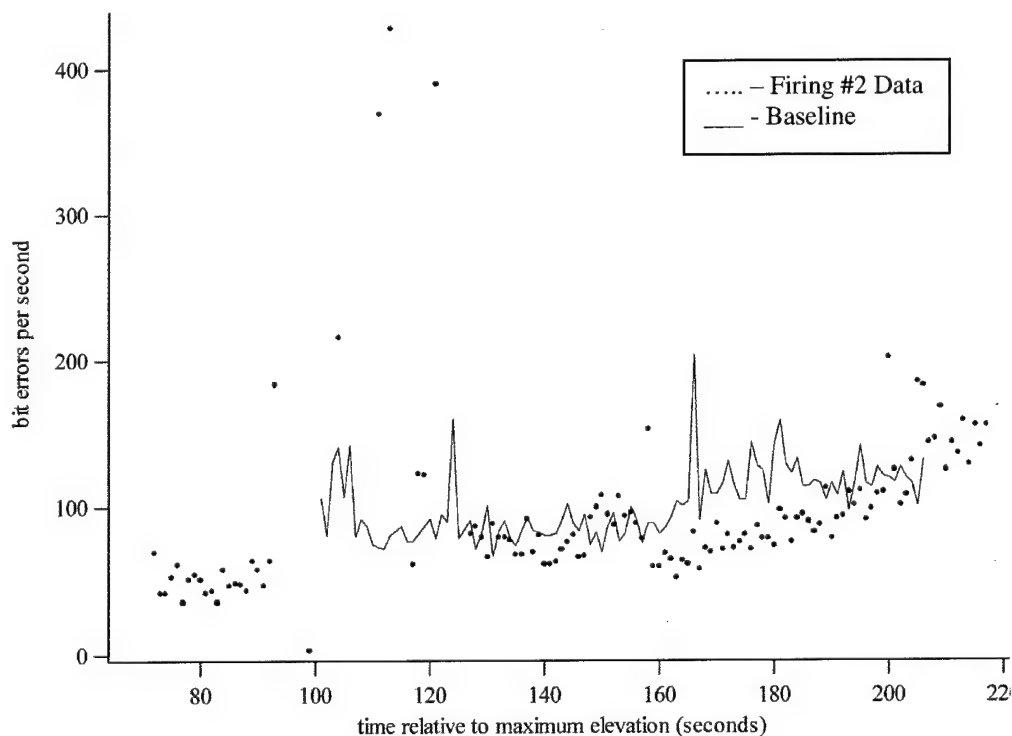


Figure 59 - Representative Bit Error Rate Data For Firing #2 (F-2) Displayed With Baseline Pass Taken Under Similar Conditions

In general the ESEX results are very promising for the integration of high power electric propulsion on commercial and government satellites. Although degradation associated with contamination is observed, in each case the effect is observed only on sensors placed very near the exhaust nozzle. It is highly unlikely that sensitive material or sensors would be located this close to the arcjet exit plane in a fully-developed, high power electric propulsion system. Contamination sensors located in the backplane of the arcjet, or behind the thermal shield, show no deleterious effects.

3.5.4 Flight Anomalies. There were two ESEX anomalies experienced during the Phase II operations: one affecting battery performance and the other affecting PFS gaseous outflows.

3.5.4.1 Battery Performance. The first signs of anomalous behavior in the battery were observed during the first charging cycle, shortly following the first ARGOS sunsafe. The charging circuit operated nominally (except for a lower output current than expected) until the battery voltage approached -225 Vdc. At this point, as shown in Figure 60, the output current from the charging circuit began cycling on and off, resulting in oscillations of the open circuit battery voltage. Initially, this was thought to be a result of a higher-than-expected internal battery resistance. In an attempt to lower the charging circuit impedance, the high capacitance filters in the PCU were switched into the circuit via the KilovacTM relays. This did improve the stability somewhat, but did not eliminate the fluctuations. Since this instability was not detrimental to the ESEX battery or the spacecraft bus, it was decided to charge through this region and realize the charging inefficiencies by extending the total charging time. Subsequent charge cycles showed a

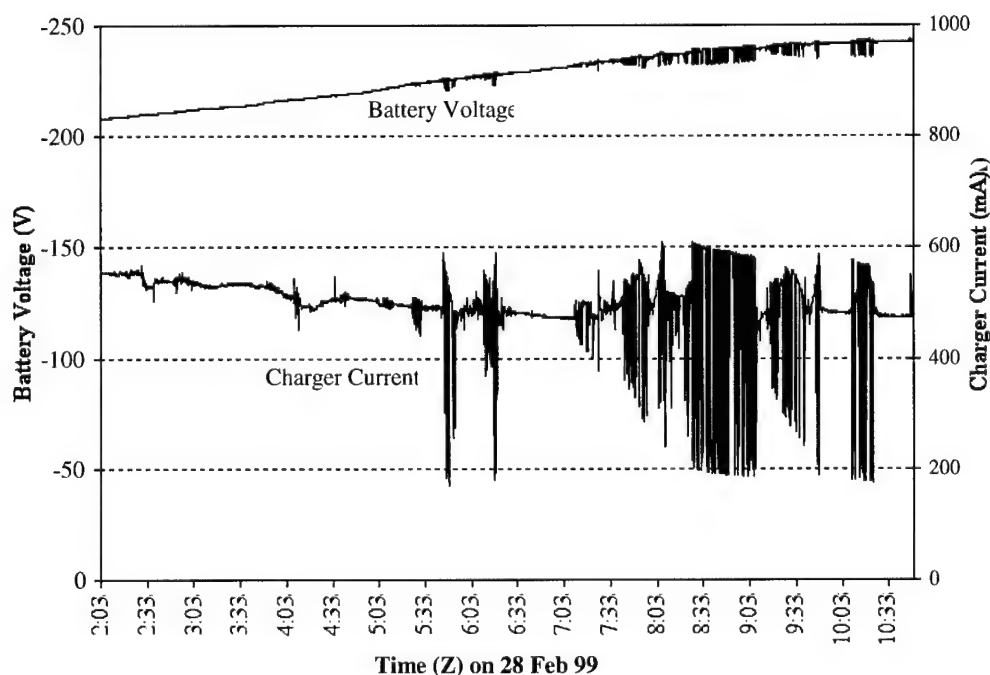


Figure 60 - Typical Battery Charging Circuit Instability

degrading instability that caused the charging circuit to shut off prior to attaining a full state of charge.

Beginning on F-4, further anomalous behavior on the battery output started appearing which resulted in a limited total firing duration. This was manifested as a low battery output voltage, resulting in unstable PCU and arcjet operation - eventually extinguishing the arc. It should be noted, however, that the voltage at which the arc extinguished was approximately -147 Vdc - well below the lower PCU specification limit of -160 Vdc. As can be seen in Table 15, the duration of each firing after F-4 steadily decreased, as the battery performance deteriorated. On F-7, the arcjet cycled on and off twice (due to the command logic in the PCU) - both firings being extremely short. After this event, the battery was reconditioned by performing a deep discharge through the bleed resistors, and restarting the charge. The initial plan was to wait until the battery was at a full state of charge (indicated by the charger circuit shutting off at the upper charge limit) before attempting the next firing. After approximately 19 days, however, the charger was commanded off and a firing was attempted. Unfortunately, as can be seen by the short duration of F-8, the reconditioning did not have the desired effect.

Following the completion of F-8, the battery voltage fluctuated erratically between -175 and -200 Vdc with periodic drops as low as -30 Vdc - where it eventually stabilized. This behavior lasted approximately 24 hours until, as subsequent analysis revealed, the battery sub-assembly on panel #1 had a catastrophic failure. This failure was probably a result of electrolyte leakage from one of the cells, causing a short circuit to the battery case. As the energy in the cell was discharging internally through the short circuit, there was a dramatic increase in the battery temperature and pressure as hydrogen gas was being generated from decomposition of the electrolyte. This process continued until there was a breach of the battery case and a release of this super-heated gas internal to the ESEX flight unit. This gas was eventually vented into space, which caused a dramatic attitude disturbance on the vehicle, resulting in a sunsafe event. Further discussion on the contamination effects from the battery venting is described elsewhere.

The cause of the battery problem will never be fully known since the flight data do not present a complete picture of the anomaly. There was, almost certainly, a combination of effects that ultimately describes the entire data set. Recent data show, for instance, a significant increase in impedance of a Ag-Zn battery as it approaches a full state of charge at a low charge rate - which would explain the charger instabilities, but not the ultimate failure. Some phenomenon was responsible for rupturing at least one of the battery cells and causing electrolyte to leak out and short to the battery case. It is also likely that some of the electrolyte was vented from the battery cells during launch as the flight unit de-pressurized, and also as the high current firings were conducted. This expelled electrolyte could have led to a variety of problems such as degraded mechanical connections or bridging the two cell electrodes and causing a short. In any case, this battery was pushed beyond its design parameters and was still able to deliver eight successful firings. In hindsight, a different battery and battery charger design might have been more appropriate for this high discharge/low recharge application.

3.5.4.2 PFS Liquid Ingestion. The PFS liquid ingestion anomaly was initially observed on the first successful NH_3 outflow. Upon initiation of the PFS algorithm, evidence of a single slug of liquid NH_3 being ingested by the plenum tank was observed on the initial DPC valve cycle. Figure 61 illustrates the issue for a typical outflow. Note that plenum tank temperature drops $\sim 70^\circ\text{F}$ as soon as the PFS flow control algorithm is initiated, indicating that liquid NH_3 is

expanding into the plenum tank. The plenum tank pressure and temperature soon indicate a super-heated condition and drying out of the liquid in the plenum tank as some of the NH_3 vapor is vented through the open arcjet valve. The flow meter immersion thermistor shows no similar drop in temperature, indicating that the liquid is confined to the plenum tank and never passed to the arcjet, even prior to arc initiation. To be sure that no two-phase flow reached the arcjet, however, the arcjet start was delayed until a dry plenum was achieved in all cases. After this initial ingestion, all PFS temperatures and pressures indicate no liquid was passed to the plenum tank or arcjet.

A schematic representation of the PFS is shown in Figure 26. The operational profile is presented in detail elsewhere,^{13,14,15} but basically consists of two heating periods prior to the outflow, one at t-17 hours, and one much closer to the firing/release. This first pre-heat period is to ensure sufficient pressure in the propellant tank to support flow, and the second is to heat the system to ensure the impending outflow to the arcjet is vaporized. The PFS algorithm is started just before the firing and controls the NH_3 flow rate by cycling the DPC valve to maintain pressure in the plenum tank corresponding to the specified flow rate.

The problem appears to be a cold spot in the propellant line somewhere between the EFH and the DPC valve. This cold spot allows NH_3 to condense and collect just upstream of the DPC valve. The liquid ingestion seems to occur only at the initiation of the PFS algorithm, which causes a single cycle of the DPC valve regardless of the plenum tank pressure. This valve cycle releases this slug of liquefied NH_3 into the plenum tank resulting in the behavior described above.

This phenomenon was not readily observed in any of the ground tests. Initially, there were some differences between the flight operations profile and the ground test, primarily the heater setpoints and timing, but ultimately the flight profile was changed to mirror the test flow. This did not, however, alleviate the problem. Further modifications were made to the flight profile (mostly adjusting heater setpoints) but none of these proved successful either.

The root cause of the problem - the cold spot in the system - was possibly a result of a cooler PFS platform than experienced during test. This platform temperature is not actively controlled, and can drift significantly - perhaps leading to a low enough temperature to condense NH_3 at the pressure in the propellant line.

To further support this possibility, there were some variations from the normal procedure on the last firing (F-8) and no liquid ingestion was observed. For that case, the PFS heaters were turned on days before the actual firing attempt as a result of waiting for the battery reconditioning to complete. This may suggest the cold spot in the propellant line had enough time to heat up and vaporize the condensed NH_3 .

In summary, the liquid ingestion proved to be an annoyance, but did not seriously detract from the arcjet operation. If the ESEX mission had continued, a heater configuration that alleviated this problem would almost certainly have been determined.

4.0 SUMMARY

During Phase I of the program, the engineering design of all the subsystems and the flight unit was performed. Preliminary developmental testing was also performed using a government-furnished arcjet and a breadboard PCU in order to attempt to establish detailed technical criteria regarding the start-up of the arcjet with the PCU. However, as was subsequently learned in Phase II with additional integrated testing of the arcjet and PCU, the starting requirements of the arcjet were not entirely understood. Phase I was concluded with the presentation of the flight unit design to AFRL at the PDR in July 1991.

During Phase II, fabrication and testing of development hardware was conducted and detailed design changes were incorporated based on these test results. Examples of these design changes include:

- Integrated testing of a development PCU with a government-furnished arcjet identified the inability of the PCU to break down (i.e. ignite) the thruster with the existing start circuit. Additional testing was accomplished at AFRL and PAC that defined the true start-up criteria for the arcjet. The necessary changes were successfully implemented into the PCU design.
- Numerous tests were conducted to develop a PFS which was capable of conditioning liquid NH_3 to vapor for the full 15 minute outflow required for thruster operation.
- Eagle PicherTM, a subcontractor to TRW, performed discharge tests using a 20-cell battery to verify performance capability and stability and to provide thermal design data before fabricating the full 126-cell battery.
- A development PCU, an EM arcjet, and an EM of the propellant feed subsystem were integrated and tested to verify performance. A full-scale EM of the battery was subsequently added to the entire system-level assembly to demonstrate the capability of the propulsion system end to end.
- EMs of the PIU and the CCU were assembled and functionally tested prior to and after a vibration test to verify functionality and their ability to endure the anticipated launch environment.
- A breadboard EMI electronics unit was upgraded to an EM and exposed to vibration, thermal cycle and burn-in tests to verify the integrity of the design for the Arcjet ATTD application.
- The flight unit structure was fabricated and subjected to a static load test and was inspected and verified to have survived the test without damage.

Following these tests, the overall flight unit design was presented to AFRL at the program CDR.

Following the CDR and AFRL approval of the flight unit design, some EM hardware was refurbished for flight use. Specifically, this hardware included the PIU, the EMI electronics unit, the CCU, and the flight unit structure. PAC fabricated and assembled from all new components, the flight PFS, a flight arcjet and a flight PCU. Prior to integration into the flight unit, protoflight-level acceptance tests were conducted to verify compliance of the arcjet, PCU, and PFS with environmental requirements. TRW assembled the diagnostic package and the thermal management system. OSC integrated the various subsystems into the flight unit. Both TRW and OSC refurbished, as necessary, all hardware to assure its status as flight-ready.

Phase III of the program began at the completion of flight unit assembly and initial functional testing. During this phase, TRW subjected the flight unit to the protoflight acceptance tests. This testing consisted of thermal vacuum, random vibration, EMC, proof pressure and leak testing of the propulsion subsystem, and integrated system tests. Having completed its ground

qualification test, the flight unit was delivered to AFRL at the Boeing Company in Seal Beach, CA for integration onto the ARGOS spacecraft.

ESEX is the culmination of over ten years of effort to validate high power electric propulsion on-orbit and verify its compatibility with USAF, DoD and commercial satellites. There were a total of eight firings conducted over the course of the 60-day mission, for a total duration of 2,023 seconds. There were two anomalies associated with the flight operations - a liquid ingestion problem that had only a minor affect on the mission, and a battery failure that precluded any further firings. Approximately 76% of the ESEX mission success was attained, with the biggest deficiencies resulting from the optical signature characterization and the lack of GPS data. All of the demonstration aspects of the experiment were completed successfully, and all of this hardware - the arcjet, PCU, and PFS - operated very well, and within their specifications. All of the data analyzed to date indicate the thruster operated nominally, and operated completely independently of the normal operations of the host spacecraft (ARGOS).

5.0 RELATED PUBLICATIONS

Kriebel, M. M. and Sanks, T. M., "Electric Propulsion Space Experiment (ESEX) - Spacecraft Design Issues for High Power Electric Propulsion", CPIA-PUB-580-VOL 1, *JANNAF Propulsion*, Indianapolis, IN, February 24-26, 1992, P 503-516

Cassady, R. J., Vaughan, C.E., and Aadland, R. S., "A 26 kW Arcjet System for On-Orbit Demonstration", CPIA-PUB-580-VOL 1, *JANNAF Propulsion*, Indianapolis, IN, February 24-26, 1992, P 517-526.

Kay, R. J., Golden, C. M., and Fisher, J. R., "Power Conditioning Unit for 30 kW Class Arcjet Flight Experiment", CPIA-PUB-580-VOL 1, *JANNAF Propulsion*, Indianapolis, IN, February 24-26, 1992, P 527-537.

Kriebel, M. M., and Stevens, N. J., "30-kW Class Arcjet Advanced Technology Transition Demonstration (ATTD) Flight Experiment Diagnostic Package", AIAA Paper 92-3561, July 1992, *AIAA Joint Propulsion Conference*, Nashville, Tennessee, July 6-8, 1992.

On September 13-17, 1993, Mary Kriebel of TRW and Joe Cassady and Charlie Vaughan of PAC attended the 23rd International Electric Propulsion Conference in Seattle, WA. During the conference, PAC presented the following two papers related to the Arcjet ATTD program:

Vaughan, C., Cassady, R., and Fisher, J., "Design, Fabrication, and Test of a 26 kW Arcjet and Power Conditioning Unit," IEPC-93-048, September 1993.

Aadland, R. and Vaughan, C., "Achieving Reliable, Repeatable Starts of a 26 kW Arcjet," IEPC-93-049, September 1993.

Aadland, R.S., Vaughan, C.E., Cassady, R.J., and Kay, R.J., "Integrated Mission Simulation of a 26-kW Flight Arcjet Propulsion System," AIAA-93-2395, June 1993, *AIAA/ASME/SEAE/ASEE Joint Propulsion Conference and Exhibit*, Monterey, CA., June 28-30, 1993.

Vaughan, C.E., and Morris, J.P., "Propellant Feed Subsystem for a 26-kW Flight Arcjet Propulsion System," AIAA-93-2400, June 1993, *AIAA/ASME/SEAE/ASEE Joint Propulsion Conference and Exhibit*, Monterey, CA., June 28-30, 1993.

Biess, J. J., Sutton, A. M., "Integration and Verification of a 30 kW Arcjet Spacecraft System", AIAA Paper 94-3143, *30th Joint Propulsion Conference*, Indianapolis, IN, June 27-29 1994.

6.0 REFERENCES

1. Olin Aerospace Company, *Arcjet Advanced Technology Transition Demonstration (ATD) Engineering Model Test Report*, submitted to TRW on 11 April 1995.
2. Paul, Fred W. and Burrowbridge, Donald, *The Prevention of Electrical Breakdown in Spacecraft*, NASA SP-208, NASA Goddard Space Flight Center, 1969.
3. Dunbar, W., *High Voltage Design Criteria*, NASA 50M05189, NASA George C. Marshall Space Flight Center, 1972.
4. Farber, B., Goldin, D., Markus, B., and Mock, P., *Transmitter Experiment Package for the Communication Technology Satellite*, NASA CR-155035, NASA Lewis Research Center, 1977.
5. Mendell, W. D., *Electric Propulsion Space Experiment (ESEX) EMC Test Report*, TRW Document Number 95.M541.4-035, 1 June 1995.
6. Barone, T. J., *Arcjet Payload Protoflight Test Report*, TRW Document Number M533.5.95-071, 31 May 1995.
7. Lee, D. W., *Arcjet Thermal Vacuum Test Report*, TRW Document Number 96.M532.1.15-001, 15 January 1996.
8. Bromaghim, D. R., LeDuc, J. R., Salasovich, R. M., Zimmerman, J. A., Matias, D. C., Sutton, A. M., Spanjers, G. G., Fife, J. M., Hargus, W. H., Spores, R. A., Dulligan, M. J., Engelman, S. F., "An Overview Of The On-Orbit Results From The Electric Propulsion Space Experiment (ESEX)," IEPC Paper No. 99-192, October 1999.
9. Johnson, L., Spanjers, G., Bromaghim, D., LeDuc, J., Salasovich, R., Zimmerman, J., Sutton, A., Fife, J., Hargus, W., Spores, R., Dulligan, M., Schilling, J., and White, D., "First Results From Optical Diagnostics Applied to the Air Force Electric Propulsion Space Experiment (ESEX)," AIAA Paper 99-2710, June, 1999.

10. Dulligan, M.J., Zimmerman, J.A., Salasovich, R.M., Bromaghim, D.R., and Johnson, L.K., "Electromagnetic Effects of the ESEX 26 kW Ammonia Arcjet on Normal Spacecraft Operations," AIAA Paper 99-2708, June 1999.
11. Fife, J.M., LeDuc, J.R., Sutton, A.M., D.R. Bromaghim, Chart, D., Hoskins, W.A., Vaughan, C.E., and Johnson, L.K., "Preliminary Orbital Performance Analysis of the Air Force Electric Propulsion Space Experiment (ESEX) Ammonia Arcjet," AIAA Paper 99-2707, June 1999.
12. Spanjers, G.G., Schilling, J.H., Engelman, S.F., Bromaghim, D.R., and Johnson, L.K., "Contamination Analysis from the ESEX 26 kW Ammonia Arcjet Flight Experiment," IEPC Paper 99-038, October 1999.
13. Vaughan, C. E., and Morris, J. P., "Propellant Feed Subsystem for a 26 kW Flight Arcjet Propulsion System," AIAA Paper 93-2400, June 1993.
14. Bromaghim, D.R. and Sutton, A.M., "Electric Propulsion Space Experiment Integration and Test Activities on the Advanced Research and Global Observation Satellite," AIAA Paper 96-2726, July 1996.
15. Salasovich, R.M., Bromaghim, D.R., and Johnson, L.K., "Diagnostics and Flight Planning for the US Air Force Phillips Laboratory Electric Propulsion Space Experiment (ESEX)," AIAA Paper 97-2777, July 1999.

APPENDIX A: MATERIALS RESEARCH AND DEVELOPMENT REPORT

As a part of the overall arcjet development effort, three separate material process development efforts were undertaken. The first was to develop a process that would produce tungsten (W100) in densities high enough to be suitable for the high power/high temperature operating conditions anticipated for the 30 kW arcjet. The second development effort was to develop a means by which to weld the high density tungsten to Mo/41Re in order to join the anode body to the anode nozzle. The third effort was to develop a flight-qualified means by which to braze InconelTM 625 to Mo/41Re in order to duplicate the arcjet manifold-to-barrier-tube braze joint.

A.1 High Density Tungsten Development. The process needed to produce the desired density of tungsten for the anode was initiated during Phase I of the program. This was a significant contribution to the development of the flight-unit arcjet. Tungsten is not usually fabricated in diameters greater than 1.5 inches and powder metallurgy does not produce full density material in the center of large bars where the critical anode dimensions are. GTE-SylvaniaTM performed a test run of a Hot Isostatic Press (HIP) technique that yielded positive results. The chemical composition of the tungsten billets produced in this manner met PAC's specification. To meet the density requirement (99%), however, forging of the billet was required. The material, produced in two-inch diameter by 7-inch long billets, were then forged at Northwest Industries into 3-inch diameter by 5-inch long billets and machined into the weld samples and anodes. The actual welding and testing of the samples was performed in Phase II.

A.2 Tungsten to Mo/41Re Weld Development. At the end of Phase I, a process to produce the desired density of tungsten for the anode was completed. The output of this effort was a number of tungsten weld samples and anodes to be welded and tested in Phase II. The weld process development testing for the anode to barrier tube EB weld was completed early in Phase II. Six sets of bi-metallic weld mock-ups were machined out of tungsten (W100) and Mo/41Re. The EB weld schedule parameters were established to join the Mo/41Re barrier tube to the tungsten anode. Three mock-ups were welded. Once two of the mock-ups were welded, they were subjected to thermal cycle exposure between -150°F and 2300°F for up to 200 cycles and a single -320°F cold cycle. Post-thermal cycle penetrant inspections of the weld joint face and the weld heat affected zone revealed no defects in either the Mo/41Re or tungsten.

Two of the weld mock-ups were sectioned for metallographic weld quality inspection. One was in the post-weld stress relieved condition as noted above with 200 thermal cycles. The results of this metallographic cross sectioning revealed that both EB welds contained root cracks on the tungsten side of the weld in the heat affected zone. These cracks penetrated the weld from the weld root heat affected zone to a depth of approximately 0.134-inch which left a remaining weld thickness of approximately 0.045 inch including the weld face reinforcement. No external surface cracking, or weld leakage, was observed.

From these metallographic cross section results it appears that the EB weld joint root heat affected zone of the tungsten is cracking during post-weld cooling and that cyclic thermal exposures are not causing crack propagation through the material. The nature of the cracks is such that applied vibration loads would probably not lead to further propagation through the joint. However, due to the generally unpredictable nature of the cracking phenomena, an effort was undertaken to redesign these welds to reduce the post-weld residual stress. Three geometries, shown in Figure A1, were identified and analyzed.

The first proposed geometry change was to reduce the joint thickness to 0.088 inch from 0.125 inch to more closely approximate the joint geometry of the successful TelstarTM 4 anode weldment. This would not appreciably reduce the joint stresses, but would make the welding process more similar to past practices. A transition section was also considered in order to reduce the coefficient of thermal expansion (CTE) mismatch between the tungsten anode and the adjacent material. The selected transition material was W/25Re, which has a CTE that is very close to that of pure tungsten, but is less ductile than the Mo/41Re currently used in the joint. The optimum length for the transition section was estimated to be 0.175 inch to 0.525 inch. Stresses in the W/25Re to Mo/41Re barrier tube joint were anticipated to be similar in magnitude to the baseline anode weld, but less crack prone due to the increased weldability of W/25Re over that of pure tungsten. Changing the joint from a butt weld to a scarf weld was also examined. This geometry was thought to provide the benefit of retaining the current two materials, and requiring just one weld joint.

Finite element analysis was used to model the existing anode joint, and each of the alternative configurations. The stresses at the root of the weld are quite high at the inner diameter, but are very localized, and are alleviated by small amounts of yielding. Variations in finite element mesh geometries can lead to significant differences in the stress calculation at this interface. The best way to avoid this numerical difficulty was to model all competing designs with the same size finite element mesh and compare the results relative to each other. In this way a linear static finite element analysis provided results usable for design assessment.

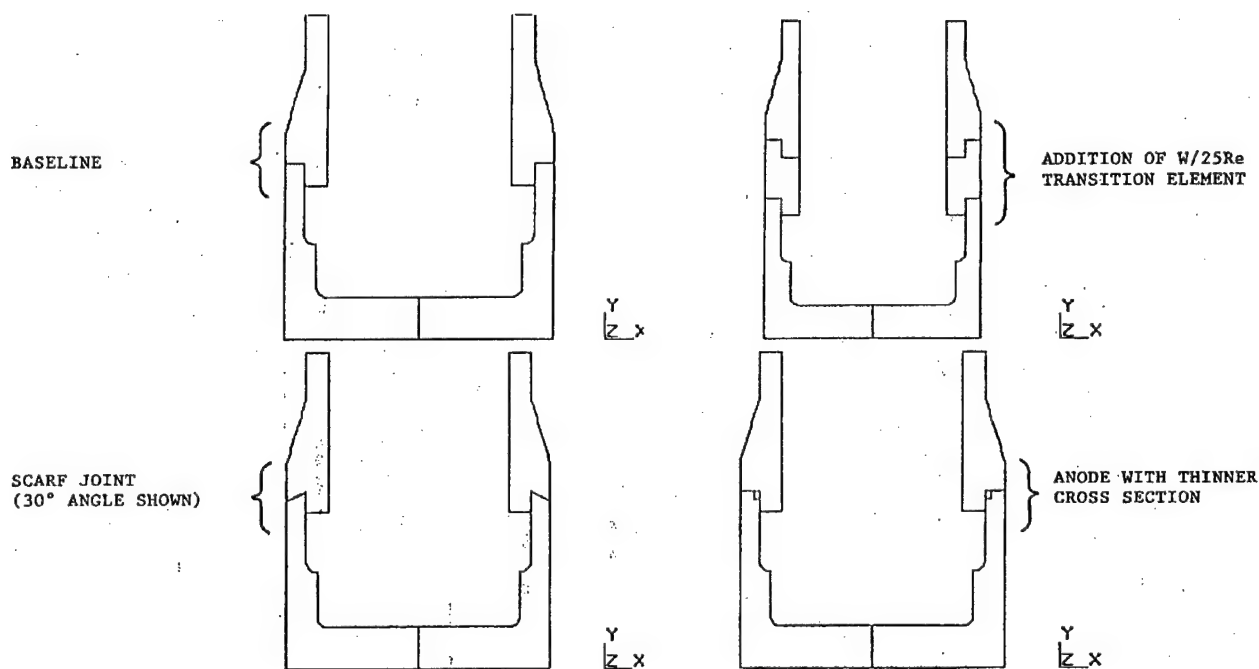


Figure A1. Analyzed Anode Joint Configurations

An examination of the stress field near the weld joint showed that the radial and hoop stresses were compressive for all of the weld joints considered in this analysis. The axial yy stress component did vary however, and was felt to be the best indicator of crack formation. Tensile yy stresses at the weld interface tended to pull the joint open, and could propagate a radial crack, while

a compressive yy stress field inhibited radial cracking. Stresses in the anode were of primary interest since the tungsten material was the least ductile component in this assembly.

Three joint configurations were examined and compared to the existing design. Each case was analyzed using a linear axisymmetric finite element model with loading produced by differential contraction of the various metals from a stress free state at the 2000°F welding temperature. Figure A1 shows the basic configurations that were modeled. For the transition sleeve and scarf joint options, various transition lengths and joint angles were modeled in order to identify the best possible geometries in each case.

The proposed use of a W/25Re transition element between the anode and the barrier tube represented the greater departure from the current configuration. Transition lengths of 0.175 inch to 0.525 inch were analyzed. Figure A2 shows the configuration and finite element model. As was mentioned earlier, the yy stress component was used as the figure of merit when comparing the performance of various joints. Figure A3 plots the yy stress results as a function of transition element length for the inner and outer joint diameter, and the anode body at the location where circumferential cracking occurred in one earlier weld sample. The corresponding stresses from the baseline configuration are also included for comparison purposes.

Addition of the W/25Re transition element completely changed the stress distribution in the joint from that of the baseline weld. The joint I.D. was loaded in compression at the weld root, which inhibited crack formation in this region, but the outer surface was in tension instead of compression. The surface of the anode body remained in tension, but the stresses were lower than in the baseline configuration. A transition element length of 0.350 inch appeared to provide a good amount of compression at the weld root, while keeping the tensile stresses at the O.D. within acceptable limits. Shorter transition lengths could present some difficulty in fabrication because the weld region for both joints would be heated simultaneously, and longer lengths would increase the amount of W/25Re stock required.

After identifying the 0.350-inch transition joint as the most favorable, the yy stresses in the weld joints at both ends of the 0.350 inch-long W/25Re transition element were determined. The root of the barrier tube weld has a stress distribution very similar to that of the anode weld that cracked. The difference was that the materials involved should be more able to tolerate these stresses without cracking than the pure tungsten of the anode.

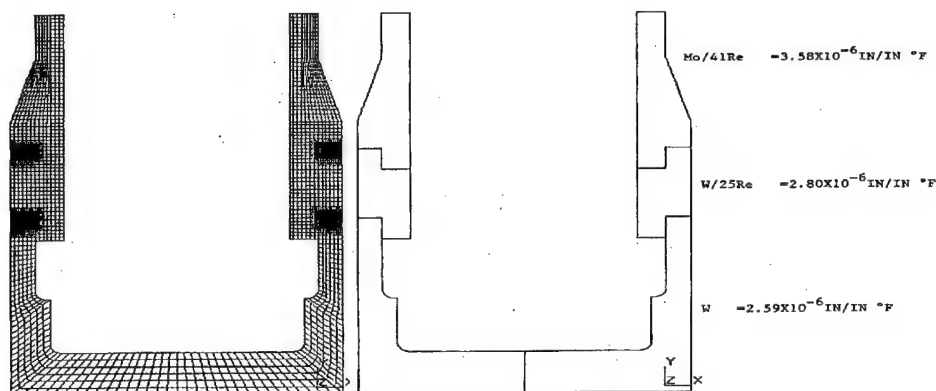


Figure A2. Finite Element Model of Weld Joint with W25Re Transition Element

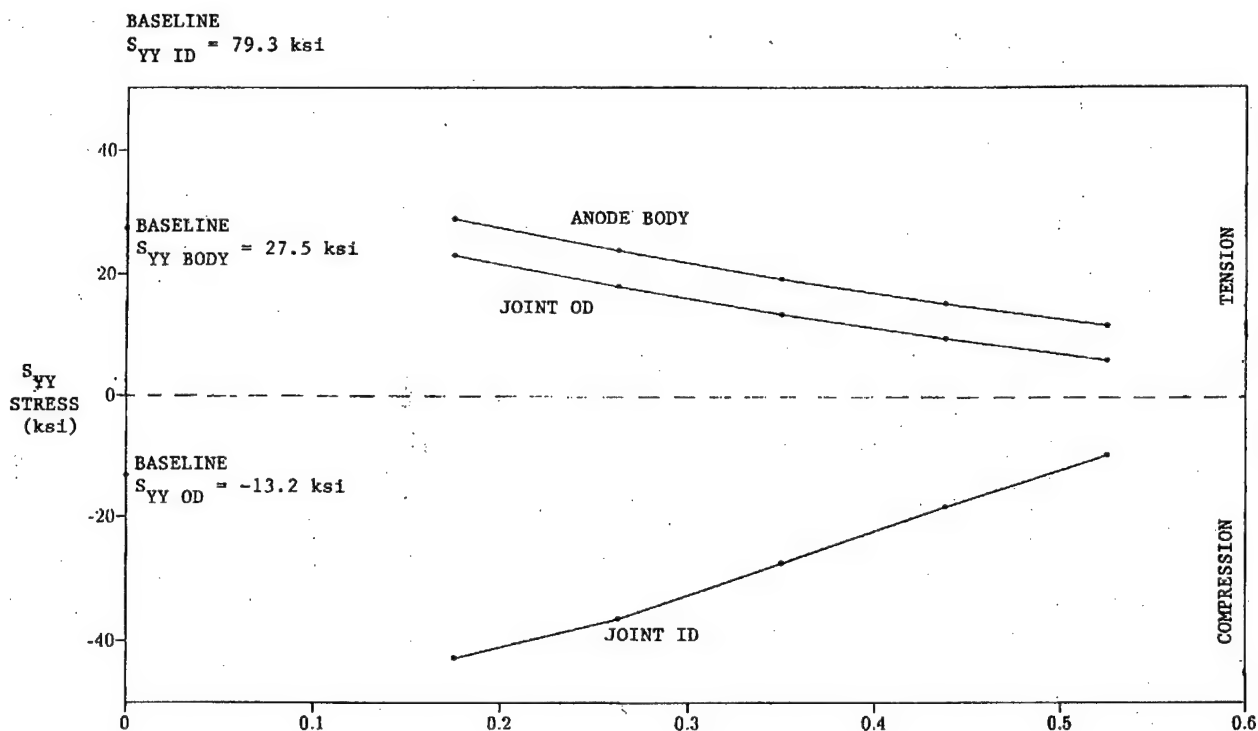


Figure A3. Anode Stresses in Weld Region of Modified Joint

After it became clear that the tungsten portion of the anode weld root could be kept in compression by using a different mating material, an attempt was made to duplicate this effect using the tungsten and Mo/41Re joint materials with a revised geometry. The existing straight butt weld was modified to include a scarf angle at the interface. A finite element model of this joint is shown in Figure A4.

Negative scarf angles reduced the yy stresses at the joint I.D., but allowed the joint O.D. stresses to rise dramatically over those of the baseline configuration. The relationships between the joint scarf angle, and the resulting joint stresses are shown in Figure A5. Stresses in the anode body are fairly insensitive to the scarf angle used in the anode weld joint. An angle of negative 15° represented a good compromise that reduced stresses at the joint I.D. without overloading the joint O.D.

The last joint investigated simply reduced the tungsten anode cross section by removing material at the inner diameter as shown in Figure A6. This resulted in a joint that had the same interface geometry as a commercial program anode weld that has proven to be successful in production. The stresses in the thinner joint were somewhat higher at the weld root than in the baseline design. The potential advantage to this configuration was that if the root cracking was a function of the welding methodology, returning to dimensions used in past designs could eliminate the cause of the cracking.

Stress analysis results for the baseline design and the three proposed alternatives are tabulated in Table 5. The use of a scarf joint provided some benefits, but they were of a more incremental nature than those obtained by including the W/25Re in the anode weldment. The -15° scarf joint was less attractive from a stress minimization standpoint and was removed from consideration. The option of using a thinner anode section provided no benefit other than

increasing the compressive axial load at the O.D. of the weld. Addition of the W/25Re transition element was the only analyzed option that resulted in compressive loading of the anode weld root. A sample with a 0.350-inch long W/25Re element to connect the anode to the barrier tube was subsequently fabricated.

Since it was not anticipated that the cracks in the existing EM welded hardware would result in any hardware failure during EM testing, this EM arcjet fabrication using the baseline weld configuration proceeded in parallel with the weld-joint trade study. During the TiC high emissivity coating of the EM arcjet anode, a circumferential crack formed approximately 0.25 inch from the tungsten to Mo/41Re EB weld on the tungsten side of the weld when the arcjet body assembly was grit blasted for surface preparation. This occurred in an area of known high external surface stress and was similar to a failure that occurred with one of the weld development samples. The grit blasting generated a flaw in the surface of the material that allowed the crack to form in the stress field. In order to minimize schedule impact, assembly and EB welding of a new EM arcjet was performed using the spare tungsten anode (formerly the flight anode), the original EM barrier tube and internal hardware, and a new manifold. The new assembly, referred to as EM', was not TiC coated to avoid introducing surface flaws.

Seven alternate flight configurations were also developed, but subsequently reduced to the W25/Re ring and a tape-tungsten insert in a Mo/41Re anode tube shown in Figure A7. A sample with the W/25Re ring was welded, but the weld cracked in the heat-affected zone on the tungsten side of the tungsten-to-W/25Re weld. It became obvious the tungsten-to-Mo/41Re weld had to be eliminated and the anode insert approach was pursued. The anode insert design shown in Figure A8 was fabricated and integrated with a new arcjet manifold and refurbished portions of the EM' arcjet. This arcjet thruster was referred to as EM'' and used in the IMS-testing.

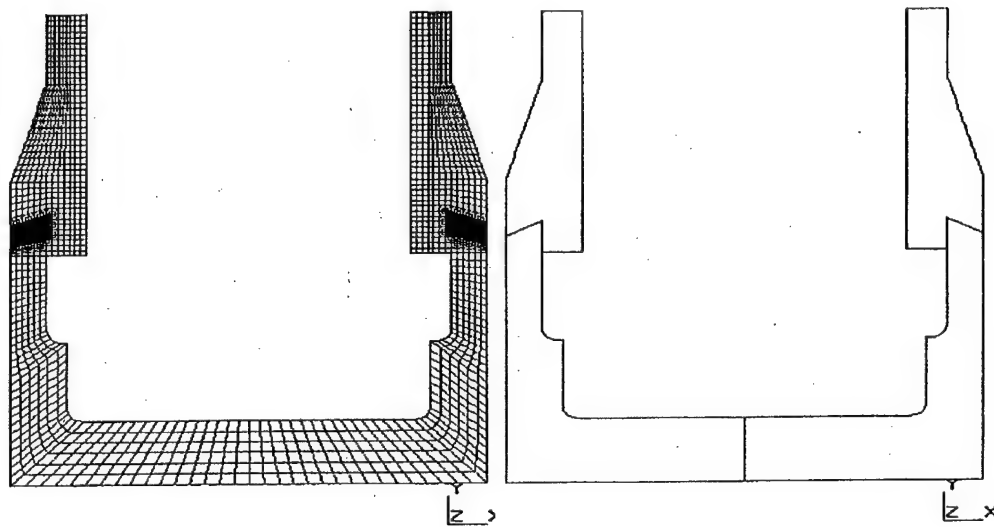


Figure A4. Finite Element Model of Weld Joint with a -30° Scarf Angle

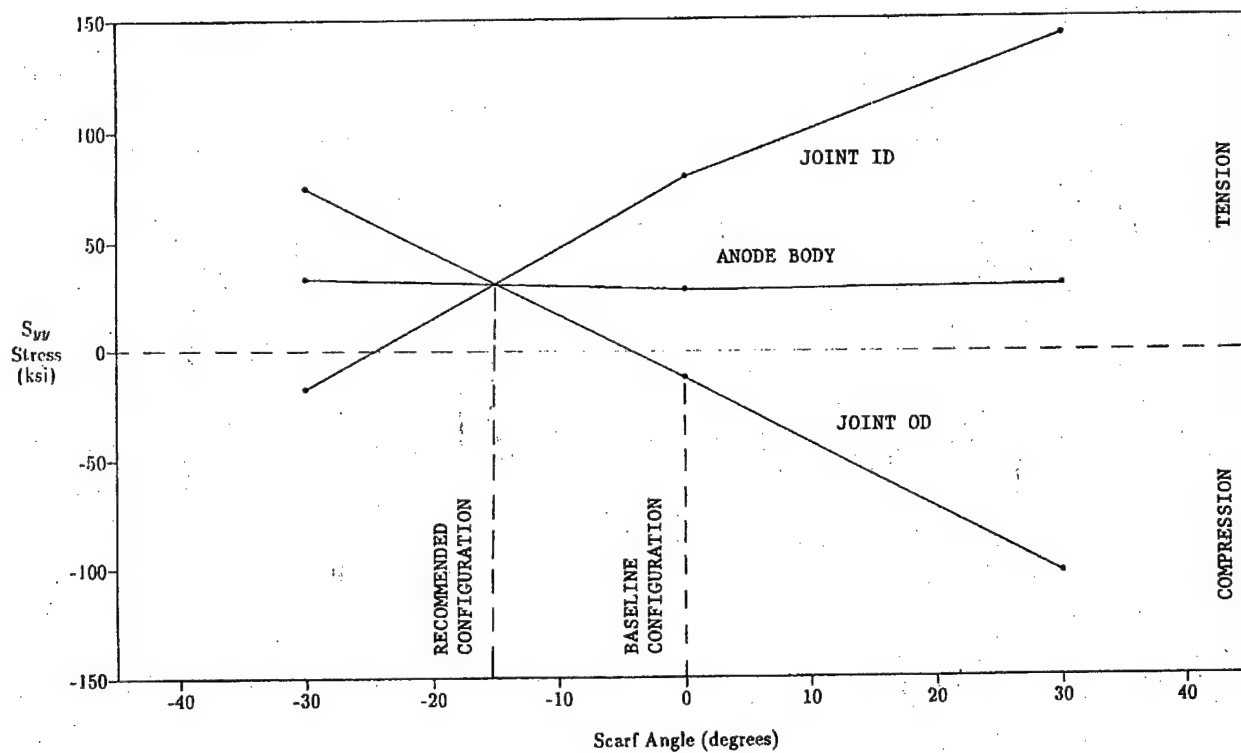


Figure A5. S_{yy} Anode Stresses in Weld Region of The Scarf Joint

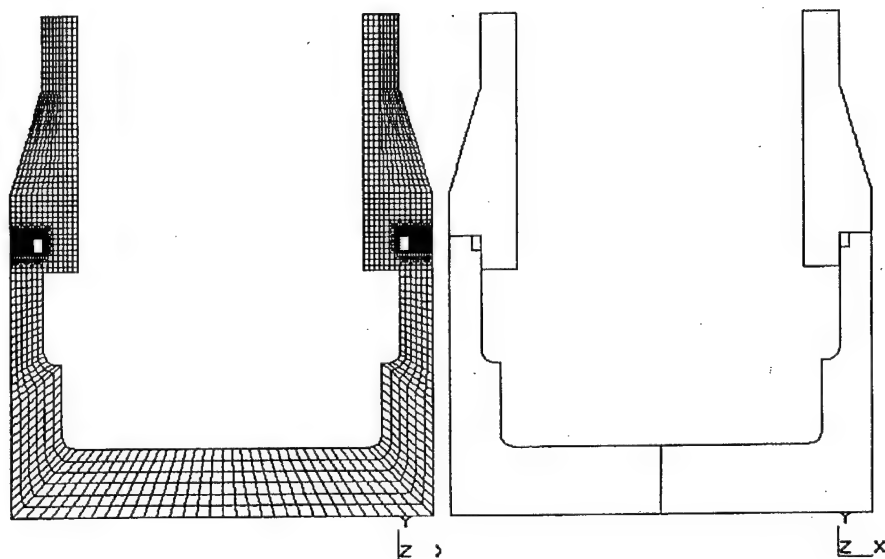


Figure A6. Finite Element Model of Weld Joint with Thinned Anode at Weld Interface

Table A1. Stress Summary for Anode Weld Alternatives (S_{yy} Stress Used as Figure of Merit)

Location	W Anode to Mo/41Re Barrier Tube	W Anode to 0.350 inch W/25Re Transition Sleeve	W Anode to Mo/41Re Barrier Tube With -15° Scarf Angle	W Anode to Mo/41Re Barrier Tube With 0.037 inch Relief at I.D.
Joint I.D.	79.3 ksi	-27.5 ksi	30.0 ksi	104.1 ksi
Joint O.D.	-13.0 ksi	13.3 ksi	30.0 ksi	-26.0 ksi
Anode Body	27.5 ksi	19.1 ksi	30.0 ksi	31.7 ksi

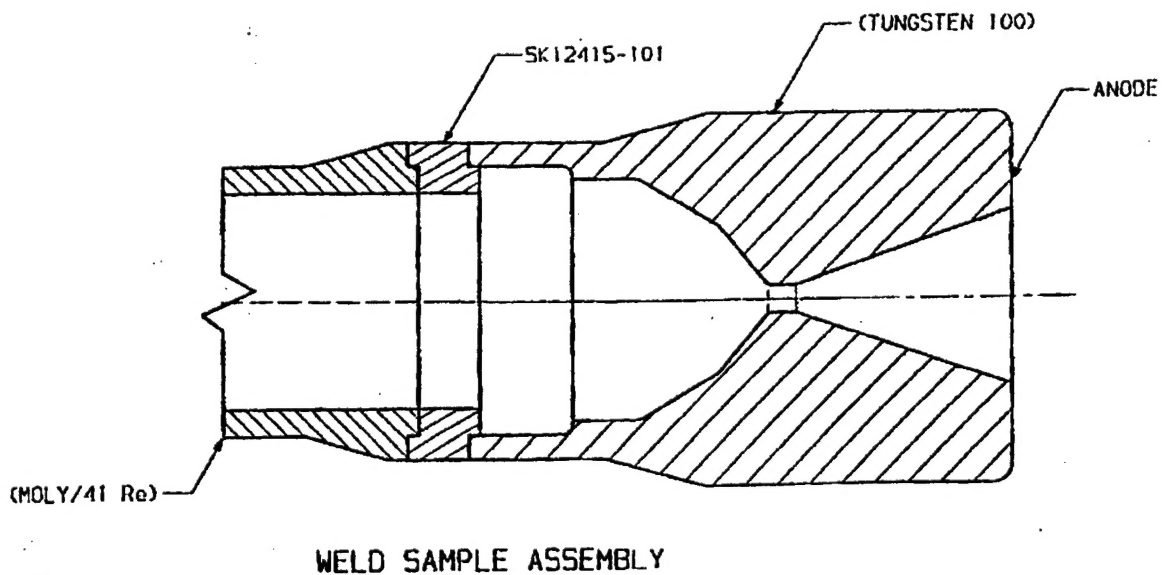


Figure A7. Alternate EB Weld Configuration with a W24/Re Ring

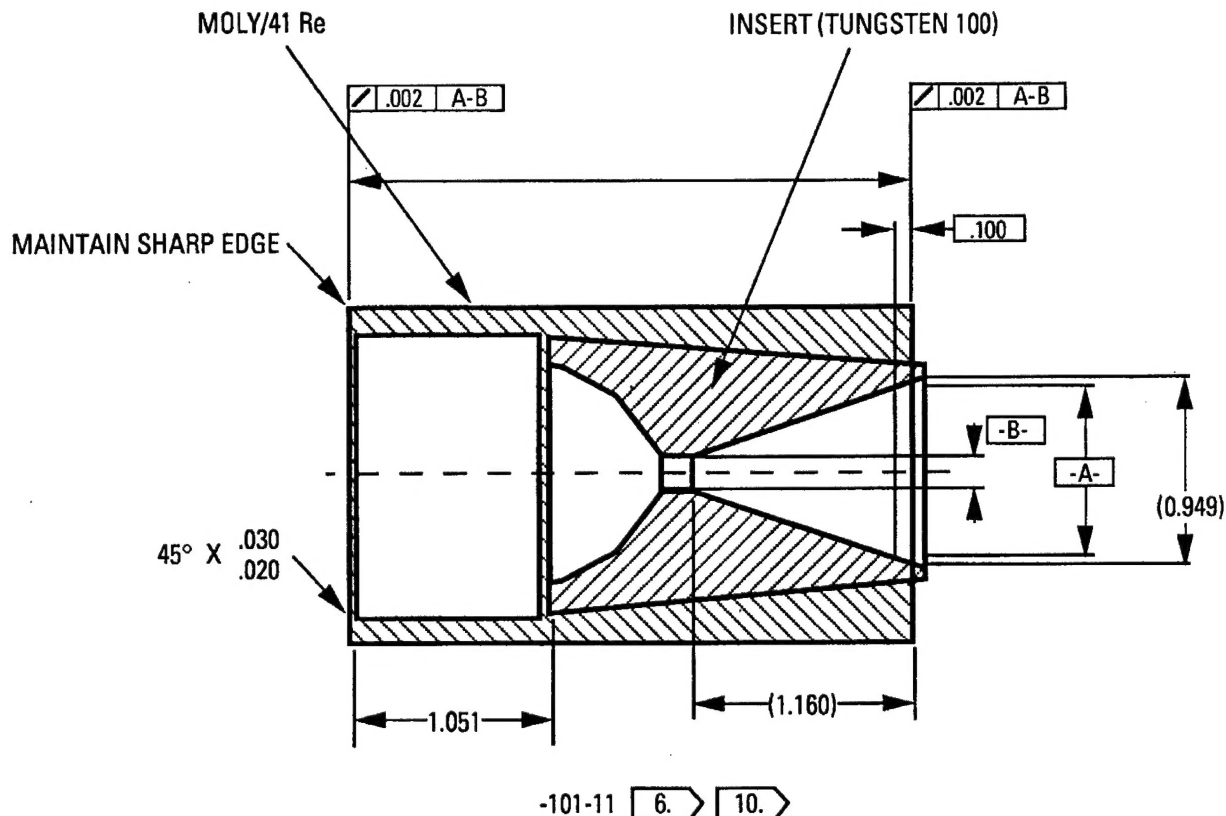


Figure A8. EM" Anode Design

A.3 Inconel™ 625-to-Mo/41Re Braze Development. A set of five Inconel™ 625-to-Mo/41Re braze samples were fabricated to duplicate the manifold-to-barrier-tube braze joint, but only three samples were actually brazed. The braze alloy filler metal rings were fabricated using 0.087-inch diameter gold wire. Internal visual inspection of the braze joints pull-through side was performed using a bore scope. The visual inspection showed braze material fillets around the entire circumference of all three samples, however, filler size was considered too small. An additional operation of adding gold braze powder to the external surface of the joint was performed on two of the samples as a technique for increasing alloy feed side fillet uniformity. Based on the results of re-brazing the joints with additional gold powder filler metal, this technique was abandoned. The braze ring used for the EM braze joint utilized 0.093-inch-diameter wire pre-flattened to obtain an oblong cross-section. In order to provide additional braze filler metal for fillet formation at both the fillet feed and pull-through side of the braze joint.

All three braze samples that were fabricated with the added gold braze powder were proof pressure tested using helium at 45-50 psig for five minutes minimum. They were then leak

checked under an alcohol bath using helium at 30-35 psig for one-minute minimum. There was no leakage from any of the three samples.

Sample Number 2 was submitted for thermal cycling between 90°F and 150°F. The test fixture was a pneumatic cylinder driving a ¼" diameter CRES sample holder in and out of a quartz tube furnace with the temperature set at 90°F into a water jacket cooling zone. The atmosphere in the furnace was N₂, however, the port through the end plate was not sealed and some oxidation did occur. A programmable timer was used to cycle a solenoid 3-way valve (supplying the gas to the pneumatic cylinder) which controlled the position of the part with respect to the heating and cooling zones. Forty-five minutes in each position supplied adequate heating to obtain the desired temperature extremes.

The braze joint was checked at 29, 114, and 209 cycles for appearance and leak checked with bubble leak-check solution using 50 psig helium pressure. There was discoloration due to oxidation, but no evidence of leakage was found at any time. The braze joint was then sectioned for metallographic examination, and successfully completed inspection.

Primary Distribution for AFRL-PR-ED-TR-1999-0034:

AFRL/PRRS (5)
Daron R. Bromaghim
4 Draco Drive
Edwards AFB CA 93524-7160

Ranney Adams (1)
AFRL/PROI (PAO)
2 Draco Drive
Edwards AFB CA 93524-7800

Mary M. Kriebel (5)
TRW Space & Technology Division
Space & Electronics Group
One Space Park
Redondo Beach CA 90278

AFRL/PR Technical Library (3)
6 Draco Drive
Edwards AFB CA 93524-7130

Air University Library (1)
AUL/SE
600 Chennault Circle
Maxwell AFB AL 36112-6424

Chemical Propulsion Information Agency (1)
Attn: Tech Lib (Dottie Becker)
10630 Little Patuxent Parkway, Suite 202
Columbia MD 21044-3200

Defense Technical Info Center (Orig + 1)
Attn: DTIC-ACQS (Acquisitions)
8725 John J. Kingman Road, Suite 94
Ft. Belvoir VA 22060-6218